Tesis Doctoral

Programa Doctorado: Cibernética y Telecomunicación (2002/2004)

UNIVERSIDAD DE LAS PALMAS
DE GRAN CANARIA

Nuevos Esquemas para el Procesado de Señales Tensoriales

New Schemes for Tensor Signal Processing

E.T.S. Ingenieros de Telecomunicación
Departamento de Señales y Comunicaciones

Director:
Dr. Juan Ruiz Alzola

Codirector:
Dr. Carl-Fredrik Westin

Autor:
Carlos Alberto Castaño Moraga

Las Palmas de Gran Canaria, Diciembre 2006

A mi esposa

Agradecimientos

Al echar la mirada atrás y recordar las experiencias vividas durante los cuatro años en los que he estado trabajando en esta tesis, no me cabe la menor duda de que el trabajo recogido en este documento es trabajo de equipo, en el que muchas personas han aportado su granito de arena para que esta tesis fuera tomando forma progresivamente.

En primer lugar, quiero agradecer a mis directores de tesis, el Dr. Juan Ruiz Alzola y el Dr. Carl-Fredrik Westin, el apoyo y la confianza que han puesto en mí para llevar a cabo este trabajo de investigación. De forma especial quiero agradecer a Juan las largas conversaciones que hemos mantenido discutiendo el planteamiento más acertado de esta tesis, estudiando a fondo los problemas a los que nos enfrentábamos. También quiero agradecerle todo lo que me ha enseñado en lo que se refiere a mi formación profesional, algo que abarca desde lo puramente conceptual hasta valores tan importantes como la perseverancia en el trabajo. ¡Gracias!

También quiero agradecer a C.-F. que me haya acogido durante tres meses en su grupo de investigación en Boston, el Laboratory of Mathematics in Imaging *en el* Brigham and Women's Hospital, *que fue muy fructífera tanto a nivel profesional como personal. Mi agradecimiento se hace extensivo para todos los miembros de este laboratorio de los que he aprendido mucho. De forma especial quiero agradecer al Dr. Raúl San José Estepar sus muchas y valiosas indicaciones para mejorar los algoritmos presentados en esta tesis, así como para interpretar adecuadamente los resultados. También quiero agradecer a C.-F. que me proporcionara una parte de los datos tensoriales reales con los que se han realizado algunos experimentos en esta tesis. ¡Gracias!*

No puedo olvidarme de mis compañeros del Centro de Tecnología Médica, *especialmente de mis compañeros el Dr. Miguel Ángel Rodríguez, el Dr. Eduardo Suárez y el Dr. Rubén Cárdenes, a los que considero como hermanos mayores en el terreno profesional, puesto que he ido aprendiendo con vuestro ejemplo y vuestras experiencias. Tampoco puedo olvidarme de otros compañeros como el Dr. Eduardo Rovaris, Reny, Darío, Víctor, Marcos y otros muchos que han ido pasando por el laboratorio como proyectandos. Gracias también a Lidia, por su ayuda siempre necesaria con los trámites burocráticos.*

¡Gracias!

Mi más sincero agradecimiento también al Dr. Olivier Faugeras y muy especialmente al Dr. Rachid Deriche, directores del Proyecto Odyssée *en* INRIA-Sophia Antipolis, *que durante nueve meses me acogieron en su grupo de investigación, ayudándome con gran interés en mi trabajo. Un agradecimiento muy especial también a Christophe Lenglet, por su inestimable ayuda y paciencia para explicarme los conceptos de geometría diferencial, métricas Riemannianas, etc. etc. Tampoco me puedo olvidar de mi compañero de despacho Jerome Piovano, del que también tanto he aprendido. Gracias también a Nicolas Wotawa por proporcionarme los datos tensoriales con los que hemos realizado algunos de los experimentos mostrados en esta tesis. Y, por supuesto, mi agradecimiento a todos los miembros de este laboratorio por vuestro trato humano y por haberme acogido tan calurosamente durante mi estancia en Sophia-Antipolis. ¡Gracias!*

Gracias también a todos los miembros del Laboratorio de Procesado de Imágenes *de la Universidad de Valladolid, especialmente al Dr. Carlos Alberola López, por motivarme para realizar la tesis doctoral que estoy a punto de finalizar y por ponerme en contacto con Juan para llevar a cabo esta tarea. Gracias también por los consejos que me has dado como profesor, como director del PFC y como amigo. Y también quiero agradecer al Dr. Marcos Martín Fernández las largas conversaciones aclarando conceptos y por compartir tus conocimientos. ¡Gracias!*

Un agradecimiento muy especial también al Dr. Luis Álvarez León del que tanto he aprendido a lo largo de estos años. Gracias por tu inestimable ayuda en los cursos de doctorado que me dirigiste, por los buenos consejos que siempre me has sabido dar tanto en el dominio de esta tesis como en el ámbito personal. Gracias también por acordarte de mí para el proyecto FLUID. También quiero dar gracias al resto de compañeros del grupo AMI, empezando por el Dr. Karl Krissian por ayudarme con la visualización de los tensores con tu querido AMILAB, así como a Miguel García, Agustín Salgado, al Dr. Luis Mazorra, al Dr. Javier Sánchez, al Dr. Agustín Trujillo y al Dr. Julio Esclarín. Por vuestra amabilidad, simpatía y amistad. ¡Gracias a todos!

También quiero agradecer a todos mis profesores de cursos de doctorado todo lo que me han enseñado en sus clases. En especial al Dr. Luis Álvarez, al Dr. Manuel Cubero, al Dr. Francisco Eugenio, al Dr. Roberto Moreno, al Dr. Rafael Pérez, al Dr. Luis Gómez y al Dr. Iván Alejandro Pérez. ¡Gracias!

Por último, aunque no por ello con menos intensidad, he querido dejar a todas aquellas personas que me han ayudado con su apoyo y con los ánimos que necesitaba en los momentos duros. En primer lugar agradecer a mis padres y hermanos que siempre hayan estado ahí, aportando serenidad y esa ayuda silenciosa que casi no se nota pero resulta imprescindible para continuar día tras día. También quiero agradecer a todos mis amigos

esos consejos que tanto me han ayudado durante todo este tiempo. Gracias al Dr. Félix López por haber estado ahí desde la distancia. Gracias al Dr. Sylvain Jaume, por todas esas largas conversaciones en el comedor de INRIA-Sophia Antipolis, *nuestras grandes excursiones por la Costa Azul y por tu amistad. Gracias a todos mis amigos franceses: Pascal, Mike, Georges, Paul, Michel, etc. etc. por vuestra amistad y por hacerme sentir uno más entre vosotros. Gracias a D. Álvaro, por su empujón y por contagiarme su fortaleza. Gracias Jorge por estar siempre preocupado por mí (prometo hacer más deporte a partir de ahora). Gracias Carlos, Antonio, Ángel, Javier, José Luis y D. Francisco José, por vuestra ayuda. ¡GRACIAS!*

De forma muy especial, quiero agradecer a Elena, mi esposa, su apoyo constante e incondicional durante todo este tiempo. Quizás es la persona que mejor conoce el esfuerzo que hay detrás de este documento, con sus momentos duros y sus alegrías. Gracias por estar siempre ahí. Por eso quiero dedicarte esta tesis, por ser la mejor compañera de viaje que uno puede desear. ¡GRACIAS!

Contents

Abstract

The overall objective of this thesis is to originally contribute to the development of the new field of Multidimensional Tensor Signal Processing as a branch of Signal Processing. Tensors arise in multiple areas of science and technology, e.g., diffusion tensor, fabric tensor, electrical conductivity tensor, thermal conductivity tensor, strain tensor, etc. Different sensing modalities provide tensor measurements are not fully reliable since any real sensor will provide noisy and possibly incomplete and degraded data. Therefore, all problems dealt with in conventional multidimensional signal processing - such as filtering, restoration, reconstruction, classification, etc. - are also present when dealing with tensor signals.

Tensor data processing has been mainly approached as a specific case of multichannel signal processing. This procedure is obviously insufficient, as tensors are much more general structures than vectors, and writing tensor signals as a succession of vectors fails to preserve intrinsic algebraic relationships among its elements. In this thesis, we argue for considering the whole nature of second and higher order tensor signals in order to preserve all their intrinsic algebraic and geometric information. In this sense, new algorithms developed under this context have to consider the random nature of tensor data and their own algebraic structure with the constraint of keeping the algorithmic complexity as low as possible.

Computer vision is a field of science where tensors arise as an important tool. Based on three axiomatic requirements, Knutsson demonstrated that the image local structure is more conveniently described by a second order symmetric positive semidefinite tensor. This new representation leads to the definition of the local structure tensor *which, in addition, profits from a solid mathematical body that supports a complete analysis in the tensor domain. In this sense we will also focus on the applications that the local structure tensor may have in the development of anisotropic processing systems, either with scalar or tensor data. As an example, fundamental tools of differential geometry like metrics will be used to constitute a data-dependent geometry on the image which allow us to compute distance measures that can be used to derive filter kernels, interpolate images or derive anisotropic models of covariance structure.*

The development of multidimensional tensor signal processing is of potential interest of several applications such as electrical conductivity or mechanics, among others. But in this dissertation, we are specially interested in the applications that multidimensional tensor signal processing may have in the field of medical imaging. In particular, we use a relatively new medical image modality called Diffusion Tensor Magnetic Resonance Imaging (DT-MRI) as proof-of-concept to validate our processing algorithms. A major constraint to deal with this kind of tensor signals is to preserve the positive semidefiniteness of the tensors as long as tensors that do not satisfy this condition have no physical meaning.

In conclusion, we present in this thesis different approaches to deal with conventional signal processing problems, but with the special requirements that tensor datasets demand. As a result of our research work, we have set several theoretical frameworks that lead us to the development of New Schemes for Tensor Signal Processing.

Resumen

Introducción

Esta primera sección presenta al lector un resumen del trabajo realizado en el contexto de esta tesis, expuesto en los seis capítulos escritos en inglés que componen la parte principal de este documento. Este resumen aborda de forma suficientemente extensa tanto los objetivos propuestos en este trabajo de investigación, el planteamiento del problema que se pretende resolver, la metodología empleada para resolverlo, las aportaciones a la literatura científica, junto con las conclusiones más importantes, así como las futuras líneas de investigación que se pretenden abordar como continuación natural de las conclusiones de esta tesis doctoral. Puesto que nuestro objetivo se centra principalmente en el desarrollo de algoritmos para el procesado de señales tensoriales, en este resumen se hace continua referencia tanto a la formulación matemática desarrollada en la parte principal del documento y en la que se fundamentan nuestros algoritmos, así como a las imágenes y figuras que presentan los resultados, que nos permiten extraer las conclusiones apropiadas. De este modo, se evita incluir dos veces las mismas figuras, aunque obviamente formen parte de este resumen.

El objetivo primordial de esta tesis es contribuir de forma original al establecimiento y desarrollo del Procesado de Señales Tensoriales Multidimensionales, considerando tanto sus fundamentos matemáticos como la implementación práctica de los algoritmos desarrollados en computadores digitales. En los últimos años, el procesado de señales tensoriales de segundo orden ha despertado un gran interés en la comunidad científica, ya que en diversas áreas de conocimiento como la dinámica, elasticidad, fluidos, termodinámica, electricidad y magnetismo o geometría diferencial, surge la necesidad de trabajar con este tipo de señales.

Los campos de datos tensoriales de segundo orden, al ser estructuras de datos más complejas que los campos de datos escalares (tensores de orden cero) o vectoriales (tensores de orden uno), requieren algoritmos de procesado especializados capaces de tratar con tales entidades. Uno de los principales problemas que surge en el procesado de este tipo

de datos es la conservación de determinadas propiedades, como que los tensores sigan siendo semidefinidos positivos tras aplicar algún filtro. Esta restricción impone condiciones adicionales a los filtros que se puedan utilizar, lo que complica su diseño.

El procesado de datos tensoriales se ha abordado en numerosas ocasiones como un caso particular de procesado multicanal. Sin embargo, esta forma de proceder es insuficiente ya que los tensores son estructuras mucho más generales que vectores y el hecho de escribir un tensor como tal no permite preservar las relaciones algebraicas intrínsecas entre sus elementos. Es decir, operaciones tan sencillas como la descomposición espectral o realizar transformaciones de coordenadas son difíciles de manejar cuando los tensores se escriben como vectores. Además, tratar las señales tensoriales como señales multicanales implica ignorar información importante de las relaciones algebraicas y geométricas que deben tenerse en cuenta a la hora de procesar los datos.

Por estos motivos, en esta tesis se respeta la propia naturaleza de las señales tensoriales a la hora de desarrollar los distintos algoritmos que aquí se consideran. Por tanto, estos nuevos modelos no se pueden considerar extensiones de los algoritmos multicanal, sino algoritmos con un fundamento matemático propio que engloba al caso multicanal, del mismo modo que este último engloba al caso escalar.

Los campos de tensores aparecen en multitud de dominios de la ciencia. Por ejemplo, en el campo del procesado de imágenes, está muy extendido el uso del tensor de estructura local como herramienta para describir la forma en la que varía la señal localmente. De este modo, además de beneficiarse de un marco matemático muy completo, el uso del tensor de estructura local aporta información de incertidumbre sobre la orientación dominante. Es decir, aporta información sobre la orientación dominante y en la dirección ortogonal. Por tanto, un análisis de los autovalores y autovectores ayuda a discriminar el tipo de vecindario local.

En esta tesis se ha contribuido al desarrollo de filtros anisótropos en el dominio espacial partiendo de la información proporcionada por el tensor de estructura, lo que permite distinguir el caso en el que la señal no varía (caso homogéneo) o lo hace en más de una dirección. Además, en presencia de discontinuidades - caso no homogéneo - la cuantificación de la variabilidad de la señal en la dirección ortogonal proporciona la información necesaria para que el filtro sepa como tiene que mezclar la información introduciendo el deseado comportamiento anisótropo.

El desarrollo del procesado de señales tensoriales tiene mucho interés en distintos casos prácticos, como el estudio de la conductividad eléctrica, visión por ordenador, elastografía, etc. Sin embargo, este interés se ha visto reforzado gracias a la aparición de una nueva modalidad de imagen llamada Resonancia Magnética de Difusión Tensorial, del inglés Diffusion Tensor Magnetic Resonance Imaging (DT-MRI), que define para cada voxel un

tensor de difusión, esto es, una matriz simétrica y semidefinida positiva con la información sobre la magnitud y la dirección en la que se produce la difusión de las moléculas de agua en los tejidos en presencia de un fuerte gradiente. Esto, aplicado al cerebro y junto con las técnicas de procesado adecuadas, permite realizar una reconstrucción in vivo de las fibras nerviosas que recorren la materia blanca del cerebro, así como estudiar la evolución o detectar determinadas patologías neurológicas relacionadas con el deterioro de la materia blanca, como por ejemplo el Parkinson o Alzheimer.

Un tipo de restricción para tratar con este tipo de señales tensores es que los tensores a la salida del sistema de procesado sigan siendo semidefinidos positivos, puesto que aquellos tensores que no cumplen este requisito no tienen significado físico, del mismo modo que una matriz de covarianza negativa no tiene sentido. Para resolver este problema, en esta tesis se ha propuesto una transformación homeomórfica que nos permite definir una cadena de procesado que permite garantizar una respuesta semidefinida positiva.

Este mismo problema también es estudiado desde el punto de vista de la geometría diferencial. Los tensores de orden dos se pueden identificar con el subconjunto de matrices simétricas y definidas positivas, donde se puede obtener una métrica, de forma que aquellas matrices que no son definidas positivas se encuentran a una distancia infinita. Además, es posible obtener una expresión analítica de la geodésica, es decir, el camino más corto entre dos elementos de un subconjunto. De este modo, es posible calcular distancias entre dos matrices definidas positivas y calcular estadísticos sobre ellos, estableciendo una formulación equivalente a los filtros definidos utilizando una geometría euclídea para el caso de datos escalares y vectoriales.

En resumen, en esta tesis se han investigado diferentes formas de tratar algunos problemas convencionales de procesado de señales, pero teniendo en cuenta los requisitos demandados por los datos tensoriales. Como resultado de nuestro trabajo se han definido ciertos marcos matemáticos que nos conducen al desarrollo de Nuevos Esquemas para el Procesado de Señales Tensoriales.

Antecedentes

Antes de comenzar con el desarrollo específico de este trabajo de investigación, en la sección 1.4 se describe la notación que se utilizará en este documento. Básicamente, se utiliza la convención de que los datos escalares se escriben con letras minúsculas, los vectores con letras minúsculas en negrita, las matrices y tensores de segundo orden con letras mayúsculas en negrita, mientras que sus elementos se indexan con letras minúsculas con el número de subíndices apropiados.

El capítulo 2 introduce los conceptos básicos que son utilizados en todo el documento. En este sentido, la sección 2.2 presenta conceptos importantes de la teoría de procesado de señal, como energía local, fase local y filtros en cuadratura, en los que se basan algunos algoritmos de los desarrollados en esta tesis. Esta teoría básica se complementa con la sección 2.3, donde describimos los conceptos básicos de la estimación en sentido óptimo, una rama clásica del procesado de señal, con especial interés en la teoría del filtro de Wiener. Después, en la sección 2.4, se describen las matemáticas involucradas en el álgebra tensorial, lo que incluye la definición de señales tensoriales, como las que aparecen, por ejemplo en Diffusion Tensor Magnetic Resonance Imaging (DT-MRI), una modalidad de resonancia magnética de particular interés en esta tesis.

Conceptos Previos

Algunos conceptos básicos que se usan en todo este documento son los siguientes:

- *Fase local: La fase local de una señal $s(t)$ es el argumento de su señal analítica (Ec. 2.2): $\varphi(t) = \arg[s_A(t)]$. Esta magnitud ofrece una descripción contínua de la variación de la señal en términos unidimensaionales en un cierto vecindario y a una cierta escala.*
- *Amplitud local: La amplitud local de una señal $s(t)$ is la magnitud de la señal analítica (Ec. 2.2): $A = |s_A(t)|$, que representa la energía de la estructura de la señal en un cierto vecindario y a una cierta escala.*

Estos dos conceptos son realmente importantes para una representación apropiada de la estructura local puesto que permiten interpretar el comportamiento de la señal en dos componentes independientes. Por una parte la amplitud local varía al mismo tiempo que cambia la estructura local, pero es invariante con respecto al tipo de estructura. Por otra parte, la fase local da una descripción del tipo de estructura, siendo independiente de las variaciones locales de la señal.

La generalización de estos conceptos para señales multidimensionales no es trivial. En este sentido, se suele realizar el análisis definiendo previamente una dirección dominante, tal como se muestra en la ecuación 2.3. Esto nos conduce a la definición de filtros direccionables, desarrollados en la sección 2.2.3. La teoría de los filtros direccionables se basa en explotar la propiedad de linealidad, utilizando unos filtros orientados en unas direcciones que forman una base en dicho espacio. Después, para calcular la respuesta del filtro en una determinada dirección arbitraria tan solo es necesario realizar una combinación lineal de las respuestas del filtro orientadas según las direcciones base, tal como se muestra en las ecuaciones de la sección 2.2.3 y en la figura 2.1.

Filtros en Cuadratura

Intimamente ligados a la definición de transformada de Hilbert, se encuentran los filtros en cuadratura, que son los que se usan en la práctica para calcular la señal analítica, cuya definición está en la Ec. 2.2, puesto que la transformada de Hilbert no es causal o no tiene soporte finito en muchas ocasiones.

Los filtros en cuadratura, por tanto, se usan para aproximar la función analítica, convolucionando una señal con un filtro $q(t)$ cuyo efecto es eliminar todas las frecuencias negativas.

Estimación Óptima

La estimación en sentido óptimo tiene un soporte teórico muy bien establecido en el campo de procesado de señal. Bajo este marco, asumimos que es posible estimar el valor correcto de una señal basándonos en el estudio del comportamiento estadístico de la señal, lo que nos conduce a hablar de estimación óptima bajo algún criterio estadístico, normalmente minimizar el error cuadrático medio.

Una implementación Finite Impulse Response (FIR) de este tipo de filtros implica que la estimación del valor de una señal en el punto objetivo $\mathbf{x}$ *se realiza usando un número finito de observaciones tomadas en un cierto vecindario de dicho punto. Distintas configuraciones de dicho vecindario conducen a distintos esquemas de estimación, aunque lo usual es tomar una rejilla regular con el punto objetivo en el centro de la misma.*

El valor estimado se obtiene mediante una combinación lineal de las observaciones dentro de ese vecindario ponderadas con unos pesos que optimizan el criterio de calidad. Cuando los pesos se obtienen de forma global para toda la señal esto nos conduce a la utilización de la convolución, donde el kernel se define con los correspondientes pesos.

En este sentido, el filtro de Wiener es la solución óptima para la minimización del error cuadrático medio, usando información estadística. En la sección 2.3.1 se detallan las características de este filtro y la forma de calcular los pesos a partir del análisis estadístico de primer y segundo orden de la señal, lo que nos conduce a la expresión final mostrada en la Ec. 2.16. Un problema fundamental a la hora de llevar a la práctica este filtro es la caracterización estadística de la señal, puesto que normalmente solo se tiene acceso a observaciones de la señal que vienen distorsionadas por el ruido.

Por tanto, en muchas ocasiones se utilizan modelos para la función de autocovarianza, como el de la Ec. 2.18 que dependen de una serie de parámetros que se obtienen a partir de las observaciones disponibles de la señal. En esta tesis, se estudian también métodos para mejorar estos modelos a partir de la información existente.

Señales Tensoriales

En una primera aproximación, se puede afirmar que un tensor es una entidad que se puede expresar como un array multidimensional con respecto a una base, aunque como entidad matemática en sí misma, un tensor es independiente del sistema de referencia utilizado. El rango de un tensor es el número de índices del array requerido para describir tal cantidad.

En sentido más estricto, un tensor de rango n en un espacio m-dimensional es un objeto matemático que tiene n índices y m^n componentes y que obedece a ciertas reglas de transformación. Visto de este modo, los tensores son generalizaciones de los escalares - que son tensores de rango 0 - de los vectores - que son tensores de orden 1 - de las matrices - tensores de orden 2 -, así hasta un número arbitrario de índices. Por tanto, los tensores proporcionan un marco matemático natural y compacto para la formulación y resolución de problemas en áreas tan independientes como la elasticidad, mecánica de fluidos y relatividad general.

La notación de tensores de orden genérico se hace expresando la magnitud con subíndices (índices covariantes) y superíndices (índices contravariantes). Esta distinción es significativa para tensores de orden genérico, sin embargo, en el caso particular de tensores definidos en un espacio Euclídeo tridimensional, ambas posibilidades son equivalentes. Como entidades matemáticas que son, los tensores pueden operar con otros tensores, como tensores de métrica o tensores de permutación. También hay operadores que actúan sobre tensores como las derivadas covariantes o contravariantes. La manipulación de tensores para formular ecuaciones implica subir y bajar índices, lo que permite establecer una notación especial para las operaciones más comunes, como la multiplicación.

En la sección 2.4 se describen las operaciones más comunes con tensores y se muestran las definiciones de conceptos tensoriales tales como tensor de métrica, tensor covariante y contravariante, base de tensores, tensor simétrico y semidefinido positivo, norma de tensores, etc.

- ***Regularización de Datos Tensoriales:*** *Normalmente, como en todo proceso de adquisición de datos, suele ser necesario regularizar el campo de datos tensoriales obtenido con el objetivo de reducir el ruido introducido en la estimación. En este sentido, se han realizado muchas aportaciones en la literatura lo que demuestra el interés de este problema. Los métodos y algoritmos propuestos hasta el momento se pueden clasificar en dos grandes categorías, tal como se ha hecho en la sección 2.4.6.*

  Por una parte están los métodos en los que se trata el tensor como una entidad matemática en sí misma dentro del algoritmo de procesado. Dentro de este grupo hay muchas aportaciones basadas en modelos matemáticos tan dispares como Partial Differential Equations (PDE), modelos estadísticos o aproximaciones algebraicas.

Por otra parte, algunos autores defienden que es más acertado realizar una descomposición espectral del tensor y regularizar por separado las direcciones de difusión y las magnitudes de difusión, es decir, los campos de autovectores y autovalores, respectivamente.

En general, esta última descomposición tiene sentido porque la velocidad de regularización de los autovalores es mayor que la de los autovectores, por lo que suele darse lo que se denomina efecto de inflado. *Sin embargo, utilizando herramientas matemáticas definidas en los espacios geométricos más adecuados para el procesado de datos tensoriales es sencillo solucionar este problema. Esto se estudiará a lo largo de los capítulos 4 y 5.*

- ***Visualización:*** *La visualización de datos tensoriales es un problema que también ha despertado mucho interés, puesto que requiere mostrar mucha información con complejas interrelaciones entre los valores de un mismo tensor y de éste con sus vecinos más próximos. Durante la última década se han presentado muchas alternativas para visualizar este tipo de datos, tal como se muestra en la sección 2.4.7. La mayoría están basadas en la reducción de la dimensiones de los datos mediante la extracción de la información más relevante del tensor. Así, se pueden distinguir algunas aportaciones que reducen la información de anisotropía a un valor escalar, mostrando toda la información en una imagen de escala de grises. También existen alternativas que proponen la utilización de imágenes en color con una codificación RGB en la que cada canal está parametrizado por la forma dominante del tensor: forma lineal, plana o esférica. Finalmente, se han propuesto otras técnicas que permiten visualizar la totalidad de la información geométrica del tensor utilizando formas geométricas como elipsoides o* superquadrics.

  En esta tesis, se utilizarán elipsoides para la representación de campos tensoriales. Cada elipsoide estará representada de un color que dependerá de la forma geométrica predominante del tensor, utilizando la codificación RGB que normalmente se utiliza como forma de representación vectorial. De este modo, los tensores predominante lineales llevarán estarán asociados al color rojo, los planos al color verde y los esféricos al azul.

Imágenes Médicas

El diagnóstico por imagen se ha convertido en los últimos años una de las herramientas que más ha ayudado a los médicos en sus tareas de diagnóstico y seguimiento de las enfermedades que sufren sus pacientes, sin olvidar sus aplicaciones en el campo de la

investigación médica, ayudando a comprender el funcionamiento y leyes internas de organismos vivos.

Una de las principales razones por las que estas tecnologías se han convertido en una herramienta fundamental radica en el hecho de que proporciona información objetiva de lo que se está evaluando, reduciendo en gran medida la probabilidad de una interpretación errónea de los síntomas que conduzcan a un diagnóstico equivocado, reduciendo también los recursos necesarios para la evaluación y el tiempo dedicado a esta tarea. Además, las imágenes digitales pueden ser inteligentemente archivadas en sistemas de almacenamiento digitales, lo que ayuda a salvar mucho espacio y recursos humanos dedicados a esta tarea.

La evolución de las distintas modalidades de imágenes médicas está ligada a la evolución de los sistemas informáticos, beneficiándose de los nuevos avances tanto en capacidad de computación como en sistemas de almacenamiento que facilitan y mejoran la calidad de las imágenes obtenidas y la forma de presentación a la persona que debe interpretar los resultados.

En este sentido, se están realizando numerosos esfuerzos a nivel de investigación que continuamente conducen al desarrollo de nuevas modalidades de imágenes médicas para la visualización de procesos con requisitos específicos. En este sentido, la sección 2.5 presenta una lista de las modalidades de imágenes médicas más importantes desarrolladas en los últimos años.

Resonancia Magnética de Difusión Tensorial (DT-MRI)

La Resonancia Magnética de Difusión Tensorial, DT-MRI, es una modalidad de imagen médica que mide la difusión media de las moléculas de agua en los tejidos aplicando un gradiente de campo eléctrico en distintas direcciones. El protocolo de adquisición de datos se muestra en la Fig. 2.10, en la que se usan dos pulsos fuertes posicionados de forma simétrica sobre un pulso de 180^0 *que permite ponderar la difusión de las moléculas de agua. En esta secuencia, el primer pulso invierte la fase de giro y durante el periodo* Δ *entre los dos pulsos se producirá un cambio de posición de las moléculas debido al movimiento Browniano, lo que se traduce en una pérdida de señal al aplicar el segundo pulso que es proporcional a la difusión.*

Para eliminar la dependencia con la densidad de moléculas, han de tomarse varias imágenes de resonancia magnética con y sin ponderación de la difusión. Una vez eliminada esta dependencia la difusión en esa dirección puede calcularse con la fórmula expresada en la Ec. 2.53, donde el significado de los parámetros de esta ecuación y sus valores por defecto se detallan en la sección 2.6.

Sin embargo, la difusión de las moléculas de agua no es isótropa en todas las direcciones debido principalmente a la presencia de tejidos que obstaculizan el movimiento en unas determinadas direcciones. Por este motivo, una medida escalar de la difusión no es suficiente para caracterizar la difusión. Por este motivo se propuso inicialmente la utilización de un tensor de orden dos para caracterizar esta magnitud, utilizando una formulación tensorial del proceso de difusión anisótropa, expresado en la Ec. 2.55.

Por tanto, la estimación de un campo de tensores 3×3*, que en nuestro contexto es equivalente a un campo de matrices simétricas y semidefinidas positivas, requiere tomar al menos seis medidas tomadas con gradientes electromagnéticos en diferentes direcciones. Además, también es necesaria una medida de referencia sin ponderado de difusión que se toma como aproximación a la situación de equilibrio o estado inicial. La razón por la que al menos se necesitan seis direcciones diferentes está relacionado con los grados de libertad del tensor de difusión, puesto que tan solo hay seis componentes que son desconocidas al ser el tensor simétrico.*

A la hora de resolver el sistema de ecuaciones mostrado en la Ec. 2.55, se han propuesto distintos modelos que se detallan en la sección 2.6. Básicamente, la diferencia entre ellos radica en las restricciones que se imponen a la hora de construir los tensores de difusión y en el método matemático empleado para resolver el sistema de ecuaciones. En este sentido, nos encontramos algunas aproximaciones que garantizan que los tensores son simétricos semidefinidos positivos mientras que otros métodos propuestos en la literatura no garantizan esta condición, ya que el ruido inherente a la medida puede provocar que esta condición se pierda, provocando que los resultados sean incorrectos.

Los datos proporcionados por esta modalidad de imagen médica han demostrado ser de gran utilidad en gran cantidad de problemas médicos, especialmente en el campo de la neurociencia. Quizás, una de las aplicaciones de mayor interés es la tractografía, cuya finalidad es la construcción de modelos virtuales de las fibras nerviosas que recorren el cerebro de un hemisferio al otro formando auténticas redes de comunicaciones. Asumiendo que la mayoría de los tensores obtenidos en el proceso de adquisición de datos son bastante anisótropos, algo que no es muy alejado de la realidad, es posible reconstruir el camino seguido por las fibras siguiendo la dirección marcada por el autovector principal de la matriz de difusión. Esta técnica suele fallar en aquellas regiones donde dos o más fibras se cruzan, ya que el perfil medio de la difusión en estas regiones es muy similar al caso isótropo donde no exista una dirección de preferencia. Para solucionar esta limitación, se ha propuesto la utilización de tensores de orden superior con los que es posible cuantificar correctamente estos casos.

Estos mapas virtuales tienen una utilidad práctica muy importante ya que permiten la planificación de una operación quirúrgica en órganos tan delicados como el cerebro de una

persona, tratando de minimizar el daño que se pueda ocasionar en la intervención y, sobre todo, evitar lesiones en zonas importantes. Además, actualmente se está investigando la relación que existe entre el tensor de difusión y el tensor de conductividad eléctrica pues parece existir una gran similitud entre ambos. Por tanto, el modelo físico proporcionado por DT-MRI proporciona la base en la que resolver las ecuaciones de conducción eléctrica.

Además, DT-MRI es de gran interés para detectar algunas enfermedades como isquemia cerebral, infarto cerebral, Alzheimer o esquizofrenia.

Un Nuevo Esquema para el Filtrado Anisótropo de Señales

Los sistemas de procesado convencionales que utilizan la hipótesis de que la variación de señal es semejante en todas las direcciones espaciales, es decir, bajo la hipótesis de isotropía presentan la desventaja de que en presencia de cambios abruptos de señal su respuesta introduce un error que se traduce, por ejemplo, en el suavizado de dichos cambios. Para solucionar estos problemas se suelen proponer sistemas anisótropos que incluyen información sobre la variación espacial de las señales.

Normalmente, el gradiente es el operador utilizado para obtener una estimación de la dirección de máxima variación de la señal es. Sin embargo, es sabido que este operador presenta algunas limitaciones, por ejemplo, en presencia de una línea fina se obtiene una cierta ambigüedad, puesto que si se mira el gradiente no se sabe si corresponde a dos bordes seguidos o una sola estructura. Además, cuando la señal varía por igual en más de una dirección, por ejemplo en las esquinas de un cuadrado, la información también es ambigua, puesto que no es posible distinguir esta situación de la presencia de un simple borde.

Por tanto, parece razonable utilizar un descriptor que no introduzca este tipo de ambigüedades. Siguiendo esta idea, Knutsson detalló los requisitos imprescindibles que debería tener un descriptor de la estructure local y que se estudian en la sección 3.2, proponiendo el uso de tensores para llevar a cabo esta tarea, que finalmente terminó denominándose Tensores de Estructura Local. *Los tensores, además de permitir una representación compacta de este tipo de información tienen un cuerpo matemático muy sólido que permite realizar un análisis de cualquier problema en el dominio tensorial. La representación tensorial de la estructura local está basada en la utilización de una matriz simétrica y semidefinida positiva para expresar la variación de orientación a una escala determinada.*

En el capítulo 3 se investigan nuevas técnicas para explotar la información proporcionada por el tensor de estructura local con el objetivo de construir sistemas de

procesado anisótropo de señales de propósito general. En este sentido, en la sección 3.4 presentamos un marco general para realizar sistemas anisótropos de procesado basados en la información proporcionada por el tensor de estructura local.

En una primera aproximación, en la sección 3.4.1 se plantea un método para definir los datos con los que se pretende hacer la estimación. La idea básica consiste en el cálculo de un vecindario local alrededor de la muestra que se está procesando teniendo en cuenta la información proporcionada por el tensor de estructura. En este sentido, en zonas homogéneas las muestras que utilizaremos para la estimación estarán distribuidas por igual en todas las direcciones, mientras que en zonas con alta anisotropía, sólo utilizaremos aquellas muestras que se encuentran a lo largo del borde, evitando así mezclar información de distinto tipo. La idea propuesta, al ser bastante genérica, puede ser particularizada para cualquier tipo de sistema de procesamiento de datos.

En segundo lugar, la sección 3.4.2 propone un esquema de filtrado anisótropo Gaussiano donde la forma de la Gaussiana, y por tanto los coeficientes del kernel, dependen del tensor de estructura, que es interpretado como una matriz de covarianza. Este marco también es aplicable al problema de interpolación anisótropa, que normalmente se realiza pesando muestras en un vecindario siguiendo alguna regla (lineal, cúbica, etc.), tal como se describe en la sección 3.4.3. El comportamiento anisótropo se introduce pesando más las muestras encontradas a lo largo del borde que las encontradas a lo largo de la dirección de máxima variación de la señal. En nuestro esquema, acentuamos este comportamiento usando vecindarios adaptativos y el tensor de estructura como métrica para medir distancias entre muestras.

Finalmente, también proponemos en la sección 3.4.4 el uso de la información proporcionada por el tensor de estructura local para construir modelos anisótropos de la autocovarianza de la señal, lo que nos conduce a poder definir versiones anisótropas de estimadores óptimos en sentido estadístico, como el famoso filtro de Wiener.

Por último, se este esquema es generalizado para su utilización no sólo con datos escalares, sino también con señales tensoriales. La generalización básicamente radica en la definición de un tensor de estructura local que codifica la variación de señales tensoriales del mismo modo que se hace para el caso escalar. Nuestro método, además, asegura que su respuesta siempre es un campo de tensores semidefinidos positivos, puesto que la combinación lineal mediante la que se produce la estimación siempre se realiza con pesos positivos. En la sección 3.6 se muestran algunos resultados obtenidos tanto con señales escalares como tensoriales en datos sintéticos y reales.

Representación de la Estructura Local

La representación tensorial para describir la orientación local de las señales se basa en la utilización de una matriz simétrica y semidefinida positiva que codifica la variación de la señal en un cierto vecindario. Para una señal multidimensional, un tensor de orden 2 es suficiente para codificar la complejidad si, y sólo si, existe una sola orientación dominante. En el caso de existir más de una orientación, sería necesario usar tensores de órdenes superiores para representar debidamente la señal. Sin embargo, con ejemplos reales, un tensor de orden dos es suficiente puesto que proporciona la información necesaria para clasificar las características de las imágenes.

Los requisitos de una representación tensorial los satisface el mapeado propuesto en la Ec. 3.4, que a partir de un vector proporciona un tensor simétrico y semidefinido positivo cuya orientación dominante es precisamente la del vector original. La condición de simetría garantiza la invarianza ante rotaciones además de que sus autovalores sean reales. Entre otras características, este mapeado requiere un tratamiento especial puesto que intrínsecamente es no lineal y las operaciones de filtrado deben ser aplicadas con cuidado.

La principal ventaja de esta representación es que los tensores proporcionan información no sólo de la dirección dominante, sino que también proporcionan información sobre la variación de la señal en las direcciones ortogonales a la principal. Por tanto, con un análisis de los autovalores de la matriz $\lambda_1 \geq \ldots \geq \lambda_m$ *y sus autovectores* $\mathbf{e_1}, \ldots, \mathbf{e_m}$*, tal como se muestra en la fig. 3.3, se pueden distinguir distintos casos en 3D* $m = 3$ *(una clasificación análoga se puede hacer en 2D):*

1. *Caso plano* ($\lambda_1 \gg \lambda_2 \simeq \lambda_3 \simeq 0$)*: Sólo hay una dirección principal en la que varía la señal. El vecindario, por tanto, es aproximadamente una estructura plana cuyo vector normal viene dado por* $\mathbf{e_1}$*.*

2. *Caso lineal* ($\lambda_1 \simeq \lambda_2 \gg \lambda_3 \simeq 0$)*: En este caso, hay dos direcciones principales de variación lo que nos lleva a un vecindario con estructura lineal orientado según* $\mathbf{e_3}$*, como por ejemplo los lados de un cubo.*

3. *Caso puntual* ($\lambda_1 \simeq \lambda_2 \simeq \lambda_3 \gg 0$)*: No hay orientación preferente de variación de la señal, lo que equivale a una esquina o una unión de varias estructuras lineales.*

4. *Caso homogéneo* ($\lambda_1 \simeq \lambda_2 \simeq \lambda_3 \simeq 0$)*: En este caso, no hay variación de la señal, lo que corresponde al caso de un valor constante de señal.*

Además de lo expuesto anteriormente, la representación tensorial elimina algunos problemas fundamentales de otras medidas de la estructura local, como puede ser el

gradiente. Un problema básico es el presentado en la fig. 3.1, donde se puede ver que la magnitud del gradiente no responde igual ante la presencia de líneas finas o bordes. Además, en la fig. 3.2 se muestra que la respuesta del gradiente no es invariante ante el cambio de fase. En dicha imagen se puede ver que aunque la orientación principal de la señal es constante, la respuesta del gradiente no lo es.

Procesado Anisótropo de Señales

La herramienta fundamental en la que se basan nuestros esquemas de procesado anisótropo es el tensor de estructura. En la sección 3.3 se repasan las distintas técnicas que han sido propuestas en la literatura para estimarlo a partir de los datos, incluyendo el denominado tensor de estructura no lineal, que introduce un postprocesado diferente al habitual, puesto que propone el uso de algoritmos no lineales de regularización para incorporar al tensor información de escala evitando los comunes efectos de delocalización de estructura. Estos métodos se pueden clasificar en dos grandes grupos atendiendo a la filosofía en la que se basan para realizar la estimación.

- *Métodos basados en el gradiente: Estos métodos usan el gradiente espacial para determinar la orientación de la señal y a partir de esa información calcular el tensor.*
- *Métodos basados en el cálculo de la energía local: Estos métodos usan el concepto de energía local para determinar los elementos de estructura de la señal, mediante la utilización de filtros en cuadratura.*

Un problema común, independientemente del método de estimación que se haya utilizado, es el denominado efecto de delocalización de la estructura, producido principalmente por el método de postprocesado empleado para regularizar el campo de tensores. Tiene sentido, por tanto, comparar la robustez de las estimaciones obtenidas con cada uno de los métodos, pues este problema es una importante fuente de error, especialmente para el diseño de filtros anisótropos. Este estudio se realiza en la sección 3.3.4 midiendo el error introducido al estimar la localización de elementos de estructura importantes como son las esquinas. En la fig. 3.5 se muestran los resultados de la precisión con que son capaces de calcular la posición de las esquinas y en la fig. 3.6 se muestra la robustez de estos métodos frente al ruido.

El marco genérico para el procesado anisótropo de señales desarrollado en el contexto de esta tesis queda completamente descrito en la sección 3.4. La idea básica en este marco es la utilización de la información proporcionada por el tensor de estructura para introducir un comportamiento anisótropo en filtros, empleando conceptos de geometría diferencial como las métricas para definir una geometría que depende de la estructura de la señal.

La aplicación más directa es la utilización de la información del tensor de estructura para determinar la forma del vecindario que usaremos para realizar la estimación de la señal. En particular, para estimar el valor de la señal alrededor de la posición $\mathbf{x}$ *usaremos las muestras dentro del vecindario* $\mathcal{N}(\mathbf{x})$*, definido por la elipse* $\mathbf{xT(x)x}^T = 1$*, representada en la fig. 3.7, cuya forma depende del tensor de estructura local distinguiéndose los casos explicados anteriormente, y que se muestran de forma esquemática en la fig. 3.8.*

Una vez que se ha calculado el vecindario centrado en el punto de procesado, se puede realizar la estimación mediante una combinación lineal, tal como se muestra en la Ec. 3.30 donde los pesos vienen determinados por cualquier técnica de estimación. En este sentido, se pueden definir versiones anisótropas de cualquier filtro comúnmente utilizado, como por ejemplo el filtro de Wiener, Linear Minimum Mean Square Error (LMMSE) estimation, Kriging, etc.

También es importante señalar que el cálculo del vecindario también es independiente de la técnica de estimación del tensor de estructura que se haya utilizado. Sin embargo, a la vista de los resultados presentados en la sección 3.3.4 en los que se evalúa la precisión con la que es posible detectar ciertos elementos de estructura como las esquinas, parece razonable pensar que los métodos que utilizan filtros en cuadratura junto con una regularización no lineal son más precisos, por lo que es la técnica con la que trabajaremos a lo largo de esta tesis.

Sin embargo, aún es posible explotar la información del tensor de estructura en otras aplicaciones, que también se presentan en la sección 3.4:

- ***Filtrado Anisótropo Gaussiano:*** *Una aplicación interesante es el diseño de máscaras en el dominio espacial con un comportamiento anisótropo. Esta idea se ilustra en la sección 3.4.2 mediante el diseño de un filtro anisótropo Gaussiano, donde la forma de la Gaussiana viene determinada por el tensor de estructura en ese punto. De este modo, además, se pone de manifiesto la estrecha relación entre tensor de estructura y matriz de covarianza, puesto que el primero es utilizado como tal en el kernel Gaussiano. La ventaja principal que proporciona esta implementación es que el efecto de delocalización se reduce sensiblemente puesto que el suavizado se favorece a lo largo de las orientaciones privilegiadas.*

- ***Interpolación Anisótropa:*** *El marco expuesto en la sección 3.4.1 también es válido para el problema de la interpolación. En el esquema propuesto en la sección 3.4.3, una vez calculado el vecindario alrededor del punto de interpolación, para enfatizar el comportamiento anisótropo cada muestra se pondera de forma inversamente proporcional a la distancia utilizando el tensor de estructura local como métrica para calcular esa distancia, de forma que muestras separadas por un*

borde resultan estar mucho más lo lejos de lo que estarían en un espacio Euclídeo. Esta idea se muestra de forma gráfica en la fig. 3.9

- ***Estimación Anisótropa de la Función de Autocovarianza:*** *Finalmente, también proponemos el uso del tensor de estructura local para estimar de forma anisótropa la función de autocovarianza de la señal a través de modelos de señal. Esta generalización nos conduce a la formulación de estimadores óptimos en sentido estadístico con un comportamiento anisótropo, donde la caracterización estadística de segundo order juega un papel crucial. En este contexto, en la sección 3.4.4 se describe con detalle la forma de estimar esta función de autocovarianza de forma anisótropa para construir una versión anisótropa del filtro de Wiener 2.3.1.*

Por último, en la sección 3.5, se ha propuesto una formulación tensorial de los algoritmos anteriormente expuestos. La generalización radica en la definición del tensor de estructura para datos tensoriales de orden dos propuesta en la Ec. 3.39. De este modo, todos los conceptos y formulaciones utilizados para el caso escalar pueden ser directamente trasladados para el caso tensorial con la ventaja de que el nuestros esquemas de filtrado e interpolación siempre proporcionarán tensores semidefinidos positivos, puesto que los datos de entrada siempre son ponderados con pesos positivos.

En la sección 3.6 se muestran los resultados obtenidos con los métodos desarrollados anteriormente en comparación con otras técnicas de procesado comúnmente utilizadas. A la vista de los resultados mostrados en las figuras comprendidas entre la 3.10 y la 3.20 se puede ver el buen comportamiento de nuestros algoritmos.

Filtrado Homomórfico de Datos Tensoriales

En el capítulo 4, nuestra atención se centra únicamente en el problema de filtrado de datos tensoriales, cuyo objetivo es mejorar la calidad de las imágenes reduciendo el ruido aleatorio inherente al proceso de adquisición de datos. En el caso concreto de DT-MRI, la relación señal a ruido suele ser baja debido a que la adquisición de datos está condicionada por factores humanos, tales como su capacidad de permanecer inmóviles mientras se realiza el escaneo.

La principal restricción que deben respetar los algoritmos de filtrado diseñados para tratar este tipo de imágenes, es que su respuesta debe proporcionar un campo de tensores simétricos y semidefinidos positivos. Además, las operaciones aritméticas sobre tensores deben realizarse cuidadosamente puesto que producen algunos efectos no deseados, tales como el efecto de inflado o la obtención de tensores isótropos como resultado de tensores anisótropos orientados con diferentes ejes.

Para tratar estos problemas, en el capítulo 4 se propone un marco teórico para diseñar filtros tensoriales. La principal contribución del marco propuesto se basa en el hecho de que la respuesta del filtro siempre va a ser semidefinida positiva independientemente del filtro utilizado para llevar a cabo la regularización. Nuestro método se basa en una interpretación algebraica del conjunto de tensores simétricos y semidefinidos positivos que, mediante una aplicación, son transportados al espacio vectorial formado por tensores simétricos donde se realiza la regularización apoyándonos en las herramientas definidas en un espacio vectorial. Finalmente, mediante la transformación inversa, los datos son transportados al dominio original.

El esquema propuesto está inspirado en la descomposición homomórfica comúnmente utilizada para señales escalares, explicado en la sección 4.3, tras revisar algunos conceptos matemáticos fundamentales relacionados con los espacios vectoriales y las aplicaciones lineales en la sección 4.2. A continuación, en la sección 4.4, se presenta el marco homomórfico para tratar con datos tensoriales, basándonos en la interpretación algebraica descrita en la sección 4.4.1. Por último, en la sección 4.5 se muestran los resultados en comparación con otros esquemas comúnmente utilizados.

Filtrado Homomórfico

La base del procesado homomórfico radica en la generalización del principio de superposición descrito en la sección 4.2.3 y en las ecuaciones 4.9 y 4.10. Por tanto, el formalismo para la representación de sistemas con estas propiedades se basa en la interpretación de las señales de entrada y salida como elementos de espacios vectoriales con unas determinadas reglas de operación entre los elementos del espacio vectorial y de éstos con escalares. Bajo esta perspectiva, el sistema homomórfico se interpreta como un operador algebraico que relaciona elementos del espacio de señales a la entrada del sistema con los elementos del espacio de señales a la salida.

La teoría del procesado homomórfico demuestra que cualquier sistema de este tipo se puede representar como una cascada de tres subsistemas, tal como se muestra en la Fig. 4.2 y cada uno con las propiedades que a continuación se describen:

- ***Subsistema de entrada:*** *El primer subsistema transforma elementos del espacio de señales a la entrada en elementos de un espacio vectorial lineal en el sentido convencional.*

- ***Subsistema de filtrado:*** *El segundo subsistema es un sistema lineal en el sentido convencional que realiza las operaciones de filtrado o suavizado.*

- ***Subsistema de salida:*** *El tercer subsistema realiza la transformación desde el espacio vectorial lineal al espacio vectorial definido a la salida del sistema homomórfico. En el caso particular de que el espacio vectorial a la entrada y a la salida sean el mismo, como suele ser habitual, este tercer subsistema resulta ser el inverso del primero.*

En la figura 4.3 se muestra una representación de la descomposición homomórfica explicada anteriormente, donde se puede ver el camino y las transformaciones realizadas desde el espacio de entrada hasta el espacio de salida.

En el caso escalar, esta descomposición tiene muchas aplicaciones tales como la descomposición de señales convolucionadas, utilizando logaritmos y transformadas de Fourier como subsistemas de entrada y salida. De este modo, como subsistema central se puede utilizar un filtro lineal diseñado bajo la hipótesis de que las señales a su entrada son aditivas.

Pero un caso de especial interés análogo a nuestro problema tensorial es la descomposición de señales multiplicativas utilizando como subsistemas de entrada y salida el logaritmo y la función exponencial, respectivamente. El conjunto de números positivos reales forma un Grupo de Lie bajo la multiplicación habitual y su álgebra de Lie es el grupo aditivo de todos los números reales. El álgebra de Lie se puede interpretar como el espacio tangente al grupo de Lie sobre la identidad y existe una aplicación lineal desde el espacio tangente al álgebra de Lie llamado exponential map.

Esta formulación algebraica permite una interpretación de la descomposición homomórfica en el que a través del exponential map *es posible realizar las transformaciones entre subespacios anteriormente descritas.*

Filtrado Homomórfico de Datos Tensoriales

En el caso de señales tensoriales, el exponential map *también se puede utilizar, aunque su interpretación algebraica tiene una pequeña variación. En el caso tensorial, tal como se demuestra en la sección 4.4.1, esta transformación define un* homeomorfismo *entre el espacio vectorial de matrices simétricas y el conjunto de tensores de segundo orden simétricos y definidos positivos. En otras palabras, esta transformación respeta la estructura topológica de ambos grupos, transformando los elementos cercanos del primer conjunto en elementos cercanos del segundo conjunto y los que están lejos, siguen lejos en el espacio final.*

Por tanto, ambos conjuntos son idénticos desde el punto de vista topológico, lo que permite hacer el procesado tanto en un dominio como en el otro. En este sentido, parece

lógico realizar el procesado en el espacio vectorial definido por el conjunto de matrices simétricas, puesto que contamos con las herramientas matemáticas propias de este espacio: escalado por escalares, propiedad distributiva y conmutativa, producto escalar, etc. Por tanto, es necesario transformar el espacio original de la señal, es decir, el conjunto de tensores simétricos y definidos positivos en el espacio vectorial de matrices simétricas mediante el logarithm map *y, tras procesar la señal en dicho espacio vectorial, transformar la señal al espacio original mediante el* exponential map.

Una diferencia importante con respecto al filtrado homomórfico de datos escalares es que las transformaciones no son homomorfismos, por lo que la descomposición de una señal multiplicativa en la suma de sus logaritmos ya no es posible en el caso tensorial. Tan sólo en el caso particular de que los tensores involucrados conmutaran, sería posible hacer esta descomposición y, por tanto, una generalización directa del caso escalar.

No obstante, hay un doble interés en esta descomposición homeomórfica. Por una parte, es de interés cualquier otra transformación que defina un homomorfismo entre el conjunto de tensores de segundo orden simétricos y semidefinidos positivos y otra estructura algebraica. Por otra parte, el procesado de señales se puede separar de imponer la restricción para conservar los tensores definidos positivos.

En la sección 4.5 se muestran los resultados obtenidos utilizando nuestro marco de procesado en comparación con otras técnicas de procesado usadas en la literatura. A la vista de los resultados mostrados en las figuras comprendidas entre la 4.5 y la 4.17 se puede ver el buen comportamiento de nuestro esquema homomórfico.

Un Marco Riemanniano para el Procesado de Señales Tensoriales

En el capítulo 5 abordamos el mismo problema planteado en el capítulo 4, pero desde un marco matemático distinto presentado en la literatura y que nos permite calcular estadísticas en campos tensoriales. En este caso, abordamos el problema desde la perspectiva de la geometría diferencial del espacio de las distribuciones normales multivariadas. En este marco de procesado, consideramos la familia de distribuciones normales tridimensionales con media nula parametrizándolo como un espacio de seis dimensiones de varianzas y covarianzas, identificándolo además con el conjunto de matrices reales y definidas positivas.

En este espacio geométrico es posible definir una métrica Riemanniana en términos de la matriz de información de Fisher, como se presenta en el Teorema 5.4, lo que además nos permite definir conceptos tales como distancia geodésica, curvatura, media y matriz de

covarianza en dichos espacios. En la sección 5.3 se describen los detalles matemáticos que conducen al desarrollo de las herramientas estadísticas que utilizaremos para desarrollar nuestro esquema de procesado.

La contribución más importante de este capítulo es el desarrollo de un esquema de procesado anisótropo controlado por la magnitud del gradiente del campo tensorial, que es calculado utilizando las herramientas matemáticas desarrolladas dentro de este marco computacional. La idea general, como viene siendo habitual en el contexto de esta tesis, es pesar más aquellas muestras que se encuentran a lo largo del borde que aquellas que están en la dirección perpendicular a éste. Lo realmente original de este algoritmo es la forma de calcular los pesos, basada en cálculo del módulo del gradiente Riemanniano y en la forma de calcular la media local teniendo en cuenta la métrica definida en este espacio.

Finalmente, la sección 5.6 presenta los resultados obtenidos con este nuevo algoritmo anisótropo en comparación con otros esquemas anisótropos desarrollados en la literatura.

Media Local y Cálculo del Gradiente

Para estimar la media local en el marco definido en el capítulo 5, se hace uso de la definición clásica de centro de masas y del concepto de distancia geodésica entre dos matrices, definido en el Teorema 5.3.2. Bajo este contexto, es posible calcular la matriz media como el mínimo local de la Ec. 5.8. Como no existe una expresión cerrada para ese mínimo local, es necesario hacer evolucionar un esquema numérico iterativo (Ec. 5.13) hacia el centro de masas, empezando con una estimación inicial cualquiera.

Aunque este esquema iterativo suele converger en no más de 4 ó 5 iteraciones independientemente de la estimación inicial, es posible detectar la convergencia cuando la norma de Frobenius de la velocidad de evolución está por debajo de un determinado umbral. Como consecuencia, el esquema numérico está libre de parámetros.

Filtrado Anisótropo Riemanniano

Sin embargo, en el esquema propuesto anteriormente todas las muestras contribuyen igualmente a la media local, por lo que no resulta idóneo para diseñar un algoritmo de procesado anisótropo de datos. Este problema es abordado en la sección 5.4.2, donde se evoluciona un esquema numérico similar que sí incluye un ponderado de las muestras que se procesan, cuya formulación final, obtenida siguiendo los mismos pasos que para la versión isótropa se encuentra definido en la Ec. 5.15.

En lo que se refiere al cálculo de los pesos, se ha propuesto el cálculo del módulo del gradiente dentro de este marco Riemanniano mediante la suma ponderada de los cuadrados

de las distancias geodésicas entre los tensores dentro de un vecindario alrededor del punto central, tal como muestra la ecuación 5.16. Esta formulación del módulo del gradiente Riemanniano se basa en una interpretación equivalente del gradiente en espacios Euclídeos para aproximar el gradiente espacial, tal como se demuestra en la sección 5.4.3.

Cuando comparamos las propiedades del gradiente bajo el marco Riemanniano con las del caso Euclídeo, cabe destacar que el primero proporciona una magnitud que resulta independiente de la escala. Es decir, el módulo del gradiente en la frontera entre dos regiones con tensores diferentes a ambos lados es independiente del valor de los autovalores, tan solo depende de la relación entre ellos. En la Figura 5.2 se realiza una comparación de los módulos del gradiente Riemanniano y del Euclídeo, donde queda reflejado este comportamiento con respecto a la escala. Mientras que uno resulta independiente de la magnitud de los autovalores, el Euclídeo viene determinado por la raíz cuadrada de la suma de los autovalores al cuadrado, por lo que cuanto mayores son los autovalores mayor es el módulo del gradiente.

En nuestro estudio, también hemos estudiado el caso en el que la frontera en el campo tensorial está generada por tensores rotados un cierto ángulo. En la Figura 5.3 se pueden ver distintas respuestas del módulo del gradiente en función del ángulo de rotación. Como cabía esperar, cuanto más anisótropos son los tensores, mayor es el módulo del gradiente, aunque en el caso Riemanniano su dependencia con el valor de los autovalores es menos importante que en el caso Euclídeo.

Finalmente, la sección 5.5 describe algunos detalles de la implementación del algoritmo de filtrado basado en los principios expuestos anteriormente. En la sección 5.6, se muestran los resultados en comparación con otras técnicas de filtrado anisótropo de campos tensoriales basadas en ecuaciones en derivadas parciales, comprendiendo las figuras comprendidas entre la 5.4 y la 5.12. En comparación con las técnicas de regularización en derivadas parciales, nuestro algoritmo presenta un comportamiento más preciso y no presenta problemas tales como el inflado de los tensores para un tiempo de regularización demasiado grande.

Conclusiones

El objetivo de esta tesis es el desarrollo de Nuevos Esquemas para el Procesado de Señales Tensoriales *abordando problemas clásicos del procesado de señales pero con los requisitos que los datos tensoriales necesitan. Esta nueva rama del procesado de señales se ha convertido en los últimos años en un campo fundamental con contribuciones tan importantes como el tensor de estructura local.*

En este sentido, en el capítulo 3 se ha desarrollado un marco general para el procesado anisótropo de señales utilizando la información del tensor de estructura local, con diversas aplicaciones que surgen de manera natural. En primer lugar, dicha información se ha utilizado para definir de forma adaptativa un vecindario alrededor del punto de estimación. Otra de las aplicaciones que se han desarrollado es un algoritmo de filtrado Gaussiano en el que, además de seleccionar las muestras de forma anisótropa, se utiliza el tensor de estructura para definir la forma de la matriz Gaussiana, como si se tratara de una matriz de covarianza. Por otra parte, también hemos desarrollado un algoritmo anisótropo de interpolación en el que el tensor de estructura se utiliza como tensor de métrica para calcular distancias entre tensores de forma que las muestras en la dirección de máxima variación parecen estar más lejos de lo que en realidad están. Por último, la información proporcionada por el tensor de estructura también se ha utilizado para elaborar de forma anisótropa modelos de la función de autocovarianza comúnmente utilizados en el diseño de filtros óptimos en sentido estadístico, lo que nos permite diseñar versiones anisótropas de este tipo de filtros, como el filtro de Wiener.

Puesto que la forma de estimación del tensor de estructura tiene cierta influencia en el resultado final, también se ha llevado a cabo un estudio comparativo para ver el método que menor error introduce en la delocalización de las estructuras más importantes del campo de datos, incluyendo las denominadas versiones no lineales del tensor de estructura. A la vista de nuestros resultados, la estimación del tensor de estructura con formulaciones basadas en filtros de cuadratura junto con un suavizado no lineal al final parece la más apropiada para ser utilizada en nuestro algoritmo.

La generalización desde el caso escalar al caso tensorial de nuestros algoritmos pasa por la generalización del tensor de estructura para datos tensoriales. Una vez hecho esto, se pueden aplicar los mismos conceptos para desarrollar los algoritmos, con la ventaja de que de forma natural nuestros algoritmos proporcionarán una respuesta semidefinida positiva, puesto que los pesos utilizados están restringidos de forma natural a valores positivos.

En el capítulo 4 se ha abordado el problema específico de regularización de datos tensoriales desde una nueva perspectiva, basada en la generalización de la descomposición homomórfica para este problema. La base matemática recae en la interpretación algebraica del espacio de matrices simétricas y del conjunto de matrices simétricas y semidefinidas positivas. Aunque estas dos estructuras algebraicas son aparentemente distintas, existe una relación entre ellas que nosotros explotamos para generalizar la teoría homomórfica.

En este sentido, aunque la interpretación algebraica difiere un poquito, nos conduce a una formulación matemática totalmente análoga utilizando el logaritmo matricial y la exponencial matricial como subsistemas de entrada y salida y en medio un filtro lineal en el sentido habitual. Además, relajando ligeramente algunos requisitos también se puede

utilizar una cadena de procesado que como subsistema de entrada utiliza la raíz cuadrada del tensor y como subsistema de salida el cuadrado del mismo. La principal ventaja de esta nueva formulación es que también es válida para tensores semidefinidos positivos, evitando también problemas numéricos cuando los autovalores son muy pequeños.

Finalmente, el capítulo 5 presenta un nuevo esquema basado en la teoría de geometría diferencial para la regularización anisótropa de datos tensoriales, vistos como campos de distribuciones normales. Basándonos en las propiedades de este espacio de distribuciones normales, es posible introducir una métrica Riemanniana que proporciona un marco teórico para definir geodésicas y distancias entre tensores en las que se fundamenta el algoritmo presentado en este capítulo.

El comportamiento anisótropo se introduce mediante el cálculo del módulo del gradiente en sentido Riemanniano, calculado usando la distancia geodésica entre distribuciones. El módulo del gradiente, al contrario del caso Euclídeo se beneficia de la invarianza afín de la distancia. En nuestro estudio de sus propiedades hemos comprobado que la versión Riemanniana no es sensible a la escala de los tensores lo que permite discriminar mejor interfaces de tejidos y regularizar tensores desorientados a causa del ruido. En comparación con otras versiones anisótropas de regularización para campos tensoriales basadas en Partial Differential Equations (PDE), hemos visto que nuestro esquema no presenta algunas limitaciones de estos esquemas, como por ejemplo el efecto de inflado.

Publicaciones Relacionadas

En esta sección mostramos una breve descripción de los artículos que han sido publicados en el contexto de esta tesis:

- ***Homomorphic Filtering of DT-MRI Fields** [Castaño03b]:*

  En este artículo, publicado en la conferencia internacional Medical Image Computing and Computer Aided Intervention *se propusieron las bases en las que se fundamenta el filtrado homomórfico para datos tensoriales presentado en el capítulo 4 y que consiste en una cadena de procesado que garantiza una respuesta semidefinida positiva independientemente del filtro utilizado en dicha cadena para reducir el ruido.*

- ***Filtrado Homomórfico de Datos Tensoriales** [Castaño03a]:*

  Los campos de datos tensoriales, como los proporcionados por modalidades de imágenes médicas como DT-MRI, deben cumplir la propiedad de ser simétricos y semidefinidos positivos. Sin embargo, debido a una serie de razones esto no

siempre es cierto en los datos reales. Además, sería deseable que dicha propiedad se mantuviera incluso después de procesar estos datos con los sistemas de procesado apropiados. En este sentido, esta publicación complementa el trabajo realizado en [Castaño03b] mediante una cadena de procesado que garantiza esta propiedad.

- ***Anisotropic Interpolation of DT-MRI*** *[Castaño04b]:*

  En este artículo, se presenta una nueva técnica para interpolar campos de tensores de difusión de forma anisótropa respetando correctamente las fronteras entre regiones y con la condición de que la respuesta sea semidefinida positiva. Nuestra propuesta se basa en el uso de la inversa del tensor de estructura local como métrica para calcular distancias entre el punto de interpolación y las muestras encontradas en un determinado vecindario. La interpolación es una herramienta esencial en el manejo de imágenes digitales en gran diversidad de aplicaciones. Para ilustrar el comportamiento de nuestra técnica, se muestran resultados de remuestreo (zooming) en campos tensoriales sintéticos y reales de DT-MRI. Este nuevo esquema proporciona un nuevo marco de filtrado anisótropo, incluyendo aplicaciones en el filtrado, registrado o segmentación.

- ***Esquema Variacional para el Filtrado de Imágenes Médicas Tensoriales*** *[Castaño04a]:*

  En este artículo, se propone un esquema de filtrado para regularizar campos de datos de DT-MRI. Nuestra propuesta se basa en la utilización de métodos variacionales combinados con el uso del tensor de estructura local de estos campos. Algunos ejemplos con datos sintéticos y reales de DT-MRI ilustran el comportamiento de nuestro método.

- ***Estudio Comparativo de Estimadores no Lineales del Tensor de Estructura Local*** *[Castaño05]:*

  En este artículo, proponemos el uso de un proceso de difusión no lineal para mejorar la robustez de los métodos que utilizan la energía local de la señal para estimar el tensor de estructura local. Además, se realiza un análisis comparativo de la robustez con que los distintos métodos presentados en la literatura son capaces de detectar elementos de estructura como las esquinas.

- ***A Generalized Local Structure Measure to Regularize Tensor Fields*** *[SS05]:*

  Este trabajo describe algunas aplicaciones del tensor de estructura de datos tensoriales en el procesado de señales bajo un marco estadístico. El tensor de estructura, obtenido a partir de los datos iniciales, se usa como elemento clave para regularizar de forma anisótropa dichos datos. El desarrollo realizado en este trabajo

se hace desde un punto de vista estocástico, incluyendo también una implementación invariante en fase. Además, se presenta un esquema de filtrado general para imágenes tensoriales y aplicaciones en interpolación y registrado de datos tensoriales multidimensionales.

- ***Anisotropic Filtering with Nonlinear Structure Tensors*** *[Castaño06b]:*

  En este artículo, presentamos un esquema de filtrado anisótropo que usa una versión no lineal del tensor de estructura local para adaptar de forma dinámica la forma del vecindario usado para llevar a cabo la estimación. De esta forma, sólo las muestras a lo largo de la dirección ortogonal a la de máxima variación son utilizadas para estimar el valor en la posición actual, lo que ayuda a respetar de forma adecuada las fronteras y la información de estructura. Esta idea general es directamente trasladable para implementar todo tipo de filtros FIR, como el filtro de Wiener o LMMSE entre otros. En este artículo se describe la idea subyacente usando un esquema de filtrado anisótropo gaussiano lo que nos permite, al mismo tiempo, estudiar la influencia del tensor de estructura no lineal en los esquemas de filtrado, puesto que se realiza una comparación con las respuestas obtenidas utilizando las definiciones clásicas de tensor de estructura.

- ***A Homomorphic Filtering Framework for DT-MRI*** *[Castaño06c]:*

  En este artículo se establecen las bases matemáticas de un marco de filtrado para señales tensoriales usando la teoría de espacios vectoriales. Desde este punto de vista, las señales se interpretan como elementos de espacios vectoriales y los operadores como mapeados de un espacio de entrada a uno de salida. Esta formulación, nos permite generalizar el principio de superposición para cualquier operador definido en espacios de señales. Los sistemas que obedecen esta generalización se denominan homomórficos y pueden descomponerse en una cadena de tres subsistemas. El primero opera en el espacio de entrada de la señal, el segundo es un sistema lineal en el sentido habitual y el tercero opera en el espacio de salida. Por tanto, es posible elegir diferentes subsistemas de entrada y salida apropiados para tratar con todo tipo de señales, definiendo de este modo una completa familia de filtros homomórficos. En el caso particular de las señales tensoriales, identificamos los espacios de entrada y salida como el conjunto de matrices reales, simétricas y semidefinidas positivas y, además, se proponen subsistemas específicos para garantizar que todas esas propiedades se satisfacen a la salida de la cadena de procesado.

- ***A Fast and Rigorous Anisotropic Smoothing Method for DT-MRI*** *[Castaño06]:*

En este artículo, se explotan las proiedades de geometría diferencial del espacio de distribuciones normales multivariadas, donde es posible definir una métrica Riemanniana para calcular estadísticas en el manifold de matrices simétricas positivas definidas. Nuestra contribución en este caso se centra en el uso de estas herramientas estadísticas en el filtrado anisótropo de campos de datos tensoriales.

- ***A Riemannian Approach to Anisotropic Filtering of Tensor Fields*** *[Castaño06a]:*

  Los algoritmos de filtrado desarrollados para tratar con tensores están basados en la interpretación del campo tensorial como un espacio vectorial de matrices con la limitación de permanecer simétricos y definidos positivos. Por el contrario, nuestra propuesta en este artículo está fundada en la interpretación de los datos desde el punto de vista de la geometría diferencial, donde se puede definir un marco matemático riguroso y explotar las propiedades del manifold de las distribuciones normales multivariadas, donde es posible definir una métrica Riemanniana y expresar estadísticas en el manifold de matrices simétricas definidas positivas. En este artículo, centramos nuestra atención en la contribución de estas herramientas para el procesado de filtrado anisótropo y regularización de campos tensoriales, ilustrando el comportamiento de nuestro algoritmo tanto en datos sintéticos como reales.

Líneas Futuras

El trabajo presentado en esta tesis presenta varias líneas de investigación donde es posible realizar nuevas aportaciones y que constituyen algunas de las líneas futuras en las que se va a continuar trabajando con el objetivo de desarrollar nuevos conceptos y algoritmos para el procesado de señales tensoriales. Entre otras, hemos identificado las siguientas líneas de trabajo futuras:

- *Una línea de investigación que en la que se va a continuar trabajando es la elaboración y completa caracterización de filtros anisótropos tradicionales como el filtro de Wiener, Kriging, etc. bajo el marco de procesado anisótropo presentado en esta tesis.*

- *El uso del tensor de estructura local como tensor métrico para calcular distancias entre dos muestras cualquiera usado en nuestro esquema de interpolación tiene aplicaciones en otros problemas de procesado convencionales, como por ejemplo el segmentado o registrado de imágenes, que quedaron fuera de los objetivos de esta tesis, pero que son de enorme importancia en el campo de procesado de imágenes.*

- *En lo que se refiere a los marcos de procesado homomórfico y Riemanniano, se pretende realizar un estudio más detallado para intentar establecer las relaciones que puedan existir entre ambos algoritmos, dada la similitud existente entre ambas formulaciones que resulta evidente al comparar visualmente las ecuaciones que rigen sus respectivos comportamientos.*

Chapter 1

Introduction

1.1 Motivation

The overall objective of this thesis is to originally contribute to the development of the new field of Multidimensional Tensor Signal Processing as a branch of Signal Processing. Tensors arise in multiple areas of science and technology, e.g., diffusion tensor, fabric tensor, electrical conductivity tensor, thermal conductivity tensor, strain tensor, etc. Different sensing modalities provide tensor measurements, though they are not fully reliable since any real sensor will provide noisy and possibly incomplete and degraded data. Therefore, all problems dealt with in conventional multidimensional signal processing - such as filtering, restoration, reconstruction, classification, etc. - are also present when dealing with tensor signals.

Tensor data processing has been mainly approached as a specific case of multichannel signal processing. This procedure is obviously insufficient, as tensors are much more general structures than vectors, and writing tensor signals as a succession of vectors fails to preserve intrinsic algebraic relationships among its elements. For example, operations that are commonly applied to tensors, such as making their eigen-decompositions or applying general coordinate transformations, are difficult to manage when tensors are written as vectors. Moreover, statistics estimated from the stacked components of the tensor fields, such as the covariance matrix, offer no insights into the way noise or features of the experimental design affects their distribution. In addition, treating tensors signals as unrestricted multichannel signals implies to ignore important algebraic and geometric information that should be accounted for during the whole processing procedure.

In this thesis, we argue for considering the whole nature of second and higher order tensor signals in order to preserve all their intrinsic algebraic and geometric information. It must be stressed that new models and algorithms based on multidimensional tensor signal processing are not extensions of currently available multi-channel algorithms. In this sense, new algorithms developed under this context have to consider the random nature of tensor data and their own algebraic structure with the constraint of keeping the algorithmic complexity as low as possible. Since scalar and vector data correspond to 0^{th} and 1^{st} order tensor fields respectively, multidimensional tensor signal processing includes

them as particular cases of current signal processing schemes, much in the same way as multichannel signal processing includes scalar signal processing.

Computer vision is one field of science where tensors arise as an important tool. Based on three axiomatic requirements, Knutsson demonstrated that the image local structure is more conveniently described by a second order symmetric positive semidefinite tensor than it is done with other more common descriptors used before [Knutsson89]. This representation leads to the definition of the *local structure tensor* which, in addition, profits from a solid mathematical body that supports a complete analysis in the tensor domain. The main contribution of the local structure tensor is that tensors contain more information than only the dominant orientation, since they also quantify uncertainty about this orientation being actually dominant. Thus, an analysis of the eigenvalues and eigenvectors helps to discriminate the type local neighborhood.

In this sense, the local structure tensor has become an important image processing tool with applications in several computer vision domains, such as techniques based on optical flow analysis, representation of spatio-temporal features, feature detection or medical data segmentation and registration among others. In this thesis we will also focus on the applications that the local structure tensor may have in the development of anisotropic processing systems, either with scalar or tensor data. As an example, fundamental tools of differential geometry like metrics will be used to constitute a data-dependent geometry on the image which allow us to compute distance measures that can be used to derive filter kernels, interpolate images or derive anisotropic models of covariance structure.

The development of multidimensional tensor signal processing is of potential interest of several industrial applications, such as the study of electrical conductivity, computer vision, elastrography, face detection, mechanical strain tensor, among others. But in this dissertation, we are specially interested in the applications that multidimensional tensor signal processing may have in the field of medical imaging. In particular, we use a relatively new medical image modality called Diffusion Tensor Magnetic Resonance Imaging (DT-MRI) as proof-of-concept to validate our processing algorithms. A DT-MRI dataset consists of noisy samples drawn from an underlying macroscopic diffusion tensor field, which is assumed continuous and smooth at a coarse anatomical scale. Within this context, a symmetric positive semidefinite second order tensor describes the voxel-averaged diffusion of water molecules in tissues due to Brownian motion [Basser96]. A major constraint to deal with this kind of tensor signals is to preserve the positive semidefiniteness of the tensors as long as tensors that do not satisfy this condition have no physical meaning, much in the same way as a negative covariance matrix has no sense.

In conclusion, we present in this thesis different approaches to deal with conventional signal processing problems, but with the special requirements that tensor datasets demand. As a result of our research work, we have set several theoretical frameworks that lead us to the development of *New Schemes for Tensor Signal Processing.*

1.2 Outline of this thesis

This thesis is organized in several chapters. Each chapter presents the work we have done concerning the topic that is discussed therein as well as the state-of-the-art literature in

which our contributions are founded. For each new processing scheme presented in this thesis we also present experimental results in order to validate our approaches. The thesis is split into 6 different chapters, whose contents are described next:

- **Chapter 1: Introduction.** This chapter is the current introduction, where the main motivations and objectives are described.

- **Chapter 2: Background.** This chapter deals with some preliminary topics that are described in order to provide a background to the reader with tensor datasets.

  First, we review some of the important concepts that are used throughout this document to develop our tensor signal processing algorithms, with special attention to tensor algebra. Finally, an introduction to medical imaging modalities is presented with particular interest on DT-MRI, since datasets from this medical imaging modality are used to validate the algorithms developed for tensor signal processing in this thesis.

- **Chapter 3: A New Approach for Anisotropic Signal Processing.** The limitations presented by standard descriptors of signal variation such as the gradient, may lead to a wrong identification of signal structures [Knutsson03b]. For instance, when the signal varies in more than one direction, for example at corners or junctions, the direction given by the gradient is ambiguous since it is not possible to distinguish these image features from simple edges. This leads to the use of tensors in order to get a more robust descriptor of local structure [Knutsson89]. The basic idea is to represent the signal orientation at a given scale by a symmetric Positive Semi-Definite (PSD) tensor, called *Local Structure Tensor*.

  Based on these ideas, we investigate new techniques to exploit the information given by the local structure tensor in order to derive anisotropic signal processing systems for general purposes. After a complete revision of the different methods proposed in the literature to estimate the local structure tensor, including nonlinear counterparts, we study the robustness of these methods in terms of structure delocalization in order to reduce as much as possible this undesirable effect on anisotropic signal processing systems.

  Then, we present our processing framework to develop anisotropic signal processing systems. It is remarkable that the ideas behind our approach are quite general and, hence, they can be particularized for any classical anisotropic signal processing technique. In this sense, we particularize our approach for different application purposes. First, we derive anisotropic Gaussian smoothing kernels using the local structure tensor to compute anisotropic neighborhoods around a given sample and to model the shape of the Gaussian distribution. Furthermore, we also derive an anisotropic interpolation scheme where the local structure tensor is also used as a metric tensor to compute distances. Finally, we also propose the use of the information provided by the local structure tensor to build an anisotropic estimator of the covariance estructure of the signal, yielding to anisotropic versions of traditional statistically optimal estimators, such as the well-known Wiener filter.

  Our approach is validated with scalar and tensor datasets. An interesting characteristic on the generalization for tensor data is that our approach naturally

provides a PSD response, since the response is given by a linear combination of PSD matrices with positive coefficients.

- **Chapter 4: Homomorphic Filtering of Tensor Data.** This chapter presents a new filtering framework for tensor images. The main restriction that filtering algorithms that deal with tensor data is to remove noise with the constraint of preserving the tensors positive definite after processing the signal.

  This limitation has also been addressed in [Chefd'hotel02] which provides a geometric interpretation of constrained flows for tensor-valued functions. This yields, through the use of exponential maps, suitable numerical schemes that are also constraints preserving. Another approach presented in [Weickert02] provides a generalization of anisotropic and nonlinear diffusion process to tensor-valued data. However, tensor eigenvalues tend to regularize faster than the associated eigenvectors. This phenomenon is known as the *eigenvalue swelling effect*.

  In this chapter we propose a theoretical framework for the design of filters which presents the advantage that the response of the filter is assured to be symmetric positive semidefinite independently from the filter used to regularize the tensor field [Castaño06c]. The basis of our approach relies on the algebraical interpretation of the set of symmetric positive semidefinite tensors which are mapped to the vector space of symmetric matrices following a generalization of the homomorphic decomposition for scalar signals developed in [Oppenheim67].

- **Chapter 5: A Riemannian Framework for Tensor Signal Processing.** This chapter also deals with the problem of filtering tensor images with the constraint of preserving the tensors positive definite. In this case, we derive an anisotropic filtering framework based on a geometrical interpretation of the set of positive definite second order tensors, which yields to a rigorous mathematical framework to compute statistics on tensor fields.

  We use the mathematical framework, developed in [Skovgaard81], [Amari90] and [Lenglet05b] where the differential geometrical properties of the space of multivariate normal distributions are used to define a Riemannian metric, which allow us to compute distances between tensors and, hence, compute some statistics.

  The main contribution of this chapter is an anisotropic filtering algorithm controlled by the magnitude of the Riemannian spatial gradient of the tensor field. A complete characterization of the Riemannian gradient magnitude is also performed, since it does not exhibit the same properties as the usual gradient magnitude. A detailed analysis of the performance of our approach on noisy and synthetic data is also carried out. In our experiments, we obtain better qualitative and quantitative results than with the method proposed in [Weickert02].

- **Chapter 6: Conclusions** This chapter summarizes the main conclusions we have obtained from our work and the tensor processing schemes we have developed in the context of this thesis. Moreover, it presents the related papers that have been published in the context of this thesis which contain our core work.

1.3 Our Main Contributions

In order to facilitate the identification of the main contributions of this dissertation, we summarize them listed by chapters:

- **Contributions in chapter 3:**

  A New Approach to Anisotropic Signal Processing (Section 3.4): In this section we present a new approach to derive adaptive neighborhoods for anisotropic signal processing systems. The idea behind is to wisely adapt the local neighborhood used to perform the estimation depending on the information provided by the local structure tensor by means of the ellipsoid associated to that positive semidefinite matrix.

  Comparison of the local structure tensor estimation methods (Section 3.3.4): Since the estimation methods of local structure do not provide an equal response, we have studied the structure delocalization effect in order to choose the most robust method in our approach, including the so-called *nonlinear structure tensors* recently presented and applied to the Knutsson's formulation.

  Anisotropic Gaussian Smoothing (Section 3.4.2): We derived an adaptive anisotropic Gaussian filtering scheme to reduce noise in scalar images, where the shape of the Gaussian kernel is modeled by the local structure tensor.

  Anisotropic Interpolation (Section 3.4.3): We derived an adaptive anisotropic interpolation scheme to upsample scalar images. In addition to using the local structure tensor to compute the local neighborhood, we use it as a metric tensor to measure distances between samples. The effect is that samples found in the same direction of the maximum signal variation seem to be further, while those in the direction of minimal signal variation seem to be closer.

  Anisotropic Covariance Structure Estimation (Section 3.4.4): We also used the information provided by the local structure tensor to build an anisotropic estimator of the covariance estructure of the signal. This formulation leads to the development of anisotropic versions of traditional statistically optimal estimators, such as the well-known Wiener filter.

  Generalization for Tensor Data (Section 3.5): Finally we generalized all the previous approaches for tensor-valued datasets by means of the generalization of the local structure tensor. An interesting characteristic on the generalization for tensor data is that our approach naturally provides a Positive Semi-Definite (PSD) response, since the response is given by a linear combination of PSD matrices with positive coefficients.

- **Contributions in chapter 4**

  Algebraic Interpretation of Homomorphic Systems (Section 4.3.2): We have performed a reinterpretation of the homomorphic theory from an algebraical point of view as a preceding step for the generalization for tensor data.

  Processing Cascade for Positive Definite Tensor Data (Section 4.4.1): We proposed a processing chain inspired on the homomorphic decomposition to ensure

that tensors at the output are positive definite independently of the filter used in that chain to reduce the noise.

Processing Cascade for Positive Semidefinite Tensor Data (Section 4.4.2): In order to deal with positive semidefinite tensor signals, we propose a different processing cascade using other input and output subsystems in the processing chain.

- **Contributions in chapter 5:**

  Estimation of the spatial gradient magnitude (Section 5.4.3): We proposed the estimation of the spatial gradient magnitude through the sum of squared geodesic distances between tensors in orthogonal directions on a discrete grid.

  Characterization of the Riemannian spatial gradient (Section 5.4.3): We characterized the properties of the Riemannian spatial gradient magnitude to demonstrate the differences between the Riemannian framework and the traditional Euclidean framework.

  Anisotropic Riemannian Smoothing Algorithm (Section 5.5): We developed an anisotropic Riemannian smoothing algorithm to deal with tensor data. This algorithm uses the statistical tools defined for tensors in the manifold of positive definite matrices by the definition of a Riemannian metric.

1.4 Notation

Next is presented the notation used throughout this document. We will follow the convention that vectors will be denoted by bold lowercase letters $\mathbf{v}$, second order tensors and matrices will be denoted by bold capital letters $\mathbf{T}$. Their elements will be indexed with one or two subscripts, respectively, using lowercase italic letters $\mathbf{v} = v_i$, $\mathbf{T} = t_{ij}$. Vectors are considered as column vectors, unless the contrary is outlined in a specific context.

The following vector operations are used throughout this document with the notation used in the following list:

- Sets of elements:

$\mathbb{R}^n$	n-dimensional set of real numbers
$\mathbb{R}^{+n}$	n-dimensional set of positive real numbers
$\mathbb{C}^n$	n-dimensional set of complex numbers
$S(n)$	Set of $n \times n$ symmetric matrices
$PS^+(n)$	Set of $n \times n$ positive definite matrices
$PS_0^+(n)$	Set of $n \times n$ positive definite matrices

- Signal Transformations:

$\mathcal{F}(\cdot)$	Fourier Transform
$\tilde{\mathcal{S}} = \tilde{\mathcal{H}}\{s(t)\}$	Hilbert Transform of signal $s(t)$
$s_A(t)$	Analytic Function of signal $s(t)$

- Magnitude of complex or real number z:

$$|z| \tag{1.1}$$

- Basis of a vector space $V \in \mathbb{R}^n$:

$$\{\mathbf{e}_i\}, \text{with} i = 1, \ldots, n \tag{1.2}$$

- Vector inner product:

$$< \mathbf{v}, \mathbf{w} >= \mathbf{v}^T\mathbf{w} = \sum_i^m a_i b_i \tag{1.3}$$

- Vector norm:

$$\| \mathbf{v} \|^2 = \mathbf{v}^T\mathbf{v} \tag{1.4}$$

- Vector outer product:

$$\mathbf{A} = \mathbf{v}\mathbf{w}^T = [v_i w_j] \tag{1.5}$$

- Frobenius norm:

$$\| \mathbf{T} \|_F = \sqrt{\sum_{ij} |t_{ij}|} = \sqrt{trace(\mathbf{T}\mathbf{T}^T)} = \sqrt{\sum_i \lambda_i^2} \tag{1.6}$$

- Eigenvalues λ_i and Eigenvectors $\mathbf{e}_i$ of a second order tensor $\mathbf{T}$:

$$\mathbf{T} = \sum_{i=1}^{n} \lambda_i \mathbf{e}_i \mathbf{e}_i^T \tag{1.7}$$

- The Spectral Radius of a second order tensor $\mathbf{T}$:

$$\rho(\mathbf{T}) = \max_{1 \leq i \leq n} \tag{1.8}$$

- Math symbols:

$\mathcal{D}(\boldsymbol{\Sigma_1}, \boldsymbol{\Sigma_2})$	Distance between two second order tensors $\boldsymbol{\Sigma_1}, \boldsymbol{\Sigma_2}$
$\mathcal{N}(\mathbf{x_0})$	Local neighborhood around point $\mathbf{x_0}$
$H\{\cdot\}$	Impulse response of a system
$H^{-1}\{\cdot\}$	Inverse impulse response of a system
$\mathfrak{g}$	Lie Algebra associated to the Lie Group G
$\delta(x)$	Dirac delta.

Tensor operations are completely described in section 2.4, where we perform a detailed description on this mathematical concept.

Chapter 2

Background

2.1 Introduction

In this chapter we introduce some basic concepts that will be used throughout this dissertation. In this sense, we define in section 2.2 important concepts of signal processing theory, such as local energy, local phase and quadrature filters, on which rely the schemes we develop in other chapters. This basic theory is extended in section 2.3, where we describe some basic concepts of a classic branch of signal processing such as optimal estimation, with special interest on Wiener filter theory. Then, in section 2.4 we review the mathematics involved in tensor algebra, which includes the definition of tensor signals. Since in this dissertation we are specially interested in the applications that multidimensional tensor signal processing may have in the field of medical imaging, we present in section 2.5 a brief review of some medical imaging modalities. In particular, we focus our attention in DT-MRI, which is widely described in section 2.6, since we use it as proof-of-concept to validate our processing algorithms.

2.2 Previous Concepts

In this section we define some concepts that are used throughout this dissertation in order to provide a background to the reader.

2.2.1 Local phase and Local energy

The *Hilbert transform* of a real-valued signal $s(t)$ is the integral transform given by:

$$\tilde{\mathcal{S}}(t) = \tilde{\mathcal{H}}\{s(t)\} = h(t) * s(t) = \frac{1}{pi} \int_{-\infty}^{\infty} \frac{s(\tau)}{t-\tau} d\tau \tag{2.1}$$

where $h(t) = \frac{1}{\pi t}$ is the convolution kernel. Because of the possible singularity at $t = \tau$, the integral is to be considered as a Cauchy principal value.

In the frequency domain, the Hilbert transform is given by product of the Fourier transforms of the signal and the kernel: $\mathcal{F}\{\tilde{\mathcal{S}}\} = \mathcal{H}(\omega)\mathcal{S}(\omega)$, where $\mathcal{H}(\omega) = -i \cdot \text{sgn}(\omega)$, with i the imaginary unit and $\text{sgn}(\omega)$ the *sign* function, which returns the sign of the argument. Hence, the Hilbert transform has the effect of shifting the negative frequency components $\pi/2$ radians and the positive frequency components by $-\pi/2$.

We are now able to introduce the concept of *analytic signal* of a real-valued signal $s(t)$, which was first proposed in [Gabor46] and it is defined as:

$$s_A(t) = s(t) + i\tilde{\mathcal{S}}(t) \tag{2.2}$$

where $\tilde{\mathcal{S}}(t)$ is the Hilbert transform of the signal $s(t)$ and i is the imaginary unit. The basic idea of the analytic representation is that the negative frequency components of the Fourier transform of a real-valued function are superfluous, due to spectral symmetry. Thus, they can be suppressed with no loss of information, but instead the signal becomes a complex-valued function.

The analytic signal allows us to define two important concepts used in this dissertation:

- *Local Phase:* The local phase of a signal $s(t)$ is the argument of its analytic signal $\varphi(t) = \arg[s_A(t)]$, which offers a continuous shape description of a neighborhood at a given scale in terms of one-dimensional events.
- *Local Amplitude:* The local amplitude of a signal $s(t)$ is the magnitude of the analytic signal $A = |s_A(t)|$, which represents the energy of a structure in a neighborhood at a given scale.

These two concepts are really important for a proper representation of local structure since they allow an interpretation in two independent components. On the one hand, local amplitude varies with the variation of local structure, but it is invariant to the type of structure itself. On the other hand, the local phase gives a description of the type of structure, being independent of the local variations of the signal.

Multidimensional Generalization

The generalization of the previous concepts for multidimensional datasets is not a trivial issue. First of all, it is necessary to generalize the notion of Hilbert transform, which for multidimensional data is associated to a reference direction $\hat{\mathbf{n}}_k$. Thus, given a n-dimensional function $s(\mathbf{x})$, its Hilbert transform is given by:

$$\tilde{\mathcal{S}}(\mathbf{x}) = s(\mathbf{x}) * \frac{-1}{\pi \mathbf{x}^{\mathbf{T}} \hat{\mathbf{n}}_{\mathbf{k}}} \delta_{\hat{\mathbf{n}}_k}(\mathbf{x}) \tag{2.3}$$

where $\delta_{\hat{\mathbf{n}}_k}(\mathbf{x})$ is a delta function which passes through the origin and it is parallel to the vector $\hat{\mathbf{n}}_k$. From this definition, the concepts of local phase and local energy can be straightforward generalized from the unidimensional case.

2.2.2 Quadrature filters

The computation of the analytic signal for general signals cannot be made in practice since it involves convolutions with the function $\frac{1}{\pi t}$ which is difficult to approximate as a filter which is either causal or of finite support. However, it is possible to obtain a nice approximation of the analytic signal as the convolution of the signal $s(t)$ with a filter $q(t)$ such that it eliminates all the negative frequencies.

A general expression of a quadrature filter in the Fourier domain is given by:

$$\mathbf{Q}(\mathbf{u}) = \mathcal{R}(\| \mathbf{u} \|)\mathbf{D}(\mathbf{u}) \tag{2.4}$$

where $\mathcal{R}(\| \mathbf{u} \|)$ is the radial part, which determines the bandpass character of the quadrature filter and $\mathbf{D}(\mathbf{u})$ is the directional part. In general, the quadrature filter is a vector valued function $\mathbf{Q}(\mathbf{u}) : \mathbb{R}^n \mapsto \mathbb{R}^d$, yielding to several definitions of quadrature filters. For a complete review, the reader is referred to [San Jose05].

2.2.3 Steerable filters

The term *steerable filter* is used to describe a class of filters in which a filter of arbitrary orientation is synthesized as a linear combination of a set of basis filters oriented along some predefined orientations. This kind of filters has been widely used in many signal processing domains, such as orientation estimation, adaptive filtering, feature detection, etc.

Let us illustrate this idea with an example drawn from the pioneer work [Freeman91] and [Freeman92]. Consider the 2-dimensional, circularly symmetric Gaussian function $G(x, y)$ written in Cartesian coordinates, x and y where scaling and normalization constants have been set to 1 for convenience:

$$G(x, y) = e^{-(x^2+y^2)} \tag{2.5}$$

Let us write the n-th derivative of a Gaussian in the x direction as G_n. Let $(\ldots)^\theta$ represent the rotation operator, such that, for any function $f(x, y)$, the function $f^\theta(x, y)$ represents $f(x, y)$ rotated through an angle θ about the origin. Then, the first derivative of a Gaussian ($G_1^{0^\circ}$ in our notation) is:

$$G_1^{0^\circ} = \frac{\partial}{\partial \times} e^{-(x^2+y^2)} = -2xe^{-(x^2+y^2)} \tag{2.6}$$

That same function rotated 90 degrees, is:

$$G_1^{90^\circ} = \frac{\partial}{\partial y} e^{-(x^2+y^2)} = -2ye^{-(x^2+y^2)} \tag{2.7}$$

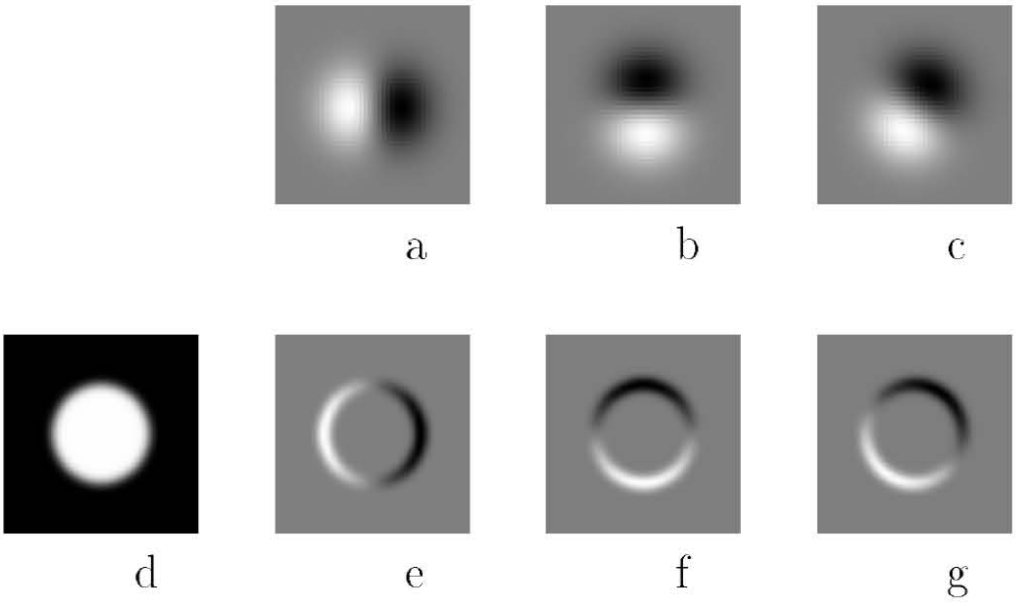

Figure 2.1: Example of Steerable Filters. First Row: Kernels to compute the spatial first derivatives in the horizontal, vertical and diagonal directions. Second Row: In the left, signal to be convolved with the kernels. e),f) are the respones of the respective kernels convolved with the input signal in d). d) is the same linear combination of the outputs e) and f) used to synthetise the kernel in c).

It is straightforward to show that a G_1^θ filter at an arbitrary orientation θ can be synthesized by taking a linear combination of $G_1^{0^\circ}$ and $G_1^{90^\circ}$:

$$G_1^\theta = \cos(\theta) G_1^{0^\circ} + \sin(\theta) G_1^{90^\circ} \tag{2.8}$$

Since $G_1^{0^\circ}$ and $G_1^{90^\circ}$ span the set of G_1^θ filters we call them *basis filters*. The $\cos(\theta)$ and $\sin(\theta)$ terms are the corresponding interpolation functions for those basis filters. In the same way, since convolution is a linear operation, we can synthesize any signal $s(\mathbf{x})$ at an arbitrary orientation by taking linear combinations of the images filtered with $G_1^{0^\circ}$ and $G_1^{90^\circ}$. Let $R_1^{0^\circ} = G_1^{0^\circ} * s(\mathbf{x})$ and $R_1^{90^\circ} = G_1^{90^\circ} * s(\mathbf{x})$, then:

$$R_1^\theta = \cos(\theta) R_1^{0^\circ} + \sin(\theta) R_1^{90^\circ} \tag{2.9}$$

Figure 2.1 shows this idea. In the first row of that figure we represent the kernels to compute the spatial first derivatives in the horizontal direction (left), vertical direction (middle) and diagonal direction (right), respectively. The diagonal direction filter response was obtained through a linear combination of the first two filter responses. The second row shows the response to the spatial filters shown on the first row applied to the image of a disk. The response of the image on the right was obtained through a linear combination of the responses of the image to the basis filters, which is equivalent to applying the spatial filter described in the right side of the first row.

The idea of steerable filters will be used in section 3.3 to obtain a descriptor of the local structure. However, we refer the interested reader to [Freeman92, Freeman91], where a complete description of steerable filters is performed with special interest on the required number of basis filters or the requirements on the interpolation functions.

2.3 Optimal Estimation

Optimal estimation is a well established theory in the field of signal processing. Under this framework, we assume that we can estimate the correct value of a signal value based on statistically related data, yielding to an optimal estimation according to some known criterion, usually the minimization of the Mean Square Error. This approach has been succesfully used in a wide range of science fields, such as computer vision, signal processing or econometry, among others [Kay93, Moon99].

A Finite Impulse Response (FIR) implementation of this kind of estimators implies that the estimation of a signal value at the *target* point $\mathbf{x}$ is performed using a finite number K of observations taken from a given neighborhood of the target point. Different neighborhood configurations yield to different estimation schemes, although the common procedure is to take a regular grid centered at the target point with every node corresponding to an observation [Dudgeon83].

The estimation is then performed by a linear combination of the observations within the neighborhood with such weights that optimize a quality criterion. When the neighborhoods for every target are described by regular grids this leads to convolution operators, where the kernel is defined by the corresponding weights. In the case of irregular grids, the convolution operation can no longer be used.

In this sense, the Wiener filter is the well-known solution for linear minimum mean square error Linear Minimum Mean Square Error (LMMSE) signal estimation, i.e., it provides the weights that minimize the Mean Square Error using statistical signal information. Next, we describe the basic theory of Wiener filters with special attention to the practical implementation issues that have to be taken into account.

2.3.1 Wiener Filter

In order to derive the Wiener filter, let us describe first some previous assumptions on which this theory relies. The signal $s(\mathbf{x})$ is considered a random field, i.e., each point $\mathbf{x}$ in the signal space is considered a random variable. The estimation problem, then, consists in the estimation of the unobservable signal $s(\mathbf{x})$ using other observable measure $z(\mathbf{x})$. A *measurement model* that has to be assumed relates both, the observable and the unobservable signals. The standard measurement model is that of signal in noise [RA05]:

$$z(\mathbf{x}) = s(\mathbf{x}) + w(\mathbf{x}) \tag{2.10}$$

where $w(\mathbf{x})$ is a zero-mean random noise field with autocovariance function $c_w(\mathbf{x_i}, \mathbf{x_j})$ and uncorrelated with respect to the signal $s(\mathbf{x})$, whose mean is given by $\eta_s(\mathbf{x}) =$

$E\{s(\mathbf{x})\}$ and its auto-covariance function is $c_s(\mathbf{x_i}, \mathbf{x_j})$. Finally, since signal and noise are uncorrelated, the auto-covariance function of the observable measure is given by $c_z(\mathbf{x_i}, \mathbf{x_j}) = c_w(\mathbf{x_i}, \mathbf{x_j}) + c_n(\mathbf{x_i}, \mathbf{x_j})$ and its mean is $\eta_z(\mathbf{x}) = E\{z(\mathbf{x})\} = \eta_s(\mathbf{x})$.

The estimation is performed by means of a linear combination of the observations $\mathbf{z} = [z(\mathbf{x_1}), z(\mathbf{x_2}) \dots z(\mathbf{x_K})]^T$ within a given neighborhood $\mathcal{N}(\mathbf{x_0})$ centered at the target point $\mathbf{x_0}$, as shows the following expression:

$$\hat{s}(\mathbf{x_0}) = \sum_{i=1}^{K} k_i z_i + b = \mathbf{k}^T \mathbf{z} + b \tag{2.11}$$

Since the estimator must remain unbiased in a bayesian sense, i.e., $\eta_s(\mathbf{x_0}) = \eta_{\hat{s}}(\mathbf{x_0}) = \mathbf{k}^T \boldsymbol{\eta}_\mathbf{z} + b$, where $\boldsymbol{\eta}_\mathbf{z} = [\eta_z(\mathbf{x_1}), \eta_z(\mathbf{x_2}) \dots \eta_z(\mathbf{x_K})]^T$. Thus, the constant b can be easily determined, yielding to the final expression of the Wiener filter estimator:

$$\hat{s}(\mathbf{x_0}) = \mathbf{k}^T (\mathbf{z} - \boldsymbol{\eta}_\mathbf{z}) + \eta_s(\mathbf{x_0}) \tag{2.12}$$

Hence, we want to obtain the coefficient vector $\mathbf{k}$ such that it minimizes the mean square error of the estimator given by:

$$\text{MSE} = E\{(s(\mathbf{x_0}) - \hat{s}(\mathbf{x_0}))^2\} = E\{(s(\mathbf{x_0}) - \eta_s(\mathbf{x_0}) - \mathbf{k}^T(\mathbf{z} - \boldsymbol{\eta}_\mathbf{z}))^2\} \tag{2.13}$$

To that end, we look for the local minimum of the previous expression differentiating with respect to the coefficients k_j:

$$\frac{\partial MSE}{\partial k_j} = E\{2((z(\mathbf{x_j}) - \eta_z(\mathbf{x_j}))(s(\mathbf{x_0}) - \eta_s(\mathbf{x_0}) - \mathbf{k}^T(\mathbf{z} - \boldsymbol{\eta}_\mathbf{z})))\} = 0 \quad j = 1 \dots K \tag{2.14}$$

This system of equations can be expressed using matrix notation as:

$$\mathbf{C_{zz}} \mathbf{k} = \mathbf{c_{sz}} \tag{2.15}$$

where $\mathbf{C_{zz}}$ is the covariance matrix of the observable data and $\mathbf{c_{sz}}$ is the cross-covariance vector between the signal and the observable data. Then, the coefficients are given by $\mathbf{k} = \mathbf{C_{zz}^{-1}} \mathbf{c_{sz}}$, which yields to the final expression of the estimator:

$$\hat{s}(\mathbf{x_0}) = (\mathbf{C_{zz}^{-1}} \mathbf{c_{sz}})^T (\mathbf{z} - \boldsymbol{\eta}_\mathbf{z}) + \eta_s(\mathbf{x_0}) \tag{2.16}$$

Some simplifications can be performed if the signal has certain properties:

- If signal and noise can be assumed to be independent: $\mathbf{C_{zz}} = \mathbf{C_{ss}} + \mathbf{C_{ww}}$ and $\mathbf{c_{sz}} = \mathbf{c_{ss}}$.
- If noise is white: $\mathbf{C_{ww}} = \sigma^2 \mathbf{I}$, where $\mathbf{I}$ is the identity matrix.

- If the signal can be assumed wide sense stationary (WSS): the mean $\eta_s(\mathbf{x_0}$ is constant η_s and the covariance matrix $\mathbf{C_{ss}}$ is Toepliz, which takes the advantage that it can be efficiently inverted.

From the Eq. 2.16, it can be seen that in order to obtain an estimate some *a priori* information about the signal has to be known, such as the mean and the autocovariance function . Although there might be cases in which the first and second order characterization of the signal may be known, the typical situation is that these parameters have to be estimated from available data, by means of Eq. 2.17. In [RA05] there is a complete review on alternative procedures to estimate these parameters from available data using ideas from geostatistics.

$$c_s(\mathbf{x_i}) = \frac{1}{K}\sum_{j=1}^{K}(s(\mathbf{x_i}) - \eta_s(\mathbf{x_i}))(s(\mathbf{x_{k+i}}) - \eta_s(\mathbf{x_{k+i}})) \tag{2.17}$$

Another resource commonly accepted is the use of a signal model which allow us to compute a theoretical autocorrelation function which depends on some parameters which have to be fitted in order to correctly describe the available data. For instance, take the example of the following autocovariance function model proposed in [Cressie93]:

$$c_s(\mathbf{h}) = \sigma^2 \exp\left(-\frac{|\mathbf{h}|}{r}\right) \tag{2.18}$$

where $\mathbf{h} = \mathbf{x_i} - \mathbf{x_j}$ denotes the distance between samples at positions $\mathbf{x_i}$ and $\mathbf{x_j}$, σ^2 is the autocovariance at the target point and r is a free parameter that has to be fixed and depends on the statistical dependence of data.

Concerning the signal mean η_s, the usual procedure is to assume that it is either null or known, so it can be subtracted from the process and added back once the filtering procedure has been carried out.

As it can be supposed, the better the mean and autocovariance models fit the real behavior of data, the better the estimation can be performed and, hence, the lower is the mean square error.

2.4 Tensor Signals

Before any further development, it is an interesting task to understand the mathematical concept of *tensors* in order to better exploit their properties for the development of specific signal processing algorithms.

2.4.1 Definition

In an informal sense, a tensor is a generalized linear quantity or geometrical entity that can be expressed as a multi-dimensional array relative to a choice of basis; however, as

an object itself, a tensor is independent of any chosen frame of reference. The rank of a particular tensor is the number of array indices required to describe such a quantity. For example, mass, temperature, and other scalar quantities are tensors of rank 0; force, displacement and other vector-like quantities are tensors of rank 1; diffusion, electrical impedance and other anisotropic measurements are tensors of rank 2.

In a more strict sense, a nth-rank tensor in an m-dimensional space is a mathematical object that has n indices and m^n components and obeys certain transformation rules. Each index of a tensor ranges over the number of dimensions of the space. However, the dimension of the space is largely irrelevant in most tensor equations (with the notable exception of the contracted Kronecker delta). Tensors are generalizations of scalars (that have no indices), vectors (that have exactly one index) and matrices (that have exactly two indices) to an arbitrary number of indices. Tensors provide in this way a natural and concise mathematical framework for formulating and solving problems in areas of physics such as elasticity, fluid mechanics and general relativity.

In tensor notation, a vector $\mathbf{v}$ would be written v_i, where $i = 1, \ldots, m$ and a matrix is a tensor of type $(1, 1)$, which would be written a_i^j. A more general tensor may have an arbitrary number of indices $r + s$ which may be of mixed type, consisting of r so-called *contravariant* (upper indices) and s *covariant* (lower indices). While the distinction between covariant and contravariant indices must be made for general tensors, the two are equivalent for tensors in three-dimensional Euclidean space, and such tensors are known as Cartesian tensors. Note that the positions of the slots in which contravariant and covariant indices are placed are significant so, for example, a_{ij}^k is distinct from a_i^{jk}.

Tensors may be operated on by other tensors, such as metric tensors, the permutation tensor or the Kronecker delta or by tensor operators such as the covariant or semicolon derivatives. The manipulation of tensor indices to produce identities or to simplify expressions is known as index gymnastics, which includes index lowering and index raising as special cases. These can be achieved through multiplication by a so-called metric tensor g_{ij}, g^{ij}, g_i^j.

Tensor notation also provides a very concise way of writing vector and more general identities. For instance, in tensor notation, the scalar product is simply written:

$$\mathbf{u} \cdot \mathbf{v} = u_i v^i \tag{2.19}$$

where repeated indices are summed over according to Einstein notation. Similarly, the vector product can be written as:

$$(\mathbf{u} \times \mathbf{v}) = \epsilon_{ijk} u^j v^k \tag{2.20}$$

where ϵ_{ijk} is the permutation tensor.

The definition of covariant or contravariant tensors is more easily understood under the context of tensor operations following certain transformation rules. Under this context, we can distinguish:

- **Contravariant Tensor:** Given a 1st-rank tensor v^i in a certain reference system $(x^1, x^2, \ldots, x^m)$ and $\tilde{v}^i$ in another reference system $(\tilde{x}^1, \tilde{x}^2, \ldots, \tilde{x}^m)$. If the transformation rule between $\tilde{v}^i$ and v^i is as follows:

$$\tilde{v}^i = \mathbf{J}\frac{\partial \tilde{x}^i}{\partial x^j} v^j \tag{2.21}$$

  where $\mathbf{J}$ is the Jacobian matrix. In that case, it is said that they are the components of a contravariant 1st-rank tensor.

- **Covariant Tensor:** Analogously, given the same 1st-rank tensor v^i in the same reference system previously used $(x^1, x^2, \ldots, x^m)$ and $\tilde{v}^i$ in the other reference system $(\tilde{x}^1, \tilde{x}^2, \ldots, \tilde{x}^m)$. If the transformation rule between $\tilde{v}^i$ and v^i is as follows:

$$\tilde{v}^i = \mathbf{J}\frac{\partial x^j}{\partial \tilde{x}^i} v^j \tag{2.22}$$

  where $\mathbf{J}$ is the Jacobian matrix. In that case, it is said that they are the components of a covariant 1st-rank tensor.

In the general case of a tensor (p, q), $T^{i_1, i_2, \ldots, i_q}_{j_1, j_2, \ldots, j_p}$, the transformation rule is defined as follows:

$$\tilde{T}^{i_1, i_2, \ldots, i_q}_{j_1, j_2, \ldots, j_p} = \left[\mathbf{J}(\frac{x}{\tilde{x}}\right] T^{a_1, a_2, \ldots, a_q}_{b_1, b_2, \ldots, b_p} \frac{\partial \tilde{x}^{i_1}}{\partial x^{a_1}} \frac{\partial \tilde{x}^{i_2}}{\partial x^{a_2}} \cdots \frac{\partial \tilde{x}^{i_q}}{\partial x^{a_q}} \cdot \frac{\partial x^{b_1}}{\partial \tilde{x}^{j_1}} \frac{\partial x^{b_2}}{\partial \tilde{x}^{j_2}} \cdots \frac{\partial x^{b_p}}{\partial \tilde{x}^{j_p}} \tag{2.23}$$

where the Jacobian matrix is given by:

$$\mathbf{J}(\frac{x}{\tilde{x}}) = \frac{\partial(x^1, x^2, \ldots, x^n)}{\tilde{x}^1, \tilde{x}^2, \ldots, \tilde{x}^n} \tag{2.24}$$

If two tensors $\mathbf{A}$ and $\mathbf{B}$ have the same rank and the same covariant and contravariant indices, then they can be added in the obvious way,

$$a^{ij} + b^{ij} = c^{ij} \tag{2.25}$$

Metric Tensor

The metric tensor appears when we define the scalar product between two vectors $\mathbf{u} = u^i \hat{\mathbf{b}}_i$, $\mathbf{v} = v^i \hat{\mathbf{b}}_i$ defined in a basis $\{\hat{\mathbf{b}}_\mathbf{1}, \hat{\mathbf{b}}_\mathbf{2}, \ldots, \hat{\mathbf{b}}_\mathbf{m}\}$:

$$< \mathbf{u}, \mathbf{v} >= u^i v^j < \hat{\mathbf{b}}_i, \hat{\mathbf{b}}_j > \tag{2.26}$$

The term $< \hat{\mathbf{b}}_i, \hat{\mathbf{b}}_j >= g_{ij}$ is called metric tensor $\mathbf{g}$, since with this tensor we obtain a scalar product and, hence, a norm.

In a formal sense, the metric tensor is a second order tensor $(0,2)$ whose components are given by:

$$g_{ij} =< \hat{\mathbf{b}}_i, \hat{\mathbf{b}}_j >, \quad g^{ij} =< \hat{\mathbf{b}}^i, \hat{\mathbf{b}}^j >, \quad g^i_j =< \hat{\mathbf{b}}^i, \hat{\mathbf{b}}_j >= g^j_i = \delta^j_i \tag{2.27}$$

where δ^j_i is the *Kronecker delta*:

$$\delta^j_i \equiv \begin{cases} 1 & i = j \\ 0 & i \neq j \end{cases} \tag{2.28}$$

An interesting practical case is the conventional Euclidean space with Cartesian coordinates, where the metric tensor defined in this space is the identity tensor, that is, the second order tensor represented by the identity m-dimensional matrix. The metric tensor, used in the definition of scalar product is also used for contravariant and covariant coordinates transformations. In this sense, taking into account that the coordinates are given by the projection of the vector over the basis elements, that is, they are given by the scalar product of both, it can be written as:

$$v^i = g^{ij} v_j, \quad v_j = g^i_j v_i, \quad v_i = g_{ij} v^j, \quad v^i = g^i_j v^j. \tag{2.29}$$

In the case of a higher rank tensor, the metric tensor also allows us to perform this kind of transformations, called *contraction*.

Types of Tensors

Tensors can be classified following different criteria. For this thesis we are particularly interested in tensors with the following properties:

- **Symmetric Tensors:** A tensor is called symmetric if we can change the order of the indices and the tensor still remains the same. For instance, a second-order tensor is symmetric if it satisfies the following property:

$$a^{mn} = a^{nm} \tag{2.30}$$

- **Semidefinite Positive:** A second-order tensor is called semidefinite positive if its eigenvalues are always equal or greater than zero.

2.4.2 Scalar Product of Tensors

The generalization of the scalar product applied to tensors is related to tensor contraction. The contraction of a tensor is a sum of products of scalar components of one or more tensors caused by applying the summation convention to a pair of dummy indices which are bound to each other in an expression. The contraction of a single mixed tensor occurs when a pair of literal indices (one a subscript, the other a superscript) of the tensor are set equal to each other and summed over. For instance, take the example $\mathbf{D}^k = \mathbf{T}^i \mathbf{S}^k_i$.

In our work, we are specially interested in the scalar product of second-order tensors, where all the indices are contracted, that is, we obtain a zero-order tensor: a scalar. This scalar product is also called double contraction and is given by:

$$\mathbf{T} \bullet \mathbf{M} =< \mathbf{T}, \mathbf{M} >= t^{ij} \cdot m_{ij}, \tag{2.31}$$

where t^{ij} and m_{ij} are the components of the second order tensors $\mathbf{T}$ and $\mathbf{M}$, respectively.

Tensor Norm

From the definition of scalar product defined in Eq. 2.31, we can define a tensor norm or magnitude of a given tensor $\mathbf{T}$.

$$\| \mathbf{T} \| = \sqrt{\mathbf{T} \bullet \mathbf{T}} = \sqrt{t^{ij} t_{ij}} \tag{2.32}$$

In the particular case of $\mathbf{T}$ being a symmetric second order tensor with real elements, the norm is expressed as the square root of the sum of the absolute squares of its elements:

$$\| \mathbf{T} \| = \sqrt{\sum_{ij} |t_{ij}|^2} = \sqrt{trace(\mathbf{TT})} = \sum_{i} \lambda_i^2 \tag{2.33}$$

where λ_i are the eigenvalues of the second order tensor $\mathbf{T}$. This representation is also called *Frobenius Norm* and it is denoted as $\| \mathbf{T} \|_F$. But this is not the unique norm commonly used for second order tensors:

- *Norm-1*: This norm is the maximum absolute column sum and it is defined as:

$$\| \mathbf{T} \|_1 = \max_j \sum_{i=1}^{n} |a_{ij}| \tag{2.34}$$

- *Norm-2* or *spectral norm*: This norm is the square root of the maximum eigenvalue of the symmetric matrix $\mathbf{TT}^T$:

$$\| \mathbf{T} \|_2 = \sqrt{\max_i \lambda_i(\mathbf{TT}^T)} \tag{2.35}$$

- *Norm*-inf: This norm is the maximum absolute row sum and it is defined as:

$$\| \mathbf{T} \|_{\text{inf}} = \max_i \sum_{j=1}^{n} |a_{ij}| \tag{2.36}$$

2.4.3 Tensor Basis

The concept of basis is also important in the context of tensor algebra. In this way, we can define a tensor basis $\{\mathbf{B}_i\}$ as a set of tensors which allow us to represent any other tensor $\mathbf{T}$ as a linear combination of the basis elements, as it is expressed in the following equation:

$$\mathbf{T} = \sum_i c_i \mathbf{B}_i \tag{2.37}$$

where c_i are the coordinates of the tensor $\mathbf{T}$ in the basis $\{\mathbf{B}_i\}$.

The concept of orthonormal basis can also be applied for tensors. In this way, a tensor basis is said orthonormal if it verifies the following property:

$$\mathbf{B}_i \bullet \mathbf{B}_j = \begin{cases} 1 & i = j \\ 0 & i \neq j \end{cases} \tag{2.38}$$

In general, the number of tensors we need to have a basis is equal to the number of independent components of the tensor $\mathbf{T}$. The coefficients c_i are given by the scalar product of the tensor with each element of an orthonormal basis:

$$\mathbf{T} = c_i \mathbf{B}_i \Rightarrow \mathbf{T} \bullet \mathbf{B}_j = c_i \mathbf{B}_i \bullet \mathbf{B}_j = c_i g_{ij} \tag{2.39}$$

Dual Basis

The concept of *dual basis* arises when the basis $\{\mathbf{B}_i\}$ is not orthonormal. In that case, the coordinates of $\mathbf{T}$ have to be computed in terms of the dual basis $\{\hat{\mathbf{B}}_i\}$, which is related to the original basis by the bi-orthogonality condition:

$$\hat{\mathbf{B}}^i \bullet \mathbf{B}_j = \begin{cases} 1 & \text{if} i = j \\ 0 & \text{otherwise} \end{cases} \tag{2.40}$$

The previous condition provide us a closed-form expression to obtain the elements of the dual basis by means of the pseudoinverse:

$$\hat{\mathbf{B}}^i = \sum_k (\mathbf{B}_i \bullet \mathbf{B}_k)^{-1} \mathbf{B}_k \tag{2.41}$$

The concept of dual basis is important whenever a tensor element is decomposed on a tensor basis, as it is done in Eq. 2.37. Then, the coefficients c_i in that equation are always obtained by the inner products of the element $\mathbf{T}$ with the dual basis elements. By symmetry, the coordinates can also be obtained by projecting onto the dual of the dual basis, which is the original basis itself:

$$\mathbf{T} = \sum_k (\hat{\mathbf{B}}_i \bullet \mathbf{T}) \mathbf{B}_i = \sum_k (\mathbf{B}_i \bullet \mathbf{T}) \hat{\mathbf{B}}_i \tag{2.42}$$

However, for an orthonormal basis, the dual basis coincides with the original basis: $\mathbf{B}_i = \hat{\mathbf{B}}_i$.

2.4.4 Outer Product of Vectors

A particular case of second order tensors is that obtained from the outer product of two vectors $\mathbf{u}$ and $\mathbf{v}$:

$$\mathbf{T} = \mathbf{x} \cdot \mathbf{y}^T \tag{2.43}$$

where the superindex T is for the vector transpose.

For this kind of tensors the following property is satisfied:

$$\mathbf{T} = \mathbf{N} \bullet \mathbf{M} = (\mathbf{x}_N \cdot \mathbf{y}_N^T) \bullet (\mathbf{x}_M \cdot \mathbf{y}_M^T) = (\mathbf{x}_N^T \cdot \mathbf{x}_M)(\mathbf{y}_N \cdot \mathbf{y}_M) \tag{2.44}$$

The magnitude of a tensor obtained in this way can be expressed as follows:

$$\| \mathbf{T} \|^2 = \| \mathbf{x} \|^2 \cdot \| \mathbf{y} \|^2 \tag{2.45}$$

A second-order tensor obtained through the outer product of two vectors is called *dyadic tensor* or *polydyadic tensor* if a higher order tensor is obtained through the outer product of tensors of lower rank. In the particular case of second-order tensors, the dyadic tensor of a vector with itself represent projector over the given vector. For instance, a tensor $\mathbf{T}$ can be decomposed into a sum of dyadic tensors associated to the projectors over the principal directions of the tensors, that is, their eigenvectors $\hat{\mathbf{e}}_i$.

$$\mathbf{T} = \sum_{i=1}^{m} \lambda_i \hat{\mathbf{e}}_i \hat{\mathbf{e}}_i^T \tag{2.46}$$

where λ_i are the eigenvalues associated to each eigenvector.

2.4.5 Application of Tensor Signals

In this section we identify several domains of science where tensor signals arise. In general, the use of second order tensors suits whenever the feature to be measured is intrinsically anisotropic, like electrical conductivity, diffusion of particles, etc.

Elasticity

In continuum mechanics there are two tensor magnitudes that are of great importance. The first one is the stress tensor σ^{ij} that measures the internal distribution of force per unit area. The second one is the strain tensor ε_{kl} that measures the deformation per unit

area caused by the action of stress on a physical body. Both tensor fields are linked by the generalized Hooke's law:

$$\sigma^{ij} = c^{ijkl}\varepsilon_{kl} \tag{2.47}$$

where c^{ijkl} is the 4th rank elasticity tensor. Since stress and strain are symmetric tensors ($\sigma^{ij} = \sigma^{ji}$ and $\varepsilon_{kl} = \varepsilon_{lk}$, the elasticity tensor obeys the symmetries $c^{ijkl} = c^{jikl} = c^{ijlk}$. These three tensors completely describe the mechanical properties of the material under study.

Fluid Dynamics

In the field of fluid dynamics tensor information is used to characterize the important fluid flow features such as vortices, separation and shocks. In this context, let us denote by $\mathbf{v}(\mathbf{x}) = [u(\mathbf{x}), v(\mathbf{x}), w(\mathbf{x})]^T$ the velocity vector field that determines the motion of the fluid flow, where $\mathbf{x} \in \mathbb{R}^3$ denotes the spatial coordinates. Then, the spatial gradient of the velocity vector field, also known as *Velocity Gradient Tensor*, contains the information on how the velocity is changing in space and is defined as:

$$\mathbf{V}(\mathbf{x}) = \begin{pmatrix} \frac{\partial u}{\partial \times} & \frac{\partial u}{\partial y} & \frac{\partial u}{\partial z} \\ \frac{\partial v}{\partial \times} & \frac{\partial v}{\partial y} & \frac{\partial v}{\partial z} \\ \frac{\partial w}{\partial \times} & \frac{\partial w}{\partial y} & \frac{\partial w}{\partial z} \end{pmatrix} \tag{2.48}$$

A common practice to identify the relevant features of the fluid flow is to decompose $\mathbf{V}$ into its symmetric and antisymmetric parts, which yields to the definition of the symmetric tensor $\mathbf{V}_S = \frac{1}{2}(\mathbf{V} + \mathbf{V}^T)$ and the antisymmetric tensor $\mathbf{V}_A = \frac{1}{2}(\mathbf{V} - \mathbf{V}^T)$ [Raffel98]. The symmetric part represents the *strain tensor* with the elongational strains on the diagonal and the shearing strains on the off-diagonal, whereas the non-null elements of the antisymmetric part contain the components of the *vorticity* vector, which measures the circulation per unit area of the fluid flow and allow us to detect and measure the strength of vortices [Hunt87].

An eigenanalysis of the velocity gradient tensor is used to classify the local features of the flow pattern [Haimes99]. In general, we can distinguish two general types of flow types characterized by the fact that the 3 eigenvalues of $\mathbf{V}$ are real numbers or only 1 is real and 2 complex conjugate numbers.

The sign of the real eigenvalues indicates whether the flow is accelerating, if it is positive, or decelerating, if it is negative, along the direction determined by the associated eigenvector. The magnitude of the eigenvalues determines the strength. When there is a complex conjugate pair of eigenvalues it indicates that there is a spiral flow. The magnitude of the imaginary part indicates the strength of the spiraling flow. If the value is small the flow is hardly swirling, whereas a big magnitude means that the flow is rotating rapidly about the point. The sign of the real part indicates whether the flow is converging, if it is negative, or diverging, if it is positive, with the magnitude of the real part reflecting the strength of the attraction or repulsion. The special case where the real part is zero, the flow produces concentric periodic paths [Haimes99]

Electromagnetism

Electromagnetism is a field of science where tensors also arise. The *Electromagnetic Tensor* is an antisymmetric 4×4 second order tensor that describes the electric and magnetic fields, yielding to a simplification in notation of the Maxwell equations. It is usually written as:

$$\mathbf{F} = \begin{pmatrix} 0 & \frac{1}{c}e_x & \frac{1}{c}e_y & \frac{1}{c}e_z \\ -\frac{1}{c}e_x & 0 & -b_z & b_z \\ -\frac{1}{c}e_y & b_z & 0 & b_x \\ -\frac{1}{c}e_z & b_y & b_x & 0 \end{pmatrix} \tag{2.49}$$

where $[e_x, e_y, e_z]^T$ are the components of the electric field $\mathbf{e}$, $[b_x, b_y, b_z]^T$ are the components of the magnetic field $\mathbf{b}$ and c is the speed of light. The tensor representation allows us a compact representation of the Maxwell's equations in terms of this tensor and its dual $\mathbf{G}$, which is obtained by replacing the electric components by the magnetic components and viceversa:

$$\frac{\partial f^{\alpha\beta}}{\partial x^{\beta}} = \mu_0 j^{\alpha} \tag{2.50}$$

$$\frac{\partial g^{\alpha\beta}}{\partial x^{\beta}} = 0 \tag{2.51}$$

where α, β denote the indices of the tensor and j^{α} is a four dimensional vector which denotes the current density. Hence, the electromagnetic field tensor not only is a mathematical object to simplify notation, but it also completely describes the inherent electromagnetic field.

2.4.6 Tensor Signal Regularization

As it was seen in the previous section, tensor fields arise in several areas of knowledge. In many cases, raw tensor data are corrupted by noise and specific regularization methods are needed to obtain more coherent diffusion tensor maps. Recently, several methods have been proposed in the literature to regularize second-order symmetric and positive semidefinite tensors, which, broadly speaking, can be divided into two classes.

Non-spectral regularization methods:

- **Smoothing the raw images s_k:** In [Vemuri01], an approach was proposed for direct regularization of the raw images s_k which are used to build the tensors, using a Partial Differential Equation (PDE) scheme that takes into account the coupling between the different channels.

$$\forall k = 0 \ldots n, \quad \frac{\partial s_k}{\partial t} = div\left(\frac{g(\lambda_+, \lambda_-}{\parallel \nabla s_k \parallel} \nabla s_k\right) - \mu(s_k - s_{k_{t=0}}) \tag{2.52}$$

The coupling is done through the two eigenvalues $\lambda_{\pm}$ coming from a first estimation of the diffusion tensors $\mathbf{D}$, with a least square method. After regularization, the tensor field is re-estimated from the regularized version $\tilde{s}_k$, resulting in a smoother version of $\mathbf{D}$.

- **Smoothing as multivalued images:** Another approach, proposed in [Chefd'hotel02, Brox02], is to estimate the tensor field $\mathbf{D} : \Omega \mapsto PS_0^+(n)$ from raw data s_k, then consider it as a multi-valued image with 6 components, that is, the number of different coefficients in a 3×3 matrix. This multivalued image is then processed with classic vector-valued smoothing algorithms such as those proposed, for instance, in [Kimmel00], [Sapiro01] or [Tschumperle03c].

- **Statistical smoothing methods:** Smoothing tensor datasets has also been studied from a statistical point of view. For instance, in [MF04] a Bayesian regularization approach was presented to deal with this problem. The approach uses Markov random field ideas and is based upon the definition of a n-dimensional neighborhood system ($n = 2, 3$) in which the spatial interactions of the tensors are modeled. As for the prior, the behavior of the tensor field is modeled by means of a multidimensional multivariate Gaussian local characteristic. As for the likelihood, the noise process is modeled by means of conditionally independent multidimensional multivariate Gaussian variables. The models include inter-tensor correlations, intra-tensor correlations and colored noise. Finally, the solution tensor field is obtained by using the simulated annealing algorithm to achieve the maximum *a posteriori* estimation.

- **Riemannian smoothing algorithms:** More recently, several algorithms have been proposed in the literature [Pennec05, Castaño06a] which are grounded on the theoretically well-founded differential geometrical properties of the space of multivariate normal distributions, where it is possible to define an affine-invariant Riemannian metric and express statistics on the manifold of symmetric positive definite matrices. From this perspective, an elegant and accurate mathematical framework is provided to deal with tensor signal processing and solves some problems derived from the interpretation of symmetric positive matrices as elements of a vector space, such as the *swelling* effect. In this sense, several approaches have been already proposed. For instance, in [Fletcher04], a statistical analysis of diffusion tensors was proposed based on a Riemannian computational framework or in [Pennec04], where the regularization task was addressed with a Riemannian PDE point of view. In chapter 5 we will study in further detail this approach.

Non-spectral methods cannot have a direct control on the spectral elements of the tensors, which carry the relevant information of the tensor. The use of non-spectral regularization processes, usually leads to an eigenvalue swelling effect due to a different speed of convergence of tensor eigenvectors and eigenvalues [Tschumperlé03].

Spectral regularization methods

The idea behind spectral regularization methods of tensor fields lies in the separate regularization of the tensor eigenvalues and eigenvectors. The smoothing process must also consider the tensor constraints (positivity and symmetry) in the spectral space, which is equivalent to impose that all the eigenvalues remain positive and the eigenvectors remain orthogonal, that is, their scalar product is zero.

Usually, tensor eigenvalues are considered as a multi-channel image with 3 components and can be smoothed by any standard procedure found in the literature [Alvarez94, Weickert99, Charbonnier94]. The positivity constraint of these eigenvalues λ_i is simply ensured by using a scheme that satisfies the maximum and minimum principle [BMtHR94].

The difficult part of the spectral regularization methods come from the regularization of the tensor orientations. In [Coulon01], the authors propose to regularize only the field of the principal eigenvector, using a modified version of the norm constrained Total Variation (TV) Regularization approach, as defined in [Chan99]. Then, the two other tensor directions are rebuilt from the original noisy eigenvectors and the regularized principal component. There are also some authors that argue for the regularization of the complete eigenvector matrix by means of an anisotropic Partial Differential Equation (PDE)-based scheme [Tschumperlé01].

2.4.7 Tensor Signal Visualization

Meaningful visualization of second-order symmetric positive semidefinite tensor fields is challenging because they are multivalued, with complex interrelationships among the values within a single tensor as well as among different tensors. The last decade has seen several approaches to visualize tensor data, most of them based on reducing the dimensionality of the data by extracting relevant information from the tensor [Zhang04]. One possible classification of the different visualization techniques is by the dimensionality to which the tensor is reduced. Another important characteristic is the ability of these algorithms to show local or global information, where global information means the complex spatial relationships of tensors. Our discussion here groups the visualization methods on the basis of these two criteria. Anisotropy indices reduce the 6D information to a scalar value (1D). Volume rendering uses anisotropy indices to define transfer functions that show the anisotropy and shape of the tensor. Tensor glyphs do not reduce the dimensionality of the tensor, instead using visual representations that show the 6D tensor as such; however, these techniques cannot show global information. Vector-field visualization reduces the tensor field to a vector field, and therefore to 3D information at each point. Several techniques can be used for vector-field visualization that show local as well as global information.

Ellipsoids

The natural geometric representation of tensors is by means of ellipsoids, which represent isosurfaces of the related feature under measurement (e.g. diffusion, electrical impedance, strain, etc.). The shape of the ellipsoid is inherently related to the eigenvalues and

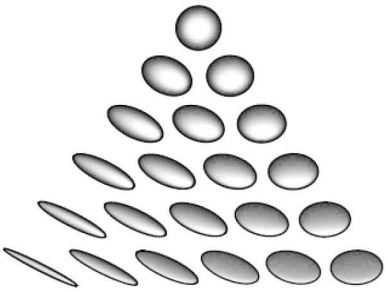

Figure 2.2: Barycentric space of tensor ellipsoids

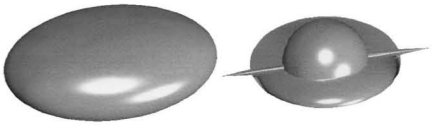

Figure 2.3: Comparison of an ellipsoid and a composite shape depicting the same tensor with eigenvalues $\lambda_1 = 1$, $\lambda_2 = 0.7$ and $\lambda_3 = 0.4$

eigenvectors of the tensor: the three principal radii are proportional to the eigenvalues and the axes of the ellipsoid aligned with the three orthogonal eigenvectors.

Figure 2.2 shows the associated ellipsoids to the tensors, represented as a barycentric space where the corners of a triangle are the three extreme cases: linear, planar, and spherical. The orientation of the ellipsoid axes corresponds to the tensor's eigenvector system, while their length depends on the associated eigenvalues. However, using this representation some ambiguity may be introduced, since it is difficult to distinguish between and edge-on, flat ellipsoid and an oblong one or between a face-on, flat ellipsoid and a sphere one.

To overcome that ambiguity, a new representation was proposed in [Westin97] which is based on the decomposition of the tensor into their linear, planar and spherical components. Figure 2.3 compares the ellipsoidal representation of a tensor with the proposed composite shape. The components are scaled according to the shape measures c_l, c_p and c_s. Additionally, coloring based on these shape measures can be used for visualization. Figure 2.4 shows a coloring scheme where the color is interpolated between the blue linear case, the yellow planar case and the red spherical case.

Scalar Indices

The complexity of a tensor field requires a complicated visualization scheme; however, for end-user applications it is more comfortable to present those data sets as scalar fields on gray-level images slice by slice. Scalar data sets, although limited in the amount of information they can convey, can be visualized with simplicity and clarity and thus interpreted quickly and easily. In this sense, several scalar indices have been designed for a successful visualization of interesting features, which usually complement another

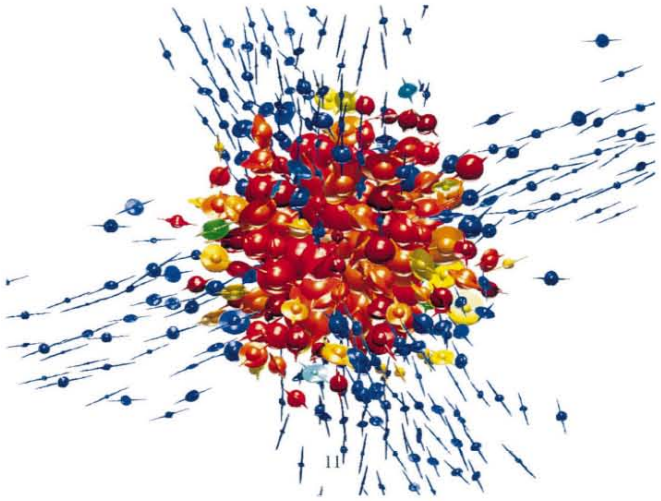

Figure 2.4: Visualization of tensors. The tensors are color coded according to the shape: linear case is blue, planar case is yellow and spherical case is red. The radius of the sphere is the smallest eigenvalue of the tensor; the radius of the disk is second largest and the length of the rod is twice the largest eigenvalue.

visualization technique in order to better present the results [Vilanova05].

The challenges of reducing a tensor measurement to a scalar index include mapping to a meaningful physical quantity, maintaining invariance with respect to rotation and translation, and reducing the effect of noise. Some scalar indices for tensor data are listed in Table 2.1.

Mean Diffusivity (MD), which measures the overall rate, providing the average of the tensor eigenvalues, which is a rotationally invariant magnitude. In [vG94], it was demonstrated that, after a stroke, the trace of the diffusion tensor delineates the affected area much more accurately than the diffusion image in one orientation.

Several different anisotropy indices were used, such as anisotropic diffusion ratio [Douek91]. Unfortunately, these anisotropy indices depend on the choice of laboratory coordinate system and are rotationally variant: their interpretation varies according to the relative orientations of the reference system in the laboratory, usually resulting in an underestimation of the degree of anisotropy [Pierpaoli96a]. Therefore it is important to use rotationally invariant anisotropy indices such as Volume Ratio (VR), Rational Anisotropy (RA) or Fractional Anisotropy (FA), which are based on the rotationally invariant eigenvalues. Note that both RA and FA can be derived from tensor norms and traces without calculating the eigenvalues.

However, rotationally invariant indices such as RA and FA are still susceptible to noise contamination. Also in [Pierpaoli96a] it was proposed the computation of an intervoxel anisotropy index, the Lattice Intex (LI), which locally averages inner products between tensors in neighboring voxels. LI decreases the sensitivity to noise and avoids underestimation of the anisotropy when the neighbor voxels have different orientations.

Because they contract the tensor to one scalar value, FA, RA and LI do not indicate the

Scalar Index	Equations
Mean Diffusivity (MD) ($< d >$)	$\frac{\lambda_1+\lambda_2+\lambda_3}{3}$
Volume Ratio (VR) [Pierpaoli96a]	$\frac{\lambda_1\lambda_2\lambda_3}{\left(\frac{\lambda_1+\lambda_2+\lambda_3}{3}\right)^3}$
Fractional Anisotropy (FA) [Basser96]	$\sqrt{\frac{3}{2}}\frac{\|\mathbf{D}-<d>\mathbf{I}\|}{\|<d>\mathbf{I}\|}$
Lattice Intex (LI)	$\sum_{n=1}^{N} a_n \left(\sqrt{\frac{3}{8}}\frac{\sqrt{<\mathbf{T},\mathbf{T_k}>}}{<\mathbf{D},\mathbf{D_k}>}+\frac{3}{4}\frac{<\mathbf{T},\mathbf{T_k}>}{\sqrt{<\mathbf{D},\mathbf{D}>}\sqrt{<\mathbf{D_k},\mathbf{D_k}>}}\right)$
Linear anisotropy, c_l [Westin97]	$\frac{\lambda_1-\lambda_2}{\lambda_1+\lambda_2+\lambda_3}$
Planar anisotropy, c_p [Westin97]	$\frac{2(\lambda_2-\lambda_3)}{\lambda_1+\lambda_2+\lambda_3}$
Isotropy, c_s [Westin97]	$\frac{3\lambda_3}{\lambda_1+\lambda_2+\lambda_3}$

Table 2.1: Some scalar indices for tensor data. In LI equation, a_k is a spatial mask with sum of coefficients equal to one, and $\mathbf{T}$ is the anisotropic part of the tensor $\mathbf{D}$, which is computed as $\mathbf{T} = \mathbf{D} - \frac{1}{3}trace(\mathbf{D})\mathbf{I}$

directional variation of the anisotropy in a unique sense. For example, a cigar-shaped and a pancake-shaped ellipsoid can have equal FA while their shapes differ greatly. Geometrical measures developed in [Westin97] can be used to overcome these limitations. In this sense, linear anisotropy, c_l, planar anisotropy, c_p and spherical anisotropy or isotropy, c_s can be used to introduce color in the images, as it was already presented in Fig. 2.4, overcoming such ambiguities. These three metrics parameterize a barycentric space in which the three shape extremes (linear, planar, and spherical) are at the corners of a triangle, in a similar way as it is done in Fig. 2.2. It is worth noting that, unlike FA or RA, geometrical metrics depend on the order of the eigenvalues and are thus prone to bias in the presence of noise [Pierpaoli96a].

Figure 2.5 shows one way to compare qualitatively some of the metrics described above by sampling their values on a slice of a DT-MRI data set of a brain. Notice that the MD is effective at distinguishing between cerebrospinal fluid (where MD is high) and brain tissue (lower MD), but fails to differentiate between different kinds of brain tissue. High fractional anisotropy, FA, on the other hand, indicates white matter, because the directionality of the axon bundles permits faster diffusion along the neuron fiber orientation than across it. FA is highest inside thick regions of uniformly anisotropic diffusion, such as inside the corpus callosum. Finally, while both c_l and c_p indicate high anisotropy, their relative values indicate the shape of the diffusion ellipsoids with a color coding different from the one used in 2.4.

Vector Field Visualization

The tensor field can also be simplified to a vector field defined by the main eigenvector, $\mathbf{u_1}$. This simplification is based on the assumption that in the areas of linear anisotropy, $\mathbf{u_1}$ defines the orientation of linear structures. The sign of $\mathbf{u_1}$ has no meaning.

One commonly used method to visualize tensor data is to map $\mathbf{u_1}$ to color, e.g., directly using the absolute value of the $\mathbf{u_1}$ components for the Read Green Blue (RGB) channel: $R =\mid \mathbf{e_1^T} \cdot \mathbf{x} \mid$, $G =\mid \mathbf{e_1^T} \cdot \mathbf{y} \mid$ and $B =\mid \mathbf{e_1^T} \cdot \mathbf{z} \mid$. The saturation of this color is weighted by

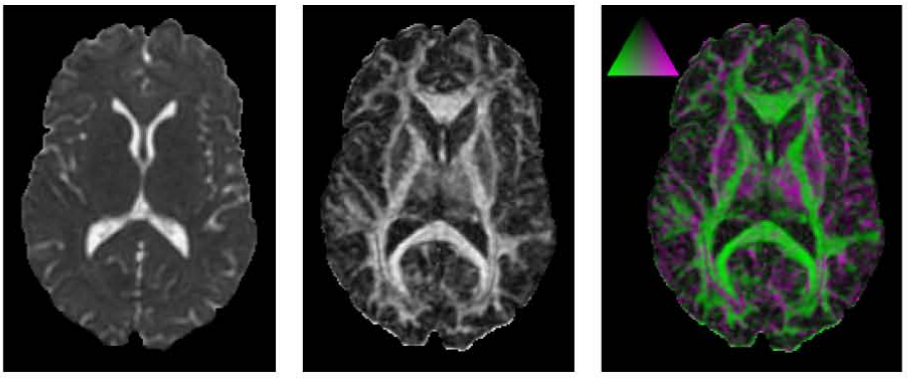

Figure 2.5: Shape metrics applied to one slice of a brain DT-MRI scan. Left: Mean Diffusion (MD). Middle: Fractional Anisotropy (FA). Right: Geometrical representation: $c_l green$ and c_p magenta.

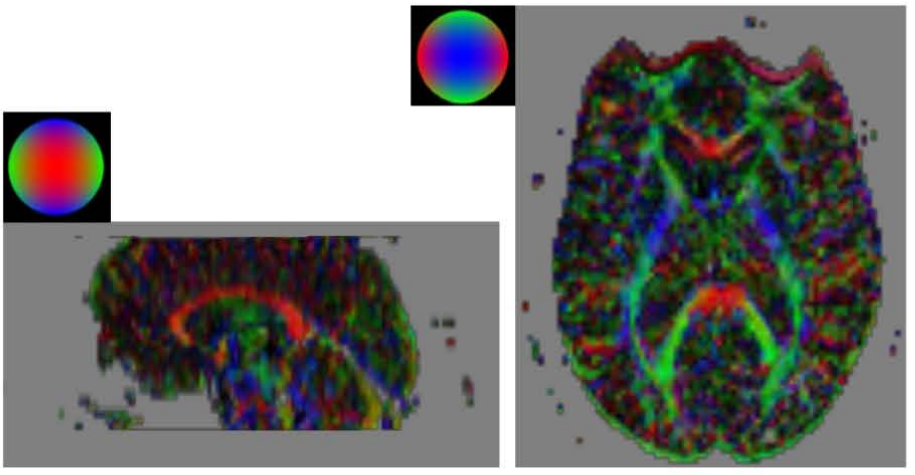

Figure 2.6: Mapping of $\mathbf{e_1}$ to the RGB channel shown in 2D slices of a human brain.

an anisotropy index to de-emphasize isotropic areas, as shown in Fig. 2.6 in the particular application of DT-MRI data visualization.

Tensor Glyphs

Another avenue of tensor visualization has focused on using tensor glyphs to visualize the complete tensor information at one point. A tensor glyph is a parameterized graphical object that describes a single tensor with its size, shape, color, texture, location, etc. Most tensor glyphs have six or more degrees of freedom and can represent a tensor completely. However, tensor glyphs do not expose relationships and features across a tensor field; rather, they imply these relationships from the visual correlation and features of the individual glyphs. While exploiting many different types of tensor glyphs, from boxes to ellipsoids to superquadrics, tensor glyph designers aim to make the mapping between glyphs and tensors faithful, meaningful and explicit.

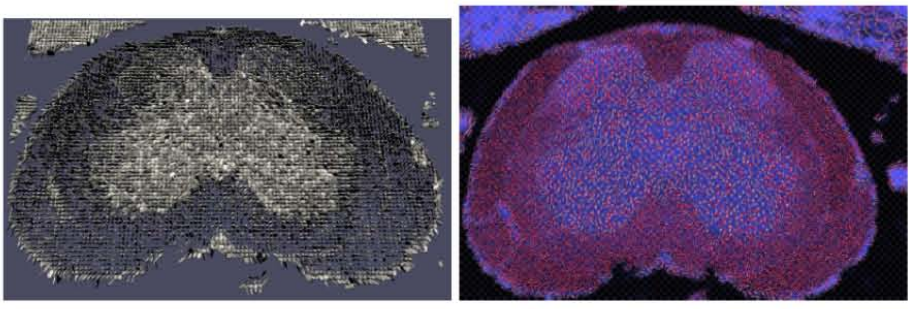

Figure 2.7: Left: Arrays of normalized ellipsoids show the tensors in a single slice. Right: Brush strokes illustrate the orientation and magnitude of the tensors: background color and texture-map show additional information.

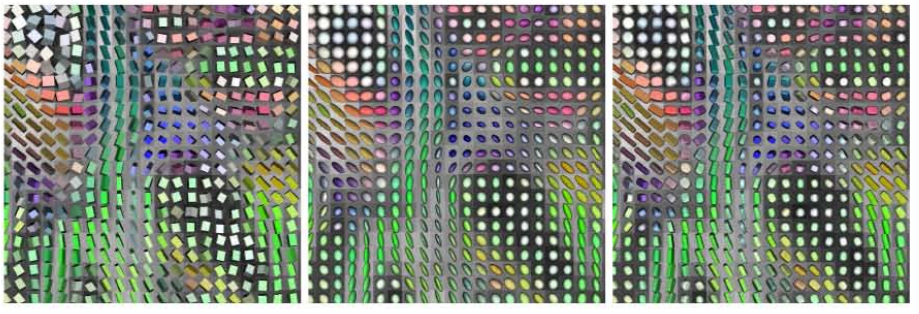

Figure 2.8: A portion of a brain DT-MRI scan visualization with three different glyph methods. Left: Using boxes. Middle: Using ellipsoids. Right: Using Superquadrics.

Ellipsoids are the most commonly used representation for tensors. In the first use of ellipsoids as tensor glyphs, the size of the ellipsoids was associated with the mean of the tensor eigenvalues. Arrays of ellipsoids were arranged together in the same order as the data points to show a 2D slice of tensor data [Pierpaoli96a]. The normalization of the size of the ellipsoids to fit more of them in a single image was proposed in [Laidlaw98] (see left side of Fig. 2.7). In the context of DT-MRI visualization, this method creates more uniform glyphs that show anatomy and pathology over regions better than the non-normalized ellipsoids.

A different method also proposed in [Laidlaw98] uses the concepts of brush strokes and layering from oil painting to emphasize the signal patterns. They used 2D brush strokes both individually, to encode specific values, and collectively, to show spatial connections and to generate texture and a sense of speed corresponding to the magnitude of tensors. They also used layering and contrast to create depth. An example of this visualization technique can be seen in right side of Fig. 2.7, where it was applied to visualize spinal cords of mice with Experimental Allergic Encephalomyelitis (EAE).

Boxes and cylinders have also been used to show the directions and relative lengths of all three eigenvectors. Boxes clearly indicate the orientation of the eigenvectors. They also have fewer polygons and are thus faster to render. But their flat faces usually make it hard to infer the 3D shapes from a 2D image, as shown in Fig. 2.8.

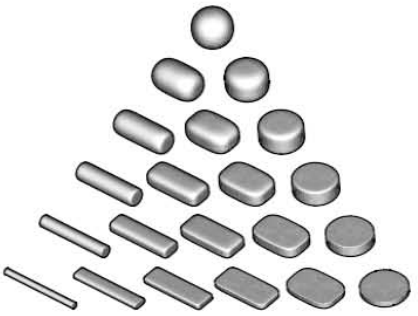

Figure 2.9: Superquadrics as tensor glyphs, sampling the same barycentric space as in Fig. 2.2

Superquadrics, a traditional surface modeling technique, was also adapted to generate tensor glyphs in [Kindlmann04]. The class of shapes created by this technique includes spheres in the isotropic case, while emphasizing the differences among the eigenvalues in the anisotropic cases. As shown in figure 2.9, cylinders are used for linear and planar anisotropy and intermediate forms of anisotropy are represented by approximations to boxes. As with ellipsoid glyphs, a circular cross-section accompanies equal eigenvalues, for which distinct eigenvectors are not defined.

The differences among some of the glyph methods can be appreciated by comparing their results on a portion of a slice of a DT-MRI brain scan, as shown in Fig. 2.8. The individual glyphs have been colored with the principal eigenvector colormap. The directional cue given by the edges of box glyphs (left image in Fig. 2.8) is effective in linearly anisotropic regions, but can be misleading in regions of planar anisotropy and isotropy, since in these cases the corresponding eigenvectors are not well defined numerically. The rotational symmetry of ellipsoid glyphs (middle image in Fig. 2.8) avoids misleading depictions of orientation, with the drawback that different shapes can be difficult to distinguish. The superquadric glyphs (right image in Fig. 2.8) aim to combine the best of the box and ellipsoid methods.

2.5 Medical Imaging

Medical Imaging is the process by which physicians evaluate an area of the subject's body that is not externally visible. The goal is to facilitate doctors to do their job providing them with additional information to diagnose, to examine the evolution of diseases in specific human patients or to understand processes in living organisms. Before the development of several imaging modalities, the only choice for doctors (appart from invasive techniques) was simply feeling an area of the body in order to imagine the condition of internal organs. Fortunately for patients, this subjective methodology has been removed by medical imaging, which provides a more objective vision of the reality. It can be said, then, that medical imaging is the art by which physicians see where human eye cannot.

A big part of the success of this relatively new branch of medicine is due to the development of computer science, which provides more sophisticated and powerfull

computers that can handle huge amounts of information in a short period of time. In fact, a major milestone in medical imaging history is the introduction of Analog to Digital (A/D) converters adapted to conventional fluoroscopic image intensifiers and Television (TV) systems in the 1970's. Then, the analog signal from imaging systems could be converted to a digital picture which could be enhanced for clearer diagnosis and also digitally stored for future reviews. In this sense, computers become an usual tool of doctors, helping them to better detect or diagnose any disease.

Since that moment, a lot of research is done in order to develop better and better algorithms to deal with digital medical datasets. Moreover, as long as algorithms become more sophisticated, also new medical applications and needs arise. For instance, data is presented to doctors depicted with different colors depending on the tissue properties or on the organs shown in the image which is done by means of accurate segmentation approaches that have been developed first. Another example is motivated by the fact that usually doctors need to compare two images of the same patient but they are taken with a different reference system which may lead to a misinterpretation. This issue motivated the development of registration algorithms. Similar examples also motivated the development of other signal processing techniques, such as data fusion, classification, transformations, edition, etc.

Thus, the main advantage of medical imaging techniques is the fact that they provide a non-invasive diagnosis method which provides objective information about the disease under evaluation, which reduces the probability of symptoms misinterpretation, reducing also time and resources. In addition, digital images can be wisely archived onto compact optical disks or digital tape drives saving tremendously on storage space and manpower. Also, digital images can be sent via network to other workstations so that other specialists can share the information and assist in the diagnosis or used as learning tools for medicine students.

Due to the numerous advantages of medical imaging, a lot of research is done in this field yielding continuously to new applications and specific imaging modalities with specific requirements. The following section presents an enumeration of the most important medical imaging modalities in order to obtain an idea of the physical principle in which they are based on. Then, section 2.6 presents a detailed description of diffusion tensor magnetic resonance imaging DT-MRI, the medical imaging modality we are interested in.

Medical Imaging Modalities

- **X-rays:** X-rays are a type of electromagnetic radiation with wavelengths of around 10^{-10} meter. When medical X-rays are being produced, a thin metallic sheet (usually tungsten, but sometimes molybdenum) is placed between the emitter and the target, effectively filtering out the lower energy (soft) X-rays. The resultant X-ray is said to be hard. The basic production of X-rays is by accelerating electrons in order to collide with the metallic sheet. Here the electrons suddenly decelerate upon colliding with the metal target and if enough energy is contained within the electron it is able to knock out an electron from the inner shell of the metal atom and as a result electrons from higher energy levels then fill up the vacancy and X-ray photons are emitted.

Diagnostic radiography involves the use of both ionizing radiation and non-ionizing radiation to create images for medical diagnoses. This application is known as diagnostic radiography. Since the human body is made up of various substances with differing densities, X-rays can be used to reveal the internal structure of the body on film by highlighting these differences using attenuation, or the absorption of X-ray photons by the denser substances (like calcium-rich bones).

- **Computed tomography:** Computed Tomography (CT), originally known as Computed Axial Tomography (CAT) and body section roentgenography, is a medical imaging method employing tomography where digital geometry processing is used to generate a three-dimensional image of the internals of an object from a large series of two-dimensional X-ray images taken around a single axis of rotation. The word *tomography* is derived from the Greek *tomos* (slice) and *graphia* (describing). CT produces a volume of data which can be manipulated, through a process known as windowing, in order to demonstrate various structures based on their ability to block the x-ray beam. Although historically the images generated were in the axial or transverse plane (orthogonal to the long axis of the body), modern scanners allow this volume of data to be reformatted in various planes or even as volumetric 3D representations of structures. Although most common in healthcare, CT is also used in other fields, e.g. nondestructive materials testing.

- **Ultrasound:** Medical ultrasonography uses high frequency sound waves of between 2.0 to 10.0 MHz that are reflected by tissue to varying degrees to produce a 2D image, traditionally on a TV monitor. This is often used to visualize the fetus in pregnant women. Other important uses include imaging the abdominal organs, heart, male genitalia and the veins of the leg. While it may provide less anatomical information than techniques such as CT or Magnetic Resonance Imaging (MRI), it has several advantages which make it ideal as a first line test in numerous situations, in particular that it studies the function of moving structures in real-time. It is also very safe to use, as the patient is not exposed to radiation and the ultrasound does not appear to cause any adverse effects, although information on this is not well documented. It is also relatively cheap and quick to perform. Ultrasound scanners can be taken to critically ill patients in intensive care units saving the danger of moving the patient to the radiology department. The real time moving image obtained can be used to guide drainage and biopsy procedures. Doppler capabilities on modern scanners allow the blood flow in arteries and veins to be assessed.

- **Magnetic Resonance Imaging:** Magnetic Resonance Imaging (MRI), formerly referred to as Magnetic Resonance Tomography (MRT) or Nuclear Magnetic Resonance (NMR), is a method used to visualize the inside of living organisms as well as to detect the composition of geological structures. It is primarily used to demonstrate pathological or other physiological alterations of living tissues and is a commonly used form of medical imaging. MRI has also found many novel applications outside of the medical and biological fields such as rock permeability to hydrocarbons and certain non-destructive testing methods such as produce and timber quality characterization.

  MRI uses powerful magnets to excite hydrogen nuclei in water molecules in human

tissue, producing a detectable signal. Like a CT scan, an MRI traditionally creates a 2D image of a thin slice of the body. The difference between a CT image and an MRI image is in the details. X-rays must be blocked by some form of dense tissue to create an image, therefore the image quality when looking at soft tissues will be poor. An MRI scan is only sensitive to hydrogen based objects, so bone, which is calcium based, will be a void in the image, and will not affect soft tissue views. This makes it excellent for peering into joints. As an MRI does not use ionizing radiation, it is the preferred imaging method for children and pregnant women.

In the next section we will focus on a particular imaging modality based on Magnetic Resonance Imaging (MRI), which is called Diffusion Tensor Magnetic Resonance Imaging (DT-MRI). In this thesis, we use this imaging modality as proof-of-concept for the new schemes for tensor signal processing presented here.

2.6 Diffusion Tensor Magnetic Resonance Imaging

Diffusion Tensor Magnetic Resonance Imaging (DT-MRI) is a medical imaging modality developed in the mid- to late-1990s, based on MRI which allows us to visualize the nerve fiber tracts within the white matter of the brain. The underlying physical phenomenon is based on the diffusion of water molecules in the white matter, which mainly takes place along nerve fiber tracts since they are as natural barriers for their motion. These measures are commonly used clinically to localize white matter lesions that do not show up on other forms of clinical MRI.

In the same way that temperature is a scalar magnitude, diffusion is a tensor magnitude that can be codified by a second-order symmetric semidefinite tensor whose eigenvalues determine the amount of diffusion that takes place along the associated eigenvector. Hence, the measurement of tensor signals requires the estimation of all tensor components yielding to sophisticated procedures. Next, we describe the data acquisition protocol and some important medical applications for this imaging modality.

2.6.1 Data Acquisition

The data acquisition process is based on the measurement of water molecules diffusion in several directions $\mathbf{g_k}$. To that task, the Stejskal-Tanner imaging sequence is used [Stejskal65]. This sequence uses two strong gradient pulses, symmetrically positioned around a 180^0 refocusing pulse, allowing for controlled diffusion weighting (Fig. 2.10). The first gradient pulse will invert this phase shift, thus canceling the phase shift for static spins. Spins having completed a change of location due to Brownian Motion during the time period (Δ in Fig. 2.10) will experience different phase shifts by the two gradient pulses, which means they are not completely refocused and consequently will result in a signal loss.

To eliminate the dependence of spin density, T1, and T2 we must take at least two measurements of diffusion-weighted images that are differently sensitized to diffusion but remain identical in all other respects. By using, for instance, a measurement without

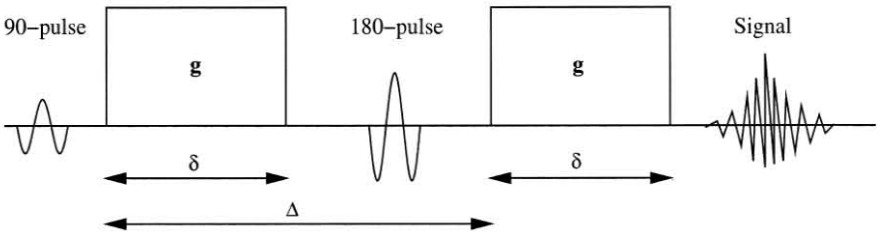

Figure 2.10: Stejskal-Tanner imaging sequence

diffusion weighting and with diffusion weighting, diffusion can be calculated using the following equation [Stejskal65]:

$$s = s_0 e^{-bD}, \tag{2.53}$$

where b is the diffusion weighting factor, introduced and defined in [Bihan86] is computed as follows:

$$b = \gamma^2 \delta^2 (\Delta - \frac{\delta}{3}) \parallel \mathbf{g} \parallel \tag{2.54}$$

where γ is the proton gyromagnetic ratio (42 MHz/Tesla), $\parallel \mathbf{g} \parallel$ is the strength of the diffusion sensitizing gradient pulses, δ is the duration of the diffusion gradient pulses, and Δ is the time between diffusion gradient Radio Frequency (RF) pulses. The diffusion values, D, are also known as Apparent Diffusion Coefficients (ADC), which emphasizes the fact that the diffusion values generated from this procedure depend on the experimental conditions such as the direction of the sensitizing gradient and other sequence parameters (δ and Δ).

For the case of anisotropic diffusion, Eq. 2.53 has to be rewritten in a more general form:

$$s = s_0 e^{-b\hat{\mathbf{g}}_\mathbf{k}^T \mathbf{D} \hat{\mathbf{g}}_\mathbf{k}} \tag{2.55}$$

where $\mathbf{D}$ is the diffusion tensor we want to measure, $\hat{\mathbf{g}}_\mathbf{k} \in \mathbb{R}^3$ is the normalized gradient vector whose coordinates represent the pulse gradient direction/magnitude, used for the acquisition of the volume s_k.

Estimating a field of 3×3 diffusion tensors (symmetric and positive-definite matrices) requires at least six measurements taken from different non-collinear gradient directions appart form the baseline image data s_0 in absence of a diffusion-sensitizing field gradient, since the diffusion tensor $\mathbf{D}$ has six degrees of freedom, that is, six independent coefficients in a matrix representation. Hence, the computation of the diffusion tensor requires solving 2.55 system of equations for each voxel. Classical methods for computing that tensor $\mathbf{D}$ from the images s_k are as follows:

- **Direct tensor estimation:** Authors in [Westin02b, Westin02a] proposed an elegant closed-form to estimate the tensors $\mathbf{D}$ directly from a set of 7 raw images. Their method is based on the decomposition of $\mathbf{D}$ into a specific orthonormal tensor basis $\tilde{\mathbf{g}}_\mathbf{k}\tilde{\mathbf{g}}_\mathbf{k}^T$ computed as the dual basis of $\{\mathbf{g}_k\mathbf{g}_k^T \mid k = 1..6\}$, the original basis used for the measurement of the s_k:

$$\mathbf{D} = \sum_{k=1}^{6} \ln\left(\frac{s_0}{s_k}\right) \tilde{\mathbf{g}}_\mathbf{k}\tilde{\mathbf{g}}_\mathbf{k}^T \tag{2.56}$$

  With this method, only 7 images s_0, ..., s_6 can be used to estimate the tensor field $\mathbf{D}$. However, this low number of images may be not sufficient for a robust estimation of $\mathbf{D}$ especially if the s_k are corrupted with noise.

- **Least Squares (LS) estimation:** It is the most classical method used for diffusion tensor computation [Basser94a, Poupon99]. The tensors $\mathbf{D}$ are estimated by solving the following least square criterion,

$$\min_{\mathbf{D}\in\mathcal{M}_3} \sum_{k=1}^{n} \left(\ln\left(\frac{s_0}{s_k}\right) - \mathbf{g}_k^T\mathbf{D}\mathbf{g}_k\right)^2 \tag{2.57}$$

  which leads to the resolution of an overconstrained system $\mathbf{Ax} = \mathbf{b}$ (where $\mathbf{x}$ is a vector containing the six unknown coefficients of $\mathbf{D}$).

  The Least Squares (LS) method is more robust, since all the n available raw images s_k (usually $n > 7$) are used for the tensor estimation.

  Note that both methods do not take the prior positive-definiteness constraint of the tensors $\mathbf{D}$ into account. For the case of noisy raw images, nothing prevents the estimation process to compute *negative tensors*. Practically, one solution could be to reproject the negative tensors into the positive tensor space after such estimation method. This is generally done by forcing negative eigenvalues of the tensors to zero.

- **Variational approaches:** In [Tschumperlé03b], it has been proposed a technique to avoid these important drawbacks by using a variational approach that estimates the tensor field $\mathbf{D}$ while introducing important priors on the *tensor positivity* and *regularity*. The idea is based on the *positive-constrained minimization* of the following functional:

$$\min_{\mathbf{D}\in PS_0^+(3)} \int_\Omega \sum_{k=1}^{n} \psi\left(\left|\ln\left(\frac{s_0}{s_k}\right) - \mathbf{g}_k^T\mathbf{D}\mathbf{g}_k\right|\right) + \alpha\,\phi(\|\nabla\mathbf{D}\|_F)\,d\Omega \tag{2.58}$$

  where $\psi : \mathbb{R} \to \mathbb{R}$ is a function allowing a robust tensor estimation, $\phi : \mathbb{R} \to \mathbb{R}$ is an increasing function acting as an anisotropic regularization term of the tensor field, $\alpha \in \mathbb{R}$ is a user-defined regularization weight and $\|\nabla\mathbf{D}\|_F = (\sum_{i,j} \|\nabla d_{i,j}\|^2)^{\frac{1}{2}}$ stands for the classical Frobenius matrix norm.

  Note that if $\psi(s) = s^2$ and $\alpha = 0$, we minimize the LS criterion presented in Eq. 2.57, but with a positive solution since our minimization is done on the constrained

space $PS_0^+(3)$ of the positive semidefinite tensors. This task is done through a gradient descent algorithm that ensures the positive-semidefiniteness of the tensors $\mathbf{D}$ for each iteration of the estimation process. Moreover, the regularization term α introduces *spatial regularity* on the estimated tensor field, while preserving important physiological discontinuities, thanks to the anisotropic behavior of the ϕ-function regularization formulation [Alvarez92, Sapiro01, Weickert98].

A related variational approach for tensor estimation has also been proposed in [Wang03]. But the proposed method does not deal with various estimation and regularization functionals.

- **Riemannian Approach:** In [Lenglet05a], a new approach to estimate the diffusion tensors has been proposed. The idea is to minimize a functional of the linearized Stejskal-Tanner equation (Eq. 2.55) by evolving an initial guess of the tensor on the manifold of symmetric positive definite matrices. The special feature of this approach is that the minimization is achieved taking into account the algebraical structure of that manifold, which yields to the definition of a Riemannian metric which modifies the computation of distances, as we will study in chapter 5. Hence, to minimize the functional proposed in [Lenglet05a], a robust gradient descent algorithm similar to the one defined in section 5.4.1 has been defined.

2.6.2 DT-MRI Applications

Diffusion Tensor Magnetic Resonance Imaging has proven to be a quite interesting imaging modality with applications in many medical domains, specially in neuroscience [Bihan01]. In this section we detail some of the most important applications.

Tractography

The main idea on which rely most classical algorithms for brain connectivity mapping [Mori99, Moseley99, Pierpaoli96b] and references therein) is that, despite the potentially multi-directional environment within a voxel, water diffusion in many regions of the white matter is highly anisotropic and thus, within the limits imposed by the Gaussianity assumption, the orientation of the major eigenvector aligns with the predominant axon's direction. It is then safe to say that we should be able to identify macroscopical three-dimensional architectures of the white matter by using simple line propagation techniques. These local approaches provide fast algorithms to estimate 3D curves, more or less accurately, by integration of the major eigenvector field. Euler or higher-order Runge-Kutta schemes are typically used with intravoxel interpolation of the diffusion tensor field to achieve subvoxel accuracy and reconstruct smooth and more precise curves. By taking into account the anisotropy information in the interpolation process, dynamically adjusting the time step (in high curvature regions for example) or constraining the angle between successive steps, various studies have shown coherent results for known anatomical regions.

All these approaches however fails to recover fibers bundles whenever they enter a region of low anisotropy. The estimate of the curve tangent becomes highly unreliable and Lazar et al. [Lazar03] proposed a method based on diffusion equations and

making use of the whole diffusion tensor in order to propagate in the most coherent fashion without getting stopped by locally isotropic regions. Well known structures such as the corpus callosum, the external capsule or cortico-spinal tracts can easily be identified using this technique. These algorithms have been augmented to incorporate some natural constraints such as regularity, stochastic behavior or local non-Gaussianity [Basser00, Campbell03, Parker03].

To better describe the complexity of the diffusion profile, high angular resolution Diffusion Weighted Imaging (DWI) [Tuch02b, Frank02] or q-space and Diffusion Spectrum Imaging [Tuch01, Lin03] have been proposed but still yield long acquisition times. Finally more global algorithms [Cicarelli03] have been introduced to better handle situations of false planar or spherical tensors (with underlying fibers crossings) or fascicles junctions [Poupon00] using some a priori knowledge of the low curvature of most of the fascicles.

More global algorithms have been proposed to better handle the situations of false planar or spherical tensors (with underlying fibers crossings) and to propose some sort of likelihood of connection. However, they either make use of the major eigenvector field [Parker02, Cicarelli03] or consider the evolution of a front in an Euclidean space while adapting its speed through the use of the complete diffusion tensor [O'Donnell02]. In this last attempt, the diffusion tensor is used to compute the metric of a Riemannian manifold but the geometry of that manifold was not exploited.

Inference of Conductivity Properties

Knowledge of electrical conductivity properties of nerves and muscles is essential if we want to establish a link between the electromagnetic fields generated by those tissues and the underlying electro-physiological currents used to mediate communications. Indeed, magneto-encephalography measure magnetic fields from which the tridimensional spatial distribution of currents can be inferred by inversion of a direct model. This process is referred to as Electromagnetic Source Imaging (ESI) and requires solving the quasi-static Maxwell equations in a resistor model. However, precision of the reconstruction is highly dependent on the precision of the conductivity estimation.

State of the art formalisms have been described for relating the effective electrical conductivity tensor of white matter tissue to the effective water diffusion tensor as measured by Diffusion tensor magnetic resonance imaging (DT-MRI) [Basser94b, Tuch01]. Basser et al. first proposed in 1994 to infer the conductivity tensor from the diffusion tensor through the use of constraints imposed by the tissues geometry. More recently, Tuch et al., based on the works [Torquato90, Torquato02] showed a strong linear relationship between the eigenvalues of the two tensors, supported by reports exhibiting comparable anisotropy of the two tensors in the white matter. Also, recent studies showed that skull and white matter conductivity anisotropy have an influence on the forward solutions for Electro-EncephaloGraphy (EEG) and Magneto-ElectroencephaloGraphy (MEG) [Haueisen02, Wolters01] as well the inverse problem in EEG/ MEG source localization [Anwander02].

Other Medical Applications

DT-MRI is particularly relevant to a wide range of clinical pathologies investigations. One of the most successful clinical applications of DT-MRI since the early 1990s has been acute brain ischemia detection [Albers00, Baird98, Sotak02], but many other potential applications like stroke, Alzheimer's disease, schizophrenia [Ardekani03] can be foreseen. Other potentially important applications of DT-MRI include characterization of cardiac muscle tissue architecture, [Reese95] liver disease diagnosis, [Muller94], temperature mapping. [Bihan89], electrical impedance tomography. The interested reader is referred to [Horsfield02] for a further reading on the current applications of diffusion-weighted and DT-MRI in diseases of the brain white matter.

A domain of major interest is that of brain surgery. Without a *prior* knowledge irreversible alterations to important fiber bundles may be caused. On the contrary, knowledge of their position and extension could minimize functional damage to the patient [Talos03]. The information provided by this imaging modality is of great help to recover the neural connectivity in the human brain, leading to a better understanding of how brain areas communicate as part of a distributed network [Tuch02a, Tuch02b, Vemuri01, Campbell03]. As of today, DT-MRI is the only non-invasive method that allows us to distinguish the various anatomical structures of the cerebral white matter such as the *corpus callosum*, the *arcuate fasciculus* or the *corona radiata*, which are examples of commisural, associative and projective neural pathways, the three major types of fiber bundles.

Chapter 3

A New Approach for Anisotropic Signal Processing

3.1 Introduction

Conventional isotropic signal processing systems present the disadvantage that borders and other important features are either blurred or delocalized. To overcome these effects, anisotropic systems have been developed. The idea behind these systems is to wisely combine information about the way the signal varies and introduce it into the processing system to discriminate among orientations. This idea, which seems very simple at a first glance, requires a lot of care when trying to put it into practice. The literature shows different approaches based either on linear filters [Geusebroek03], PDEs [Perona90] or more sophisticated methods [RF03].

In the context of image processing, the standard operator to measure the spatial signal variation is the gradient, which indicates the direction of maximum signal variation. However, as we show in section 3.2, the gradient presents some limitations as a descriptor for local structure [Knutsson03b, RF01]. Hence, to overcome those limitations Knutsson introduced the requirements of a robust descriptor of local structure, introducing the use of second-order tensors [Knutsson89]. The basic idea is to represent the signal orientation at a given scale by a symmetric Positive Semi-Definite (PSD) second order tensor, called Local Structure Tensor (LST). Tensors, besides allowing a compact representation, have a solid mathematical body that supports further analysis.

After that groundwork, a lot of research has been done on this topic yielding to different methods to estimate the LST [Bigün87]. Moreover, this image processing tool has been applied to numerous image processing techniques such as filtering [Westin94], segmentation [Rousson04], registration [SS03] or optic flow estimation [Farnebäck02].

In this chapter we investigate new techniques to exploit the information given by the local structure tensor in order to derive anisotropic signal processing systems for general purposes. In this sense, we perform a detailed description of the methods proposed in the literature to estimate the LST from data in section 3.3, including nonlinear counterparts.

Furthermore, in section 3.3.4, we also study the robustness of these estimation methods with respect to the noise and their influence on structure delocalization.

Then, in section 3.4 we present a processing framework to derive anisotropic signal processing systems. It is remarkable that the ideas behind our approach are quite general and, hence, they can be particularized for any kind of anisotropic signal processing technique. In this sense, we also particularize our approach for different application purposes.

First, we use the local structure tensor to compute a local neighborhood around a given sample. In this way, in homogeneous areas we will obtain isotropic neighborhoods, while near main structures the neighborhood will be extended along the edges. We illustrate this idea in section 3.4.2 for the specific application of anisotropic Gaussian smoothing, where in addition, the local structure tensor is used to model the shape of the Gaussian distribution.

Our second algorithm is described in section 3.4.3 for the specific application of anisotropic interpolation, which is normally performed by weighting local signal samples according to some rule (linear, cubic, etc.). The idea behind this approach is to weigh the samples in the direction of maximum variation (e.g. across and edge) less than in the orthogonal direction (e.g. along the edge) in order to reduce inter-region blurring. In our scheme this is achieved by using adaptive neighborhoods and a metric defined from the local structure tensor.

Finally, we also propose in section 3.4.4 the use of the information provided by the local structure tensor to build an anisotropic estimator of the covariance estructure of the signal, yielding to anisotropic versions of traditional statistically optimal estimators, such as the well-known Wiener filter.

In section 3.5, we present the necessary steps to generalize this approach to deal with multivalued datasets, such as vector or tensor signals. This generalization basically relies on the definition of a spatial local structure tensor for matrix-valued datasets. Moreover, since weights are naturally constrained to be positive, if the tensors in the input tensor field are PSD, the system response will be PSD as well. It is important to note that this idea can be extended to more general anisotropic tensor estimation problems. Finally, we present in section 3.6 the results we have obtained in our experiments for both, scalar and tensor valued datasets. We conclude this chapter with the main conclusions obtained from our work.

3.1.1 Contributions in this Chapter

- *A New Approach to Anisotropic Signal Processing (Section 3.4):* In this section we present a new approach to derive adaptive neighborhoods for anisotropic signal processing systems. The idea behind is to wisely adapt the local neighborhood used to perform the estimation depending on the information provided by the local structure tensor by means of the ellipsoid associated to that positive semidefinite matrix.

- *Comparison of the local structure tensor estimation methods (Section 3.3.4):* Since the estimation methods do not provide an equal response, we have studied the

structure delocalization effect in order to choose the most robust method in our approach, including the so-called *nonlinear structure tensors* recently presented and applied to the Knutsson's formulation.

- *Anisotropic Gaussian Smoothing (Section 3.4.2):* We derived an adaptive anisotropic gaussian filtering scheme to reduce noise in scalar images, where the shape of the Gaussian kernel is modeled by the local structure tensor.

- *Anisotropic Interpolation (Section 3.4.3):* We derived an adaptive anisotropic interpolation scheme to upsample scalar images. Appart from the use of the local structure tensor to compute the local neighborhood, we use it as a metric tensor to measure distances between samples. The effect is that samples found in the same direction of the maximum signal variation seem to be further, while those in the direction of minimal signal variation seem to be closer.

- *Covariance-based Anisotropic Structure Estimation (Section 3.4.4):* We also used the information provided by the local structure tensor to build an anisotropic estimator of the covariance estructure of the signal. This formulation leads to the development of anisotropic versions of traditional statistically optimal estimators, such as the well-known Wiener filter.

- *Generalization for Tensor Data (Section 3.5):* Finally we generalized all the previous approaches for tensor-valued datasets by means of the generalization of the local structure tensor. An interesting characteristic on the generalization for tensor data is that our approach naturally provides a PSD response, since the response is given by a linear combination of PSD matrices with positive coefficients.

3.2 Local Structure in Multidimensional Signals

In order to be able to design anisotropic processing systems it is mandatory to use a measure to quantify local structure of multidimensional signals. We understand by *local structure* the set of all the meaningful features of a multidimensional signal. At a coarse scale and for sufficiently small regions, the meaningful features of a multidimensional signal can be approximated to one-dimensional signals, where only a dominant orientation of signal variation is present. In this case, it is said that the region is intrinsically one-dimensional.

The measurement of the local structure is still a matter of discussion, although several methods have been proposed in the literature, such as those based on the gradient computation or those based on local energy. Next, we are going to study the advantages and limitations of both descriptors.

3.2.1 Local Structure Measurement

The gradient is a common descriptor for local structure widely used in computer vision and image processing. The gradient of a scalar field provides a vector field that determines the direction and magnitude of local maximum signal variation. The components of the

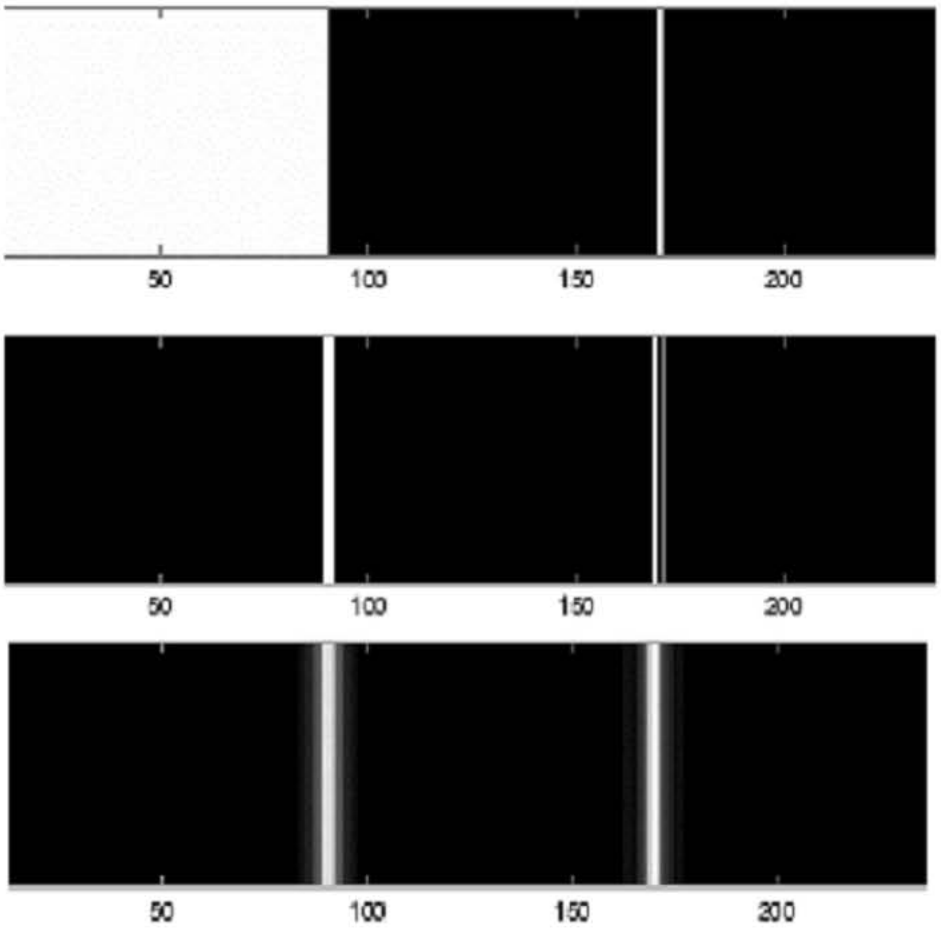

Figure 3.1: Top Row: Synthetic Signal with a step border and a line. Middle Row: Gradient Magnitude of the signal. Bottom Row: Local Energy of the signal. From the image it can be seen that the gradient magnitude does not provide the same response to signal variations with the different phase.

gradient vector are the spatial derivatives of the signal, so both concepts are somehow related. Although several numerical schemes have been developed to accurately estimate the gradient yielding to low error rates [Raffel98], it is important to remark that discrete estimation of derivatives is an operation that has to be carefully done.

Independently from the numerical problems that are inherent to the derivative estimation method, the major problem is that the gradient itself is not invariant to local phase variations. As a consequence of this, the gradient do not provide the same response for two structure elements with different local phase. For instance, take the example presented in Fig. 3.1, where in the top we can see a scalar field with two main structure areas: a border and a line. In the middle row, we represent the gradient magnitude. As it can be seen, the response is not the same for both structure elements [RF03].

This idea is also illustrated in Fig. 3.2 where we compute the gradient of sinusoidal function. As it can be seen, the gradient is maximum when the signal crosses zero and it

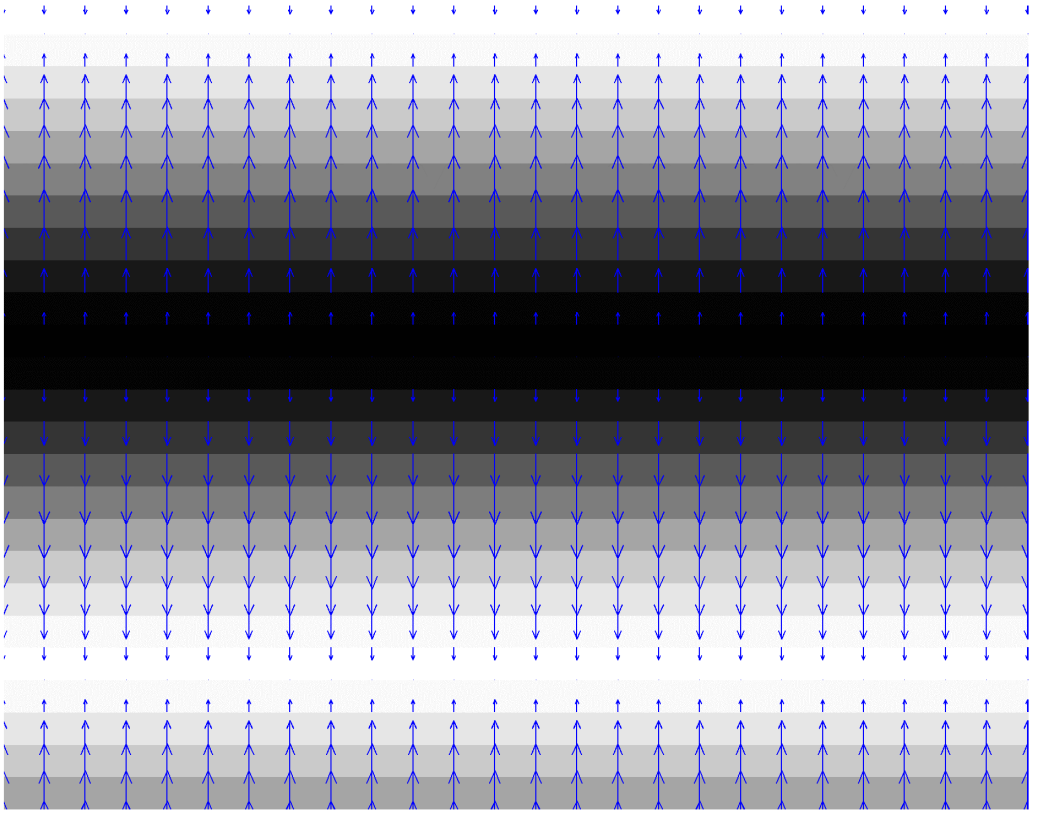

Figure 3.2: Gradient computed for a sinusoidal signal. As it can be seen the gradient presents discontinuities in locations where the signal presents a change in the local phase, although orientation is continuous.

is null when it achieves the maximum or minimum values. However, as it can be seen from the background signal, local structure and local orientation do not change from point to point, since there are no discontinuities in the signal. This fact emphasizes the relationship between both concepts [San Jose05].

To avoid these limitations some authors argue for the use of local energy to identify the relevant features of the signal, which is free of ambiguity [Knutsson03b, Morrone87] and, in addition, local energy measures give peak responses at points where human observers localize contours [Morrone87], yielding to a direct relationship between energy and meaningful features of the signal. As an example, let us examine again the lowest row of Fig. 3.1, where we show the local energy associated to the image shown on the top. As it can be seen, both structure elements are equally detected.

However, local energy itself is not enough to completely describe local structure since it does not provide orientation information, as it is a scalar measure. The representation of local structure using vectors has the additional limitation that in regions that are not intrinsically one-dimensional (such as corners or junctions, where more than one preferred orientation is present), the information provided is ambiguous, since only one direction of signal variation is provided. Moreover, simple averaging of the gradient vector field presented in Fig. 3.2 would produce cancellation effects over the discontinuities of the

gradient vector field, since neighboring vectors have opposite directions. For these reasons, the use of second order tensors was proposed as a local structure measure. Next, we study the requirements that such a local structure descriptor should hold to properly represent local structure.

3.2.2 Representation of Local Structure Using Tensors

The tensor representation for local orientation was introduced by Knutsson [Knutsson89] to encode the orientation information for signals with dimensionality greater than one. Tensors, besides allowing a compact representation, have a solid mathematical body that supports further analysis in the tensor domain. The idea is to represent the orientation of a neighborhood by a symmetric and PSD matrix.

In the case that more than one dominant orientation is present, (for instance, take the example of a corner in a scalar image), it should be necessary to use higher order tensors to completely describe local orientation in a strict sense. However, in practice, a second order tensor provides enough information to distinguish the relevant features of an image, including corners [Köthe03], although certain ambiguity might appear under certain circumstances.

Knutsson studied the requirements that a continuous representation of orientation should hold [Knutsson89]. Let $\mathbf{v_o} \in \mathbb{R}^n$ be a known vector which represents the main orientation and let $\mathcal{M}$ be a mapping $\mathcal{M} : \mathbb{R}^n \mapsto \mathbb{R}^{n\times n}$ to be defined. Then $\mathcal{M}$ should satisfy the following properties in order to properly describe local structure:

- *Uniqueness:* Antipodal vectors should be mapped onto a singular point. In this way, vectors pointing in opposite directions are treated equally removing the discontinuity at π:
$$\mathcal{M}(\mathbf{v_o}) = \mathcal{M}(-\mathbf{v_o}) \tag{3.1}$$
- *Polar separability:* The norm of the mapped vector should be rotation invariant. Information carried by the norm of the vector does not carry information about orientation:
$$\| \mathcal{M}(\mathbf{v_o}) \|_F = f(\| \mathbf{v_o} \|), \tag{3.2}$$
where $f : \mathbb{R}^+ \mapsto \mathbb{R}^+$ is an arbitrary function.
- *Uniform stretch - Equivariance:* Variations in the original spaces should be proportional to variations in the mapped space. In other words, the tensor representation must be invariant to basic transformations such as translation, rotation or scale:
$$\| \partial\mathcal{M}(\mathbf{v_o}) \|_F = b \| \partial\mathbf{v_o} \| . \tag{3.3}$$

A mapping that fulfills the above requirements is $\mathbf{M} : \mathbb{R}^n \mapsto \mathbb{R}^{n\times n}$ [Knutsson89] such that

$$\mathbf{M}(\mathbf{v_o}) = \frac{\mathbf{v_o}\mathbf{v_o}^T}{\| \mathbf{v_o} \|}. \tag{3.4}$$

This mapping is a non-linear mapping, therefore filtering operations applied to the elements of $\mathbf{M}$ have to be carefully made. This mapping provides a symmetric positive semidefinite matrix with $\frac{n(n+1)}{2}$ independent components where the dominant orientation given by the vector $\mathbf{v_o}$ is codified by the dominant eigenvector of that matrix. The symmetry condition guarantees the invariance to rotations at the same time that assures that all the eigenvalues of the matrix are real values and the positive semidefiniteness guarantees that all of them are positive. The matrix provided by this mapping is called *Local Structure Tensor* and will be denoted by $\mathbf{T}$. In section 3.3 we discuss different approaches to directly estimate the LST from data.

The main advantage of the tensor representation is that tensors contain more information than only the dominant orientation, since they also quantify uncertainty about this orientation being actually dominant [Westin02a]. In other words, they quantify how much the signal varies along the dominant orientations and also along the orientation orthogonal to the dominant within a certain neighborhood. Thus, through an analysis of eigenvalues $\lambda_1 \geq \ldots \geq \lambda_m$ and eigenvectors $\mathbf{e_1}, \ldots, \mathbf{e_m}$ we can distinguish different cases in 3D $m = 3$ (an analogous classification can be done in 2D):

1. Planar case ($\lambda_1 \gg \lambda_2 \simeq \lambda_3 \simeq 0$): There is only one main direction of signal variation. This neighborhood is approximately a planar structure whose normal vector is given by $\mathbf{e_1}$.

2. Linear case ($\lambda_1 \simeq \lambda_2 \gg \lambda_3 \simeq 0$): In this case, there are two main directions of signal variation which yields a line-like neighborhood oriented along $\mathbf{e_3}$, as the edges of a cube.

3. Point Structure case ($\lambda_1 \simeq \lambda_2 \simeq \lambda_3 \gg 0$): There is no preferred orientation of signal variation, which represents a corner or a junction in 3D.

4. Homogeneous case ($\lambda_1 \simeq \lambda_2 \simeq \lambda_3 \simeq 0$): In this case, there is neither a preferred orientation of signal variation nor significant variation, which corresponds to homogeneous regions.

From a statistical point of view, when the signals are regarded as random fields an interesting relationship can be established between the local structure tensor and the covariance matrix $\mathbf{C}$. In fact, when the expectation per element is zero (usually on homogeneous areas such as planes or lines) the local structure tensor and covariance matrix are identical. The equivalence is given by the following formulation:

$$\mathbf{C} = \mathbf{T} - E\{\nabla s\}E\{(\nabla s)^T\} \tag{3.5}$$

where ∇s represents the spatial gradient of the signal s and $E\{\cdot\}$ is the expectation operator.

As it is shown in section 2.4.7, there exists an interesting equivalence between the tensor representation and the matrix of the quadratic form associated to the equation of an ellipsoid. In this sense, it is illustrative to identify the eigenvectors $\hat{\mathbf{e}}_\mathbf{i}$ of the tensors to the main axes of the ellipsoid, where the length of each axis is determined by the associated

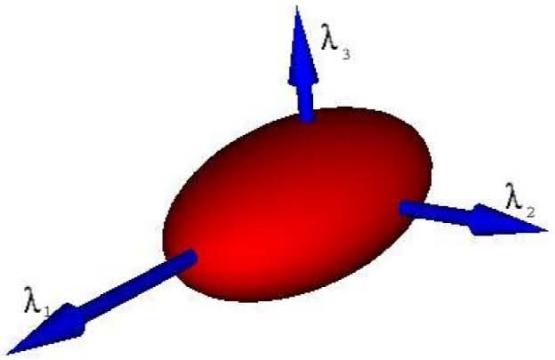

Figure 3.3: Interpretation of a symmetric semidefinite tensor as an ellipsoid.

eigenvalue λ_i. In Fig. 3.3 we represent an example of this geometric interpretation of the local structure tensor.

3.3 Estimation of the Local Structure Tensor

In this section we face the problem of local structure estimation from multidimensional images using the tensor representation described in the previous section. As we said before, local structure is related to local orientation and to the most relevant features of an image. As a consequence of this fact, estimation of local structure has been a matter of discussion in literature for years. The works [Bigün87], [Förstner87] and [Kass87] in 1987 together with [Knutsson89] in 1989 represent the seed of the tensor representation of local structure. These methods can be classified, as done in [San Jose05], in two different groups:

- Gradient methods: These methods use the spatial gradient to determine the signal orientation. Among others, the following references are of interest [Bigün87, Förstner87, Kass87, Rao91, Mester01].
- Local-energy methods: These methods involve the use of quadrature filters to quantify the energy of the signal and, hence, to be able to determine local structure. Among others, the following references are of interest [Knutsson89, Knutsson03b, Knutsson03a, Rieger04]

Let us now describe both estimation methods.

3.3.1 Gradient Methods

As it was said before, these methods use the spatial gradient to compute the local structure tensor. These methods are based on the principle that states that the Fourier transform

$\mathcal{F}_s(\mathbf{u})$ of a signal $s(\mathbf{x}) = g(\mathbf{x}^T\hat{\mathbf{n}})$ with only one main orientation $\hat{\mathbf{n}}$ is concentrated along a line through the origin

$$\mathcal{F}(\mathbf{u}) = \mathcal{G}(\hat{\mathbf{n}}^T\mathbf{u})\delta^{line}_{\hat{\mathbf{n}}}(\mathbf{u}) \tag{3.6}$$

In order to estimate the orientation $\hat{\mathbf{n}}$, Bigün tries to find the minimum of an error function $E(\hat{\mathbf{n}})$ given by the Euclidean distance $\mathfrak{d}(\mathbf{u}, \hat{\mathbf{n}})$ between a point in the Fourier domain and a candidate direction $\hat{\mathbf{n}}$ weighted by the spectrum of the signal:

$$E(\hat{\mathbf{n}}) = \int \mathfrak{d}^2(\mathbf{u}, \hat{\mathbf{n}}) \mid \mathcal{F}(\mathbf{u}) \mid^2 d\mathbf{u} \tag{3.7}$$

The error function described above can be rewritten as a quadratic form:

$$E(\hat{\mathbf{n}}) = \hat{\mathbf{n}}^{\mathbf{T}}\mathbf{J}\hat{\mathbf{n}} \tag{3.8}$$

where $\mathbf{J}$ is the inertia matrix, whose components are expressed in the following equation:

$$J_{ij} = \begin{cases} \int \sum_{j \neq i} u_i^2 \mid \mathcal{F}(\mathbf{u}) \mid^2 d\mathbf{u} & \text{if} \quad i = j \\ \int u_i u_j \mid \mathcal{F}(\mathbf{u}) \mid^2 d\mathbf{u} & \text{if} \quad i \neq j \end{cases} \tag{3.9}$$

Finally, the solution to the minimization problem is given by the eigenvector corresponding to the smallest eigenvalue of $\mathbf{J}$. Bigün showed that the problem of fitting a line in the Fourier domain is algebraically equivalent to fitting a hyperplane to $\mathcal{F}(\mathbf{u})$ that passes through the origin as well. To solve this equivalent problem, the Euclidean distance from a point in the Fourier domain to the given orientation has to be redefined as the perpendicular distance from a point in the Fourier domain $\mathbf{u}$ to the hyperplane which passes through the origin and whose normal vector is $\hat{\mathbf{n}}$. That is:

$$\mathfrak{d}(\mathbf{u}, \hat{\mathbf{n}}) = \hat{\mathbf{n}}^T\mathbf{u}\mathbf{u}^{\mathbf{T}}\hat{\mathbf{n}} \tag{3.10}$$

Again, the error function can be written as a quadratic form $E(\hat{\mathbf{n}}) = \hat{\mathbf{n}}^{\mathbf{T}}\mathbf{T}\hat{\mathbf{n}}$ where

$$\mathbf{T} = \{t_{ij}\} = \int u_i u_j \mid \mathcal{F}(\mathbf{u}) \mid^2 d\mathbf{u} \tag{3.11}$$

is the *local structure tensor*, whose eigenvector corresponding to the largest eigenvalue is the main orientation of the signal. Both, the inertia matrix and the structure tensor are positive semidefinite and have common eigenvectors but different eigenvalues. In this way, the inertia matrix is related to the structure tensor by means of

$$\mathbf{J} = tr(\mathbf{T})\mathbf{I} - \mathbf{T} \tag{3.12}$$

Then, Eq. 3.11 provides an analytic expression to compute the local structure tensor. However, in [Bigün87] it was also presented an equivalent formulation to Eq. 3.11 that

avoids the computation of the signal Fourier transform, which uses the Parseval theorem to express the local structure tensor components in the spatial domain as follows:

$$\mathbf{T}(\mathbf{x_0}) = \{t_{ij}\} = \frac{1}{4\pi^2} \int_{\mathbf{x}\in\Omega(\mathbf{x_0})} \frac{\partial s}{\partial x_i} \frac{\partial s}{\partial y_j} d\mathbf{x} \tag{3.13}$$

where $\Omega(\mathbf{x_0})$ is a local neighborhood of the function $s(\mathbf{x})$ around the point $\mathbf{x_0}$ where the local structure tensor is going to be estimated. In practice, where we assume we are working on a discrete grid, Eq. 3.13 can be written using the following expression:

$$\mathbf{T}(\mathbf{x_0}) = G_\sigma(\mathbf{x_0}) * (\nabla s(\mathbf{x_0}) \nabla^T s(\mathbf{x_0})) \tag{3.14}$$

where $G_\sigma(\mathbf{x_0})$ is a Gaussian kernel with standard deviation σ, used to regularize the outer product of the gradient introducing the information of the local neighborhood at a given scale σ in order to obtain a full rank tensor. Otherwise, the outer product of the gradient itself would not incorporate the uncertainty information since it is a rank-1 tensor. The partial derivatives in the discrete domain are computed with Gaussian derivative filters.

An analogous formulation to Eq. 3.14 can be obtained by means of a probabilistic interpretation of the signal $s(\mathbf{x})$ [Alzola01]. In other words, we can think of the signal $s(\mathbf{x})$ as a field where a random variable is assigned to each position $\mathbf{x} \in \mathbb{R}^n$. Then, to characterize the variation of the signal we make use of the second order joint statistics of the signal gradient. Assuming a zero mean gradient, an estimate of the covariance matrix of the signal gradient is given by Eq. 3.15, where $V(\mathcal{N}(\mathbf{x_0}))$ stands for the number of samples of the neighborhood $\mathcal{N}(\mathbf{x_0})$ centered at point $\mathbf{x_0}$:

$$\mathbf{C}_{\nabla s}(\mathbf{x_0}) = \frac{1}{V(\mathcal{N}(\mathbf{x_0}))} \sum_{\mathbf{x_i}\in\mathcal{N}(\mathbf{x_0})} \nabla s(\mathbf{x_i}) \nabla s(\mathbf{x_i})^T \tag{3.15}$$

The elements of the covariance matrix, i.e. local structure tensor, are estimates of the second order cross moments of the signal gradient. Thus, an analysis of the eigenvalues and eigenvectors provide information on the manner in which the gradient changes. In brief, the eigendecomposition helps to discriminate the type local neighborhood among the different cases already presented in section 3.2.2.

Both formulations are then coherent with the properties that any descriptor of orientation should hold, which were outlined in section 3.2.2. In addition, it is clear that Eqs. 3.14 and 3.15 are particular formulations of the proposed mapping $\mathbf{M}$.

3.3.2 Local Energy Method

This method, mainly developed by Knutsson [Knutsson89], involves the use of quadrature filters to quantify the local energy of the signal to infer the local structure, based on the relationship between these two concepts described in section 3.2. However, local energy itself is not enough to completely describe local structure since it does not provide

orientation information, as it is a scalar measure. Then, the estimation of the local structure tensor requires some previous steps.

Using basic theory of tensor algebra, it is known that any tensor $\mathbf{T}(\mathbf{x})$ can be expressed as a linear combination of the elements of a tensor basis $\{\mathbf{M}_k\}$ weighted by the coefficients $q_k(\mathbf{x})$, where $k = 1, \ldots, K$ is the number of elements in the basis of tensors:

$$\mathbf{T}(\mathbf{x}) = \sum_{k=1}^{K} q_k(\mathbf{x})\mathbf{M}_k \tag{3.16}$$

Knutsson, then, proposed the way to compute the tensor basis $\{\mathbf{M}_k\}$ and the coefficients $q_k(\mathbf{x})$ using a bank of K spherically separable quadrature filters oriented along a given set of directions $\hat{\mathbf{n}}_k$ symmetrically distributed in the n-dimensional space of the signal $s(\mathbf{x})$ [Knutsson89]. The set of quadrature filters is defined in the Fourier domain by:

$$\mathcal{Q}_k(\mathbf{u}) = \begin{cases} e^{(\frac{-4}{B^2 ln2})(ln^2(\frac{\|\mathbf{u}\|}{\|\mathbf{u}_0\|}))} \cdot (\hat{\mathbf{u}}^T \hat{\mathbf{n}}_k)^2 & \text{if } \hat{\mathbf{u}}^T \hat{\mathbf{n}}_k > 0 \\ 0 & \text{otherwise} \end{cases} \tag{3.17}$$

These filters can be seen as oriented Gaussian functions in a logarithmic scale, centered at $\| \mathbf{u}_0 \|$ and with bandwidth B.

Assuming a signal model like the one proposed at the beginning of this section whose Fourier transform is given by Eq. 3.6, each coefficient $q_k(\mathbf{x})$ (with $k = 1, \ldots, K$) is given by the magnitude of the complex function given by the convolution of the signal with the quadrature filter, which is more easily computed in the Fourier domain:

$$q_k(\mathbf{x}) = \| \frac{1}{(2\pi)^n} \int_{\Omega} \mathcal{G}(\hat{\mathbf{n}}^T \mathbf{u}) \delta^{line}_{\hat{\mathbf{n}}}(\mathbf{u}) \mathcal{Q}_k(\mathbf{u}) e^{i\mathbf{u}^T \mathbf{x}} d\mathbf{u} \| \tag{3.18}$$

Concerning the tensor basis, the set $\{\mathbf{M}_k\}$ is defined as the dual or reciprocal basis of the tensor basis $\{\mathbf{N}_k\}$ given by the outer product of the set of directions $\hat{\mathbf{n}}_k$, as it shown in the following expression:

$$\mathbf{N}_k = \hat{\mathbf{n}}_k \hat{\mathbf{n}}_k^T \tag{3.19}$$

Since the set $\{\mathbf{N}_k\}$ form a basis of tensors which may not be orthonormal, we have to use its dual basis $\{\mathbf{M}_k\}$ in order to get a proper representation for the tensor $\mathbf{T}(\mathbf{x})$, as it was detailed in section 2.4.3.

Finally, the K elements of the basis still have to be determined. The number K is related to the number of directions $\hat{\mathbf{n}}_k$ needed to orientate each quadrature filter in order to compute the local energy over all the orientation space of the signal, i.e. $\mathbb{R}^n$ in an n-dimensional space. A practical rule is that the directions $\hat{\mathbf{n}}_k$ should pass through the adjacent vertexes of a regular polytope (an hexagon in 2D, an icosahedron in 3D, etc.). Then, in a n-dimensional scalar dataset, the minimum number of directions required for

the quadrature filters is $K = \frac{n(n+1)}{2}$ [Granlund95]. This requirement is based on the fact that $\mathbf{T}(\mathbf{x})$ by definition is invariant to rotation of the filters [San Jose05].

A common practice is to regularize the final result with a Gaussian kernel with standard deviation σ to provide a more robust response against noise. Although this regularization is not needed in a strict sense, it also introduces an integration scale to provide a robust response. Hence, the final expression of the local structure tensor is as follows:

$$\mathbf{T}(\mathbf{x}) = G_\sigma(\mathbf{x}) * \sum_{k=1}^{\frac{n(n+1)}{2}} \parallel s(\mathbf{x}) * h_k(\mathbf{x}) \parallel \mathbf{M}_k \tag{3.20}$$

where $h_k(\mathbf{x})$ is the spatial formulation of the quadrature filter in Eq. 3.17.

The local structure tensor estimated with this method inherits the phase invariance advantage from the quadrature filters, which do not present the problems of the gradient. To illustrate this idea, let us take again the example from the Fig. 3.2, where the gradient vector field is computed for a sinusoidal signal. At locations where the signal achieves a maximum or a minimum, the gradient is zero and, hence, the outer product of the gradient is also a null tensor. On the contrary, at other locations, the gradient is not null vector and, hence, the outer product of the gradient provides a not null tensor. In fact, the gradient magnitude reaches a maximum value at locations where the signal value crosses zero. Despite this undesired effect is relaxed by means of the gaussian smoothing, this problem introduces a source of error in the estimation of the local structure.

Figure 3.4 illustrates the phase invariance property of the local structure tensor estimated with the local energy approach. On top, the ellipsoids represent the local structure tensor computed with the gradient before the Gaussian smoothing is performed, where it is clear that the tensors change as long as the phase signal does because of the phase dependence inherited from the gradient. On the bottom, the approach based on the use of quadrature filters is used. On the contrary, the tensors are constant, as it is the local structure of the signal.

3.3.3 Nonlinear Structure Tensors

In the previous section we described two different methods to estimate the local structure tensor. Although the philosophy behind them is completely different, in both cases it is a common practice to regularize the tensor field by means of a Gaussian convolution. In this way, we incorporate spatial information within a certain neighborhood at the desired integration scale and, at the same time, the estimation is more robust against noise.

However, it is known that Gaussian smoothing has two main drawbacks: the blurring effect and delocalization of main structures. This is mainly due to the use of a fixed kernel that does not depend on the local characteristics of the signal. Thus, near boundaries, where the structure information is mainly present, the result will be inaccurate since we are mixing different kinds of information.

To avoid these two effects, Brox et al. proposed the definition of the *nonlinear structure tensor* [Brox06]. The main idea is to substitute the Gaussian convolution by a nonlinear

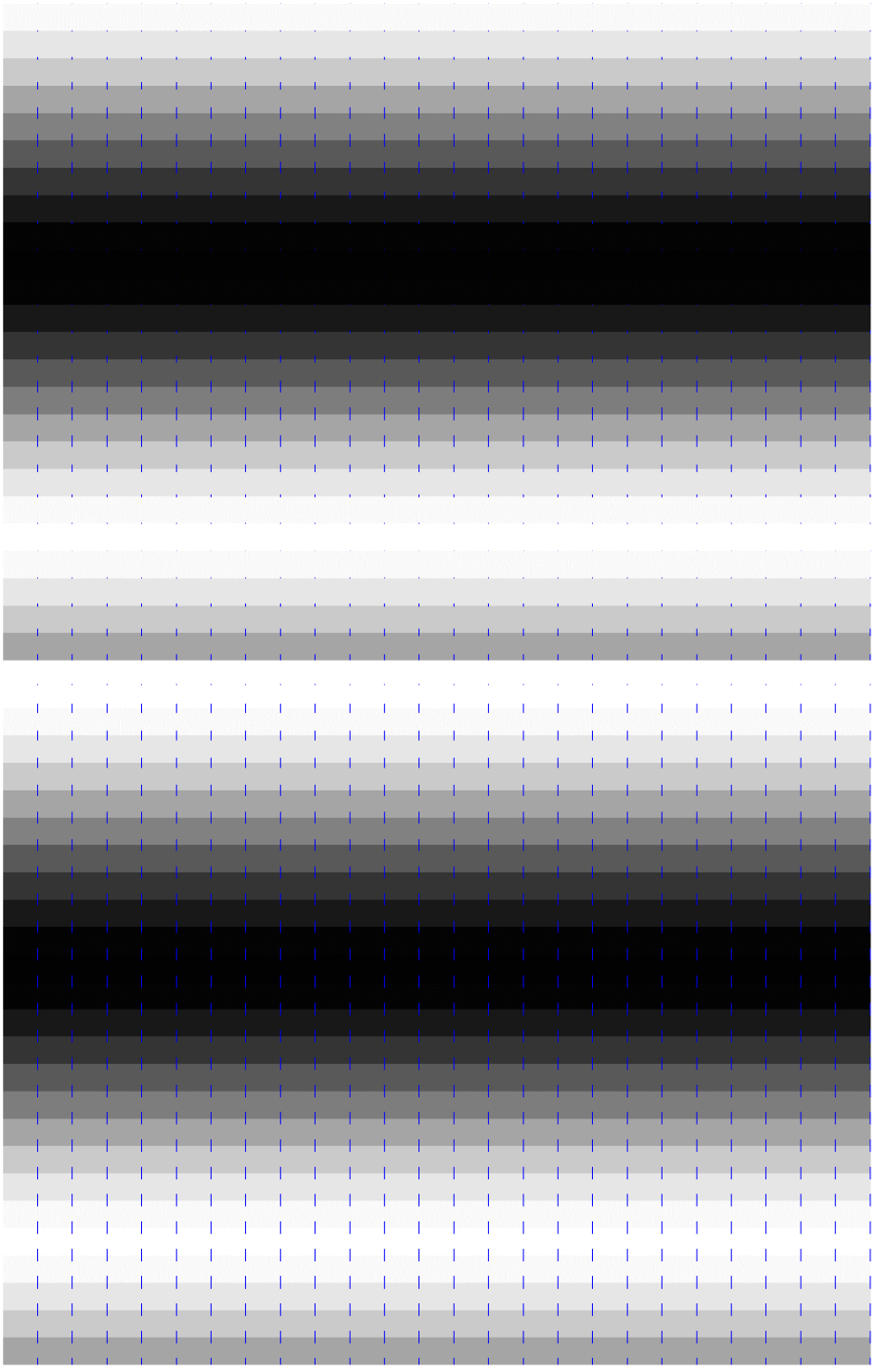

Figure 3.4: Illustrative example of the phase invariance property of the different LST estimation methods. Top: Local Structure Tensor computed with the gradient method before Gaussian regularization is performed. Bottom: Local Structure Tensor computed with the local energy method before Gaussian regularization is performed.

regularization method to avoid the delocalization and blurring effects.

In this sense, it has been shown that Gaussian smoothing can be modeled by the heat diffusion PDE shown in Eq. 3.21, where the amount of smoothing of the image $u(\mathbf{x})$ is determined by the diffusion time t, which is related to the scale-space parameter σ through the following expression $t = \frac{\sigma^2}{2}$ [Koenderink84].

$$\partial_t u(\mathbf{x}) = \triangle u(\mathbf{x}) \tag{3.21}$$

In this way, an equivalent formulation for the local structure tensor in Eq. 3.14 can be achieved with a generalized heat equation for matrices developed in [Weickert02]. Briefly, this generalization applies the heat equation 3.21 to the components t_{ij}, $i, j = 1 \dots m$ of the matrix $\mathbf{T}_0 = (\nabla s(\mathbf{x}))(\nabla s(\mathbf{x}))^T$:

$$\partial_t t_{ij}(\mathbf{x}) = div(\nabla t_{ij}(\mathbf{x})) \tag{3.22}$$

This idea can be generalized by means of nonlinear diffusion filters, which reduce smoothing across boundaries [Perona90] introducing in Eq. 3.21 a function g, called *diffusivity function*, which correlates the amount of smoothing with the gradient magnitude of the image, as follows:

$$\partial_t u(x) = div(g(\parallel \nabla u \parallel)\nabla u(x)) \tag{3.23}$$

or anisotropic diffusion filters, where a privileged direction of smoothing is introduced through the diffusion matrix $\mathbf{D}$.

$$\partial_t u(\mathbf{x}) = div(\mathbf{D}\nabla u(\mathbf{x})), \quad u(\mathbf{x}, t = 0) = I(\mathbf{x}) \tag{3.24}$$

These new formulations naturally lead to the definition of nonlinear structure tensors [Brox06], which are based on a generalized nonlinear matrix-valued heat diffusion equation [Weickert02]. As it is done for the scalar case, a diffusivity function $g(\sum_{i,j=1}^{m} \parallel \nabla t_{ij}(\mathbf{x}) \parallel)$ is introduced in Eq. 3.22 to correlate the amount of smoothing with the magnitude of the gradient of all tensor components, as shown in the following equation:

$$\partial_t t_{ij}(\mathbf{x}) = div(g(\sum_{i,j=1}^{m} \parallel \nabla t_{ij}(\mathbf{x}) \parallel^2)\nabla t_{ij}(\mathbf{x})), \quad t_{ij}(\mathbf{x}, t = 0) = t_{ij}(\mathbf{x}) \tag{3.25}$$

In this way, when the gradient in any tensor component is high due to the presence of structure, the diffusivity is low to avoid smoothing while the diffusivity is high when there is no structure in any component. As a consequence, this technique is different from just applying nonlinear diffusion independently to every component of the tensor field, since a boundary in one component reduces the amount of smoothing in all the others.

Several diffusivity functions have been proposed in the literature [Weickert98] each of them with different properties. In our case, we will use the diffusivity function expressed in Eq. 3.26, also called *total variation flow* [Dibos00, Andreu01]:

$$g(\sum_{i,j=1}^{m} \| \nabla t_{ij}(\mathbf{x}) \|) = \frac{1}{\sqrt{\epsilon^2 + \sum_{i,j=1}^{m} \| \nabla t_{ij}(\mathbf{x}) \|^2}} \tag{3.26}$$

where the parameter ϵ is a small constant that avoids singularities and allows differentiability.

There exist another natural extension for the linear structure tensor which consists on the use of an anisotropic matrix-valued diffusion process also generalized in [Weickert02]. In the anisotropic case, not only the amount of diffusion is adapted locally to the data, but also the direction of smoothing. Hence, in presence of boundaries, the smoothing will take place along the edges of the boundary but not across them. To do that, we only have to replace the diffusivity function defined in Eq. 3.26 by a diffusion tensor $\mathbf{G}(\mathbf{x})$ that determines the direction in which the diffusion takes place. The anisotropic structure tensor is given by the following expression:

$$\partial_t t_{ij}(\mathbf{x}) = div(\mathbf{G}(\sum_{i,j=1}^{m} (\nabla t_{ij}(\mathbf{x}))^T (\nabla t_{ij}(\mathbf{x})))\nabla t_{ij}(\mathbf{x})), \quad t_{ij}(\mathbf{x}, t=0) = t_{ij}(\mathbf{x}) \tag{3.27}$$

There exists an inverse relationship between the diffusion tensor and the structure tensor given by the outer product of the gradient of the tensor components [Castaño04a]. In other words, the main eigenvector of the structure tensor is the smaller one of the diffusion tensor and viceversa. Thus, the diffusion tensor is calculated applying the diffusivity function in Eq. 3.26 to the eigenvalues of the matrix $\mathbf{A} = (\nabla t_{ij}(\mathbf{x}))^T (\nabla t_{ij}(\mathbf{x}))$, exploiting the property that the function of a matrix can be expressed as follows: $g(\mathbf{A}) = \mathbf{P}^T g(\mathbf{diag}(\lambda_i))\mathbf{P}$, where $\mathbf{P}$ is a orthonormal matrix whose columns are the eigenvectors of $\mathbf{A}$ and $\mathbf{diag}(\lambda_i)$ is a diagonal matrix with the eigenvalues λ_i of $\mathbf{A}$ the diagonal elements.

To deal with digital images, whether tensor- or scalar-valued images, we have to discretize the isotropic or anisotropic PDEs and build iterative algorithms in order to obtain a filtered version of the initial digital image. The final results mainly depends on the number of iterations n and the time step δt between two consecutive iterations. The main drawback of these approaches is that there is no criterion to decide the optimal number of iterations and/or time step, and different solutions may be obtained.

Concerning the positive semidefiniteness, it can be easily shown that tensors evolving under Eq. 3.27 stay symmetric positive definite if the initial value $T(0) = (u(0)_{i,j})$ is symmetric positive definite [Brox06].

Although in the original work [Brox06] the nonlinear and anisotropic generalizations were proposed using the local structure tensor given by [Bigün87] and [Förstner87] in 3.14, it is straightforward to apply these ideas to the structure tensor given by Knutsson's formulation (Eq. 3.20), as we have done in [Castaño05], where we study the performance of both methods in order to identify their limitations and their advantages.

3.3.4 Robustness of Local Structure Tensor Estimation Methods

Local structure tensor is nowadays a common tool in the field of image processing with applications in orientation estimation [Förstner87], optic flow estimation [Lucas81] and detection of interest points such as corners or landmarks [Rohr94]. Obviously, to characterize the robustness of the local structure estimators presented in section 3.3, it should be necessary to study their influence on all these domains. However, for the aim of our work, we are more interested in the study of the structure delocalization effect, which is a common source of error in the design of anisotropic filters, in order to use the more robust method in our processing framework.

In this sense, it is useful to study how accurate the proposed estimation methods are in the task of corner detection. In 2D, corners are points where two or more intrinsically 1D structures (i.e., edges) with different orientation meet, so they are intrinsically 2D structures, that is to say, locations where two or more main orientations are present. Several methods have been proposed in the literature as a *cornerness* measure, which compute the strength of the intrinsically 2D response of the signal at that point. For instance, in [Förstner86] it has been proposed the following scalar measure based on the information provided by the structure tensor $\mathbf{T}$:

$$c = \frac{det(\mathbf{T})}{tr(\mathbf{T})} \tag{3.28}$$

Another well-known measure is the *corner response function* proposed by [Harris88], which is given by the following expression:

$$c = det(\mathbf{T}) - 0.04(tr(\mathbf{T}))^2 \tag{3.29}$$

In our experiments, we are going to use the method proposed in [Köthe03], which localizes the corners looking for the local maxima over a given threshold of the smallest eigenvalue of the smoothed local structure tensor, which is the component that quantifies the intrinsically 2D properties of the signal.

Thus, to compare the robustness of the six structure tensor estimation techniques defined in section 3.3 (linear, nonlinear and anisotropic nonlinear versions of the LST computed as the outer product of the gradient or by Knutsson's method), we use a figure with several geometric structures at given locations. Then, we add different levels of white Gaussian noise with zero mean to perturb the image and we try to localize the corners from the noisy image using all the estimation methods of the structure tensor.

Figure 3.5 shows the detected corners using the algorithm in [Köthe03]. In the images, the corners detected by the gradient methods are represented with a red cross, while those detected by the energy methods are represented with a blue circle. On the top we used linear smoothing with $\sigma = 1.4$. In the middle we used a nonlinear matrix-valued diffusion process to regularize the tensor field and at the bottom we used the anisotropic nonlinear counterpart, in both cases with diffusion time $n \cdot \delta t = 1.6$ms.

When comparing these images, we clearly see that the least accurate response is that given by the structure tensors with linear smoothing, where corners are detected some

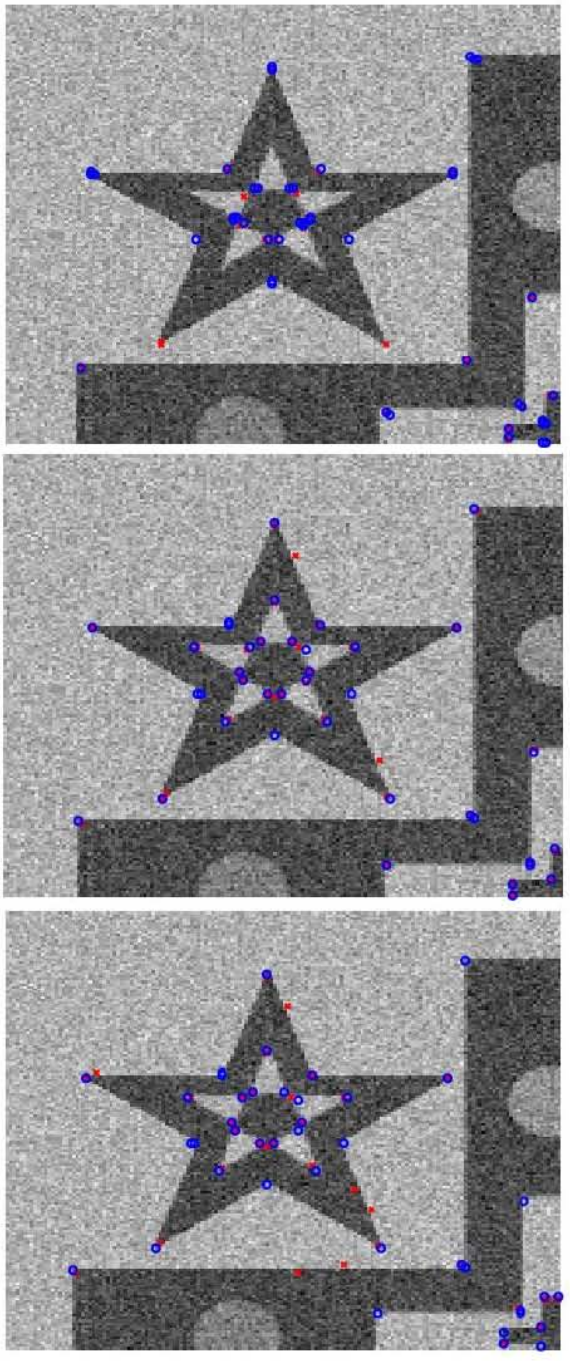

Figure 3.5: Corners detected with different estimators of the Local Structure Tensor. Red cross represents the detected corners with the gradient method while the blue circle are estimated with the energy methods. Top: linear gaussian smoothing was used to introduce an integration scale (Eq. 3.22). Middle: we used a nonlinear matrix-valued diffusion process (Eq. 3.25). Bottom: we used an anisotropic nonlinear matrix-valued diffusion process (Eq. 3.27)

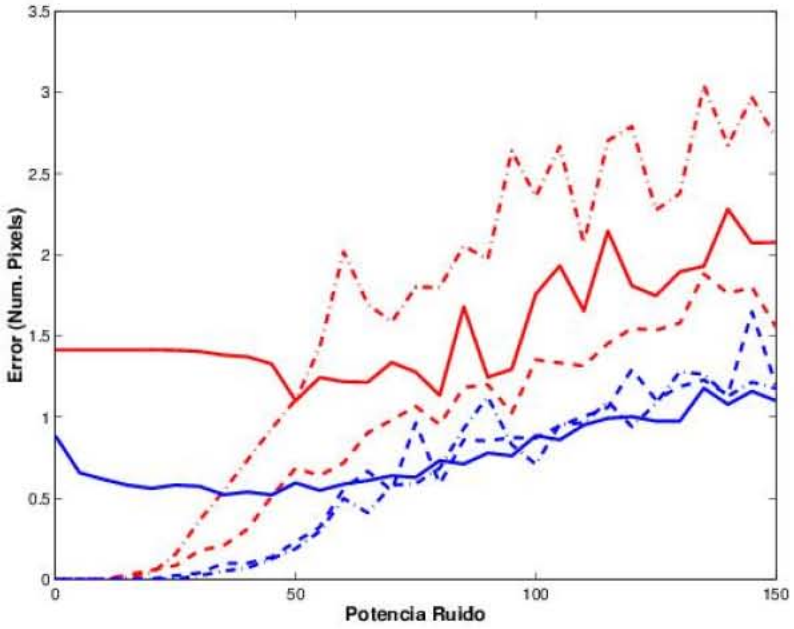

Figure 3.6: Mean localization error in pixels for increasing noise level. Red: gradient methods. Blue: energy methods. Continuous line: Gaussian smoothing. Dashed Line: Nonlinear smoothing. Dotted line: Anisotropic nonlinear smoothing.

pixels away from the true location. In addition, we observe that the energy method with linear smoothing detects *double-corners*. This effect is mainly due to the Gibbs phenomenon that appears at abrupt discontinuities in the Fourier domain [Lukin05].

On the other hand, the response provided by the nonlinear matrix-valued diffusion overcomes the problems stated before. From the middle image it is clear that the accuracy on detected corners is clearly improved at the same time that the *double-corners* effect disappears. Finally, the use of anisotropic nonlinear matrix-valued diffusion smoothing, in the right side of Fig. 3.5, still provides a very accurate response for corner detection. However, a large number of *false corners* are detected due to the contribution of noise.

Figure 3.6 shows the evolution of the error, measured in pixels, for an increasing noise level. In that figure, the red lines correspond to the gradient methods, while the energy methods are represented in blue. The type of smoothing is coded with the type of line: the continuous line means that Gaussian smoothing was used, the dashed line corresponds to nonlinear smoothing and dotted line is for anisotropic nonlinear smoothing. From the figure it is clear that as long as the noise level is increased, the error increases linearly. It is remarkable the fact that we always obtained a lower error for the energy methods for every noise level, which indicates that these methods are more robust against noise.

From these results, we argue for the use of the Knutsson method followed by a nonlinear smoothing since it is the method that produces a lower error rate.

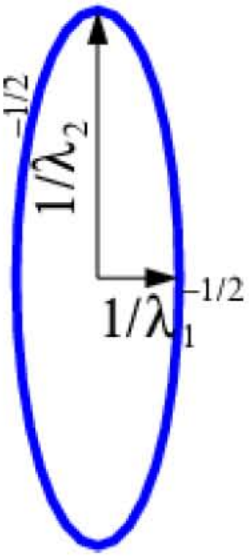

Figure 3.7: Ellipse represented by the quadratic form $\mathbf{x}\mathbf{T}\mathbf{x}^T = 1$.

3.4 A New Approach for Anisotropic Signal Processing

3.4.1 Adaptive FIR Processing Systems

The previous section showed us that the local structure tensor is a nice tool to describe local structure. Now, we present a new signal processing framework to derive anisotropic systems that uses the information provided by the local structure tensor $\mathbf{T}(\mathbf{x})$ [Castaño06b]. First, we develop in this section the complete theoretical framework of our approach and in sections 3.4.2, 3.4.3 and 3.4.4 we present some practical applications of this processing framework. For illustrative purposes, we are going to develop the theoretical framework for scalar 2D data, but results can be easily generalized for tensor data, as it is done in section 3.5 and also for the 3D case.

Many image processing techniques derived either in the spatial or frequency domains are based on the design of a kernel function $k(\mathbf{x})$ that is convolved with the signal $s(\mathbf{x})$ to provide a response. In most cases, the kernel function is designed on a neighborhood whose size is usually fixed and a paremeter of the processing system. On the contrary, the main idea of our approach is to estimate the signal value at position $\mathbf{x}$ using the samples within a neighborhood $\mathcal{N}(\mathbf{x})$ defined by the ellipse $\mathbf{x}\mathbf{T}(\mathbf{x})\mathbf{x}^T = 1$, whose size varies depending on the local structure of the signal.

Let us denote by $\lambda_1 \geq \lambda_2 > 0$ the eigenvalues of $\mathbf{T}(\mathbf{x})$ and by $\mathbf{e_1}, \mathbf{e_2}$ the associated eigenvectors. Then, the quadratic form $\mathbf{x}\mathbf{T}(\mathbf{x})\mathbf{x}^T = 1$ defines an ellipse as the one represented in Fig. 3.7, where the length of the semimajor axis is $\frac{1}{\sqrt{\lambda_2}}$ and it is oriented along the direction determined by $\mathbf{e_2}$. Analogously, the length of the semiminor axis is $\frac{1}{\sqrt{\lambda_1}}$ and it is oriented in the direction given by $\mathbf{e_1}$ and its length is $\frac{1}{\sqrt{\lambda_1}}$.

The local structure tensor can therefore be used to wisely adapt the shape of the neighborhood depending on the local structure of the signal, yielding to different

neighborhood configurations:

- Point Structure case ($\lambda_1 \simeq \lambda_2 \gg 0$): This situation represents a point with high structure such as a corner or junction. In this case, both semiaxis of the ellipse are quite small yielding to a small neighborhood with only a few samples.
- Planar case ($\lambda_1 \gg \lambda_2 \simeq 0$): There is only one main direction of signal variation, which corresponds to a structure similar to a border. In this case, the ellipsoid corresponds to a neighborhood whose semimajor axis is oriented along the border and the length of the semiminor axis is quite small. Hence, the samples within the neighborhood are only found along the border.
- Homogeneous case ($\lambda_1 \simeq \lambda_2 \simeq 0$): This case corresponds to homogeneous regions where there is no preferred orientation of signal variation. In this case, both semiaxis of the ellipse are quite long yielding to a wide neighborhood wit a lot of samples which helps to better remove noise.

Figure 3.8 shows all the possible configurations in a 2D image with two different homogeneous areas. For instance, to estimate the value at point $\mathbf{x_1}$, we are going to use only the samples along the boundary, avoiding the mixture of information of both sides of the border. Something similar happens at point $\mathbf{x_3}$ where the neighborhood $\mathcal{N}(\mathbf{x_3})$ only takes a few samples avoiding as much as possible the mixture of information from different regions. On the contrary, at point $\mathbf{x_2}$ which corresponds to an homogeneous area, the associated ellipse surrounds a lot of samples in order to better remove the inherent noise.

Hence, once the local neighborhood $\mathcal{N}(\mathbf{x_0})$ centered at point $\mathbf{x_0}$ has been computed, we can estimate the signal value at $\mathbf{x_0}$ with a linear combination of the sample values weighted by some coefficients ω_i determined by any other algorithm, as shown in the following equation:

$$\hat{I}(\mathbf{x_0}) = \frac{\sum_{i=1}^{V(\mathcal{N}(\mathbf{x_0}))} \omega_i I(\mathbf{x_0} - \mathbf{x_i})}{\sum_{i=1}^{V(\mathcal{N}(\mathbf{x_0}))} \omega_i} \tag{3.30}$$

One advantage of this framework is that the idea behind is quite general and can be used to compute anisotropic versions of any kind of filters, such as Wiener, LMMSE, etc. In such situations, once the neighborhood has been computed, we locally apply the desired filter on the selected samples to obtain an estimation of the signal value at the desired point. Moreover, it is important to remark that our approach is also independent from the method of estimation of the local structure tensor, although in the next section we study their influence on the structure delocalization.

3.4.2 Anisotropic Gaussian Filtering

As it was stated before, the coefficients that weigh the samples within the neighborhood can be chosen by any algorithm. In this section, we present the way we derive adaptive

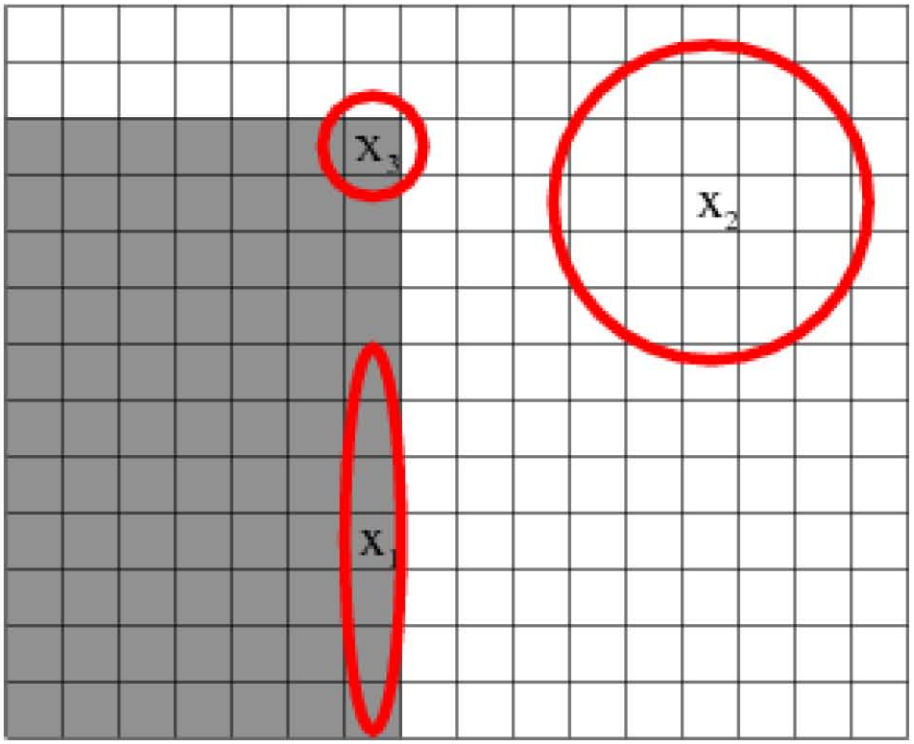

Figure 3.8: Different neighborhoods locally adapted to the structure of the image.

kernels to reduce noise in images within the proposed processing framework. To achieve that task, we illustrate this idea by means of the implementation of a non-iterative anisotropic gaussian filtering approach in the spatial domain.

The idea behind conventional isotropic Gaussian filtering in 2D images is to use the Gaussian distribution shown in Eq. 3.31 as the impulse response of the system. In practice, this is done by the definition of a square fixed-sized mask which represents a discrete approximation of the function and performing a convolution with the image. Since neither the parameters of the Gaussian function (i.e. standard deviation σ) nor the size of the neighborhood are optimized with respect to the local variation of the signal, the result is that the response is usually blurred and details are remove.

$$G(\mathbf{x}) = \frac{1}{2\pi\sigma^2} \exp(-\frac{\mathbf{x}\mathbf{x}^T}{2\sigma^2}) \tag{3.31}$$

It has been shown that Gaussian smoothing can be modeled by the heat diffusion PDE shown Eq. 3.21, where the amount of smoothing of the image determined by the diffusion time t is related to the scale-space parameter σ through the following expression $t = \frac{\sigma^2}{2}$ [Koenderink84]. This idea is quite interesting since it relates filters defined in the spatial domain with a PDE.

The main practical drawback of anisotropic diffusion schemes is the dependence on the diffusion time t, which is given by n iterations of a *time-step* ∂t, since there is no criterion to determine neither the best number of iterations nor the best *time-step*. On the other

hand, Gaussian filtering schemes take the advantage of using non-iterative approaches with a single parameter σ that determines the amount of smoothing. In addition, practical implementation is quite simple and fast since the response is obtained by the convolution of the signal with the gaussian kernel.

Thus, it is interesting to define anisotropic Gaussian filters in the spatial domain from the anisotropic diffusion PDE defined in Eq. 3.24. The anisotropic Gaussian distribution that is used to compute the kernel is given in Eq. 3.32, where the diffusion matrix $\mathbf{D}$ determines the global anisotropy of the kernel [Weickert98]. Then, the response of the filter is computed by means of the convolution $I_G(\mathbf{x}) = G(\mathbf{x}) * I(\mathbf{x})$. The main advantage of the anisotropic counterpart is that the blurring effect and the structure delocalization are significantly reduced, since the smoothing is favored along a privileged orientation. However, since the anisotropy is defined globally for the whole domain of the signal, any structure found in a different orientation from the privileged one will be blurred.

$$G(\mathbf{x}) = \frac{1}{2\pi\sqrt{det(\mathbf{D})}} \exp(-\frac{\mathbf{x}\mathbf{D}^{-1}\mathbf{x}^T}{2}) \tag{3.32}$$

To solve that limitation, one may take into consideration the use of a non-constant diffusion matrix $\mathbf{D}(\mathbf{x})$ to locally adapt the kernel to the signal variation at every point $\mathbf{x_0}$, as shown in Eq. 3.33, reducing the amount of smoothing along the direction of maximum signal variation while it is increased in the orthogonal direction. This anisotropic Gaussian smoothing is no longer equivalent to the solution of the anisotropic diffusion problem defined by the PDE with a diffusion matrix that depends on the spatial position, although a sophisticated relationship can be locally established [Nitzberg92].

$$G(\mathbf{x}-\mathbf{x_0}) = \frac{1}{2\pi\sqrt{det(\mathbf{D}(\mathbf{x_0}))}} \exp(-\frac{(\mathbf{x}-\mathbf{x_0})\mathbf{D}^{-1}(\mathbf{x_0})(\mathbf{x}-\mathbf{x_0})^T}{2}) \tag{3.33}$$

Due to the inverse relationship between the diffusion matrix and the local structure tensor $\mathbf{D}^{-1}(\mathbf{x_0}) \propto \mathbf{T}(\mathbf{x_0})$ [Castaño04a], we can introduce the latter in the Gaussian distribution equation to determine the anisotropy in the Gaussian kernel. Hence, the role of the local structure tensor in this algorithm is twofold. On the one hand, we use it to compute the neighborhood around the estimation point. On the other hand we also use it to locally adapt the shape of the Gaussian function we use to compute the weights ω_i in Eq. 3.30 following this expression:

$$G(\mathbf{x}-\mathbf{x_0}) = \frac{1}{2\pi\sqrt{det(\mathbf{T}(\mathbf{x_0}))}} \exp(-\frac{(\mathbf{x}-\mathbf{x_0})\mathbf{T}(\mathbf{x_0})(\mathbf{x}-\mathbf{x_0})^T}{2}) \tag{3.34}$$

3.4.3 Anisotropic Interpolation

The interpolation problem requires the estimation of the signal values at unsampled points in order to obtain an upsampled version of the signal. Of course, in this case it is also desirable that boundaries are well preserved, something that is not achieved with simple interpolation algorithms. In this section, we generalize our approach to derive

an anisotropic interpolation scheme. To achieve that task, we assume that the unknown signal value at a desired point can be estimated as a linear combination of signal values found within a neighborhood of the interpolation point, as previously described in Eq. 3.30. The neighborhood is chosen as described in section 3.4.1, using the local structure tensor of the nearest neighbor to build the ellipse.

Concerning the coefficients ω_i, different interpolators and signal estimators assign different weights to samples. In some cases it is possible to obtain very efficient separable kernels. Nevertheless, in order to preserve edges, the local structure should be accounted for, and the estimator must be adaptive, with weights changing from one location to another.

Consider for example the weights to be obtained as inversely proportional to the squared distance to the sample,

$$\omega_i = \frac{1}{(\mathbf{x} - \mathbf{x_i})^T (\mathbf{x} - \mathbf{x_i})}. \tag{3.35}$$

This inverse squared distance interpolator is usual in many applications with conventional scalar images, but it smooths boundaries and other highly structured regions. If only distance to the sample is accounted for, the estimator mixes samples drawn from areas that can be very different even though they are close, e.g.. samples from two sides of an edge. Therefore it is necessary to introduce a weighting factor depending on the local complexity of the signal prior to assign weights to samples in order to avoid the undesired smoothing effect.

As it was detailed in section 3.2.2, the information provided by the local structure tensor is quite useful. Through an analysis of the eigenvalues and eigenvectors of the LST we obtain a complete characterization of the sourrounding neighborhood.

The computation of the weights is then based on the use of the local structure tensor inverse as a metric tensor to compute the norm of the distance from the samples to the interpolation point. This takes the advantage that those samples found in the direction of maximum data variation, seem to be at a greater distance while those found in the orthogonal direction seem to be closer. The inversion corresponds to a $\pi/2$ radians rotation of the associated ellipsoid, and it is necessary to weigh the samples along the direction of maximum signal variation less than those in the orthogonal one. Thus, we estimate the value at the upsampled point using Eq. 3.30, but the weights ω_i are obtained from:

$$\omega_i = \frac{1}{(\mathbf{x} - \mathbf{x_i})^T \mathbf{T_x^{-1}} (\mathbf{x} - \mathbf{x_i})} \tag{3.36}$$

where $T_{\mathbf{x}}$ denotes the local structure tensor at the interpolation point.

This idea is illustrated in Fig. 3.9, where signal values from different regions are represented as black and white dots in a regular grid. For the sake of simplicity, we illustrate a 2D local neighborhood which only consists of the 4 nearest samples, although this conceptual idea is straightforward generalizable to larger neighborhoods. From the Figure, it can be seen that although the distance between the interpolated point and data samples is the same, their contributions are not.

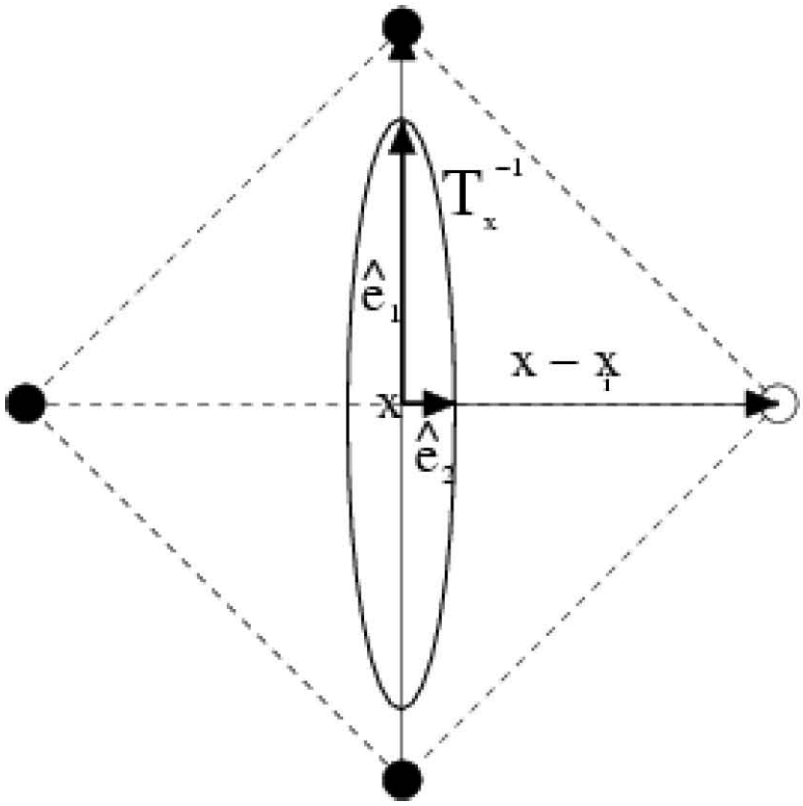

Figure 3.9: Regular grid with tensors from different regions represented as white and black dots, respectively.

Note that the local structure tensor behaves similarly to a covariance matrix in a Mahalanobbis distance computation commonly used in pattern recognition, though now the metric tensor changes from point to point (instead of from class to class).

3.4.4 Covariance-based Anisotropic Structure Estimation

As it was described in section 2.3, optimal estimation includes the design of signal processing systems that make a guess for the correct value of a signal which is optimal according to some known criterion. In order to develop these estimators, the second order probabilistic characterization is assumed to be known or fitted to a model similar to the following expression, proposed in [Cressie93]:

$$c_s(\mathbf{h}) = \sigma^2 \exp\left(-\frac{|\mathbf{h}|}{r}\right) \tag{3.37}$$

where $\mathbf{h} = \mathbf{x_i} - \mathbf{x_j}$ denotes the distance between samples at positions $\mathbf{x_i}$ and $\mathbf{x_j}$, σ^2 is the autocovariance at the target point and r is a free parameter that has to be fixed and depends on the statistical dependence of data.

This model, as it is a common practice, implicitly assumes that the signal is, at least, stationary in wide sense since the autocovariance function only depends on the distance $\mathbf{h} = \mathbf{x_i} - \mathbf{x_j}$ between the samples. This assumption, when working with real-world images, is quite strong and the model usually fails when boundaries between different regions are present, in presence of textures and, in general, when the signal varies abruptly.

However, the local structure tensor provides enough information to overcome this issue. As it was done in sections 3.4.2 and 3.4.3, we can use the local structure tensor as a metric tensor to ponderate the distances between the samples used to perform the estimation. In this sense, we want that those samples found in the direction of maximum data variation, seem to be at a greater distance while those found in the orthogonal direction seem to be closer. This can be done as it is shown in the following equation:

$$c_s(\mathbf{x_i} - \mathbf{x_j}) = \sigma^2 \exp\left(-\frac{\sqrt{(\mathbf{x_i} - \mathbf{x_j})\mathbf{T}(\mathbf{x_i} - \mathbf{x_j})}}{r}\right) \tag{3.38}$$

where the square root has the same geometric interpretation of distance as in the precedent case. The only difference is that the autocovariance function has an elliptic shape instead of a circular one.

This generalization can be easily applied to any other model given in the literature, yielding to anisotropic estimation of the covariance estructure. Hence, this generalization leads to anisotropic formulations of traditional LMMSE estimators such as Wiener filter or Kriging. In section 3.6 we applied this idea to develop an anisotropic version of the Wiener filter described in section 2.3.1 using the autocovariance model presented in Eq. 3.38.

3.5 Generalization for Tensor Signals

The concept of local structure can also be generalized for vector and higher order tensor data (multivalued data). In regions where the signal changes abruptly a local structure tensor can be defined and estimated for such data, in a equivalent way to the scalar case.

Although this generalization is almost straightforward, it is important to take into account some considerations. On the one hand, in a strict sense, the local structure tensor for tensor data should be a fourth-order tensor instead of a second-order one. With this formulation, we are able to quantify how much the tensor signal varies in the same way that the second order tensor does for scalar signals.

However, the idea of this generalization relies on the combination of the spatial variation information for every component of the tensor into a single second-order structure tensor. For instance, following the estimation method of the local structure tensor defined by Knutsson (an equivalent formulation can also be obtained for the gradient methods), we can generalize that approach using the following expression initially proposed in [RF03]:

$$\mathbf{T}(\mathbf{x}) = \sum_{k=1}^{n(n+1)/2} \left(\sum_{xyz..n} \| \, q_{[k]xyz..n} \, \|^2 \right)^{\frac{1}{2}} \mathbf{M}^k \,, \tag{3.39}$$

where we use the same notation defined in Eq. 3.20 and subscripts $xyz..n$ are associated to the components of the tensors in the field.

This generalization is consistent with the fact that each component adds its own local structure (edges, lines, etc), and the sum of the filter responses only adds isotropic information unless they provide additional high structure.

An additional constraint to deal with tensor data is that the signal estimator must provide a positive semidefinite response. This constraint is an additional requirement in the design of the processing system in order to provide a meaningfull response in the tensor signal domain. Fortunately, since the weights ω_i described for the smoothing and interpolation algorithms are always positive numbers, they naturally satisfy this requirement yielding to a straightforward generalization [Castaño04b].

3.6 Results

In this section we present some results to validate the processing scheme presented in this chapter for signal smoothing and interpolation. First, we present some results on scalar images to better illustrate the different applications of the local structure tensor information presented in this chapter and, finally we use tensor data to validate the results of the generalization.

3.6.1 Experiment 1: Filtering on Synthetic and Real Images

For this experiment we use the synthetic image shown on the left side of Fig. 3.10. Then, we add white gaussian noise with zero mean and standard deviation $\sigma_N = 30$ to obtain

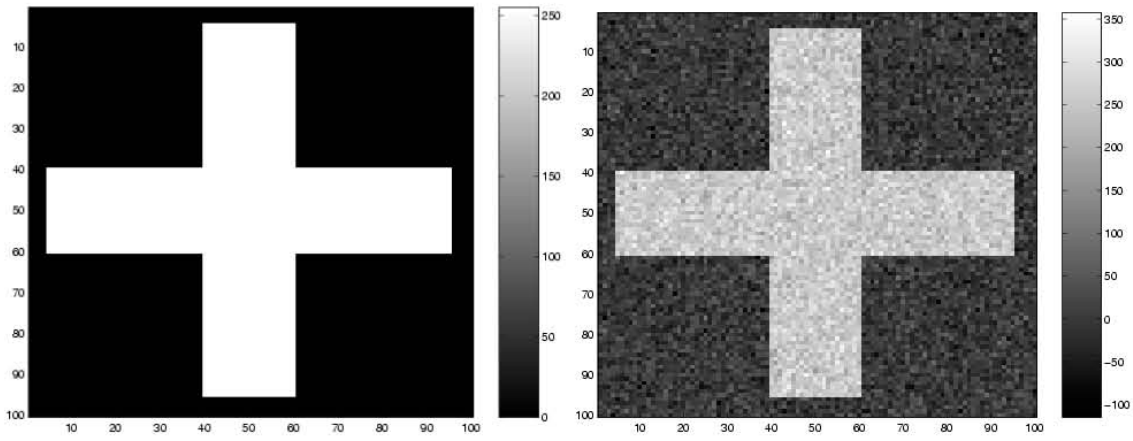

Figure 3.10: Left: Original Synthetic Image. Right: Noisy image $\sigma_N = 30$.

the noisy version in the right side of Fig. 3.10. Finally we compare in Fig. 3.11 the result of our filtering scheme with other anisotropic schemes, such as a nonlinear diffusion scheme for scalar images described in Eq. 3.23, our anisotropic Wiener filter using the autocovariance model presented in Eq. 3.38 and anisotropic gaussian smoothing driven by local structure tensors, but using fixed $N \times N$ neighborhoods, with $N = 5$.

From Fig. 3.11 we can see that the blurring effect that appears in isotropic filtering schemes is negligible. Concerning the behavior near boundaries, several effects derived from the filter responses can be shown. For instance, the response from the nonlinear diffusion scheme presents some isolated points near the boundaries that were not completely removed, even after 318 iterations with time step $\triangle t = 0.2$, which are the parameters that provide an optimal response in terms of the mean squared error. Such behavior is due to a high level of noise at those locations that is similar to the signal value and, hence, the filter believes the boundary is some pixels further.

As it can be seen, the response of the Wiener filter with anisotropic covariance structure estimation, shown at the bottom row (right), provides a similar response to that given by the anisotropic Gaussian filter with adaptive neighborhoods, preserving the boundaries quite well at the same time that the noise is also well removed from homogenous areas and boundaries. Finally, the response of Gaussian filtering with a fixed neighborhood presents a displaced boundary two pixels inside the cross due to the mixture of information achieved by the use of square neighborhoods. As it can be seen, none of these effects can be appreciated in the response of the algorithm presented here, which is shown on the top row (left), where even corners of the cross are better preserved than in other regions.

Table 3.1 shows the Mean Squared Error (MSE) error between the original image and the outputs of the filtering algorithms involved in the experiment. From that table we can see that the minimum mean square error corresponds to the nonlinear diffusion approach, although from a qualitative point of view the response from our anisotropic gaussian might seem better. In this sense, the synthetic image used for this experiment is better suited for a diffusion process, since it consists of two regions with constant values. The numerical solution of the diffusion process provides a more regular estimation of the signal since it uses global information of the whole image.

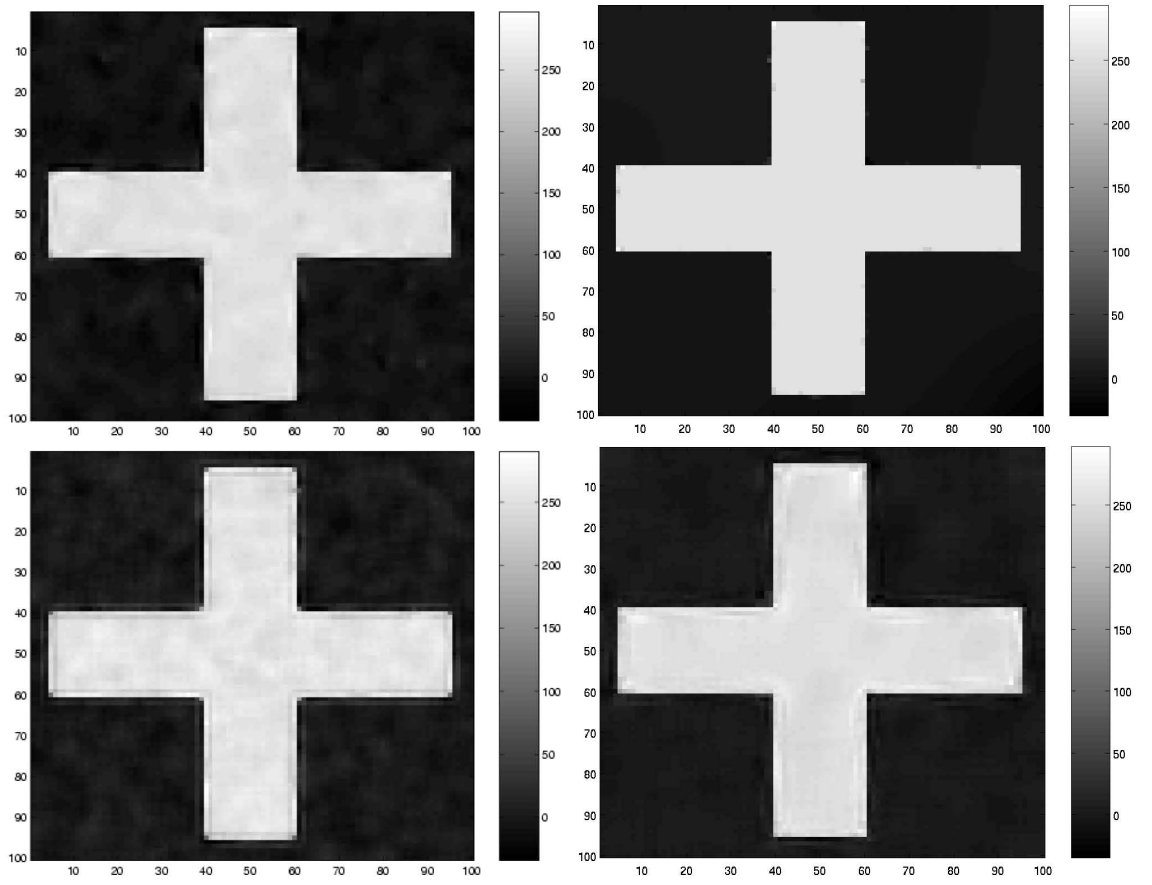

Figure 3.11: Image restored with the follwing filtering schemes. Top Left: Anisotropic Gaussian filtering described in section 3.4.2. Top Right: Nonlinear diffusion scheme. Bottom Left: Anisotropic Gaussian filtering with a fixed 5×5 neighborhood. Bottom Right: Our anisotropic Wiener filter.

Restoration Method	MSE	Std Dev. MSE	Max. $(\hat{s})$	Min. $(\hat{s})$
Nonlinear Diffusion	7.7260	63.4430	293.0800	-29.0975
Anis. Gaussian (adapt. neighb.)	40.35	158.3836	307.5281	-40.2651
Anis. Wiener	43.9271	153.3887	297.0241	-34.5161
Anis. Gaussian (5×5 neighb.)	61.8055	166.4386	307.8018	-41.6958

Table 3.1: Comparison of the Mean Squared Error between the original image in Fig. 3.10 and results in Fig. 3.11. Columns from left to right: MSE, Standard Deviation of the MSE, Maximum value of the estimated signal and Minimum value of the estimated signal.

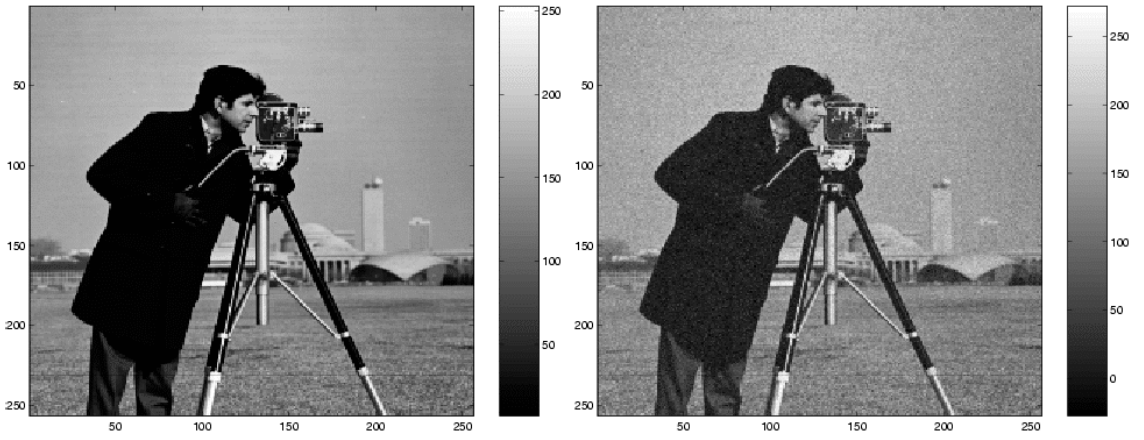

Figure 3.12: Left: Original Image. Right: Noisy image $\sigma_N = 10$.

Restoration Method	MSE	Std Dev. MSE	Max. $\hat{(s)}$	Min. $\hat{(s)}$
Anis. Gaussian (adapt. neighb.)	33.0283	74.8910	266.4196	-21.4702
Anis. Gaussian (5×5 neighb.)	36.2003	91.7741	261.4415	-16.9438
Anis. Wiener	40.0312	95.5984	267.7890	-17.5412
Nonlinear Diffusion	41.2948	102.7876	275.1842	-20.4475

Table 3.2: Comparison of the Mean Squared Error between the original image in Fig. 3.12 and results in Fig. 3.13. Columns from left to right: MSE, Standard Deviation of the MSE, Maximum value of the estimated signal and Minimum value of the estimated signal.

Then, to validate our results we use the real image shown on the left side of Fig. 3.12. As in the precedent case, we add some white Gaussian noise with zero mean and standard deviation $\sigma_N = 10$ and then we try to recover the original image with the filtering schemes previously used.

In Fig. 3.13 we present the responses from the anisotropic filtering schemes used in our previous experiment. As it can be seen, noise is well removed with the anisotropic Gaussian methods (either with a fixed neighborhood or with adaptive ones) and with nonlinear diffusion at the same time that boundaries are preserved, as it is with the Wiener filter with anisotropic covariance structure estimation.

Table 3.2 performs a comparison from a quantitative point of view. As it can be seen, the minimum mean squared error is now obtained with the anisotropic Gaussian filtering scheme that uses adaptive neighborhoods. From our results, we also observe that a fixed kernel size may provide a slightly worse behavior. A quite similar result is obtained with the anisotropic Wiener filter, where the noise is also very well removed. In this case, the mean squared error obtained for the nonlinear diffusion response is higher than the one provided by our anisotropic Gaussian algorithm, since the image is not as well suited for this method as the one presented in Fig. 3.11.

Figure 3.13: Image restored with the follwing filtering schemes. Top Left: Anisotropic Gaussian filtering described in section 3.4.2. Top Right: Nonlinear diffusion scheme. Bottom Left: Anisotropic Gaussian filtering with a fixed 5×5 neighborhood. Bottom Right: Our anisotropic Wiener filter.

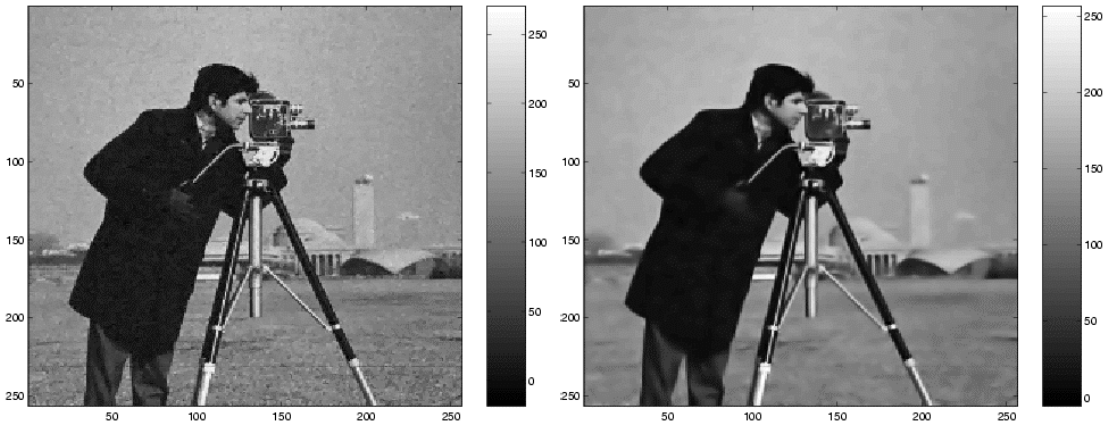

Figure 3.14: Influence of the Local Structure Tensor estimation method used in our anisotropic Gaussian filtering approach. Left: Response from our method using Knutsson's formulation with Nonlinear smoothing. Right: Response from our method using Knutsson's formulation with linear smoothing.

3.6.2 Experiment 2: Influence of the structure tensor estimation method

In this experiment we use again the images shown in Fig. 3.12 to demonstrate the influence of the structure tensor estimation method in the response of our anisotropic Gaussian filtering approach. To do that, we try to recover the original image (left side of Fig. 3.12) with the filtering scheme proposed in section 3.4.2 using, on the one hand, the linear structure tensor and, on the other hand, the nonlinear counterpart. In this way, we will be able to determine whether the nonlinear structure tensor helps to better preserve structure in the image or not.

Figure 3.14 presents on the left the filter response using Knutsson's formulation with nonlinear smoothing as a post-processing step, while on the right a linear smoothing was carried out. As it can be seen, structure and boundaries are better preserved on the left image, which is the one that uses nonlinear structure tensor. From the details depicted on Fig. 3.15, it can also be seen that the linear structure tensor also introduces a bit of blurring in some structures and textures, although the boundaries are well preserved.

Table 3.3 shows the MSE error between the original image and the output of the proposed algorithm using the nonlinear structure tensor on one hand, and on the other the classical linear structure tensor. From those results it is clear the superior performance using nonlinear structure tensors to compute the neighborhoods, something which is coherent with the comparison carried out in section 3.3.4.

3.6.3 Experiment 3: Performance of the Wiener Filter

In order to validate the anisotropic covariance estructure methodology presented in section 3.4.4, we compare four different implementations of the Wiener filter:

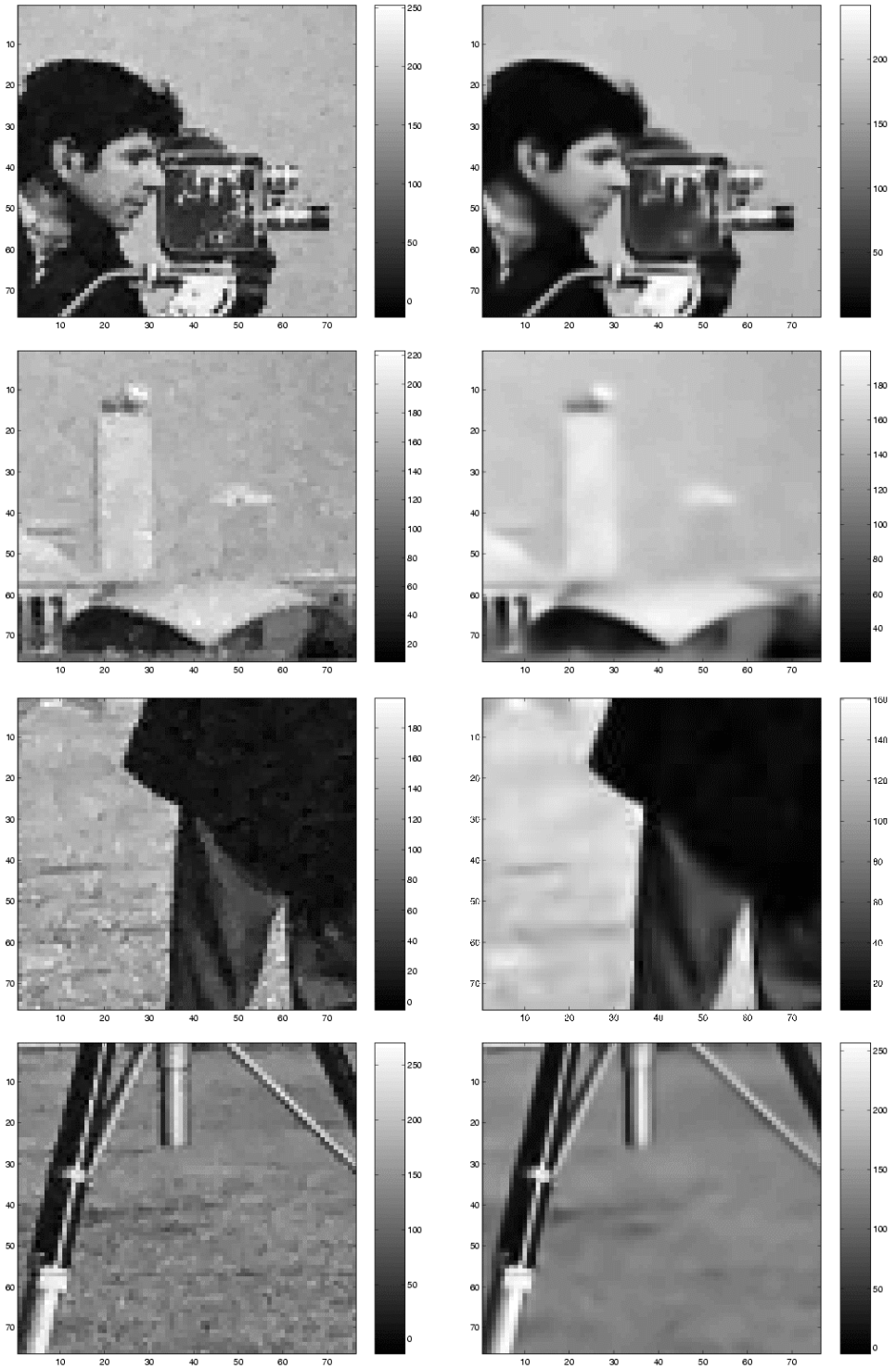

Figure 3.15: Details of the images presented in Fig. 3.14. Left Column: Details of the response from our method using Knutsson's formulation with Nonlinear smoothing. Right Column: Details of the response from our method using Knutsson's formulation with linear smoothing.

Restoration Method	MSE
Anisot. Gaussian (Adaptive Neighborhoods, nonlinear str. tensor)	42.0659
Anisot. Gaussian (Adaptive Neighborhoods, linear str. tensor)	60.5272

Table 3.3: Comparison of the Mean Squared Error between the original image and the output.

1. A FIR implementation where the covariance estructure is directly estimated from data using the following expression:

$$c_s(\mathbf{x_i}) = \frac{1}{K}\sum_{j=1}^{K}(s(\mathbf{x_i}) - \eta_s(\mathbf{x_i}))(s(\mathbf{x_{k+i}}) - \eta_s(\mathbf{x_{k+i}})) \tag{3.40}$$

2. A FIR implementation where the covariance estructure is computed using the exponential model presented here:

$$c_s(\mathbf{h}) = \sigma^2 \exp\left(-\frac{|\mathbf{h}|}{r}\right) \tag{3.41}$$

3. A FIR implementation where the covariance estructure is anisotropically estimated using the information of the local structure tensor, as expressed in the following equation:

$$c_s(\mathbf{h}) = \sigma^2 \exp\left(-\frac{\sqrt{(\mathbf{x_i} - \mathbf{x_j})\mathbf{T}(\mathbf{x_i} - \mathbf{x_j})}}{r}\right) \tag{3.42}$$

4. An Infinite Impulse Response (IIR) implementation using the adaptive Wiener filter algorithm developed by Lee [Lim90]. The impulse response in the Fourier domain $\mathcal{H}(\omega)$ is given by the following expression:

$$\mathcal{H}(\omega) = \frac{S_s(\omega)}{S_s(\omega) + S_w(\omega)} \tag{3.43}$$

   where $S_s(\omega)$ and $S_w(\omega)$ are, respectively, the signal and noise power spectra, which are directly estimated from data.

Figure 3.16 shows the results obtained with these four implementations after removing the noise introduced in the image shown in Fig. 3.12, but the noise image is built with a higher noise level $\sigma_N = 25$. In all cases, the local neighborhood used to compute the estimated value is optimized in order to obtain the best result. For instance, in implementation 1 and 2 we have used a 3×3 local neighborhood, in implementation 3 we have used a 7×7 neighborhood and in implementation 4 a 5×5 neighborhood. From the images, it can be seen that the noise perturbation is well removed, specially with our anisotropic version of the Wiener filter.

Table 3.4 shows the MSE error between the original image and the output of the different Wiener filter implementations used in our experiment. From the results, it can be seen that the noise is better removed with our anisotropic Wiener filter implementation, which provides the lowest MSE. It is interesting to remark that using the exponential covariance model without the local structure tensor we obtain the highest error rate.

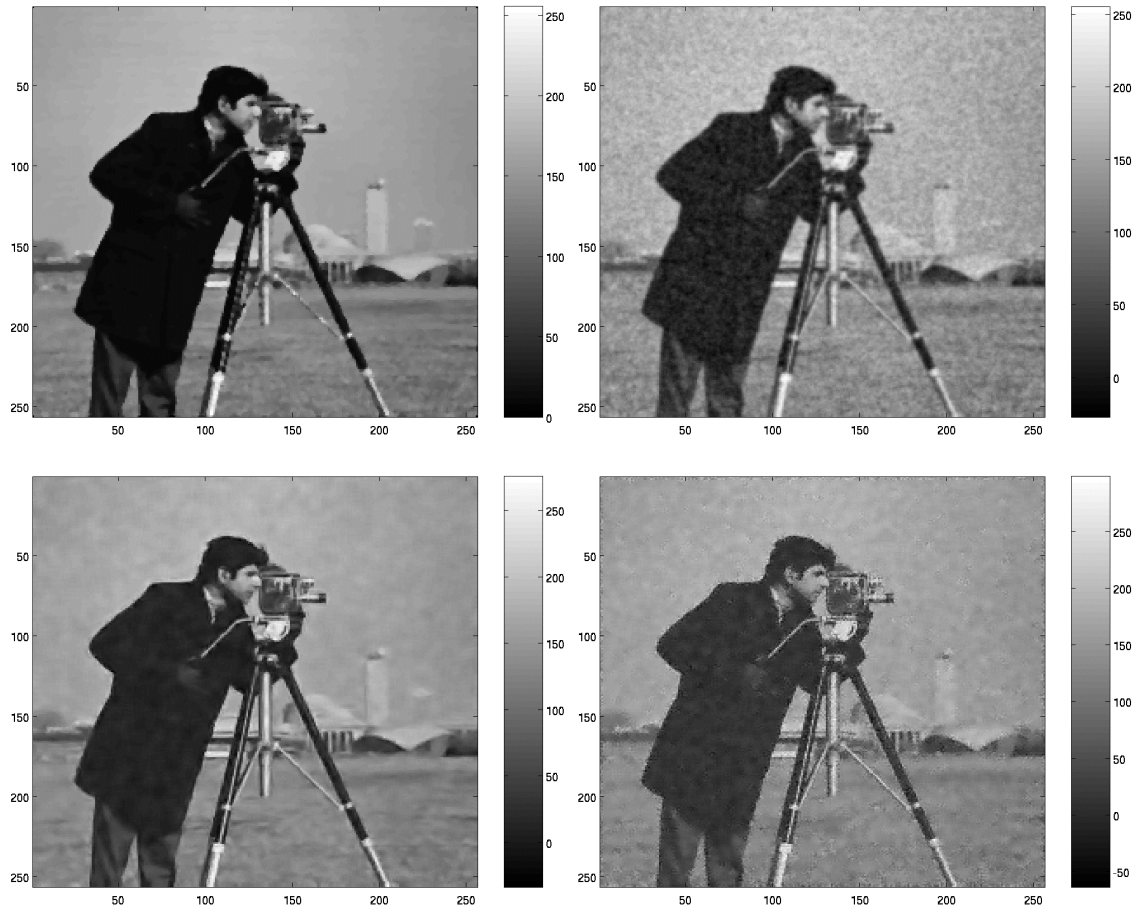

Figure 3.16: Wiener Filter responses obtained with the four implementations described in section 3.6.3. Top Left: FIR implementation with covariance directly estimated from data. Top Right: FIR implementation with an isotropic exponential covariance model. Bottom Left: FIR implementation with an anisotropic exponential covariance model using the local structure tensor. Bottom Right: Adaptive Wiener filter using Lee's algorithm [Lim90].

Restoration Method	MSE	Std Dev. MSE	Max. $(\hat{s})$	Min. $(\hat{s})$
Implementation num. 3	91.4020	235.6948	269.9761	-33.0372
Implementation num. 1	146.5894	981.6200	255.6570	0
Implementation num. 4	154.2067	360.1334	298.3844	-63.3675
Implementation num. 2	193.2791	516.5352	255.4840	-27.3688

Table 3.4: Statistics on the Mean Squared Error between the original image in Fig. 3.12 and results in Fig. 3.16. Columns from left to right: MSE, Standard Deviation of the MSE, Maximum value of the estimated signal and Minimum value of the estimated signal.

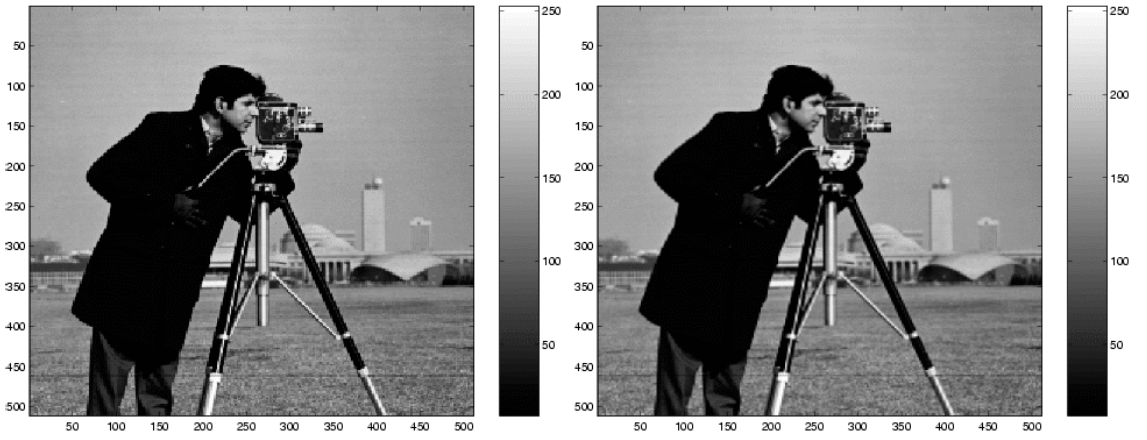

Figure 3.17: Left: Upsampled image using our anisotropic interpolation approach. Right: Upsampled image using bilinear interpolation.

3.6.4 Experiment 4: Anisotropic Interpolation

Finally, we present the results we have obtained using our anisotropic interpolation algorithm. To that end, we start from the original image shown in Fig. 3.12 to generate an upsampled image of double size. The result is shown on the left side of Fig. 3.17 in contrast with the result obtained with a bilinear interpolation technique. At a first glance, both images seem to be quite similar, but step boundaries are only well preserved with the anisotropic interpolation technique, as it was expected.

This fact can more clearly seen in Fig. 3.18, where some details of the images are shown. On the left column, we show the original image details. In the middle, we present the same details upsampled using the anisotropic interpolation technique presented in section 3.4.3. Finally, on the right we show the result of bilinear interpolation. From these results, we can clearly verify the anisotropic behavior of the proposed algorithm, since the step boundaries are not blurred, as seen, for instance, in the detail of the arm or in the background building of the image.

3.6.5 Experiment 5: Interpolation on Synthetic Tensor Data

To assess our approach in the presence of edges, we perform interpolation of a tensor field consisting of a step edge with constant tensors on one side and quite small tensors on the other side. In figure 3.19 we compare the upsampled tensor field obtained with linear interpolation (shown on the left) with the upsampled tensor field obtained using the approach presented in section 3.4.3 (shown on the right). To estimate the local structure tensor field with (3.39), we use the values $\| \omega_0 \| = \frac{\pi}{8}$, and $B = 2$ in (3.17). The quadrature filters are oriented in the directions pointing to the vertexes of a hexagon.

From that figure, it is noticeable that the edge is smeared out further using linear interpolation compared to the proposed method using the inverse structure tensor as a local metric, as it was expected. The estimated tensors that are pointed out by the arrows correspond to the values where the linear interpolation method fails because information of

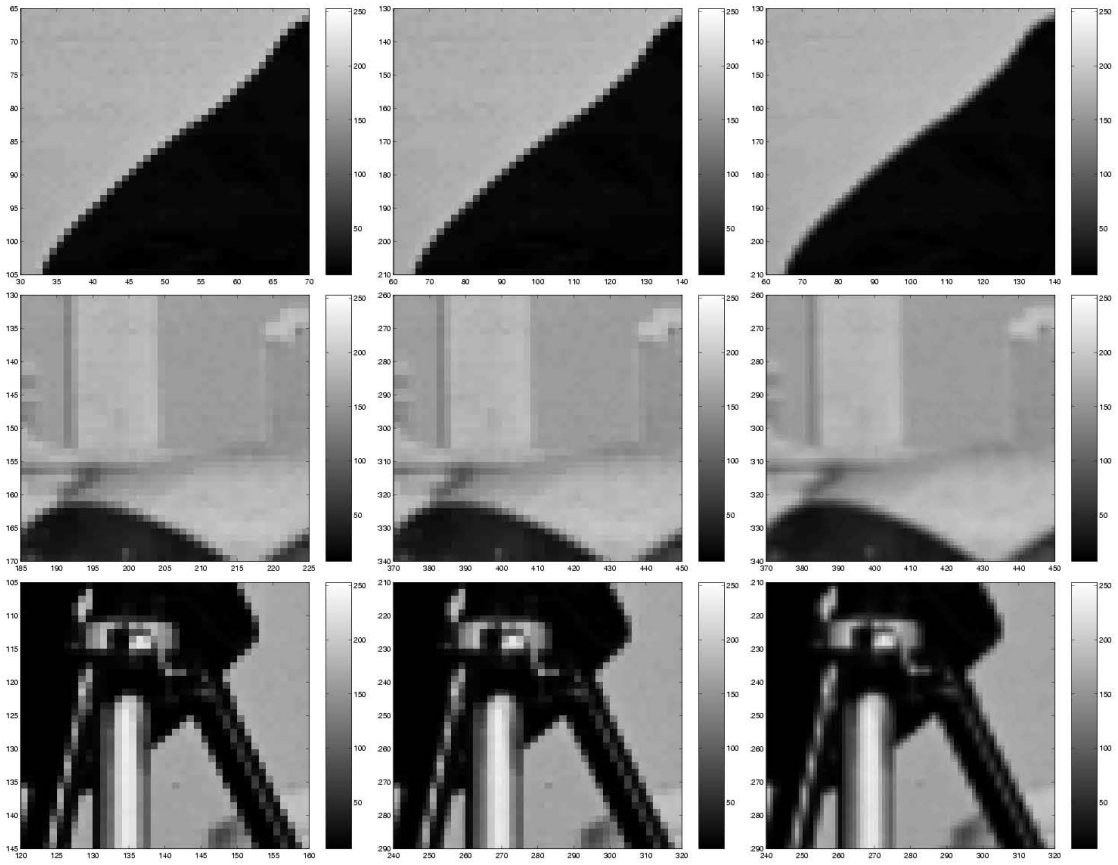

Figure 3.18: Left Column: Details from the original image. Middle Column: Details of the upsampled image using our anisotropic interpolation approach. Right Column: Details of the upsampled image using bilinear interpolation.

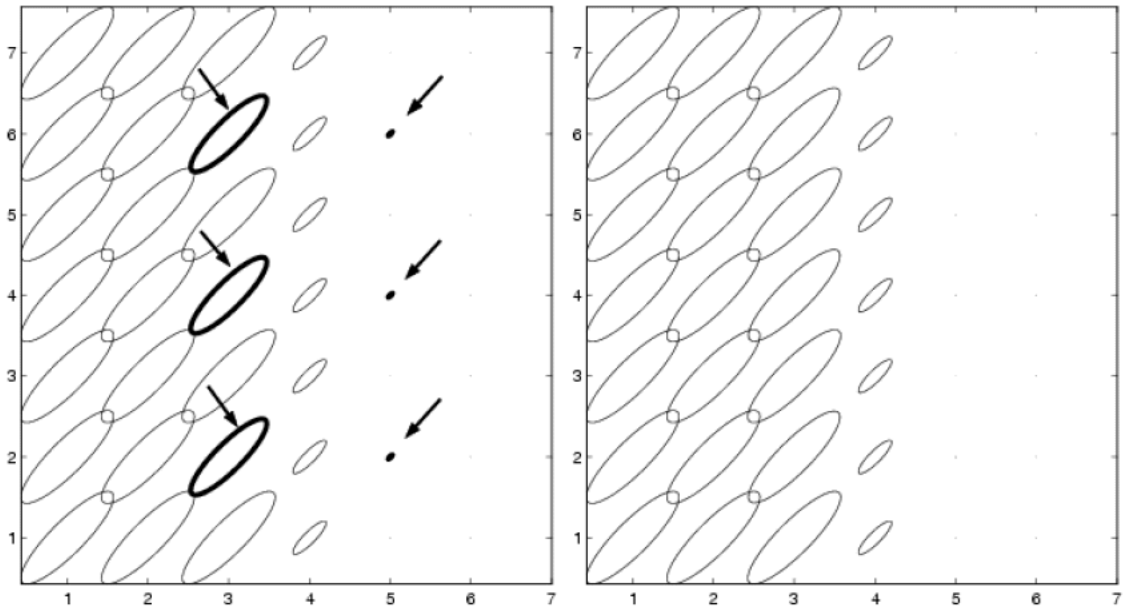

Figure 3.19: Results from interpolation of tensor valued data using linear interpolation (left), and anisotropic interpolation (right).

both sides of the edge is mixed, yielding to overestimated tensor values. On the contrary, with our approach that effect is almost negligible. Since we use the inverse of the local structure tensor as a metric, samples along the direction of maximum signal variation seems to be much further than they are. In contrast, those samples along the boundary seems to be closer. The global effect is that the contribution of tensors on the other side of the step is almost negligible, as shown in the figure.

3.6.6 Experiment 6: Interpolation on clinical DT-MRI Data

We have also tested our approach with 2D clinical DT-MRI data, which was obtained at Brigham & Women's Hospital (Boston (MA) - USA) from a GE Signa 1.5 Tesla Horizon Echospeed 5.6 system with standard 2.2 Gauss/cm field gradients. The voxel resolution is 0.85 mm$\times$0.85 mm$\times$5 mm.

Figure 3.20 shows on the left a 2D representation of an axial slice, with the corresponding anatomycal MRI T2 image in the background. On the right, we can see the highlighted area with double resolution. As it can be seen, edges are correctly preserved by the interpolation algorithm also with real data.

3.7 Conclusions

In this chapter we have studied the local structure tensor as an image processing tool to develop algorithms for scalar and tensor-valued signals. Motivated by the fact that several methods have been proposed in the literature to estimate that tensor, mainly,

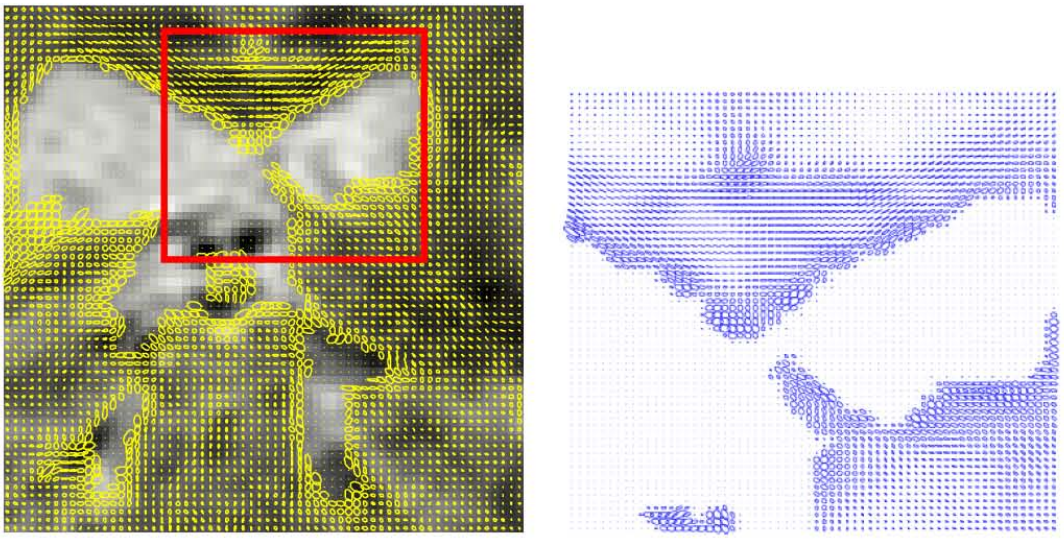

Figure 3.20: DT-MRI 64×64 slice of the *corpus callosum* superposed over the corresponding MRI T2 image (left) and a zoomed part of the central area (right).

those based on the outer product of the gradient and those based on the computation of the signal local energy, we have studied the robustness of these methods against noise. From our results, we have seen that the postprocessing smoothing usually applied to the estimated tensor field usually yields to structure delocalization, which can be reduced by means of a nonlinear smoothing technique. Also from our results, we verified that energy-based methods are more robust against noise that those based on the outer product of the gradient.

Then, we presented an anisotropic gaussian filtering scheme which uses nonlinear structure tensors to define the neighborhood to be used in the estimation and to drive an anisotropic gaussian function. On the one hand, the definition of the neighborhood by means of the local structure tensor leads us to a general framewok to build anisotropic versions of classical linear estimators, such as Wiener or constrained LMMSE. On the other hand, we introduce the use of nonlinear structure tensors in a well known filtering approach, as it is anisotropic gaussian filtering.

The local structure tensor can also be used to derive models of the signal covariance function taking into account its own structure. Statistical second order signal characterization is important in the field of signal processing since it yields to the derivation of filters that are grounded on a bayesian framework, interpreting signals as fields of random variables, using statistics to perform estimations. In this context, the use of the local structure tensor contributes to obtain covariance models that better fit the real signal behavior, yielding to improved signal estimators.

Finally, the previous ideas were also used to interpolate tensor fields, which is essential for many important tasks managing digital imagery and, in particular for data of low resolution such as clinical DT-MRI data. We presented a new method to interpolate a tensor field, preserving boundaries and assuring the positive-semidefinite constraint. Our approach interpolates tensors using the natural neighbors of the interpolation point, in

a regular grid, with weights proportional to the inverse squared distance between the samples and the interpolation point, using the inverse of a generalization of the local structure tensor as a metric to compute those distances.

Chapter 4

Homomorphic Filtering of Tensor Data

4.1 Introduction

In this chapter, we focus our attention in the problem of filtering tensor images. Filtering algorithms are mainly motivated by the necessity of improving the quality of images degraded by noise during the acquisition process. In the context of tensor images, such as those provided by DT-MRI, the Signal-to-Noise Ration (SNR) is often low because the acquisition time is restricted by human facts like patient's ability to rest immobile. Indeed, the study of the effects of noise in DT-MRI is still a matter of discussion [Anderson01, Skare00]

A DT-MRI dataset consists of noisy samples drawn from an underlying macroscopic diffusion tensor field, which is assumed continuous and smooth at a coarse anatomical scale [RF04]. Within this context, a symmetric positive semidefinite tensor describes the voxel-averaged diffusion of water molecules in tissues due to Brownian motion [Basser96]. The main restriction of filtering algorithms that deal with tensors is to remove noise with the constraint of preserving tensors positive semidefinite after processing the signal [Castaño03b]. In addition, usual arithmetic operations on tensors have to be carefully done since they produce some artifacts on the results, such as isotropic tensors as the result of the addition of two anisotropic tensors [Westin02a] or the swelling effect [Tschumperlé03a] due to a faster regularization of eigenvalues than eigenvectors.

In this chapter we propose a theoretical framework for the design of filters to deal with tensor data. The main contribution of the proposed method is the fact that the response of the filter is assured to be symmetric positive semidefinite independently from the filter used to regularize the tensor field [Castaño06c]. The basis of our approach relies on the algebraical interpretation of the set of symmetric positive semidefinite tensors which are mapped to the vector space of symmetric matrices following a generalization of the homomorphic decomposition for scalar signals developed in [Oppenheim67].

In section 4.2 we review some fundamental mathematical concepts that we will use later in our generalization of the homomorphic theory for tensor data. Then, section

4.3 explains the homomorphic theory for scalar data and the decomposition that can be achieved for homomorphic systems. A well-known practical application of homomorphic systems is detailed in Section 4.3.2, where a new perspective is offered in order to generalize the homomorphic processing for tensor signals in Section 4.4. To achieve our objective, Section 4.4.1 presents the algebraical properties of the set of positive definite matrices. Finally, some results on both synthetic and real DT-MRI data are presented in Section 4.5 in order to validate our approach.

4.1.1 Contributions in this Chapter

- *Algebraic Interpretation of Homomorphic Systems (Section 4.3.2):* We have performed a reinterpretation of the homomorphic theory from an algebraical point of view as a preceding step for the generalization for tensor data.
- *Processing Cascade for Positive Definite Tensor Data (Section 4.4.1):* We proposed a processing chain inspired on the homomorphic decomposition to ensure that tensors at the output are positive definite independently of the filter used in that chain to reduce the noise.
- *Processing Cascade for Positive Semidefinite Tensor Data (Section 4.4.2):* In order to deal with positive semidefinite tensor signals, we propose a different processing cascade using other input and output subsystems in the processing chain.

4.2 Theory of Vector Spaces and Basic Matrix Functions

Before any further development of our scheme, it is necessary to broadly review some mathematical concepts that will be used later on sections 4.3 and 4.4.

4.2.1 Groups, Subgroups and Homomorphisms

From an algebraical point of view, numbers are organized in following certain relationships that can be studied. In this section we define the concept of groups that will be used later in this chapter.

Definition 4.2.1 *A group $(G, \circ)$ under $K = \mathbb{R}$ or $\mathbb{C}$ is a non-empty set G with an internal law to combine elements of that set such that the combination results in a new element of the same set,*

$$\circ : G \times G \mapsto G \tag{4.1}$$

and, in addition, satisfies the following properties:

- *For any $a, b, c \in G$, $(a \circ b) \circ c = a \circ (b \circ c)$*
- *There exists a identity element $e_{id} \in G$ such that, for any $a \in G$, $a \circ e_{id} = a = e_{id} \circ A$.*

- *For any* $a \in G$ *there exists an inverse element* $a^{-1} \in G$ *such that* $a \circ a^{-1} = a^{-1} \circ a = e_{id}$.

A group that, in addition, satisfies the conmutative property for the group operation $a \circ b = b \circ a$ for any $a, b \in G$ is called conmutative group or Abelian.

Several matrix groups can be defined following the previous definition. In this sense, let $M_n(\mathbb{R})$ denote the set of $n \times n$ matrices with values in $\mathbb{R}$. Then, we can distinguish the following groups with matrix multiplication as group operation:

- *General Linear Group*: $GL_n(\mathbb{R}) = \{\mathbf{A} \in M_n(\mathbb{R}) | det(\mathbf{A}) \neq 0\}$.
- *Special Linear Group*: $SL_n(\mathbb{R}) = \{\mathbf{A} \in M_n(\mathbb{R}) | det(\mathbf{A}) = 1\}$.
- *Orthogonal Group*: $O_n(\mathbb{R}) = \{\mathbf{A} \in M_n(\mathbb{R}) | \mathbf{A}^T\mathbf{A} = \mathbf{A}\mathbf{A}^T = I\}$.
- *Special Orthogonal Group*: $SO_n(\mathbb{R}) = \{\mathbf{A} \in M_n(\mathbb{R}) | det(\mathbf{A}) = 1, \mathbf{A}^T\mathbf{A} = \mathbf{A}\mathbf{A}^T = \mathbf{I}\}$.

A group such that its elements have the topology of a manifold, that is, every element has a neighborhood which can be approximated to an Euclidean space, then it is called *Lie Group* .

Within a group $(G, \circ)$, we can also have a subset of elements with an algebraical structure similar to a group:

Definition 4.2.2 *Let* $(G, \circ)$ *be a group. A subgroup* $(H, \circ)$ *of* G *is a subset of* G *satisfying the following three axioms:*

- *For any* $a, b \in H$, $(a \circ b) \in H$
- *There exists a identity element* $e_{id} \in H$ *such that, for any* $a \in H$, $a \circ e_{id} = a = e_{id} \circ a$.
- *For any* $a \in H$ *there exists an inverse element* $a^{-1} \in H$ *such that* $a \square a^{-1} = a^{-1} \square a = e_i$.

The subgroup axioms ensure that a subgroup H of a group G is itself a group, with group operation, identity and inverses inherited from G.

Finally, an important concept in vector algebra is the concept of *Group Homomorphism*, which is defined as follows:

Definition 4.2.3 *Let* $(G, \square)$ *and* $(H, \circ)$ *be groups, with* $\square$ *and* $\circ$ *their respective group operations. A group homomorphism is a function* $\Phi : G \mapsto H$ *such that, for any two elements* $a, b \in G$

$$\Phi(a \square b) = \Phi(a) \circ \Phi(b) \tag{4.2}$$

If $\Phi : G \mapsto H$ is a homomorphism such that there is a one-to-one correspondence between the elements of both groups, we call it a bijection. In other words, Φ is a bijection if for each element $g \in G$ there is only one $h \in H$ such that $\Phi(g) = h$ at the same time that for each element $h \in H$ there is only one $g \in G$ such that $\Phi^{-1}(h) = g$. Then, if Φ^{-1} is also a homomorphism, we call Φ a group isomorphism and, therefore, G and H are called isomorphic.

A special isomorphism is the homeomorphism, which is a isomorphism between algebraic structures, (i.e. sets, groups, etc.) which respects their topological properties. In other words, an homeomorphism $\Psi : X \mapsto Y$ is a mapping from an algebraic structure X to a different one Y, such that Ψ is a continuous function, it is also a bijection and the inverse function Ψ^{-1} is continuous.

4.2.2 Vector Spaces

The mathematical concepts of vector spaces are widely used in signal processing techniques to derive different kinds of algorithms. This is mainly due to the solid foundation and tools they provide which make the task of designing the algorithms and understanding their behavior much easier [Moon99]. In this sense, we review in this section some important concepts of vector spaces theory and how they can be generalized in order to develop our homomorphic filtering approach for tensor signals.

Definition 4.2.4 *[Isham89] A linear vector space V under $K = \mathbb{R}$ or $\mathbb{C}$ is a non-empty set with an internal law to combine elements of that set such that the combination results in a new element of the same set,*

$$+ : V \times V \mapsto V \tag{4.3}$$

an outer law to combine scalars and elements of V such that also provides a new element of V,

$$\cdot : K \times V \mapsto V \tag{4.4}$$

and, in addition, satisfies the following properties:

1. *$(V, +)$ is a commutative group.*
2. *For any $A \in V$, and any $\alpha, \beta \in K$, $\alpha \cdot (\beta A) = (\alpha \cdot \beta) \cdot A$*
3. *For any $A \in V$, and any $\alpha, \beta \in K$, $(\alpha + \beta)A = \alpha \cdot A + \beta \cdot A$*
4. *For any $A, B \in V$, and any $\alpha \in K$, $\alpha(A + B) = \alpha \cdot A + \alpha \cdot B$*
5. *If $A \in V$ and $\alpha \in K$, $\alpha \cdot A = 0$, then it implies that $\alpha = 0$ or $A = 0$*

The canonical rule $+$ to combine elements from a vector space is the addition in the usual sense. This law is also called the inner operation since it defines how we can operate with vector space elements. On the other hand, scalar multiplication $\cdot$ is the canonical rule to operate with scalars and vectors.

Nevertheless, other internal and external rules can be defined yielding to a generalization of the notion of vector space. In this way, the necessary properties for a vector space described in definition 4.2.4 are modified as follows:

Definition 4.2.5 *A generalized linear vector space V under $K = \mathbb{R}$ or $\mathbb{C}$ is a non-empty set with an internal law to combine elements of that set such that the combination results in a new element of the same set,*

$$\square : V \times V \mapsto V \tag{4.5}$$

an outer law to combine scalars and elements of V such that also provides a new element of V,

$$: : K \times V \mapsto V \tag{4.6}$$

and, in addition, satisfies the following properties:

1. *$(V, \square)$ is a conmutative group.*
2. *For any $A \in V$, and any $\alpha, \beta \in K$, $\alpha : (\beta : A) = (\alpha : \beta) : A$*
3. *For any $A \in V$, and any $\alpha, \beta \in K$, $(\alpha + \beta) : A = (\alpha : A)\square(\beta : A)$*
4. *For any $A, B \in V$, and any $\alpha \in K$, $\alpha : (A \square B) = (\alpha : A)\square(\alpha : B)$*
5. *If $A \in V$ and $\alpha \in K$, $\alpha : A = 0$, then it implies that $\alpha = 0$ or $A = 0$*

Now, the associative and distributive properties rely on the new rules yielding to a straightforward generalization of the whole theory of vector spaces.

4.2.3 Linear Systems

Linear systems have generated a particular interest in the field of signal processing since they facilitate the analytical characterization of the system response. Any system $H\{\cdot\}$ is called linear if it satisfies the principle of superposition [Oppenheim97],

$$H\{s_1(t) + s_2(t)\} = H\{s_1(t)\} + H\{s_2(t)\} \tag{4.7}$$

$$H\{\alpha_1 \cdot s_1(t)\} = \alpha_1 \cdot H\{s_1(t)\} \tag{4.8}$$

which states that the response of the system $H\{\cdot\}$ to the combination of any two input signals $s_1(t)$ and $s_2(t)$ is the combination of the system responses for each signal. Also, the system response of a scaled version of the input signal $s_1(t)$ produces a scaled response of the system response for the input signal with the same scale factor α_1.

It is very interesting to analyze the principle of superposition from the perspective of vector spaces theory. From this point of view, the system transformation $H\{\cdot\}$ can be interpreted as a mapping from the input signal vector space, denoted as V_{input}, to

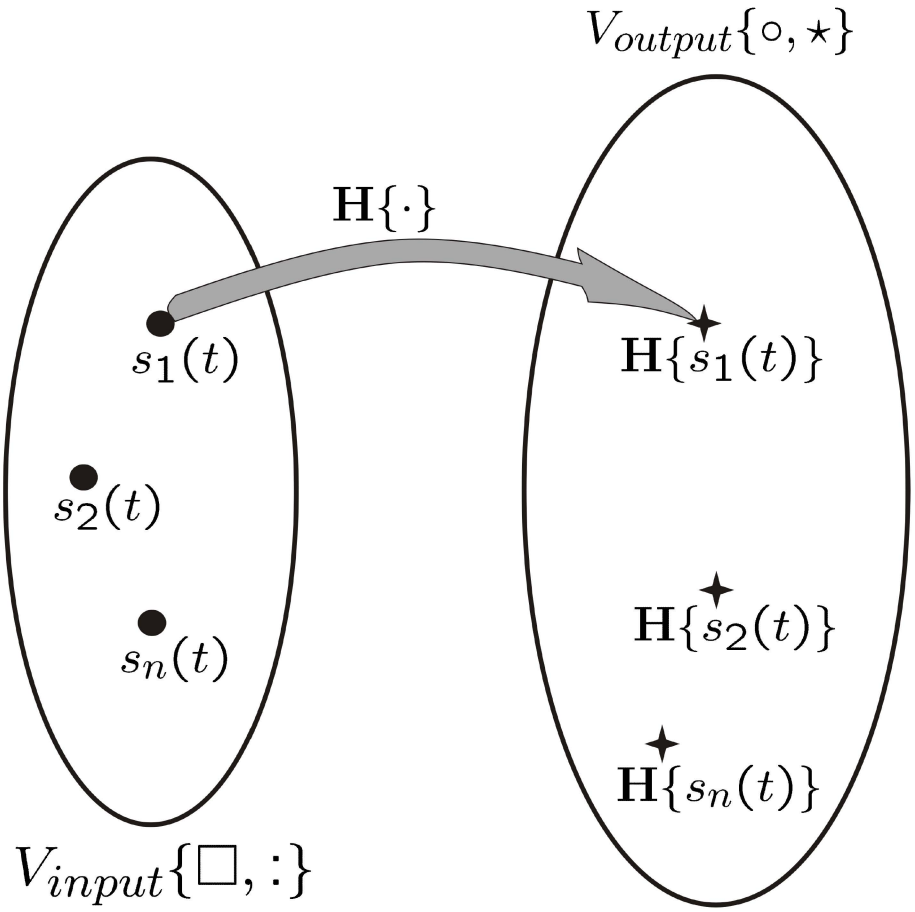

Figure 4.1: System transformation interpreted as a mapping from the input signal vector space to the output signal vector space.

the output signal vector space, denoted as V_{output}, as it is represented in Fig. 4.1 [Oppenheim65]

When this mapping is such that preserves the algebraical structure of the input space at the corresponding output space, then it is a linear system. In other words, when the basis of the output space is a linear combination of the basis elements in the input space, then, the principle of superposition is satisfied. This fact means that we can either combine the signals on the input space before computing the response of the combined input signal or compute the responses of the input signals and after that combine the responses on the output space.

From this point of view, it is not hard to generalize the principle of superposition to vector spaces with inner and outer operations different from $+$ and $\cdot$, respectively. Let us define $V_{input}(\square, :)$ and $V_{output}(\circ, \star)$ as the input and output signal spaces, respectively, with the internal laws defined by $\square$ and $\circ$ and the outer operations given by $:$ and $\star$. Then, any system $H\{\cdot\}$ that transforms the elements $s_i(t)$ on $V_{input}(\square, :)$ to $V_{output}(\circ, \star)$ satisfies the generalized principle of superposition if the following properties are met [Oppenheim67]:

$$H\{s_1(t)\square s_2(t)\} = H\{s_1(t)\} \circ H\{s_2(t)\} \tag{4.9}$$

$$H\{\alpha_1 : s_1(t)\} = \alpha_1 \star H\{s_1(t)\} \tag{4.10}$$

This generalization has the same meaning of the original principle, but in this case the combination of the signals has to be done with the correct operator, depending on the rules defined for each space [Oppenheim68b].

4.2.4 Basic Matrix Functions

Some basic matrix functions that arise in our approach are described in this section, showing the simplifications that can be achieved for the particular case of symmetric positive definite matrices. The following matrix functions are of particular interest in our approach:

1. **Matrix Square Root:** [Björck83, Higham86, Higham87, Higham97] Let $\mathbf{A} \in \mathbb{R}^{n\times n}$ be a matrix with real elements. Any $\mathbf{X}$ such that $\mathbf{X}^2 = \mathbf{A}$ is a square root of $\mathbf{A}$.

   - If $\mathbf{A}$ is positive definite, that is, all its eigenvalues are greater than zero, then there is a unique square root $\mathbf{X}$ all of whose eigenvalues are also positive, which is called *principal square root.*
   - If $\mathbf{A}$ is symmetric positive semidefinite with at least one of its eigenvalues equal to zero and, hence, a singular matrix, it has a square root since the previous sequence of numbers is always equal to zero: $dim(ker(\mathbf{A}^i)) = dim(ker(\mathbf{A}^{i-1})) = \text{numberofzero} - \text{eigenvalues}$.

2. **Matrix Exponential:** [Moler78, Ward77, Higham05b] The exponential of $\mathbf{A} \in \mathbb{R}^{n\times n}$ is defined by:

$$\exp(\mathbf{A}) = \sum_{i=0}^{\infty} \frac{\mathbf{A}^n}{n!} \tag{4.11}$$

   - $\exp(\mathbf{A}+\mathbf{B}) = \exp(\mathbf{A})\exp(\mathbf{B})$ holds if $\mathbf{AB} = \mathbf{BA}$.

3. **Matrix Logarithm:** [Kenney89, Cheng01, Higham01] Let $\mathbf{A} \in \mathbb{R}^{n\times n}$ be a matrix with real elements. Any $\mathbf{X}$ such that $\exp(\mathbf{X}) = \mathbf{A}$ is a logarithm of $\mathbf{A}$.

   - If $\mathbf{A}$ has positive eigenvalues, then there is a unique logarithm $\mathbf{X}$ of $\mathbf{A}$ all of whose eigenvalues are real numbers which is called principal logarithm of $\mathbf{A}$.
   - If $\mathbf{A}$ has a real logarithm if and only if $\mathbf{A}$ is nonsingular and $\mathbf{A}$ has an even number of Jordan blocks of each size for every negative eigenvalue.
   - If the spectral radius $\rho(\mathbf{A}) = \max_{1\leq i\leq n}\{|\lambda_i|\} < 1$, then

$$\log(\mathbf{I}+\mathbf{A}) = \sum_{i=1}(-1)^{n+1}\frac{\mathbf{A}^n}{n} \tag{4.12}$$

It is also interesting to compute any general function of a matrix. This task can be defined in several ways, for instance, through its *spectral decomposition*, a *polynomial approximation* or the definition of *Cauchy integral*. Here, we briefly describe the first and the second methods exploiting the properties of symmetric positive definite matrices in order to apply the results later. We refer the interested reader to [Higham05a] for further details on more general matrices.

1. **Spectral decomposition:** For symmetric matrices, the spectral decomposition $\mathbf{A} = \mathbf{P}^T\mathbf{D}\mathbf{P}$ is always possible where $\mathbf{P}$ is a orthonormal matrix whose columns are the eigenvectors of $\mathbf{A}$, while its eigenvalues λ_i are the diagonal elements of matrix $\mathbf{D}$. Thus, any function $\mathbf{f}(\mathbf{A})$ can be computed as $\mathbf{f}(\mathbf{A}) = \mathbf{P}^T\mathbf{f}(\mathbf{D})\mathbf{P}$, where $\mathbf{f}(\mathbf{D})$ is also a diagonal matrix whose non-zero elements are given by $f(\lambda_i)$.

   For non-symmetric matrices, the Schur decomposition can be achieved $\mathbf{B} = \mathbf{Q}^T\mathbf{T}\mathbf{Q}$, with $\mathbf{Q}$ orthonormal and $\mathbf{T}$ upper triangular, in order to simplify the computation of the function, which can be written as $\mathbf{f}(\mathbf{B}) = \mathbf{Q}^T\mathbf{f}(\mathbf{T})\mathbf{Q}$, where $\mathbf{T}$ can be efficiently computed with Parlett's recurrence algorithm [Parlett76].

2. **Polynomial Approximations:** Polynomial approximations of any matrix function, such as the given in Eq. 4.13 can be obtained by truncating a power series representation such as a Taylor series expansion. Another option is to construct a best approximation of the desired function (in some norm) of a given degree.

$$\mathbf{f}(\mathbf{X}) = \sum_{k=0}^{m} b_k\mathbf{X}^k \tag{4.13}$$

   The major concern of these methods is to efficiently evaluate a polynomial at a matrix argument. Several methods have been proposed to solve that problem, such as the method of Paterson and Stockmeyer [Golub96, Paterson73].

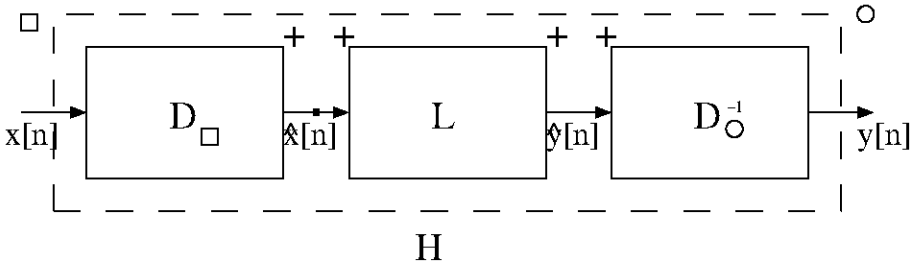

Figure 4.2: Canonic representation of a homomorphic system

4.3 Homomorphic Signal Processing of Scalar Signals

4.3.1 Homomorphic Systems

The basis of homomorphic signal processing techniques relies on the generalization of the principle of superposition described in section 4.2.3. In this sense, the system transformation $H\{\cdot\}$ is called homomorphic if it satisfies Eqs. 4.9 and 4.10 [Oppenheim68b].

As it was previously explained, the formalism for representing systems with this kind of properties lies in interpreting input and output signals as vectors within a vector space where the rules $\square$ and $\circ$ correspond to vector addition, that is, the way in which two elements of the vector space are combined; the rules : and $\star$ correspond to scalar multiplication, i.e. the way in which an element of the vector space is combined with scalars; and, finally, the system transformation $H\{\cdot\}$ is interpreted as an algebraically linear transformation on that space [Oppenheim65].

Within this framework, the traditional formulation of the principle of superposition (Eqs. 4.7 and 4.8) is a particular case when both, the input and output spaces, use traditional addition $+$ as inner rule and traditional scalar multiplication $\cdot$ as external law to combine signals and scalars [Oppenheim68b].

It has been shown that any homomorphic system can be represented as a cascade of three subsystems [Oppenheim68b], as shown in Fig. 4.2. The first subsystem $D_{\square}\{\cdot\}$, where $\square$ denotes the rule to combine two elements on the input space, which transforms elements on the input vector space to a linear vector space and satisfies the following properties:

$$D_{\square}\{s_1(t)\square s_2(t)\} = D_{\square}\{s_1(t)\} + D_{\square}\{s_2(t)\} \tag{4.14}$$

$$D_{\square}\{\tau : s_1(t)\} = \tau D_{\square}\{s_1(t)\} \tag{4.15}$$

The second subsystem $L\{\cdot\}$ is a linear system in the usual sense. Finally, the third subsystem is the inverse of $D_{\circ}\{\cdot\}$, where $\circ$ denotes the rule to combine two elements on the output space, which transforms elements on the output vector space to a linear vector space and satisfies Eqs 4.16 and 4.17. In this case, the inverse mapping $D_{\circ}^{-1}\{\cdot\}$ is required

in order to transform back from the linear space where the filtering was carried out to the output signal space.

$$D_{\circ}\{s_1(t) \circ s_2(t)\} = D_{\circ}\{s_1(t)\} + D_{\circ}\{s_2(t)\} \tag{4.16}$$

$$D_{\circ}\{\tau \star s_1(t)\} = \tau D_{\circ}\{s_1(t)\} \tag{4.17}$$

An interesting particular case, and also the most common practical situation, is the case when both input and output spaces are the same, that is to say $V_{input}(\square, :) = V_{output}(\circ, \star)$. This situation implies that the third subsystem is the same as the first one, $D_{\circ}\{\cdot\} = D_{\square}\{\cdot\}$ and satisfy the following property:

$$D_{\circ}^{-1}\{D_{\square}[s(t)]\} = D_{\square}^{-1}\{D_{\square}[s(t)]\} = s(t) \tag{4.18}$$

Figure 4.3 represents the homomorphic decomposition explained in this section, where it is clearly seen the path followed from the input vector space to the output vector space through the linear one, where we can apply the traditional mathematical concepts and tools to develop the linear filter $L\{\cdot\}$, which is an easier task than the design of the filter $H\{\cdot\}$.

4.3.2 An Example of Homomorphic Signal Processing

An example of particular interest in practical situations is to consider waveforms as the ordinary product of two signals (Eq. 4.19). For instance, amplitude modulation and image processing are two different domains where a common situation is to find two signals, one varying slowly and the other rapidly, combined as a product. In this kind of situations, the homomorphic decomposition allows us either to modify only one signal or to filter each one separately according to different objectives [Blair95].

$$s_1(t) \square s_2(t) := s_1(t) \cdot s_2(t) \tag{4.19}$$

In order to be able to apply the homomorphic decomposition we must define the rule to combine scalars and signals. Although several possibilities are possible, a particular interest is found on the rule proposed in [Oppenheim68a], where the scalar multiplication takes a signal to a scalar power:

$$c : s(t) := [s(t)]^c \tag{4.20}$$

Hence, we identify both input and output spaces as the same set of signals ($V_{input}(\cdot, .^c) = V_{input}(\cdot, .^c)$) with the operations defined in Eqs. 4.19 and 4.20. Then, to apply the homomorphic decomposition according to the canonic decomposition on Fig. 4.2, we require an input subsystem $D_{\square}\{\cdot\}$ with these three properties:

$$D_{\square}\{s_1(t) \cdot s_2(t)\} = D_{\square}\{s_1(t)\} + D_{\square}\{s_2(t)\} \tag{4.21}$$

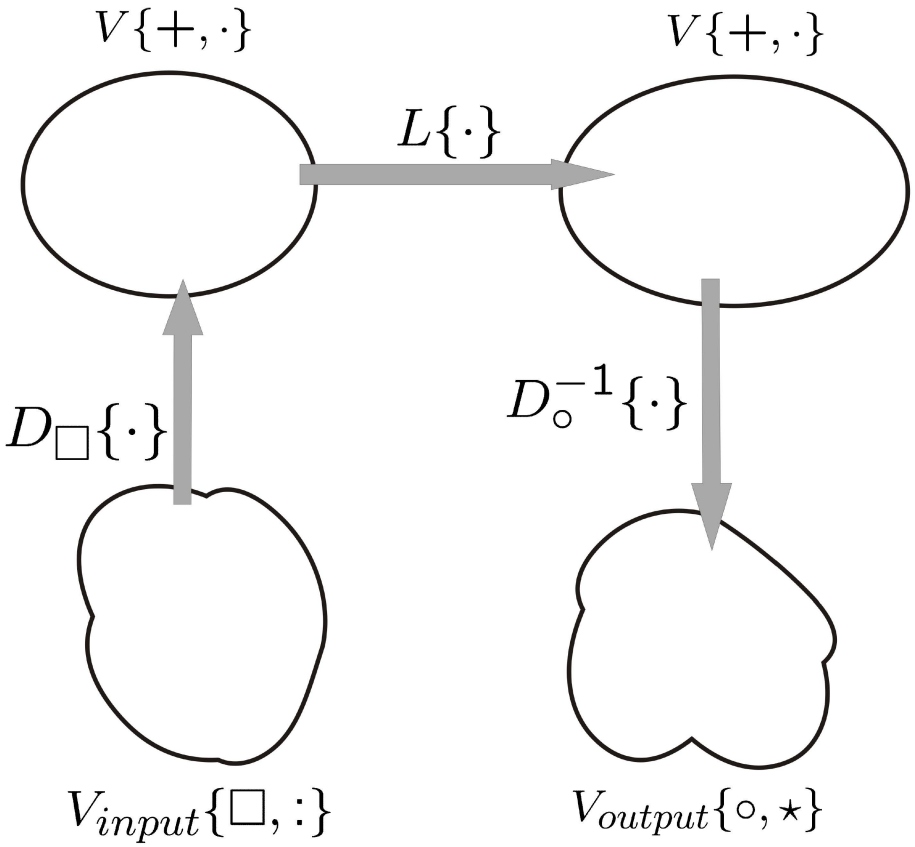

Figure 4.3: Homomorphic decomposition interpreted as a sequence of mappings from one signal space to another.

$$D_{\square}\{[s(t)]^c\} = cD_{\square}\{s(t)\} \tag{4.22}$$

$$D_{\square}^{-1}\{D_{\square}\{s(t)\}\} = s(t) \tag{4.23}$$

If we limit our consideration to include only positive real signals and real scalars, the characteristic system $D_{\square}\{\cdot\}$ may be chosen as the ordinary logarithm function and, hence, $D_{\square}^{-1}\{\cdot\}$ is the corresponding exponential function. We may think of several cases on the image processing field in which we encounter only positive real scalar signals, for instance, an image signal can be decomposed in term of light conditions where only positive values have physical meaning.

In the event that the signals to be processed cannot be restricted to positive values, we may consider complex signals and either real or complex scalars, but it is not possible to use the complex logarithm since the principal value of the logarithm of a product of complex signals is not always the sum of the principal values corresponding to the individual complex signals, as required by Eq. 4.21. However, there are some restrictions which can be placed upon complex input signals such that a satisfactory characteristic system $D_{\square}\{\cdot\}$ closely related to the complex logarithm can be found, as it is detailed in [Oppenheim68a].

An Algebraical Perspective

It is an instructive exercise to analyze the homomorphic decomposition for scalar signals from an algebraical point of view, since our generalization to deal with second-order tensors is better explained from an algebraical perspective. But before any further development, we briefly describe three important concepts:

- **Tangent Space**: Broadly speaking, the tangent space of a set M at a point $x \in M$, denoted as T_xM, is the vector space whose elements are all the possible directions in which one can pass through that point. For instance, the tangent space of a sphere in 3D at a point x of the surface is the plane which touches that point and is perpendicular to the radius of the sphere.

- **Lie Group**: A Lie Group G is a set of continuous elements, i.e. every element has a neighborhood, with a closed operation $* : G \times G \mapsto G$ that satisfies certain rules, such as associativity, neutral element and inverse element for the operation defined, which, in addition, is a continuous function of the elements. For instance, the set of positive real numbers, defined as $\mathbb{R}^+ : \{x \in \mathbb{R}, x > 0\}$ is a Lie Group under multiplication since it satisfies the associativity $(\forall a, b, c \in \mathbb{R}^+, (a \cdot b) \cdot c = a \cdot (b \cdot c))$, there exists a neutral element under multiplication $(a \cdot 1 = 1 \cdot a = a)$, there exists an inverse for each element $(a \cdot b = 1 \Leftrightarrow b = \frac{1}{a})$, every element has a neighbor and the multiplication is a continuous function of the elements.

- **Lie Algebra**: To every Lie Group G, we can associate a Lie algebra $\mathfrak{g}$, whose underlying vector space is the tangent space of G at the identity element

Following our example, the set of positive real numbers $\mathbb{R}^+$ is a group with usual multiplication as group operation. In fact, this set is also a Lie Group since it is a differentiable manifold [Moakher05]. Hence, any system whose impulse response $H\{\cdot\}$ satisfies the property in Eq. 4.24 is a homomorphism $\Phi(x) : \mathbb{R}^+ \mapsto \mathbb{R}^+$ with multiplication as group operation.

$$H\{x \cdot y\} = H\{x\} \cdot H\{y\}, \text{with} x, y \in \mathbb{R}^+ \tag{4.24}$$

However, the analysis of the homomorphism between groups with multiplicative operation might result a bit complicated. A common practice for an easier analysis is to transform the original group by means of a isomorphism, which provides a structurally identical group where the analysis can be better performed.

In this sense, the *exponential map* $\exp : \mathbb{R} \mapsto \mathbb{R}^+$ is a group isomorphism that transform the group of real elements $\mathbb{R}$ with addition as group operation into $\mathbb{R}^+$. The inverse operation, the *logarithm map*, $\log : \mathbb{R}^+ \mapsto \mathbb{R}$ is also a group isomorphism that transform back from the set of strictly positive real numbers $\mathbb{R}^+$ into the set of positive real numbers.

The initial homomorphism $\Phi(x) : \mathbb{R}^+ \mapsto \mathbb{R}^+$ is transformed into an equivalent mapping in the transformed space in order to provide the same response on the initial vector space. To find such a correspondence, it is necessary to look at the group $\mathbb{R}^+$ as a Lie Group whose Lie algebra $\mathfrak{g}$ is the additive group of all real numbers $\mathbb{R}$ [Moakher05].

The geometric link between a Lie group G and its Lie algebra $\mathfrak{g}$ is the fact that the Lie algebra can be viewed as the tangent space to the Lie group at the identity [Curtis87]. Indeed, the exponential map already defined is the map that allows to completely recapture the local group structure from the Lie algebra. More precisely, the exponential map is a map $\exp : \mathfrak{g} \mapsto G$ given by $\exp(X) = \gamma(1)$ where $\gamma : \mathbb{R} \mapsto G$ is the unique one-parameter subgroup of G whose tangent vector at the identity is equal to X, $\gamma'(0) = x$.

Then, if $\Phi : G \mapsto H$ is a homomorphism of Lie groups, and $\mathfrak{g}$ and $\mathfrak{h}$ are the Lie algebras of G and H respectively, then the induced map $d\Phi : \mathfrak{g} \mapsto \mathfrak{h}$, on tangent spaces is a Lie algebra homomorphism, where $d\Phi$ denotes its derivative at the identity.

From the above, we have the following lemma [Curtis87]:

Lemma 4.3.1 *Let $\Phi : G \mapsto H$ be a homomorphism of Lie groups and $d\Phi : \mathfrak{g} \mapsto \mathfrak{h}$ be the corresponding Lie algebra homomorphism, where $d\Phi$ denotes the derivative of Φ at the identity. Then, the diagram shown on Fig. 4.4 commutes.*

Proof By the definition of $d\Phi$, we have that $d\Phi(x) = (\Phi \circ \gamma)'(0)$. Then, $\Phi(\exp(x)) = \Phi(\gamma(1)) = (\Phi \circ \gamma)(1) = \exp(d\Phi(x))$. ∎

Hence, this algebraical interpretation of the homomorphic decomposition allow us to transform the initial group $\mathbb{R}^+$ with multiplication as group operation into the set of all real numbers with addition as group operation by means of the logarithm map. Then, we can design a linear filter $d\Phi(x)$ with the inherent property of being also a Lie algebra homomorphism. Finally, through the exponential map we can get back to the initial domain. All this process is equivalent to the definition of a Lie group homomorphism $\Phi(x) : \mathbb{R}^+ \mapsto \mathbb{R}^+$.

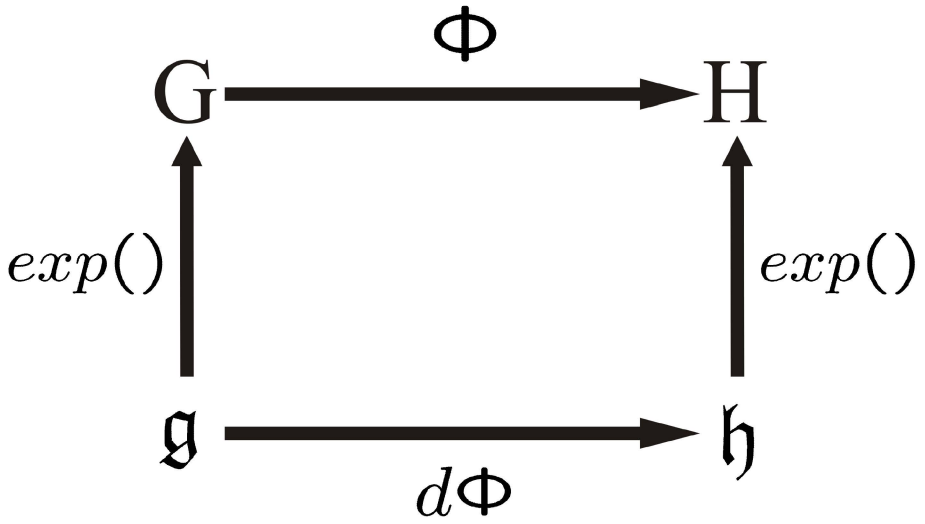

Figure 4.4: Correspondence between a Lie Group and the associated Lie algebra through the exponential map.

4.4 Homomorphic Tensor Signal Processing

The generalization of the homomorphic processing framework for tensor signals has a slightly different meaning than the scalar case. First, we review the algebraic structure of symmetric second order tensors $S(n)$ and symmetric positive definite second order tensors $PS^+(n)$ on which relies our generalization.

4.4.1 Algebraic Structure of Symmetric Positive Definite Tensors

The set of symmetric matrices $S(n)$ forms a vector space under usual matrix addition $+$ and scalar multiplication $\cdot$ [Gallier05] since the properties from definition 4.2.4 are satisfied as demonstrated as follows:

1. $(S(n), +)$ is a conmutative group.
2. For any $A \in S(n)$, and any $\alpha, \beta \in \mathbb{R}$, $\alpha \cdot (\beta \cdot A) = (\alpha \cdot \beta) \cdot A$
3. For any $A \in S(n)$, and any $\alpha, \beta \in \mathbb{R}$, $(\alpha + \beta) \cdot A = \alpha \cdot A + \beta \cdot A$
4. For any $A, B \in S(n)$, and any $\alpha \in \mathbb{R}$, $\alpha \cdot (A + B) = \alpha \cdot A + \alpha \cdot B$
5. If $A \in S(n)$ and $\alpha \in \mathbb{R}$, $\alpha \cdot A = 0$, then it implies that $\alpha = 0$ or $A = 0$

However, the set of symmetric positive definite matrices $PS^+(n)$ does not satisfy the requirements to form a vector space under usual matrix addition $+$ and scalar multiplication $\cdot$. For instance, it is not hard to see that properties 2, 3 and 4 from definition 4.2.4 may not be satisfied if scalars α, β are negative numbers. Indeed, the set $PS^+(n)$ is not even a group with matrix addition as group operation, since there is neither an identity element nor an inverse element that belongs to the group:

1. The operation is associative, that is, for any $\mathbf{A}, \mathbf{B}, \mathbf{C} \in PS^+(n)$ we have:

$$(\mathbf{A} + \mathbf{B}) + \mathbf{C} = \mathbf{A} + (\mathbf{B} + \mathbf{C}),$$

2. There exists an identity element $\mathbf{I} \in PS^+(n)$ such that:

$$\mathbf{A} + \mathbf{I} = \mathbf{I} + \mathbf{A} = \mathbf{A}$$

   The identity element under addition is the zero matrix, that is, a matrix whose elements are all equal to zero, which does not belong to the set $PS^+(n)$.

3. For any $\mathbf{A} \in PS^+(n)$ there is an element $\mathbf{A}^{-1} \in PS^+(n)$ such that $\mathbf{A} + \mathbf{A}^{-1} = \mathbf{I}$. This property also fails for $PS^+(n)$ since $\mathbf{A}^{-1}$ may not belong to the set of symmetric positive semidefinite matrices.

The algebraic interpretation of the homomorphic decomposition described in section 4.3.2, showed us that any homomorphism $\Phi : \mathbb{R}^+ \mapsto \mathbb{R}^+$ is equivalent to the composition of three different homomorphism: $\log : \mathbb{R}^+ \mapsto \mathbb{R}$, $d\Phi : \mathbb{R} \mapsto \mathbb{R}$ and $\exp : \mathbb{R} \mapsto \mathbb{R}^+$.

In the case of matrices, it is not straightforward to generalize these properties, since $PS^+(n)$ does not have the algebraical structure of a group. This means that neither the exponential map nor the logarithm map are group homomorphisms and $S(n)$ cannot be its associated Lie algebra [Gallier05].

From this point of view, the generalization we propose has a slightly different algebraical interpretation. It is founded on the fact that the exponential map $\mathbf{exp} : S(n) \mapsto PS^+(n)$ is a homeomorphism. A *homeomorphism* is a kind of isomorphism between any two algebraic structures which respects their topological properties. This means those elements that are neighbors in $S(n)$ are mapped to a local neighborhood in $PS^+(n)$, at the same time that those which are further in $S(n)$ are still far away in $PS^+(n)$, preserving the structure.

Any mapping $\Psi : X \mapsto Y$ between two topological spaces X and Y is called a homeomorphism if it has the following properties:

1. Ψ is continuous.
2. Ψ is a bijection.
3. The inverse function Ψ^{-1} is continuous.

It is straightforward that the exponential function is continuous, so in the following lemma we demonstrate that it is also a bijection [Gallier05]:

Lemma 4.4.1 *The exponential map*

$$\exp : S(n) \mapsto PS^+(n) \tag{4.25}$$

is a bijection which maps every symmetric matrix $\mathbf{A} \in S(n)$ *to another matrix* $\mathbf{B} = \exp \mathbf{A} \in PS^+(n)$ *which is symmetric positive definite and for every symmetric positive definite matrix* $\mathbf{B}$*, there is a unique symmetric matrix* $\mathbf{A}$ *such that* $\mathbf{B} = \exp \mathbf{A}$*.*

Proof A mapping $f : X \mapsto Y$ is said to be bijective if and only if for every $y \in Y$ there is exactly one $x \in X$ such that $f(x) = y$. In other words, f is bijective if and only if it is injective and surjective:

1. Let us denote by $\mathbf{A_1}, \mathbf{A_2} \in S(n)$ any two symmetric matrices whose spectral decompositions are given by $\mathbf{A_k} = \mathbf{P_{A_k}}^T \mathbf{diag}(\lambda_i^{A_k}) \mathbf{P_{A_k}}$ $k = \{1, 2\}$ where $\mathbf{P_{A_k}}$ are orthonormal matrices and $\mathbf{diag}(\lambda_i^{A_k})$ is a diagonal matrix whose non-zero elements are the eigenvalues of, respectively, $\mathbf{A_1}, \mathbf{A_2}$. Then, $\exp(\mathbf{A_k}) = \mathbf{P_{A_k}}^T \mathbf{diag}(\exp(\lambda_i^{A_k})) \mathbf{P_{A_k}}$. From that formula it is clear that $\exp(\mathbf{A_1}) = \exp(\mathbf{A_2})$ is true if and only if $\mathbf{A_1} = \mathbf{A_2}$, which implies that the mapping is injective.

2. Let us now denote by $\mathbf{B} = \mathbf{P_B}^T \mathbf{diag}(\lambda_i^B) \mathbf{P_B}$ a symmetric positive definite matrix in $PS^+(n)$. Then, for every $\mathbf{B}$ there exists a matrix $\mathbf{A} = \mathbf{P_B}^T \mathbf{diag}(\log(\lambda_i^B)) \mathbf{P_B}$ in $S(n)$ such that $\exp(\mathbf{A}) = \mathbf{B}$. This means the mapping is also surjective. ∎

The following corollary also arises for bijective mappings:

Corollary 4.4.2 *A map $f : X \mapsto Y$ is bijective if and only if there exists another relation $g : Y \mapsto X$ such that the composition $g \circ f$ is the identity function on X and $f \circ g$ is the identity function on Y. In that case g is the inverse relation of f, that is, $g = f^{-1}$ which is also a bijection. The inverse mapping for the exponential map $\exp(\mathbf{A}) : S(n) \mapsto PS^+(n)$ is the logarithm map $\log(\mathbf{A}) : PS^+(n) \mapsto S(n)$ defined in 4.12, which is also a continuous function.*

Hence, the vector space $S(n)$ and the set $PS^+(n)$ are identical from this point of view. In this sense, as it is done between group isomorphisms, it is possible to transform the original signal space $PS^+(n)$ to $S(n)$ with the logarithm where we profit from all the mathematical tools for vector spaces to process the input signal. Then, we can transform back the processed signal to its original signal space through the exponential. It is important to remark that this transformation only deals with positive definite tensors, since the matrix logarithm is not defined for symmetric positive semidefinite tensors $PS_0^+(n)$ [Cheng01].

An important consequence of this transformation is that the characteristic decomposition of multiplicative signals into additive signals ($\mathbf{AB} \rightarrow \mathbf{log(B)} + \mathbf{log(B)}$) that is usually achieved within the homomorphic processing framework does not apply for matrices any more, since the mappings are not homomorphisms. Only in the particular case that $\mathbf{A}$ and $\mathbf{B}$ conmute ($\mathbf{AB} = \mathbf{BA}$) we may have this property and, hence, a direct generalization of the homomorphic decomposition.

Thus, using the notation of the homomorphic cascade represented in Fig. 4.2, the first subsystem $\mathbf{D}_\square\{\cdot\}$ transforms our input tensor signal on $PS^+(n)$ to $S(n)$ by means of the matrix logarithm. Then, any traditional tensor linear filtering scheme $\mathbf{L}\{\cdot\}$ can be applied in order to process data. The output of this system is a tensor field of symmetric matrices not necessarily positive definite, but the third subsystem $\mathbf{D}_\square{}^{-1}\{\cdot\}$ maps back the symmetric tensors from $S(n)$ to $PS^+(n)$ by means of the exponential map.

The interesting thing about this decomposition is twofold [Castaño03b]. On the one hand, we are free to choose any pair of input and output subsystems with the only restriction of finding a homeomorphic mapping between $PS^{+}(n)$ and any other algebraic structure. On the other hand, we simplify the filter design since the problem of noise reduction is separated from the task of preserving the tensors positive definite.

4.4.2 A Relaxed Homomorphic Processing System

As it was stated in the previous section, other input and output subsystems different from the exponential and logarithm maps can be used in the processing cascade. In this section we propose the use of the principal matrix square root as input subsystem and matrix squares as output subsystem to guarantee a symmetric positive semidefinite response independently of the filter used to regularize the tensor field [Castaño06c].

The main advantage of this new approach is the fact that it can also deal with *semidefinite* tensor data robustly. This characteristic overcomes the limitation of using the exponential and logarithm maps which can only deal with *definite* tensor data, since the logarithm is not defined at 0. Moreover, the new mappings also avoid numerical unstability which may appear when tensor eigenvalues are too close to zero.

The ability to deal with *semidefinite* tensor fields is important in practice because real datasets with inherent noise usually provide tensors with negative eigenvalues. The algebraical structure of the set of positive semidefinite tensors has the shape of a cone, where inside we can find *definite* tensors, in the faces the *semidefinite* tensors (any eigenvalue equal to zero) and outside those with negative eigenvalues. In this sense, the closest tensors in a least squares sense to those with negative eigenvalues those with eigenvalues equal to zero instead of the negative ones [Niethammer06], yielding to a semidefinite tensor dataset.

The new processing cascade uses as input subsystem the principal matrix square root. Then, any matrix linear filter on the usual sense may be applied to regularize the tensor field. Finally, we transform back the matrix square assures us to get a positive semidefinite response, as it is demonstrated in the following equation:

$$\mathbf{M}^2 = (\mathbf{U}\mathbf{\Sigma}\mathbf{U}^T)(\mathbf{U}\mathbf{\Sigma}\mathbf{U}^T) = (\mathbf{U}\mathbf{\Sigma}\mathbf{\Sigma}\mathbf{U}^T) = (\mathbf{U}\mathbf{\Sigma}^2\mathbf{U}^T) \tag{4.26}$$

where $\mathbf{M}$ represents a symmetric matrix whose singular values decomposition is given by $\mathbf{U}\mathbf{\Sigma}\mathbf{U}^T$, with $\mathbf{U}$ an orthonormal matrix and $\mathbf{\Sigma}$ a diagonal matrix whose elements are the eigenvalues of $\mathbf{M}$. Thus, since the eigenvalues of $\mathbf{M}^2$ are given by the squared eigenvalues of $\mathbf{M}$, then we guarantee positive semidefinite matrices at the output.

An algebraic interpretation similar to the one performed in section 4.4.1 can also be performed in this case, where the mapping $\sqrt{\cdot} : PS_0^{+}(n) \mapsto PS_0^{+}(n)$ transforms the input signal space to itself, where the inverse mapping is the matrix squares defined as: $(\cdot)^2 : PS_0^{+}(n) \mapsto PS_0^{+}(n)$. The principal matrix square root is a continuous mapping as it is the matrix squares. It can also be demonstrated that these mappings are also a bijection from $PS_0^{+}(n)$ to itself. Hence, these system transformations define a homeomorphism, which allow us to define the corresponding processing cascade.

However, in a strict sense, we are limited to the use of a linear system whose response also provides a positive semidefinite response $\mathbf{L}\{\cdot\} : PS_0^+(n) \mapsto PS_0^+(n)$, since the input elements of the last subsystem must be in the set $PS_0^+(n)$ to be rigorous with the theoretical framework.

In practice, this requirement can be relaxed to the use of any linear filter $\mathbf{L}\{\cdot\}$ even if its response may provide negative eigenvalues. In this case, the processing framework is equivalent to project the filter response to the cone of positive semidefinite tensors using the projection method proposed in [San Jose05], which argues for taking the absolute value of the tensor eigenvalues instead of using a least square argument. This method is motivated on a physical interpretation of the tensor information, since the chances that a tensor with negative eigenvalues comes from a tensor inside the cone is higher than it comes from one in the wall.

4.5 Results

In this section we present some results to validate the performance of the proposed approach. In our experiments we use both synthetic and real DT-MRI data to compare the behavior of the homomorphic filtering framework developed in this chapter. In all of our experiments we compare the output of our homomorphic cascades to the output of the linear filter used in the middle of the chain in order to evaluate the difference.

4.5.1 Synthetic data:

Experiment 1:

To evaluate the performance of our filtering framework we used a $32 \times 32 \times 32$ synthetic volume of 3×3 tensors which simulates a small cube of tensors oriented along a horizontal direction inside a bigger cube of tensors oriented along a vertical direction, as shows the image on the left side of Fig. 4.5, where a slice of the whole volume is represented. Then, we generated the noisy tensor field shown on the right in Fig. 4.5 by using the algorithm proposed in [Lenglet05a], which allow us to easily generate a set of random positive definite tensors with the desired mean and covariance matrix. This method is a much more satisfying approach than, as it is usually done, simply building symmetric matrices with iid normally distributed components and then enforcing their positiveness since this leaves no grasp on the actual distribution of the tensors. Moreover, the algorithm proposed in [Lenglet05a] is consistent with the parametric model for noise in DT-MRI proposed in [Pajevic03] where it is proven that, assuming that the magnitude diffusion weighted images are Rician distributed, noise in diffusion tensor data within a voxel follows a 6-dimensional Normal distribution.

Then, we introduced the noisy tensor field in our homomorphic cascade. In our experiments, we have used both decompositions proposed in section 4.4: the Exponential-Logarithm cascade and the Root-Squares one. For each cascade, we have also used two different linear filters, a Gaussian filter and a Wiener filter. Finally, we also compared their respective responses to those provided by the linear filters. Figure 4.6 shows the

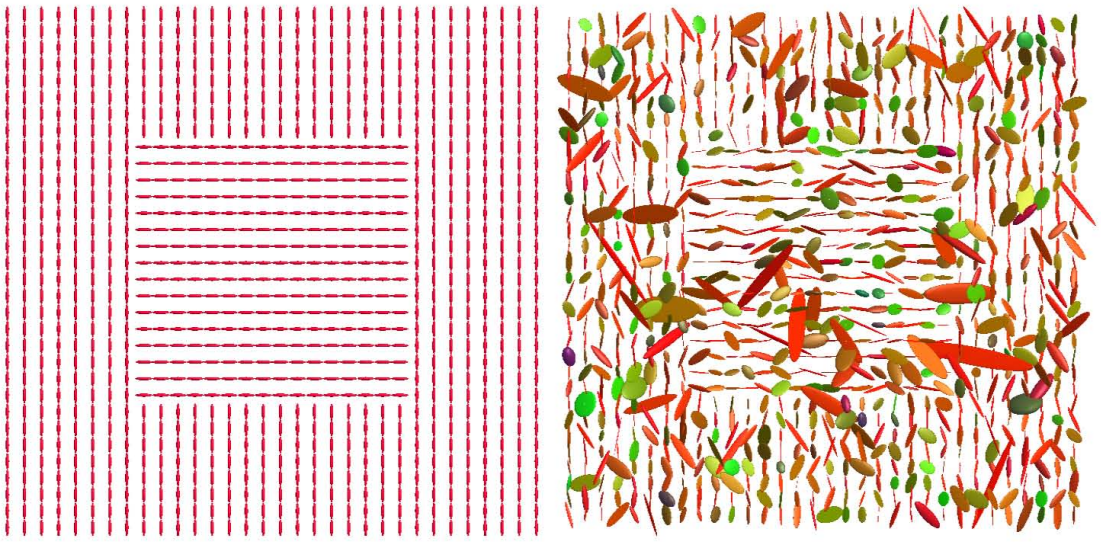

Figure 4.5: Left: Slice of the original tensor volume. Right: Same slice after noise addition.

responses of the six systems used in our experiments. On the left side, we present the systems that use the Gaussian filter and on the right, we present the responses of the systems that use the Wiener filter. On the first row, we present the responses from the linear filters, on the second one we use the root-squares approach and on the last one, the exponential-logarithm cascade.

In Figs. 4.7 and 4.8, we show some details of the images shown in Fig. 4.6. As it can be seen, the noise is better removed from images within the homomorphic framework, which provide a smoother tensor field. It is remarkable the fact that the Gaussian and the Wiener filter responses provide tensors that tend to be rounder than the ones provided by the homomorphic decomposition. This effect is produced when we perform operations on tensors within an Euclidean framework. For instance, take the example of two anisotropic tensors oriented in perpendicular directions that are summed. The result in that case is an isotropic tensor. However, we can say that using the homomorphic decomposition, the sum is performed after applying a nonlinear transformation (the root or the logarithm in our case) that reduces this effect. In any case, in the next chapter we will better understand why this swelling effect is reduced, once we had studied the geometry of the set $PS^{+}(n)$.

A quantitative comparison is also performed to evaluate our approach. In this sense, Table 4.1 compares the mean squared error between the original tensor field shown in 4.5 and the regularized versions obtained with the different approaches described in this chapter. To do that, we make use of the following error measure:

$$Error = \frac{\sum_{k=1}^{N} \parallel \mathbf{S}_0(\mathbf{x}_k) - \hat{\mathbf{S}}(\mathbf{x}_k) \parallel_F}{N} \tag{4.27}$$

which computes the mean of the Frobenius magnitude ($\parallel \mathbf{A} \parallel_F = \sqrt{\sum_{ij} |a_{ij}|} = \sqrt{trace(\mathbf{A}\mathbf{A}^T)} = \sqrt{\sum_i \lambda_i^2}$ with a_{ij} the elements of the tensor $\mathbf{A}$, and λ_i its eigenvalues)

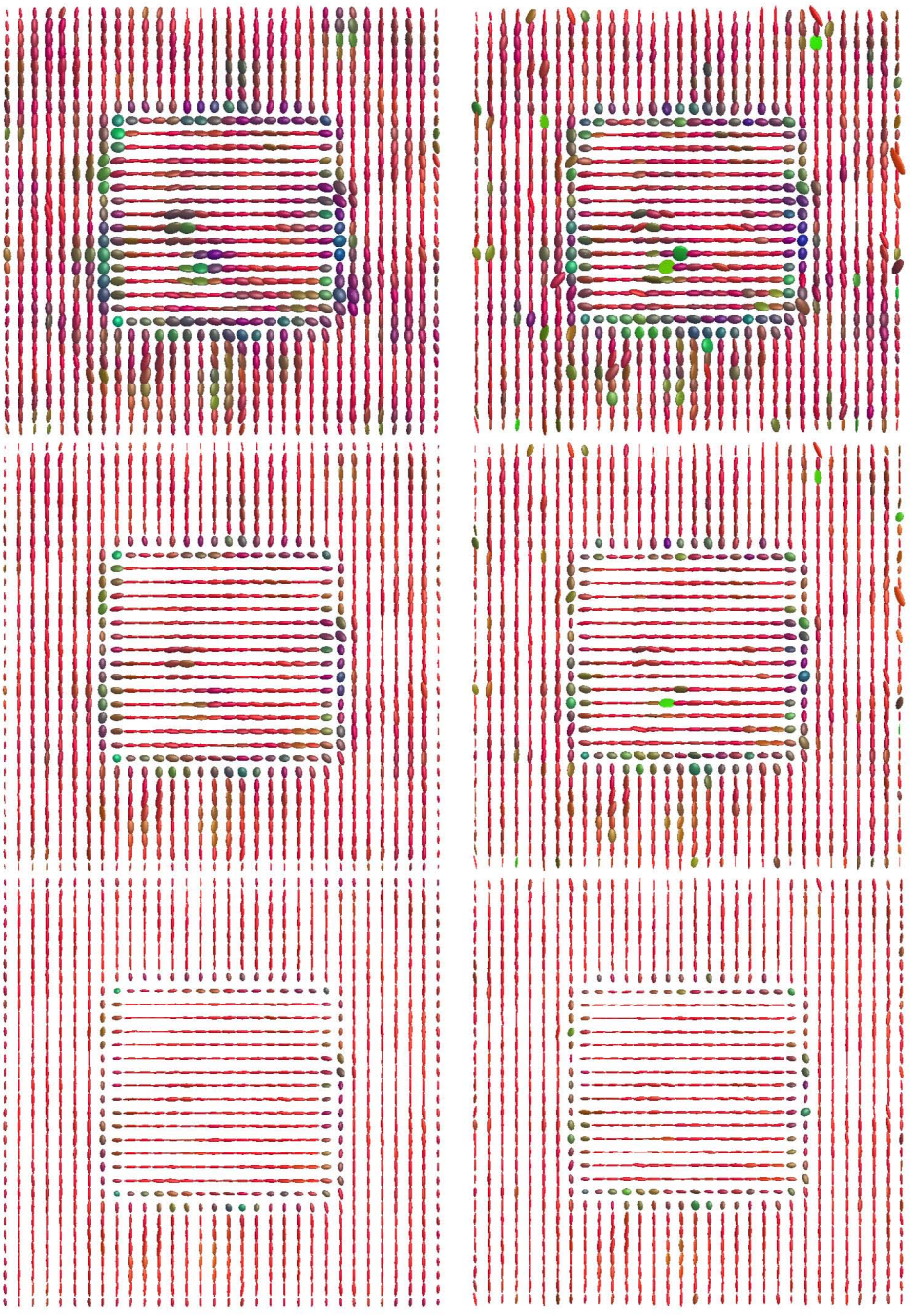

Figure 4.6: Responses of different tensor regularization methods. Top Row: Gaussian Smoothing (Left). Wiener Filter (Right). Middle Row: Root-Squares Homomorphic Filtering. $H\{\cdot\}$ is Gaussian filter (Left) and Wiener filter (Right). Bottom Row: Log-Exponential Homomorphic Filtering. $H\{\cdot\}$ is Gaussian filter (Left) and Wiener filter (Right).

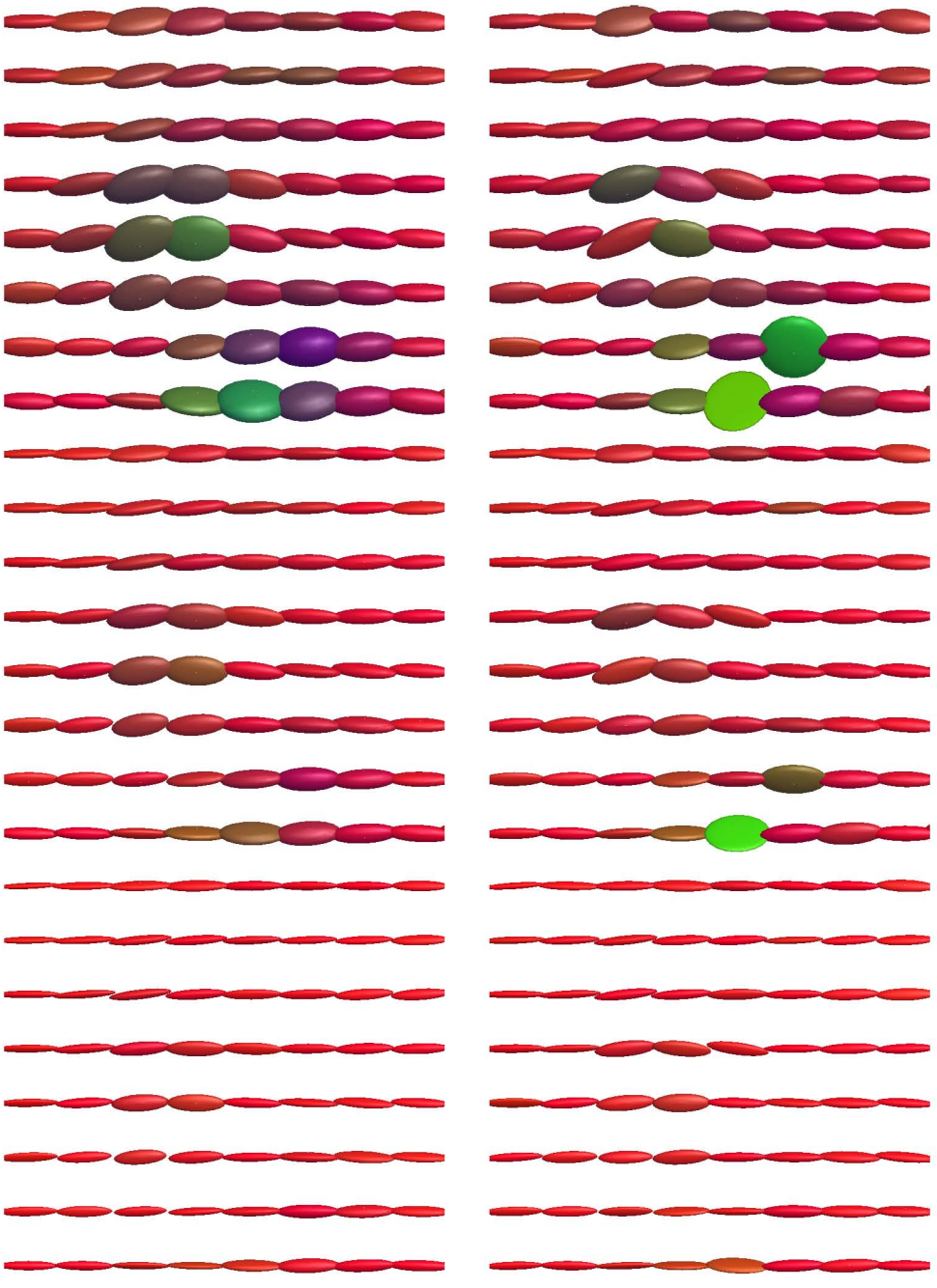

Figure 4.7: Details on the responses of different tensor regularization methods. Top Row: Gaussian Smoothing (Left). Wiener Filter (Right). Middle Row: Root-Squares Homomorphic Filtering. $H\{\cdot\}$ is Gaussian filter (Left) and Wiener filter (Right). Bottom Row: Log-Exponential Homomorphic Filtering. $H\{\cdot\}$ is Gaussian filter (Left) and Wiener filter (Right).

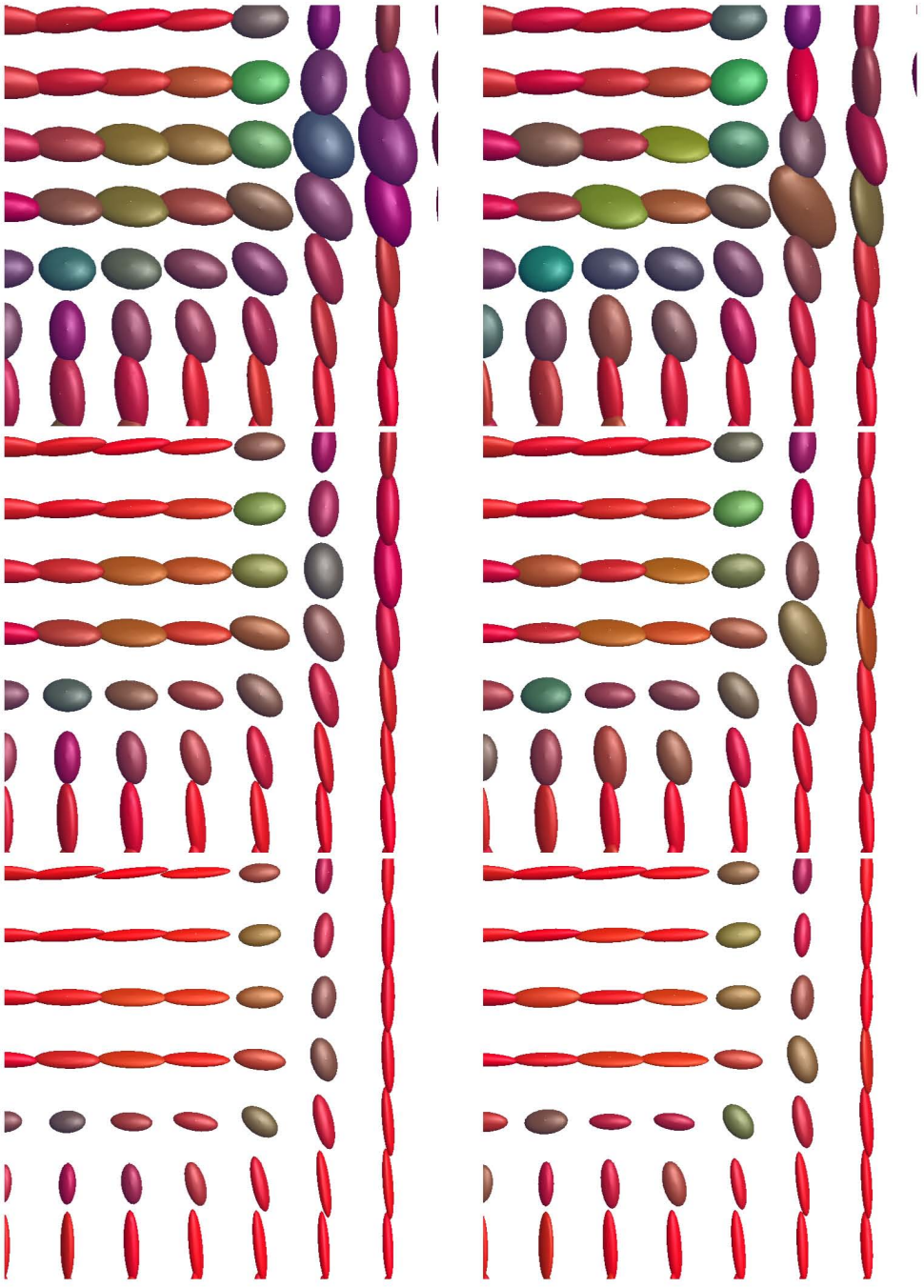

Figure 4.8: Details on the responses of different tensor regularization methods. Top Row: Gaussian Smoothing (Left). Wiener Filter (Right). Middle Row: Root-Squares Homomorphic Filtering. $H\{\cdot\}$ is Gaussian filter (Left) and Wiener filter (Right). Bottom Row: Log-Exponential Homomorphic Filtering. $H\{\cdot\}$ is Gaussian filter (Left) and Wiener filter (Right).

Method	MSE Error	Std. Dev.	Max	Min
Wiener Exp-Log Homomorphic	0.8828	0.4345	4.5647	0.1242
Gaussian Exp-Log Homomorphic	0.9885	0.5205	4.1856	0.0956
Wiener Root-Sq. Homomorphic	1.4073	0.5830	17.3132	0.2529
Gaussian Root-Sq. Homomorphic	1.5163	0.5042	4.4810	0.1340
Gaussian Filter	2.1866	0.7624	10.4433	0.3294
Wiener Filter	2.2003	0.9928	40.7226	0.1125

Table 4.1: Results from Experiment 1: Comparison of the MSE error between the original input and the regularized signals.

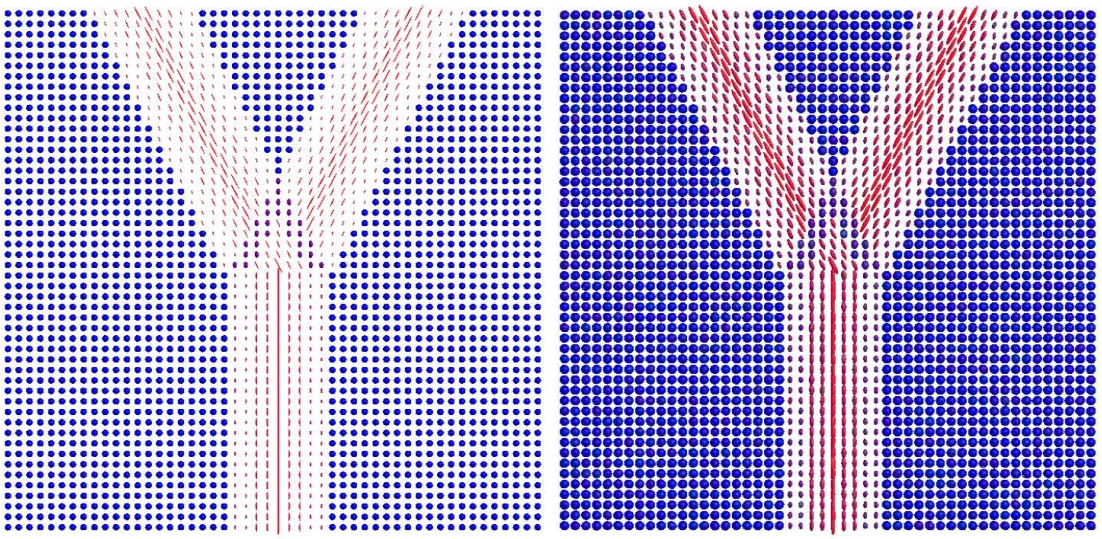

Figure 4.9: Left: Slice of the original tensor volume. Right: Same slice after noise addition.

of the error tensor field, where N denotes the number of samples in the field, $\mathbf{S}_0(\mathbf{x}_k)$ the original tensor field and $\hat{\mathbf{S}}(\mathbf{x}_k)$ the estimated one.

Experiment 2:

In our second experiment we use a $50 \times 50 \times 50$ synthetic volume of 3×3 tensors which simulates a bifurcation of a fiber bundle in the brain, as shows the image represented in the left side of Fig. 4.9. Then, we generated the noisy version of this synthetic field shown in the right side of Fig. 4.5 using the same algorithm used in the previous case.

Then, we introduced the noisy tensor field in the same filters used in the previous experiment. Figure 4.10 shows the responses of the six processing systems used in our experiments. On the left side, we present the systems that use the Gaussian filter and on the right, we present the responses of the systems that use the Wiener filter. On the first row, we present the responses from the linear filters, on the second one we use the root-squares approach and on the last one, the exponential-logarithm cascade.

In Figs. 4.11 and 4.12, we show some details of the images shown in Fig. 4.10. From those figures, we observe again the same effects of rounder ellipsoids for the linear filter

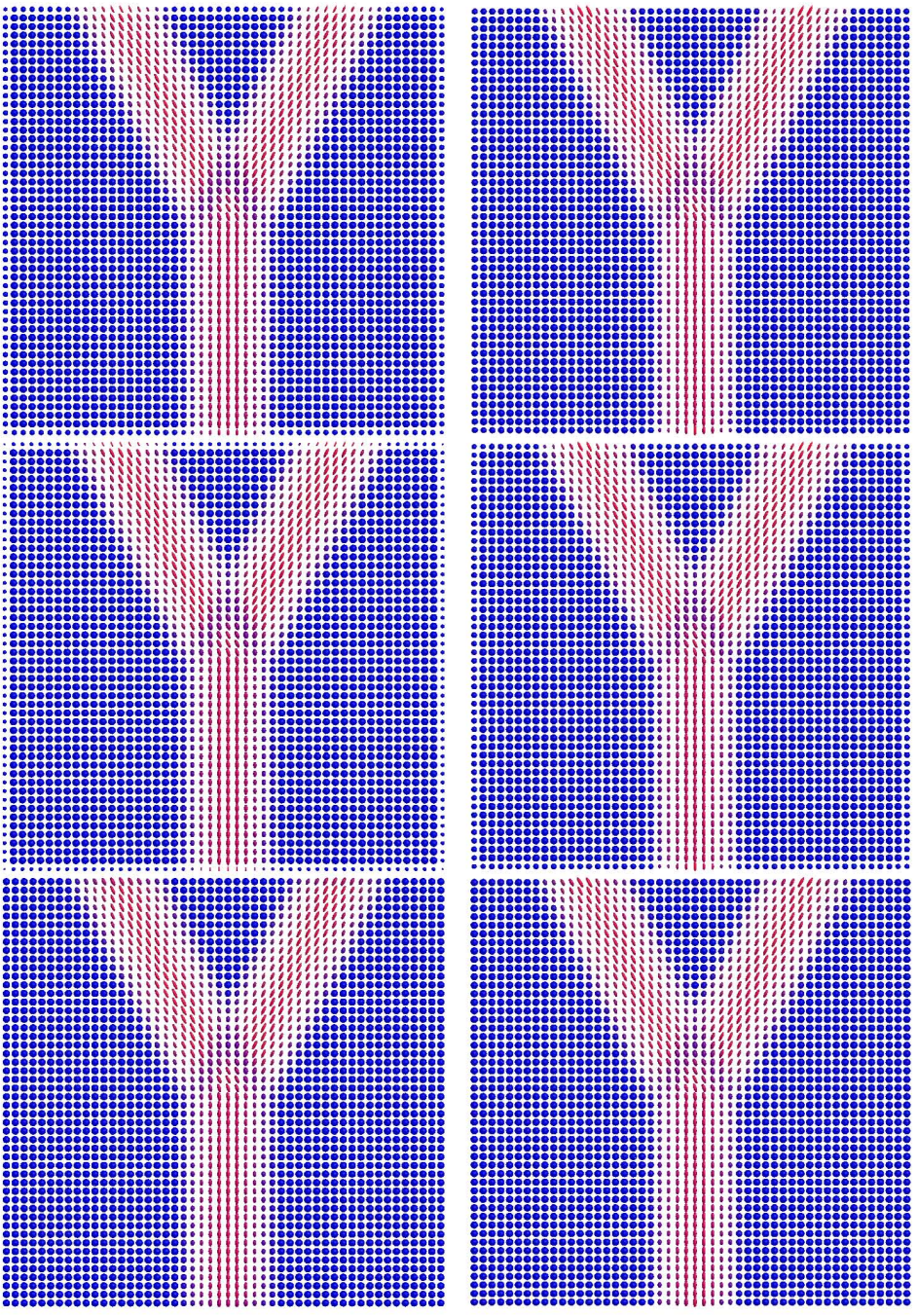

Figure 4.10: Responses of different tensor regularization methods. Top Row: Gaussian Smoothing (Left). Wiener Filter (Right). Middle Row: Root-Squares Homomorphic Filtering. $H\{\cdot\}$ is Gaussian filter (Left) and Wiener filter (Right). Bottom Row: Log-Exponential Homomorphic Filtering. $H\{\cdot\}$ is Gaussian filter (Left) and Wiener filter (Right).

Method	MSE Error	Std. Dev.	Max	Min
Wiener Exp-Log Homomorphic	0.5239	0.0455	0.9819	0.1601
Gaussian Exp-Log Homomorphic	0.5239	0.0505	0.9785	0.1734
Wiener Root-Sq. Homomorphic	0.5262	0.0462	0.9974	0.1650
Gaussian Root-Sq. Homomorphic	0.5263	0.0515	1.0141	0.1776
Wiener Filter	0.5285	0.0476	1.0134	0.1649
Gaussian Filter	0.5288	0.0541	1.0530	0.1803

Table 4.2: Results from Experiment 2: Comparison of the MSE error between the original input and the regularized signals.

responses than those provided by the homomorphic decomposition, which provide a more accurate response.

Finally, table 4.2 compares the mean error between the original tensor field shown in 4.9 and the regularized versions obtained with the different approaches described in this chapter using the same error measure previously presented:

4.5.2 Real DT-MRI Data:

For experiments with real data, diffusion weighted images were acquired on a 3 Tesla MEDSPEC 30/80 AVANCE (Bruker) at the Centre IRMf de Marseille, France, using a quadrature bird-cage head coil. We used 12 gradient directions and a b-value of 1000 s/mm^2. Acquisitions were repeated 8 times for each direction to ensure a good signal-to-noise ratio. The sequence parameters were chosen as follows: $\Delta = 38.5$ms, $\delta = 21.6$ms, $TR = 10000$ms, $TE = 79$ms and voxel size was $2 \times 2 \times 2$ mm^3.

Different views of the tensor field are shown on Fig. 4.13. They were estimated by a robust gradient descent algorithm preserving their symmetry and positive definiteness, as presented in [Lenglet05a]. The idea of this method is to minimize a functional of the linearized Stejskal-Tanner equation by evolving an initial guess of the tensor on the manifold $PS^+(3)$ with a numerical scheme similar to the one presented in the following chapter to compute the mean of a tensor field.

The most important anatomical structures present in this axial slice are labeled on the detail of the right side of Fig. 4.14. In this way we can see the tensors orientation within the *splenium of the corpus callosum* (CC(S) in the image) and in the *genu of the corpus callosum* (CC(G) in the image) inside the plane of the image from one hemisphere to the other. On the contrary, tensors within the *corona radiata* (CR in the image) are oriented in the orthogonal plane of the image from the top to the bottom of the brain volume. Finally, the *ventricles* areas (VE in the image), since they are mainly homogeneous structures are represented by isotropic tensors.

Then, we introduced the estimated tensor field in the filtering systems used in the previous experiments. Figure 4.15 shows the responses of the six processing systems used in our experiments. As it was done in the previous experiments, on the left side we present the systems that use the Gaussian filter and on the right, we present the responses of those that use the Wiener filter. On the first row, we present the outputs from the

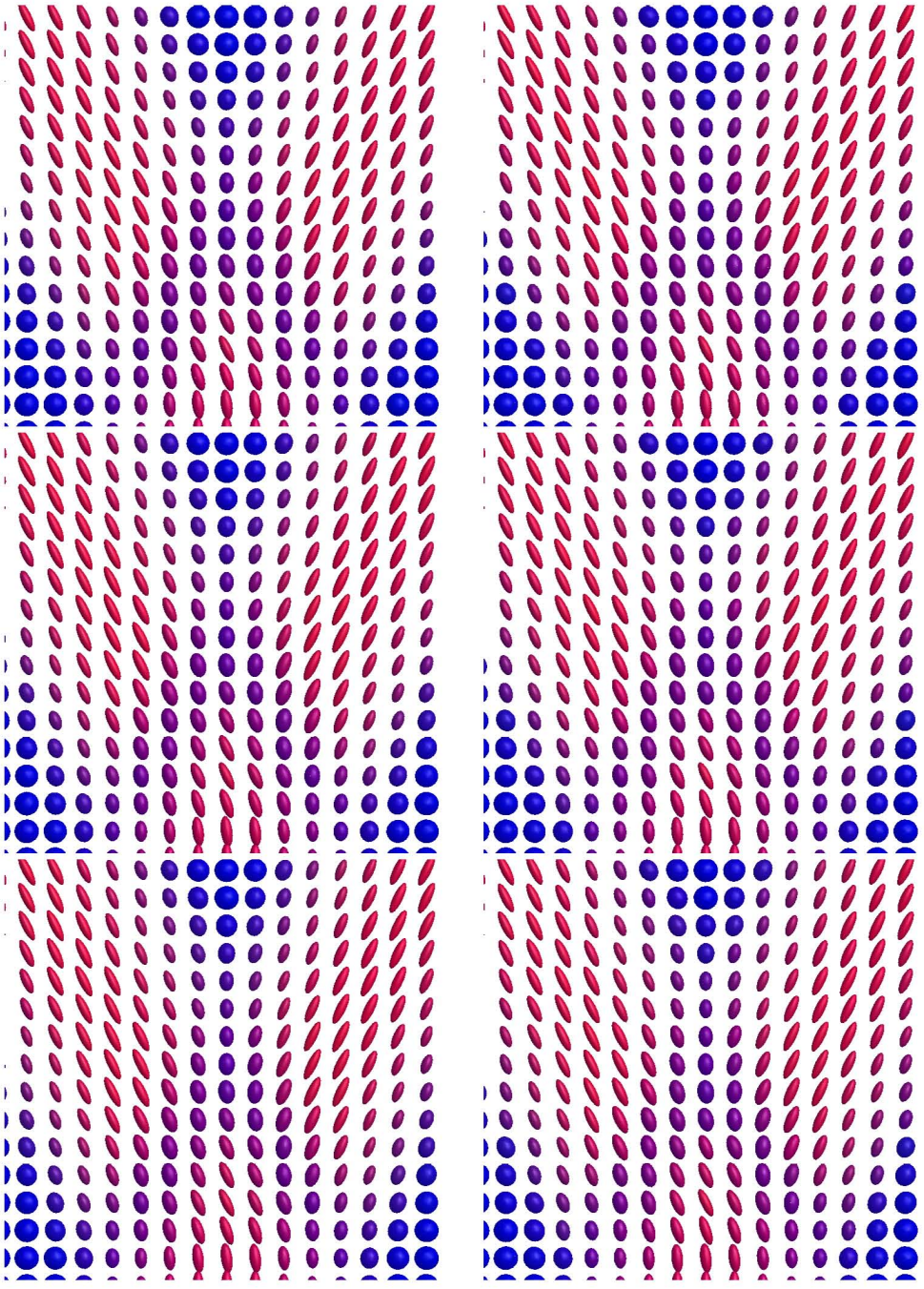

Figure 4.11: Details on the responses of different tensor regularization methods. Top Row: Gaussian Smoothing (Left). Wiener Filter (Right). Middle Row: Root-Squares Homomorphic Filtering. $H\{\cdot\}$ is Gaussian filter (Left) and Wiener filter (Right). Bottom Row: Log-Exponential Homomorphic Filtering. $H\{\cdot\}$ is Gaussian filter (Left) and Wiener filter (Right).

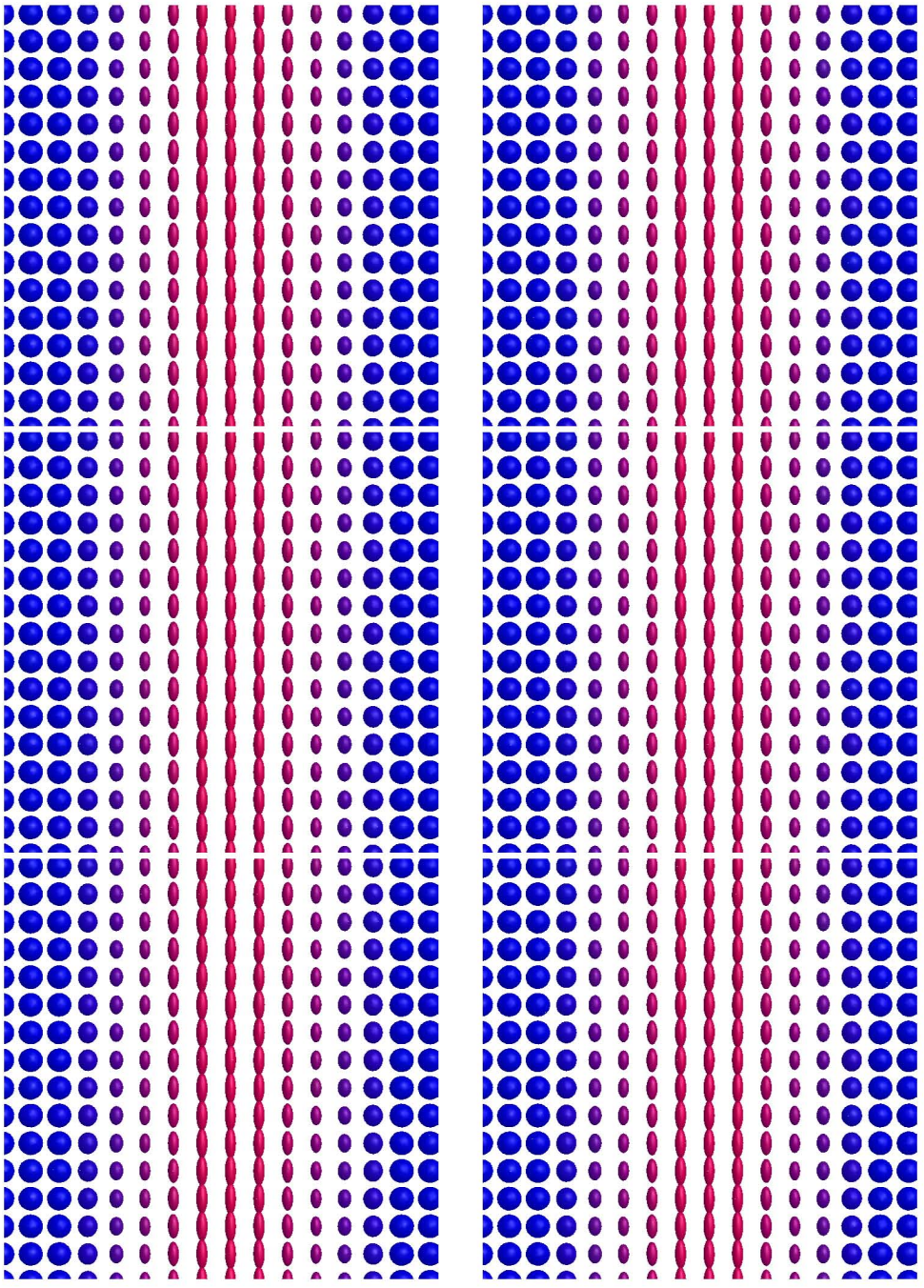

Figure 4.12: Details on the responses of different tensor regularization methods. Top Row: Gaussian Smoothing (Left). Wiener Filter (Right). Middle Row: Root-Squares Homomorphic Filtering. $H\{\cdot\}$ is Gaussian filter (Left) and Wiener filter (Right). Bottom Row: Log-Exponential Homomorphic Filtering. $H\{\cdot\}$ is Gaussian filter (Left) and Wiener filter (Right).

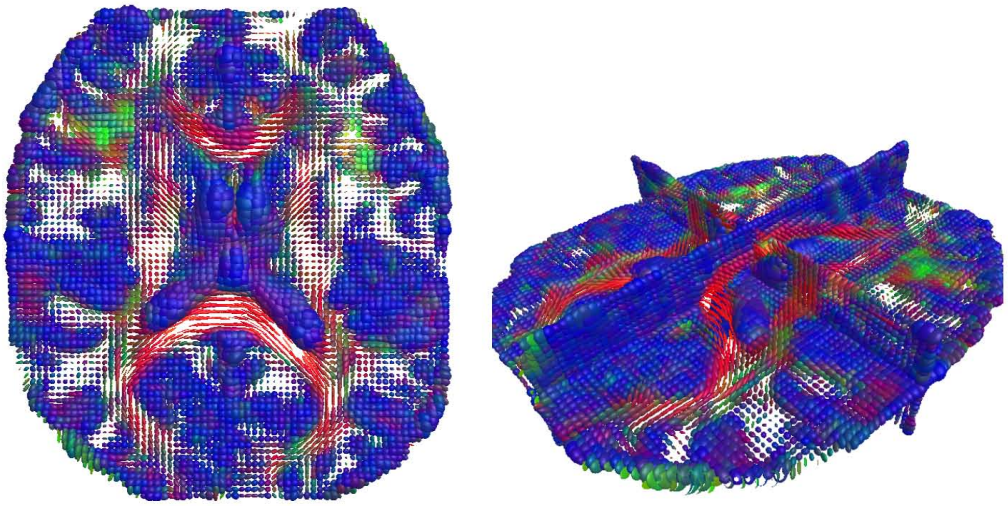

Figure 4.13: Left: Slice of the original tensor volume. Right: Same slice after noise addition.

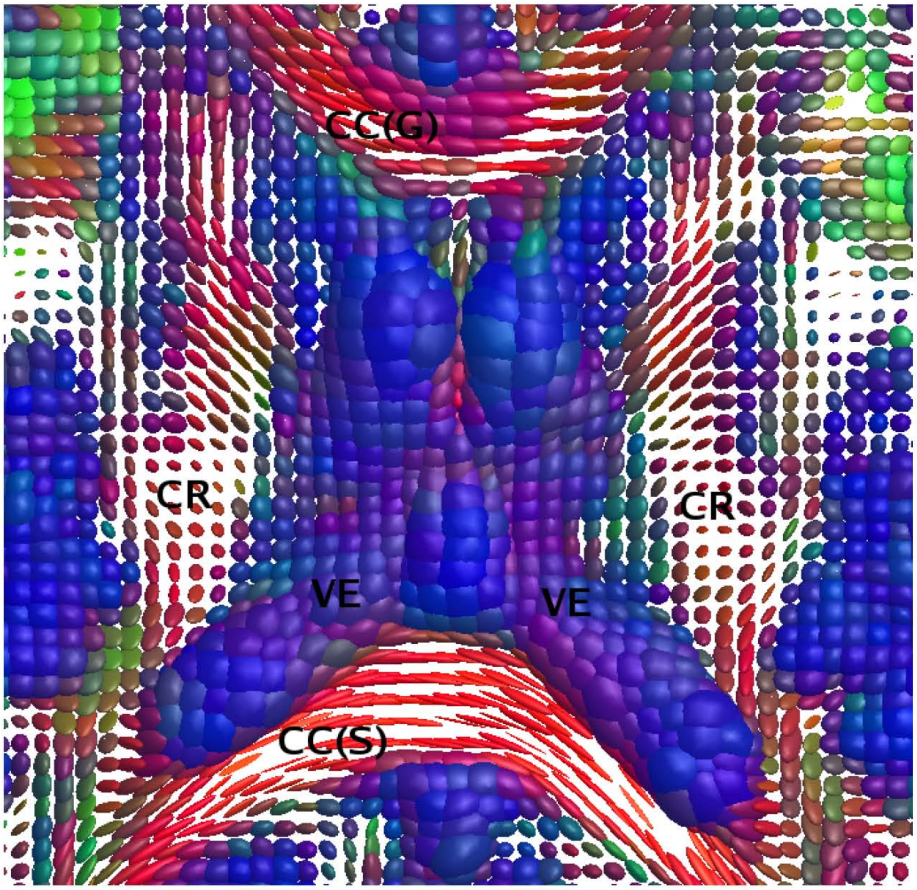

Figure 4.14: Axial view of a DT-MRI slice with the most important anatomical structures depicted in it. CC(S): *splenium of the corpus callosum.* CC(G): *genu of the corpus callosum.* CR: *corona radiata.* VE: *ventricles.*

linear filters, on the second one we use the root-squares approach and on the last one, the exponential-logarithm cascade.

In Fig. 4.16, we show some details of the images shown in Fig. 4.10. From those figures, we observe again that the anatomical structures are better preserved with the Exp-Log homomorphic cascade since tensor orientation is more coherent and anisotropies are less blurred, specially within the *Splenium of the Corpus Callosum* (CC(S) in Fig. 4.14). Figure 4.17 shows 3D views of the regularized tensor fields where the main structures of the brain can be observed from a more general perspective.

4.6 Conclusions and Discussion

In this chapter, we have addressed the specific problem of regularization of tensor fields from a new perspective. We presented a generalization of the homomorphic processing framework for the regularization of tensor fields. The mathematical background relies on the algebraical interpretation of the vector space of symmetric matrices and the set of symmetric positive definite matrices. Although these two algebraical structures seem different, there exists a relationship between them that we exploit to generalize the homomorphic theory for tensors.

In this sense, the properties of the generalized theory differ from the usual homomorphic decomposition, even though the mathematical formulation is completely analogous, using the matrix logarithm and the matrix exponential as input and output subsystems, respectively, in the processing cascade since it is the natural mapping which transforms symmetric positive definite matrices into elements of the vector space of symmetric matrices and viceversa. We show that this is not the only possibility. For instance, we relaxed some requirements to propose the use of the matrix square root and matrix squares, respectively, as input and output subsystems of the processing cascade. This approach takes the advantage that it also deals with symmetric positive semidefinite tensors.

To validate our algorithms we compared the outputs of the homomorphic processing cascades to the output of the filter used in the middle of the processing cascade. In our experiments with synthetic and true data, we obtained better results in all cases with the homomorphic framework than with the filter itself.

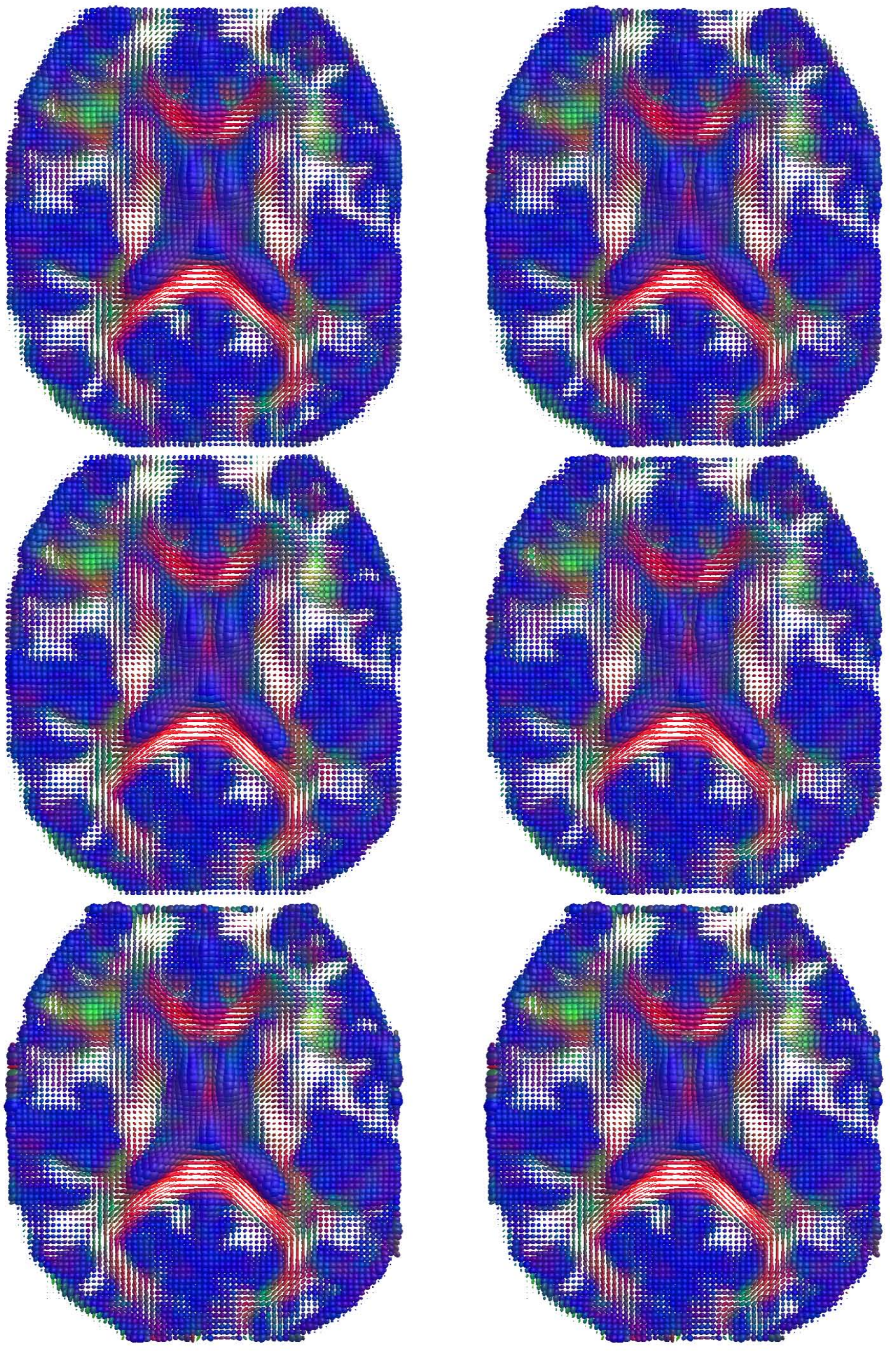

Figure 4.15: Responses of different tensor regularization methods. Top Row: Gaussian Smoothing (Left). Wiener Filter (Right). Middle Row: Root-Squares Homomorphic Filtering. $H\{\cdot\}$ is Gaussian filter (Left) and Wiener filter (Right). Bottom Row: Log-Exponential Homomorphic Filtering. $H\{\cdot\}$ is Gaussian filter (Left) and Wiener filter (Right).

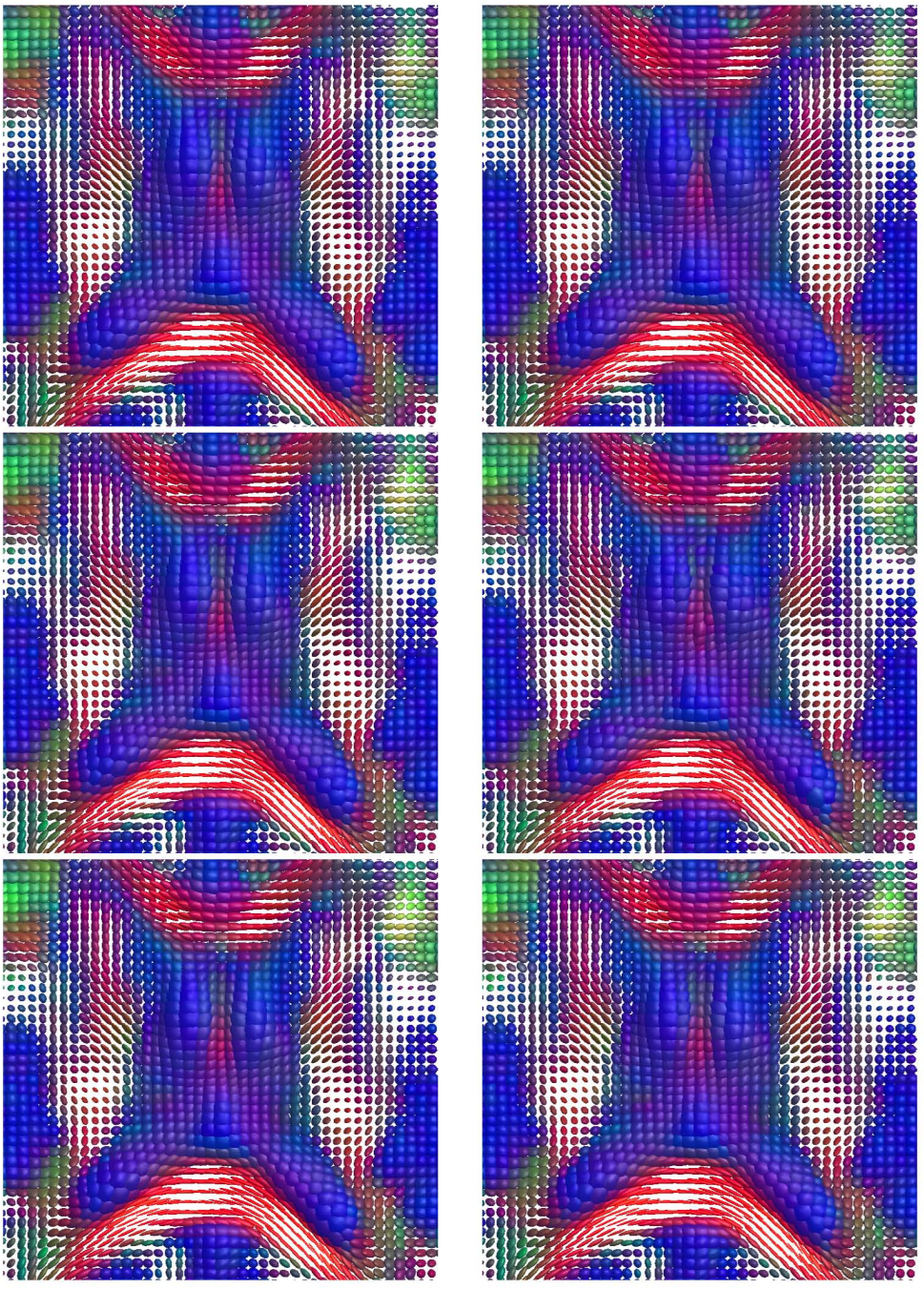

Figure 4.16: Details on the responses of different tensor regularization methods. Top Row: Gaussian Smoothing (Left). Wiener Filter (Right). Middle Row: Root-Squares Homomorphic Filtering. $H\{\cdot\}$ is Gaussian filter (Left) and Wiener filter (Right). Bottom Row: Log-Exponential Homomorphic Filtering. $H\{\cdot\}$ is Gaussian filter (Left) and Wiener filter (Right).

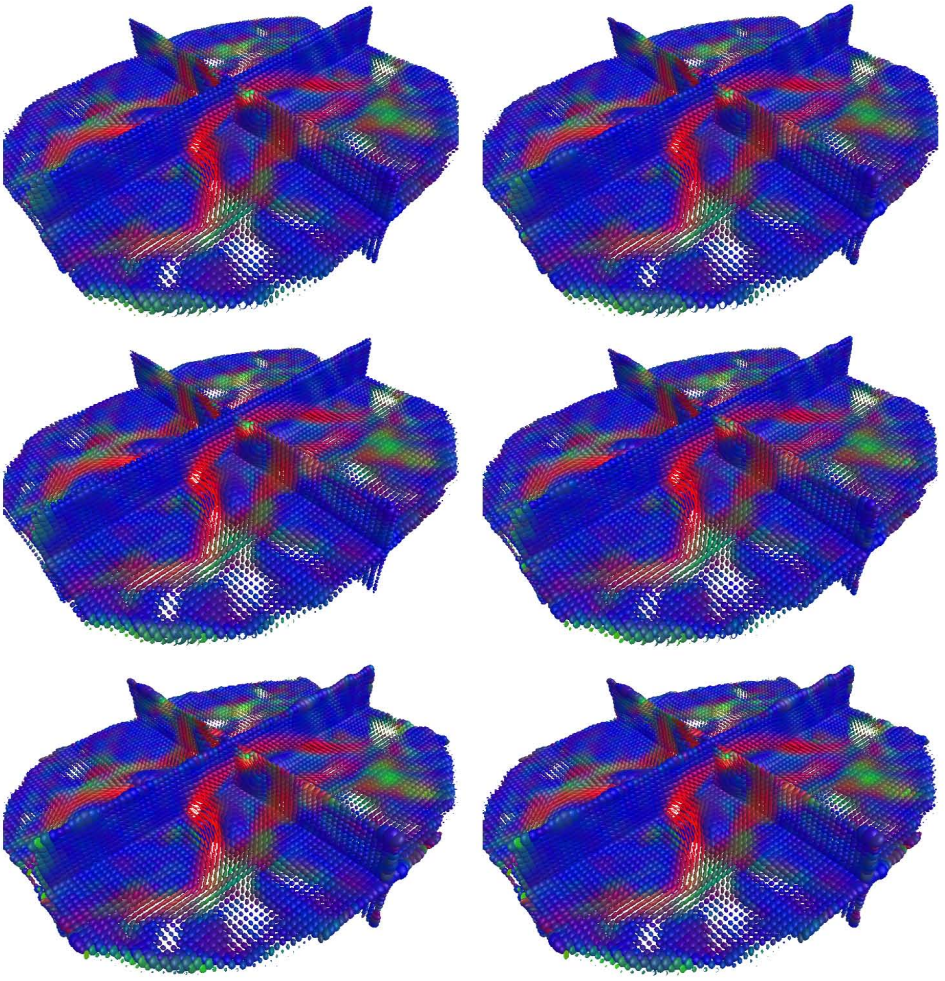

Figure 4.17: 3D Views of the tensor fields obtained with different tensor regularization methods. Top Row: Gaussian Smoothing (Left). Wiener Filter (Right). Middle Row: Root-Squares Homomorphic Filtering. $H\{\cdot\}$ is Gaussian filter (Left) and Wiener filter (Right). Bottom Row: Log-Exponential Homomorphic Filtering. $H\{\cdot\}$ is Gaussian filter (Left) and Wiener filter (Right).

Chapter 5

A Riemannian Framework for Tensor Signal Processing

5.1 Introduction

In this chapter, we will rely on a rigorous mathematical framework to compute statistics on tensor fields. We use the mathematical framework, developed in [Skovgaard81] and used in [Lenglet05b] where the differential geometrical properties of the space of multivariate normal distributions are used to define statistics on diffusion tensors, seen as covariance matrices. This work is based on the information geometry derived from the Fisher information, as proposed for instance by Amari in [Amari90].

Independently, other recent papers also addressed the issue of defining statistical quantities and filtering tools for tensor fields. [Fletcher04] first analyzes the space of symmetric, positive definite matrices from a Lie groups perspective and shows that this space does not form a vector space but can be regarded as a Riemannian symmetric space and they used these ideas to develop efficient and elegant methods for computing statistics and modes of variation of diffusion tensor data in this non linear space. More recently, [Pennec04] developed also a nice and elegant computational framework for tensor processing with a particular emphasize on interpolation, regularization and restoration of noisy tensor fields.

It is thus very interesting to note that comparable results were obtained through different means while studying the statistical variability of diffusion tensor images.

The main contribution of this chapter is an anisotropic filtering algorithm controlled by the magnitude of the Riemannian gradient of the tensor field. As opposed to [Fletcher04], where a statistical analysis of diffusion tensors was proposed but without addressing the problem of smoothing, or [Pennec04], where the regularization task was addressed with a PDE point of view, our smoothing method only relies on simple and local anisotropic averaging. Adding to that, our method is favorably compared to a state-of-the-art approach [Weickert02]. A detailed analysis of the performance of our approach is achieved using both, noisy synthetic data and real tensor data. In our experiments, we obtain

better results than those obtained with other methods in the state-of-the-art, such as the one presented in [Weickert02].

Section 5.3 recalls basic facts on the differential geometry of the space of multivariate normal distributions and section 5.4 shows how they can be used to compute local averages and spatial gradient of diffusion tensor images. Section 5.5 introduces the filtering process. Finally, section 5.6 presents and discusses numerical experiments. We will show that our Riemannian anisotropic filtering method yields better results on both synthetic and real DT-MRI datasets when compared to other approaches such as the nonlinear diffusion proposed in [Weickert02].

5.1.1 Contributions in this Chapter

- *Estimation of the spatial gradient magnitude (Section 5.4.3):* We proposed the estimation of the spatial gradient magnitude through the sum of squared geodesic distances between tensors in orthogonal directions on a discrete grid.
- *Characterization of the Riemannian spatial gradient (Section 5.4.3):* We characterized the properties of the Riemannian spatial gradient magnitude to demonstrate the differences between the Riemannian framework and the traditional Euclidean framework.
- *Anisotropic Riemannian Smoothing Algorithm (Section 5.5):* We developed an anisotropic Riemannian smoothing algorithm to deal with tensor data. This algorithm uses the statistical tools defined for tensors in the manifold of positive definite matrices by the definition of a Riemannian metric.

5.2 Theory of Differential Geometry

In this chapter we study the set $PS^+(n)$ using concepts of differential geometry. In order to facilitate the reader the understanding of this topological space, we define briefly some important concepts that will be used throughout this chapter. The basis of this study relies on the interpretation of the set of symmetric positive definite tensors $PS^+(n)$ as a differentiable manifold. Basically, a differentiable manifold is an algebraical structure that any local neighborhood resembles Euclidean space, although the global structure might be much more complicated, with a globally defined differentiable structure. In other words, for every point, its neighborhood is similar enough to Euclidean space to allow one to define differentiable equations.

For every point P in a manifold $\mathcal{M}$, we can define a vector space with the same dimension as the manifold which consists of all the possible directional derivatives at that point. This vector field is called the tangent space at point P, $T_P\mathcal{M}$. Its importance resides on the fact that it allows to define generalized differential equations on the manifold. In the particular case that the tangent space at every point is equipped with an inner product and it varies smoothly from point to point, the manifold is called *Riemannian manifold*. The continuous collection of scalar products on the tangent space at each point of the manifold is called *Riemannian metric* and it is denoted as g.

Riemannian manifolds are quite interesting structures since it is possible to define concepts such as lengths of curves, areas, volumes, gradient of functions and divergence of vector fields. Thus, if we consider a continuously differentiable curve $\gamma(t) : [a, b] \mapsto \mathcal{M}$ on the manifold $\mathcal{M}$, we can compute at each point its instantaneous speed vector $\gamma'(t_0)$ in the tangent space $T\mathcal{M}(t_0)$ at any point $t_0 \in [a, b]$ and the instantaneous speed $\| \gamma'(t_0) \|_g$, which is the norm of the speed vector induced by the inner product with metric g. To compute the length of the curve, we can proceed as usual by integrating this values along the whole curve:

$$L(\gamma) = \int_a^b \| \gamma'(t) \|_g \, dt \tag{5.1}$$

The distance between two points of a connected Riemannian manifold is the minimum length among the curves joining these points, as shows Eq. 5.2. The curves realizing this minimum for any two points of the manifold are called geodesics.

$$\mathcal{D}(a, b) = \inf\{L(\gamma)\} \tag{5.2}$$

5.3 Geometry of the Space of Multivariate Normal Distributions

The set $PS^+(n)$ has been studied from different points of view in the literature. For instance, in [Fletcher04] they identify $PS^+(3)$ with the quotient space $GL^+(3)/SO(3)$, which is the space of all the left cosets of $GL^+(3)$, the set of 3×3 matrices with positive determinant, generated by the elements of $SO(3)$, the set of 3×3 orthogonal matrices with determinant equal to one, i.e. the rotation group. We understand by the *left coset* of an element $g \in G$ (with G a group), the set of elements generated by the combination of g with all the elements $h \in H$ (with H a subgroup of G), and it is denoted as $gH = \{gh : h \in H\}$. Then, since the quotient space $GL^+(3)/SO(3)$ is a smooth manifold, it is possible to derive statistical tools to develop filtering algorithms within that framework. In another approach, [Lovric05] extended the group of rotations to $SL(3)$, the set of 3×3 general matrices with determinant equal to one, defining a slightly different manifold with a metric that turns out to exhibit an additional term in one direction. This extension was also recently formulated by [Micchelli05] in terms of a weighted Fisher information matrix, which is a symmetric positive definite matrix that defines a metric in such space. This approach can also be generalized to a wider class of elliptical densities. Although with different interpretations of the set $PS^+(3)$, it is thus very interesting to note that comparable results were obtained through different means while studying the statistical variability of tensor fields.

In our approach, we identify $PS^+(3)$, the set of 3×3 real symmetric positive definite matrices, with the family of three-dimensional normal distributions with 0-mean as the 6-dimensional parameter space of variances and covariances, that is a Riemannian manifold. We hereafter present the necessary material related to the Riemannian geometry of the multivariate normal model needed to derive our numerical schemes. For a further reading

on the fundamental mathematical tools on which is based this framework, we refer the reader to [Skovgaard81], [Burbea86], [Eriksen86], [Calvo91], [Förstner99], [Pennec05] and [Moakher05].

Following the work by Rao [Rao45] and Burbea-Rao [Burbea82], where a Riemannian metric was introduced for $PS^+(3)$ in terms of the Fisher information matrix, it is possible to define notions such as the geodesic distance, the curvature, the mean, and the covariance matrix for elements in $PS^+(3)$. The tangent space $T_{\mathbf{\Sigma}}PS^+(3)$ at $\mathbf{\Sigma} \in PS^+(3)$ is taken to be $S_{\mathbf{\Sigma}}(3)$, the vector space of symmetric matrices, as it is done in [Skovgaard81]. We denote by $\mathbf{E}_i$, $i = 1, ..., 6$ the basis of such a vector space, which is given by:

$$\begin{array}{lll} \mathbf{E}_1 = \begin{pmatrix} 1 & 0 & 0 \\ 0 & 0 & 0 \\ 0 & 0 & 0 \end{pmatrix} & \mathbf{E}_2 = \begin{pmatrix} 0 & 0 & 0 \\ 0 & 1 & 0 \\ 0 & 0 & 0 \end{pmatrix} & \mathbf{E}_3 = \begin{pmatrix} 0 & 0 & 0 \\ 0 & 0 & 0 \\ 0 & 0 & 1 \end{pmatrix} \\ \mathbf{E}_4 = \begin{pmatrix} 0 & 1 & 0 \\ 1 & 0 & 0 \\ 0 & 0 & 0 \end{pmatrix} & \mathbf{E}_5 = \begin{pmatrix} 0 & 0 & 0 \\ 0 & 0 & 1 \\ 0 & 1 & 0 \end{pmatrix} & \mathbf{E}_6 = \begin{pmatrix} 0 & 0 & 1 \\ 0 & 0 & 0 \\ 1 & 0 & 0 \end{pmatrix} \end{array} \tag{5.3}$$

The Riemannian metric for $PS^+(3)$, derived from the Fisher information matrix is given by the following theorem, which is proved in [Skovgaard81]:

Theorem 5.3.1 *The Riemannian metric for the space $PS^+(3)$ of multivariate normal distributions with zero mean is given, $\forall \mathbf{\Sigma} \in PS^+(3)$ by:*

$$g_{ij} = g(\mathbf{E}_i, \mathbf{E}_j) = \langle \mathbf{E}_i, \mathbf{E}_j \rangle_{\mathbf{\Sigma}} = \frac{1}{2}\mathrm{tr}\left(\mathbf{\Sigma}^{-1}\mathbf{E}_i\mathbf{\Sigma}^{-1}\mathbf{E}_j\right) \quad i, j = 1, ..., 6 \tag{5.4}$$

In practice, this means that for any tangent vectors $\mathbf{A}, \mathbf{B}$, their inner product relative to $\mathbf{\Sigma}$ is $\langle \mathbf{A}, \mathbf{B} \rangle_{\mathbf{\Sigma}} = \frac{1}{2}\mathrm{tr}\left(\mathbf{\Sigma}^{-1}\mathbf{A}\mathbf{\Sigma}^{-1}\mathbf{B}\right)$.

We recall that, if $\mathbf{\Sigma} : t \mapsto \mathbf{\Sigma}(t) \in PS^+(3)$, $\forall t \in [t_1, t_2] \subset \mathbb{R}$ denotes a curve segment in $PS^+(3)$ between two normal distributions parameterized by the matrices $\mathbf{\Sigma}_1$ and $\mathbf{\Sigma}_2$, its length is expressed as:

$$\mathcal{L}_{\mathbf{\Sigma}}(\mathbf{\Sigma}_1, \mathbf{\Sigma}_2) = \int_{t1}^{t2} \left(\sum_{i,j=1}^{6} g_{ij}(\mathbf{\Sigma}(t)) \frac{d\theta_i(t)}{dt} \frac{d\theta_j(t)}{dt} \right)^{1/2} dt \tag{5.5}$$

As stated for example in [Moakher05], the geodesic starting from $\mathbf{\Sigma}(t_1) \in PS^+(3)$ in the direction $\mathbf{V} = \dot{\mathbf{\Sigma}}(t_1)$ of the tangent space $T_{\mathbf{\Sigma}}PS^+(3) = S_{\mathbf{\Sigma}}(3)$, is given by the exponential map:

$$\mathbf{\Sigma}(t) = \mathbf{\Sigma}(t_1)^{1/2} \exp\left((t - t_1)\mathbf{\Sigma}(t_1)^{-1/2}\mathbf{V}\mathbf{\Sigma}(t_1)^{-1/2}\right)\mathbf{\Sigma}(t_1)^{1/2} \forall t \in [t_1, t_2] \tag{5.6}$$

We recall that the geodesic distance $\mathcal{D}$ between any two elements $\mathbf{\Sigma}_1$ and $\mathbf{\Sigma}_2$ is the length of the minimizing geodesic between $\mathbf{\Sigma}_1$ and $\mathbf{\Sigma}_2$:

$$\mathcal{D}(\boldsymbol{\Sigma}_1, \boldsymbol{\Sigma}_2) = \inf_{\boldsymbol{\Sigma}} \{\mathcal{L}_{\boldsymbol{\Sigma}}(\boldsymbol{\Sigma}_1, \boldsymbol{\Sigma}_2) : \boldsymbol{\Sigma}_1 = \boldsymbol{\Sigma}(t_1), \boldsymbol{\Sigma}_2 = \boldsymbol{\Sigma}(t_2)\}$$

It is given by the following theorem, whose original proof is available in an appendix of [Atkinson81] but different versions can also be found in [Skovgaard81] and [Förstner99].

Theorem 5.3.2 (S.T. Jensen, 1976) *Consider the family of multivariate normal distributions with common mean vector but different covariance matrices. The geodesic distance between two members of the family with covariance matrices* $\boldsymbol{\Sigma}_1$ *and* $\boldsymbol{\Sigma}_2$ *is given by*

$$\mathcal{D}(\boldsymbol{\Sigma}_1, \boldsymbol{\Sigma}_2) = \sqrt{\frac{1}{2}\mathrm{tr}\left(\log^2\left(\boldsymbol{\Sigma}_1^{-1/2}\boldsymbol{\Sigma}_2\boldsymbol{\Sigma}_1^{-1/2}\right)\right)} = \sqrt{\frac{1}{2}\sum_{i=1}^{3}\log^2(\eta_i)} \tag{5.7}$$

where η_i *denote the* 3 *eigenvalues of the matrix* $\boldsymbol{\Sigma}_1^{-1/2}\boldsymbol{\Sigma}_2\boldsymbol{\Sigma}_1^{-1/2}$.

5.4 Local Average and Spatial Gradient of Diffusion Tensor Fields

Now, we can recall how the local average and spatial gradient of a diffusion tensor image can be computed.

5.4.1 Intrinsic mean

The average of a set of elements is one of the basic statistical tools we can derive in this Riemannian framework. In this sense, the normal distribution parametrized by $\hat{\boldsymbol{\Sigma}} \in PS^+(3)$ and defined as the empirical mean of N distributions $\boldsymbol{\Sigma}_1, \boldsymbol{\Sigma}_2, \ldots, \boldsymbol{\Sigma}_N$, achieves a local minimum of the function $\mu : PS^+(3) \to \mathbb{R}^+$ given as:

$$\mu(\hat{\boldsymbol{\Sigma}}, \boldsymbol{\Sigma}_1, \boldsymbol{\Sigma}_2, \ldots, \boldsymbol{\Sigma}_N) = \frac{1}{N}\sum_{k=1}^{N}\mathcal{D}^2(\hat{\boldsymbol{\Sigma}}, \boldsymbol{\Sigma}_k) \tag{5.8}$$

It has been proved in [Karcher77] that such a local minimum, also known as the Riemannian barycenter, exists and is unique for manifolds of non-positive sectional curvature, which is the case for $PS^+(3)$. In this sense, we call the distribution parametrized by $\hat{\boldsymbol{\Sigma}} \in PS^+(3)$ the *intrinsic mean* , as it is the empirical mean of such a set of distributions which is an element of the manifold $PS^+(3)$.

Since closed-form expression cannot be obtained, we resort to a gradient descent algorithm for the computation of the intrinsic mean as shown in [Lenglet05b]. We use the classical definition of the Riemannian center of mass and the geodesic equations to derive a manifold constrained numerical integrator and thus ensure that each step forward of the gradient descent stays within the space $PS^+(3)$. To derive such a flow evolving an initial guess $\hat{\boldsymbol{\Sigma}}(0)$ towards the Riemannian barycenter of the set $\boldsymbol{\Sigma}_1, \boldsymbol{\Sigma}_2, \ldots, \boldsymbol{\Sigma}_N \in PS^+(3)$,

we denote by $\hat{\mathbf{\Sigma}}(s), s \in [0, \infty)$ the family of solution of $\partial_s \hat{\mathbf{\Sigma}}(s) = \mathbf{V}(\hat{\mathbf{\Sigma}}(s))$, where $\mathbf{V}$ is the direction of evolution. Then, we have:

$$\hat{\mathbf{\Sigma}}(s) \in PS^+(3), \forall s > 0 \Leftrightarrow \{\hat{\mathbf{\Sigma}}(0) \in PS^+(3) \; and \; \mathbf{V}(\hat{\mathbf{\Sigma}}(s)) \in T_{\hat{\mathbf{\Sigma}}(s)} PS^+(3), \forall s > 0\} \quad (5.9)$$

We thus identify $\mathbf{V}$ with the opposite of the gradient of our objective function $\mu(\mathbf{\Sigma}_1, \mathbf{\Sigma}_2, \ldots, \mathbf{\Sigma}_N)$, which is [Moakher05]:

$$\nabla\mu(\hat{\mathbf{\Sigma}}, \mathbf{\Sigma}_1, \mathbf{\Sigma}_2, \ldots, \mathbf{\Sigma}_N) = \frac{\hat{\mathbf{\Sigma}}(s)}{N} \sum_{k=1}^{N} \log(\mathbf{\Sigma}_k^{-1} \hat{\mathbf{\Sigma}}(s)) \quad (5.10)$$

Hence, the evolution is:

$$\partial_s \hat{\mathbf{\Sigma}}(s) = -\frac{\hat{\mathbf{\Sigma}}(s)}{N} \sum_{k=1}^{N} \log(\mathbf{\Sigma}_k^{-1} \hat{\mathbf{\Sigma}}(s)) \quad (5.11)$$

Moreover, numerical implementation has to be dealt with carefully and we have to build a step-forward operator such that the discrete flow provides an intrinsic approximation of the evolution in Eq. 5.11. As proved in [Lenglet05b], this can be achieved for any tangent vector $\mathbf{V} = -\nabla\mu \in S(3)$, by resorting to the geodesic equation:

$$\hat{\mathbf{\Sigma}}_{l+1} = \hat{\mathbf{\Sigma}}_l^{1/2} \exp(-dt \hat{\mathbf{\Sigma}}_l^{-1/2} \nabla\mu \hat{\mathbf{\Sigma}}_l^{-1/2}) \hat{\mathbf{\Sigma}}_l^{1/2} \quad (5.12)$$

Finally, using Eq. 5.10 in Eq. 5.12, we obtain the following evolution to calculate the intrinsic mean:

$$\hat{\mathbf{\Sigma}}_{l+1} = \hat{\mathbf{\Sigma}}_l^{1/2} \exp\left(-dt \frac{\hat{\mathbf{\Sigma}}_l^{1/2}}{N} \left(\sum_{k=1}^{N} \log(\mathbf{\Sigma}_k^{-1} \hat{\mathbf{\Sigma}}_l)\right) \hat{\mathbf{\Sigma}}_l^{-1/2}\right) \hat{\mathbf{\Sigma}}_l^{1/2}, \quad (l = 0, \ldots, N_{iter}) \quad (5.13)$$

Numerical experimentation demonstrates that the evolution toward the desired mean $\hat{\mathbf{\Sigma}}$ converges in no more than $N_{iter} = 4$ or 5 iterations for any initial guess $\hat{\mathbf{\Sigma}}_0$.

5.4.2 Weighted intrinsic mean

In the same way the intrinsic mean is defined, we can also calculate a weighted intrinsic mean which ponderates a set of N normal distributions $\mathbf{\Sigma}_1, \mathbf{\Sigma}_2, \ldots, \mathbf{\Sigma}_N \in PS^+(3)$ with the weights $\omega_1, \omega_2, \ldots, \omega_N, \omega_i \in \mathbb{R}^+$

In this case, the normal distribution parameterized by $\hat{\mathbf{\Sigma}}^w \in PS^+(3)$ and defined as the weighted empirical mean of N distributions $\mathbf{\Sigma}_1, \mathbf{\Sigma}_2, \ldots, \mathbf{\Sigma}_N$, achieves a minimum of the weighted sum of squared distances defined by

$$\mu^w(\hat{\mathbf{\Sigma}}^w, \mathbf{\Sigma}_1, \mathbf{\Sigma}_2, \ldots, \mathbf{\Sigma}_N) = \frac{\sum_{k=1}^{N} \omega_k \mathcal{D}^2(\hat{\mathbf{\Sigma}}^w, \mathbf{\Sigma}_k)}{\sum_{k=1}^{N} \omega_k} \quad (5.14)$$

Following the same steps as in section 5.4.1, the following weighted step-forward operator is readily obtained:

$$\hat{\mathbf{\Sigma}}_{l+1}^{w} = \hat{\mathbf{\Sigma}}_{l}^{w\,1/2} \exp\left(-dt \frac{\hat{\mathbf{\Sigma}}_{l}^{w\,1/2} \left(\sum_{k=1}^{N} \omega_k \log(\mathbf{\Sigma}_k^{-1} \hat{\mathbf{\Sigma}}_{l}^{w}) \right) \hat{\mathbf{\Sigma}}_{l}^{w\,-1/2}}{\sum_{k=1}^{N} \omega_k} \right) \hat{\mathbf{\Sigma}}_{l}^{w\,1/2} \tag{5.15}$$

5.4.3 Spatial gradient of tensor fields

It is possible to estimate the magnitude of the gradient of the tensor field $\mathbf{\Sigma}(x) : \Omega \subset \mathbb{R}^3 \mapsto PS^+(3)$ at $x \in \Omega$ through the sum of squared geodesic distances between tensors in orthogonal directions on a discrete grid, as indicated by the following expression:

$$| \nabla \mathbf{\Sigma}(x) |^2 \simeq \sum_{k=1}^{3} \mathcal{D}^2(\mathbf{\Sigma}(x), \mathbf{\Sigma}(x \pm e_k)) \tag{5.16}$$

where e_k denotes the elements of the canonical basis in $\mathbb{R}^3$.

To derive Eq. 5.16, we use the explicit formulation of geodesic presented in Eq. 5.6, which allows us to calculate the geodesic starting at $\mathbf{\Sigma}_0 = \mathbf{\Sigma}(x)$ in the direction $\mathbf{V} = \dot{\mathbf{\Sigma}}(0)$ as:

$$\mathbf{\Sigma}(t) = \mathbf{\Sigma}_0^{1/2} \exp(t \mathbf{\Sigma}_0^{-1/2} \mathbf{V} \mathbf{\Sigma}_0^{-1/2}) \mathbf{\Sigma}_0^{1/2} \tag{5.17}$$

Hence, as we know that $\mathbf{\Sigma}(1) = \mathbf{\Sigma}(x \pm e_k) = \mathbf{\Sigma}_1$, we obtain that:

$$\mathbf{V} = \mathbf{\Sigma}_0^{1/2} \log(\mathbf{\Sigma}_0^{-1/2} \mathbf{\Sigma}_1 \mathbf{\Sigma}_0^{-1/2}) \mathbf{\Sigma}_0^{1/2} = \dot{\mathbf{\Sigma}}(0) \tag{5.18}$$

It can be shown that this quantity is actually equivalent to the opposite of the gradient of the squared geodesic distance $\nabla \mathcal{D}^2(\mathbf{\Sigma}_0, \mathbf{\Sigma}_1)$ whose expression was given by Moakher [Moakher05]:

$$\nabla \mathcal{D}^2(\mathbf{\Sigma}_0, \mathbf{\Sigma}_1) = \mathbf{\Sigma}_0 \log\left(\mathbf{\Sigma}_1^{-1} \mathbf{\Sigma}_0\right)$$

Indeed, it is easy to see that $\mathbf{\Sigma}_0^{1/2} \log(\mathbf{\Sigma}_0^{-1/2} \mathbf{\Sigma}_1 \mathbf{\Sigma}_0^{-1/2}) \mathbf{\Sigma}_0^{1/2}$ can be rewritten as $\mathbf{\Sigma}_0 \mathbf{\Sigma}_0^{-1/2} \log(\mathbf{\Sigma}_0^{-1/2} \mathbf{\Sigma}_1 \mathbf{\Sigma}_0^{-1/2}) \mathbf{\Sigma}_0^{1/2}$.

Using the following property:

$$\mathbf{M_1}^{-1} \log(\mathbf{M_2}) \mathbf{M_1} = \log(\mathbf{M_1}^{-1} \mathbf{M_2} \mathbf{M_1}),\ \forall \mathbf{M_1}, \mathbf{M_2} \in GL(m) \tag{5.19}$$

we get

$$\mathbf{V} = \mathbf{\Sigma}_0 \log\left(\mathbf{\Sigma}_0^{-1} \mathbf{\Sigma}_1\right) = -\mathbf{\Sigma}_0 \log\left(\mathbf{\Sigma}_1^{-1} \mathbf{\Sigma}_0\right)$$

The symmetric matrix $\mathbf{V}$ can thus be used to approximate the spatial directional derivative of a tensor field. To better understand why this is correct, we can consider the Euclidean distance between tensors

$$\mathcal{D}_E^2(\mathbf{\Sigma}_0, \mathbf{\Sigma}_1) = |\mathbf{\Sigma}_0 - \mathbf{\Sigma}_1|_F^2 = \mathrm{tr}\left((\mathbf{\Sigma}_0 - \mathbf{\Sigma}_1)(\mathbf{\Sigma}_0 - \mathbf{\Sigma}_1)^T\right)$$

for which, using the fact that $\nabla \mathrm{tr}\,(XY) = Y^T$, $\forall X, Y \in GL(m)$, we have $\nabla \mathcal{D}_E^2(\mathbf{\Sigma}_0, \mathbf{\Sigma}_1) = \mathbf{\Sigma}_0 - \mathbf{\Sigma}_1$. In other words, this corresponds to the *difference* tangent vector, usually used in finite difference schemes to approximate a spatial gradient. $\mathbf{V}$ generalizes this notion by taking into account the Riemannian structure of the space $PS^+(3)$.

All we need to prove now is that the magnitude of the tangent vector $\mathbf{V}$, taking into account the Riemannian metric of $PS^+(3)$, is equal to the squared geodesic distance between $\mathbf{\Sigma}_0$ and $\mathbf{\Sigma}_1$, so that Eq. 5.16 is true.

Noting that $\mathbf{V}$ is, by definition, the *logarithm map* of $\mathbf{\Sigma}_1$ at $\mathbf{\Sigma}_0$ $\log_{\mathbf{\Sigma}_0}(\mathbf{\Sigma}_1) = \dot{\mathbf{\Sigma}}_0$, we know this is true since one of its properties is:

$$\langle \dot{\mathbf{\Sigma}}_0, \dot{\mathbf{\Sigma}}_0 \rangle_{\mathbf{\Sigma}_0} = \mathcal{D}^2(\mathbf{\Sigma}_0, \mathbf{\Sigma}_1)$$

Indeed, we have

$$\langle \mathbf{V}, \mathbf{V} \rangle_{\mathbf{\Sigma}_0} = \frac{1}{2}\mathrm{tr}\left(\left(-\mathbf{\Sigma}_0^{-1}\mathbf{\Sigma}_0 \log\left(\mathbf{\Sigma}_1^{-1}\mathbf{\Sigma}_0\right)\right)^2\right) = \frac{1}{2}\mathrm{tr}\left(\left(\log\left(\mathbf{\Sigma}_0^{-1}\mathbf{\Sigma}_1\right)\right)^2\right)$$

and since the matrices $\mathbf{\Sigma}_0^{-1}\mathbf{\Sigma}_1$ and $\mathbf{\Sigma}_0^{-1/2}\mathbf{\Sigma}_1\mathbf{\Sigma}_0^{-1/2}$ are similar, we have $\langle \mathbf{V}, \mathbf{V} \rangle_{\mathbf{\Sigma}_0} = \frac{1}{2}\mathrm{tr}\left(\log^2\left(\mathbf{\Sigma}_0^{-1/2}\mathbf{\Sigma}_1\mathbf{\Sigma}_0^{-1/2}\right)\right) = \mathcal{D}^2(\mathbf{\Sigma}_0, \mathbf{\Sigma}_1)$.

Hence, to obtain the gradient magnitude within the Riemannian framework, we simply calculate the geodesic distances in orthogonal directions following Eq. 5.16.

Let us now compare the differences between the gradient magnitude in a Euclidean sense and our definition in the Riemannian framework. For the sake of simplicity, we are going to study the case of tensors in a two-dimensional neighborhood $\mathcal{N}$ containing a boundary like that shown in Fig. 5.1, where white dots represent tensors $\mathbf{T_1} = \lambda_1 \mathbf{v_1}\mathbf{v_1}^T + \lambda_2 \mathbf{v_2}\mathbf{v_2}^T$ and black dots represent tensors $\mathbf{T_2} = k_1\lambda_1 \mathbf{v_1}\mathbf{v_1}^T + k_2\lambda_2 \mathbf{v_2}\mathbf{v_2}^T$, with $\lambda_i, (i = 1, 2)$ the eigenvalues of $\mathbf{T_1}$, associated to eigenvectors $\mathbf{v_i}$ and constants k_i.

Using Eq. 5.16 and the definition of the geodesic distance in Eq. 5.7, it is not hard to see that:

$$|\nabla \mathcal{N}|^2 = \mathcal{D}^2(\mathbf{T_1}, \mathbf{T_2}) = \frac{1}{2}(\log^2(k_1) + \log^2(k_2)) \tag{5.20}$$

while the magnitude of the Euclidean gradient is:

$$|\nabla \mathcal{N}|_E^2 = \| \mathbf{T_1} - \mathbf{T_2} \|_F^2 = \lambda_1^2(1 - k_1)^2 + \lambda_2^2(1 - k_2)^2 \tag{5.21}$$

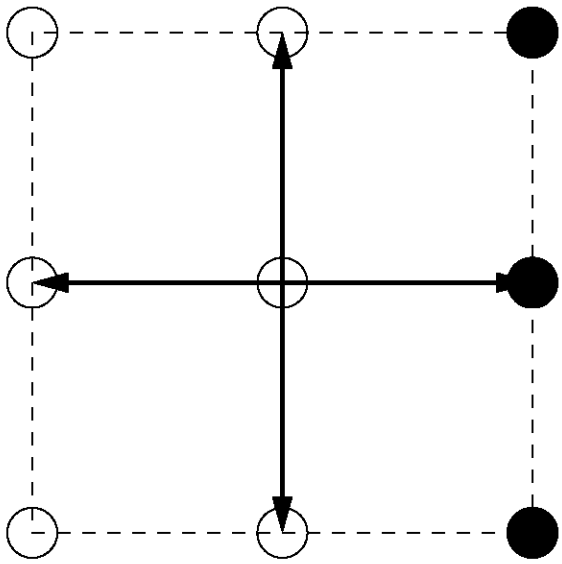

Figure 5.1: 3×3 Neighborhood $\mathcal{N}$ of a tensor field. White dots represent tensors $\mathbf{T_1}$ whereas black dots are tensors $\mathbf{T_2}$

It is remarkable that the Riemannian gradient magnitude is independent of the eigenvalues since it only depends on the constant factors, that is to say, the magnitude is scale-independent. Fig. 5.2 presents both gradient magnitudes for different values of $k_1 = k_2 = K$ and different values of λ_1, λ_2. While the Riemannian gradient is not affected by different values of λ_1, λ_2, the slope of the Euclidean gradient magnitude is determined by the square root of the sum of the squared eigenvalues, showing that the greater the eigenvalues, the bigger the slope represented by the blue lines in Fig. 5.2

Let us now study the different behaviors when we have, in our neighborhood $\mathcal{N}$, the same tensors but rotated by an angle α. The white tensors are now defined as $\mathbf{T_1} = \lambda_1 \mathbf{v_1} \mathbf{v_1}^T + \lambda_2 \mathbf{v_2} \mathbf{v_2}^T$ while $\mathbf{T_2} = \mathbf{P}^T \mathbf{T_1} \mathbf{P}$, with $\mathbf{P}$ an orthogonal unitary rotation matrix. Again, using Eqs. 5.16 and 5.7 it is not difficult to derive the following expression for the Riemannian gradient magnitude:

$$| \nabla \mathcal{N} |^2 = \mathcal{D}^2(\mathbf{T_1}, \mathbf{T_2}) = \frac{1}{2}(\log^2(A^+) + \log^2(A^-)) \tag{5.22}$$

where A^+ and A^- are, respectively

$$A^{\pm} = \frac{(2\lambda_1\lambda_2 + \sin^2(\alpha)(\lambda_1 - \lambda_2)^2 \pm \sin(\alpha)(\lambda_1 - \lambda_2)\sqrt{\sin^2(\alpha)(\lambda_1 - \lambda_2)^2 + 4\lambda_1\lambda_2})}{2\lambda_1\lambda_2} \tag{5.23}$$

On the other hand, the Euclidean gradient magnitude is:

$$| \nabla \mathcal{N} |_E^2 = \| \mathbf{T_1} - \mathbf{T_2} \|_F^2 = 2\sin^2(\alpha)(\lambda_1 - \lambda_2)^2 \tag{5.24}$$

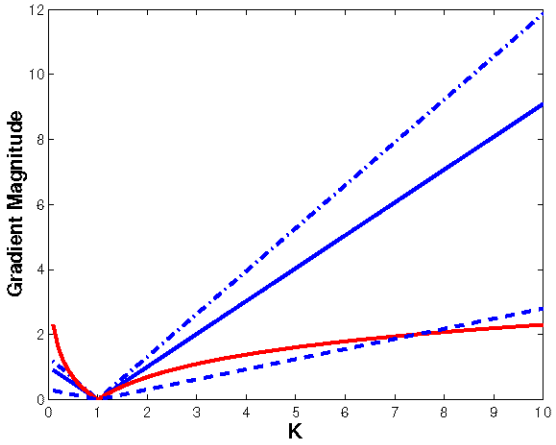

Figure 5.2: Gradient magnitudes as a function of parameter K. Red Line: Riemannian Gradient Magnitude. Blue Lines: Euclidean Gradient Magnitude for different eigenvalues Dashed Line: $\lambda_1 = 0.22, \lambda_2 = 0.22$. Solid Line: $\lambda_1 = 0.94, \lambda_2 = 0.33$. Dashed-Dotted Line: $\lambda_1 = 1.05, \lambda_2 = 0.80$.

Again, the dependence of the Riemannian gradient magnitude on eigenvalues is less important than that of the Euclidean gradient magnitude. Fig. 5.3 shows different responses of the gradient magnitudes as a function of the angle $\alpha \in [0, \pi]$. On the left, we show the gradient magnitudes for anisotropic tensors, for which eigenvalues ratio is large. In that case, for $\lambda_1 = 0.99, \lambda_2 = 0.2$ it can be seen that the response of the Riemannian gradient (solid red line) is bigger than the response of the Euclidean gradient. On the right, we show the gradient magnitudes with more isotropic tensors, with eigenvalues ratio close to one ($\lambda_1 \simeq \lambda_2$). In this case, the Riemannian gradient magnitude provides a smaller response (solid red line) than the Euclidean gradient magnitude (solid blue line). However, as the Euclidean gradient magnitude is proportional to the eigenvalues, a problem may arise with isotropic tensors if the eigenvalues are too large, as the dashed lines show. In that case, with $\lambda_1 = 19, \lambda_2 = 17.5$, the Euclidean gradient magnitude is much bigger than the Riemannian one which, on the contrary, stays almost identical to its value for small λ_i.

5.5 Riemannian Anisotropic Smoothing

We now make use of the concepts previously presented to develop our Riemannian anisotropic smoothing algorithm. We use the mathematical tools presented in section 5.4 to develop a boundary preserving smoothing algorithm. In practice, we simply use the step-forward operator shown in Eq. 5.15 to compute local weighted averages.

The anisotropic behavior is introduced by weighting each sample, within a local neighborhood, by a function that depends on the Riemannian gradient magnitude developed in section 5.4.3. This function is chosen so that, in homogeneous regions, the weights are constant and the tensors are isotropically averaged. On the contrary, when lying on an edge of the image, we would like that only samples on that boundary,

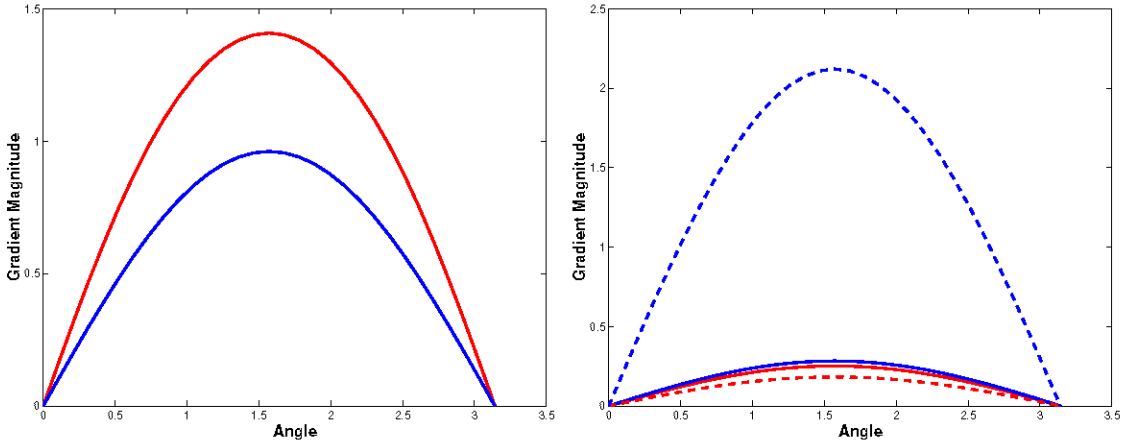

Figure 5.3: Gradient magnitudes as a function of rotation angle α. Red Lines: Riemannian Gradient Magnitude. Blue Lines: Euclidean Gradient Magnitude. Left Image: Response for anisotropic tensors. Right Image: Response for more isotropic tensors.

and not those across, contribute to the local averaging. To achieve this goal and avoid mixing structures of the image, one possible choice for the weighting function is $\omega_k = \epsilon + \mid \nabla \mathbf{\Sigma}(x) \mid^2$.

A major advantage of this approach is that a straightforward C++ implementation yields a quite computationally efficient algorithm since, to regularize a $50 \times 50 \times 50$ volume of 3×3 tensors, using a $3 \times 3 \times 3$ averaging neighborhood, we obtain an average processing time of 8 minutes on a 1.7 GHz Pentium M CPU with 1 Gb of RAM. Moreover, it is easy to automatically detect the convergence of the gradient descent, detailed in Eq. 5.15, by checking the evolution speed

$$\frac{\mathbf{\Sigma}_l^w \left(\sum_{k=1}^N \omega_k \log(\mathbf{\Sigma}_k^{-1} \hat{\mathbf{\Sigma}}_l^w) \right)}{\sum_{k=1}^N \omega_k}$$

and stopping whenever a given norm (Frobenius for instance) of this symmetric matrix has reached a certain threshold (1e-6 in practice). Hence not only do we ensure the convergence of the weighted mean but we also discard the need for a parameter such as the number of iterations.

The theoretical framework developed in sections 5.3 and 5.4 implies that the tensor field consists of symmetric positive definite tensors. Depending on the estimation procedure used to compute those tensors (see [Tschumperlé03b] and references therein), positive semidefinite tensors may arise, yielding inaccurate results, since any semidefinite tensor is at an infinite distance from a definite one. To solve this issue, it is necessary to resort to a dedicated estimation algorithm, such as the one proposed in [Lenglet05a], that ensures to stay within $PS^+(3)$.

5.6 Results

In this section, we present various numerical experiments and compare the regularization methods previously detailed on synthetic and real DT-MRI data.

5.6.1 Synthetic Data

Experiment 1

We now would like to evaluate the behavior of the different algorithms presentend in this chapter. To that end, we use the volume used in Experiment 1 from section 4.5.1 where a $16 \times 16 \times 16$ volume with tensors oriented along the horizontal direction is introduced in the central part of a $32 \times 32 \times 32$ cube with tensors oriented in the orthogonal direction, as shown on Fig. 4.5. Then, we add a high level of Gaussian noise using the algorithm proposed in [Lenglet05a], resulting in the noisy tensor field in the right side of Fig. 4.5.

Figure 5.4 shows on the left side the response obtained with the anisotropic Riemannian filtering approach presented in this chapter while on the right side it is shown the output of the nonlinear diffusion process for tensors [Weickert02]. Differences arise when comparing these two images or any of the details shown in Figs. 5.5 or 5.6. First of all, noise is better removed with the Riemannian approach than with the nonlinear diffusion, where some misoriented tensors remain even after 536 iterations with a time step of 0.01, which are the parameters that provide the optimal response. We must point out here that the optimization of the diffusion time for the nonlinear diffusion scheme is clearly both critical and difficult to adjust. It is definitely a major limitation of this last approach.

Furthermore, the well-known swelling effect, due to a faster regularization of the eigenvalues, is observed for the nonlinear diffusion, whereas it is not noticeable for our Riemannian approach. But most importantly, we can see that the regularized tensor field obtained with our approach is more anisotropic (FA is around 0.75, while the FA of the original tensor field is 0.77) than that obtained with the nonlinear diffusion (FA is around 0.60).

From a quantitative point of view, we measure the error between the original and the regularized images following two different parameters. The first one, whose expression is shown in Eq. 4.27, is a traditional error measure we already used to validate our results in previous chapters. The second one is a new error measure which computes the mean geodesic distance between the original field and the obtained one, which is given in Eq. 5.25. Table 5.1 shows the error statistics following Eq. 4.27. It is obvious that the accuracy of the Riemannian approach is much better than that achieved with the nonlinear diffusion which is consistent with the results shown in table 5.2 using Eq. 5.25.

$$Error(x) = \mathrm{tr}\left((\mathbf{\Sigma}(x) - \hat{\mathbf{\Sigma}}(x))(\mathbf{\Sigma}(x) - \hat{\mathbf{\Sigma}}(x))^T\right) \tag{5.25}$$

where $\mathbf{\Sigma}(x)$ is the original tensor field and $\hat{\mathbf{\Sigma}}(x)$ is the filtered one.

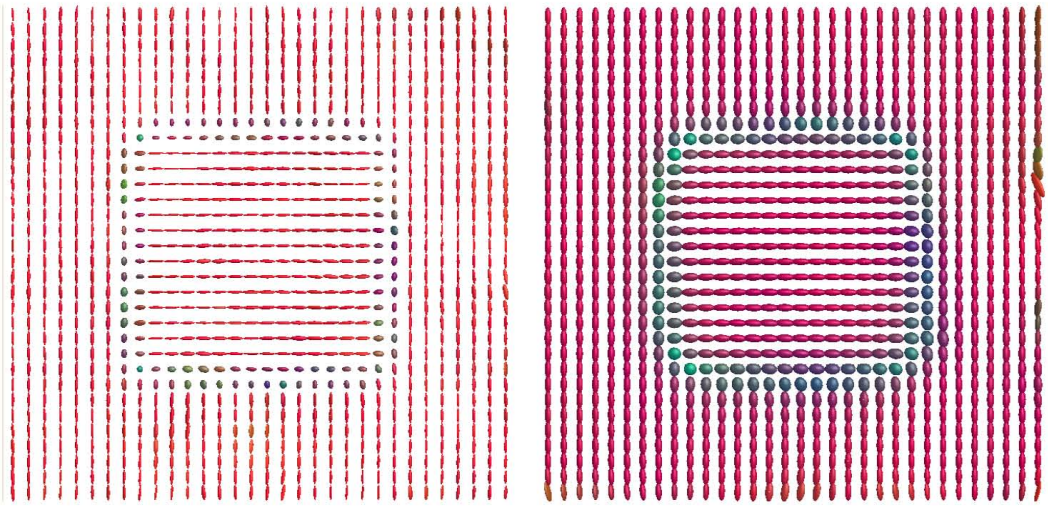

Figure 5.4: Responses of different tensor regularization methods. Left: Anisotropic Riemannian filtering approach. Right: Nonlinear diffusion filtering scheme.

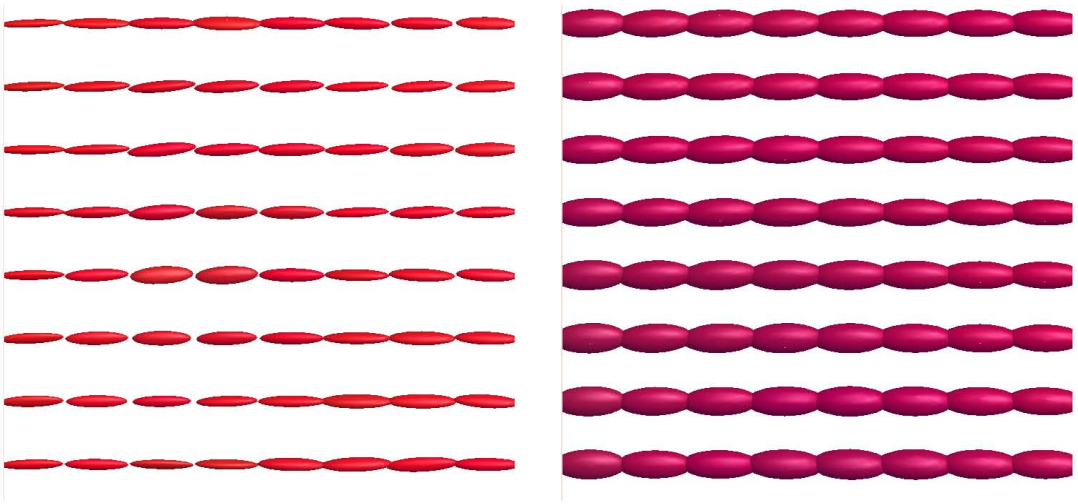

Figure 5.5: Details on the responses of different tensor regularization methods. Top Row: Gaussian Smoothing (Left). Wiener Filter (Right). Middle Row: Root-Squares Homomorphic Filtering. $H\{\cdot\}$ is Gaussian filter (Left) and Wiener filter (Right). Bottom Row: Log-Exponential Homomorphic Filtering. $H\{\cdot\}$ is Gaussian filter (Left) and Wiener filter (Right).

	Mean Error	Std. Deviation	Max	Min
Anisotropic Riemannian Filtering	0.6296	0.5166	4.4222	0.0600
Nonlinear Diffusion	2.1677	0.7970	91.2742	0.7367

Table 5.1: Statistics of the error measured following Eq. 4.27 for experiment 1.

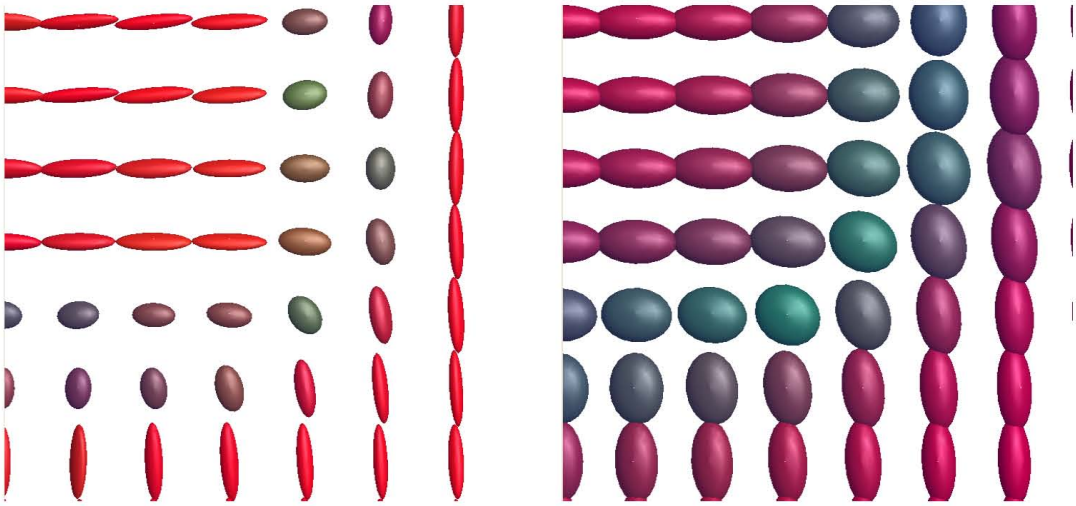

Figure 5.6: Details on the responses of different tensor regularization methods. Top Row: Gaussian Smoothing (Left). Wiener Filter (Right). Middle Row: Root-Squares Homomorphic Filtering. $H\{\cdot\}$ is Gaussian filter (Left) and Wiener filter (Right). Bottom Row: Log-Exponential Homomorphic Filtering. $H\{\cdot\}$ is Gaussian filter (Left) and Wiener filter (Right).

	Mean Error	Std. Deviation	Max	Min
Anisotropic Riemannian Filtering	0.2572	0.1313	1.3065	0.0300
Nonlinear Diffusion	0.8284	0.1209	3.2551	0.2630

Table 5.2: Statistics of the error measured following Eq. 5.25 for experiment 1.

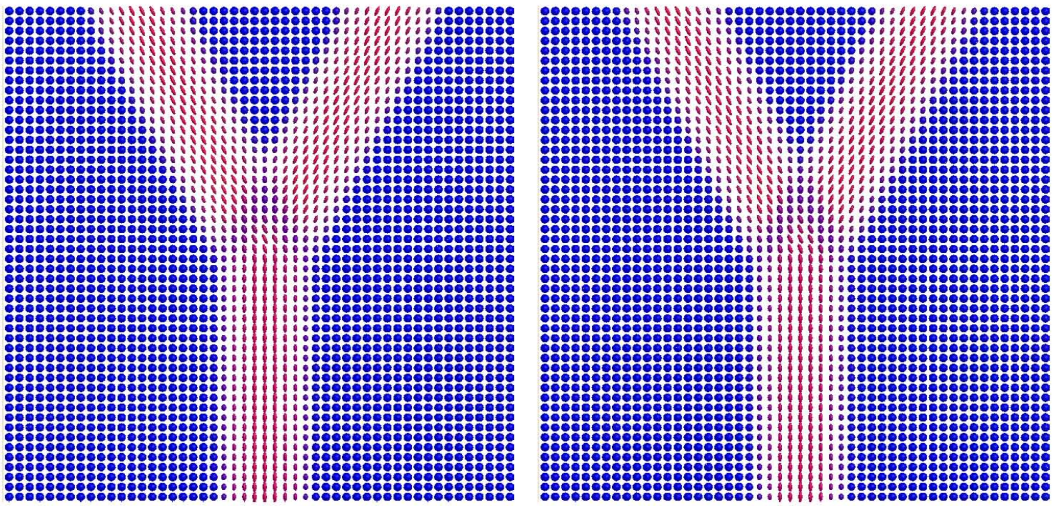

Figure 5.7: Responses of different tensor regularization methods. Top Row: Gaussian Smoothing (Left). Wiener Filter (Right). Middle Row: Root-Squares Homomorphic Filtering. $H\{\cdot\}$ is Gaussian filter (Left) and Wiener filter (Right). Bottom Row: Log-Exponential Homomorphic Filtering. $H\{\cdot\}$ is Gaussian filter (Left) and Wiener filter (Right).

	Mean Error	Std Deviation	Max	Min
Anisotropic Riemannian Filtering	0.5218	0.0712	1.0770	0.1651
Nonlinear Diffusion	0.5283	0.0409	0.9957	0.2044

Table 5.3: Statistics of the error measured following Eq. 4.27 for experiment 2 using the different regularization schemes proposed in this chapter.

Experiment 2

In order to check the performance of our approach with different datasets we use again the $50 \times 50 \times 50$ volume of 3×3 tensors synthesized for the experiment 2 in the previous chapter, which can be seen in Fig. 4.9. Then, we generate the noisy version shown in Fig. 4.9 with the procedure previously explained.

We then try to recover the original image from the noisy version. Figure 5.7 shows on the left the response from our anisotropic Riemannian smoothing algorithm, while on the right the response of the nonlinear diffusion algorithm with time step 0.01 and 36 iterations is shown. From those figures, it is obvious that boundaries are well preserved with these anisotropic methods. To more clearly emphasize the differences, Figs. 5.8 and 5.9 show some details of the referred responses near boundaries.

In order to quantify and compare the performances of the nonlinear diffusion with our Riemannian anisotropic smoothing method, we also measure the mean error with the proposed parameters described in Eqs. 4.27 and 5.25. Table 5.4 shows some statistics on the error, where it can be seen that the Riemannian approach improves the behavior of the Euclidean counterparts.

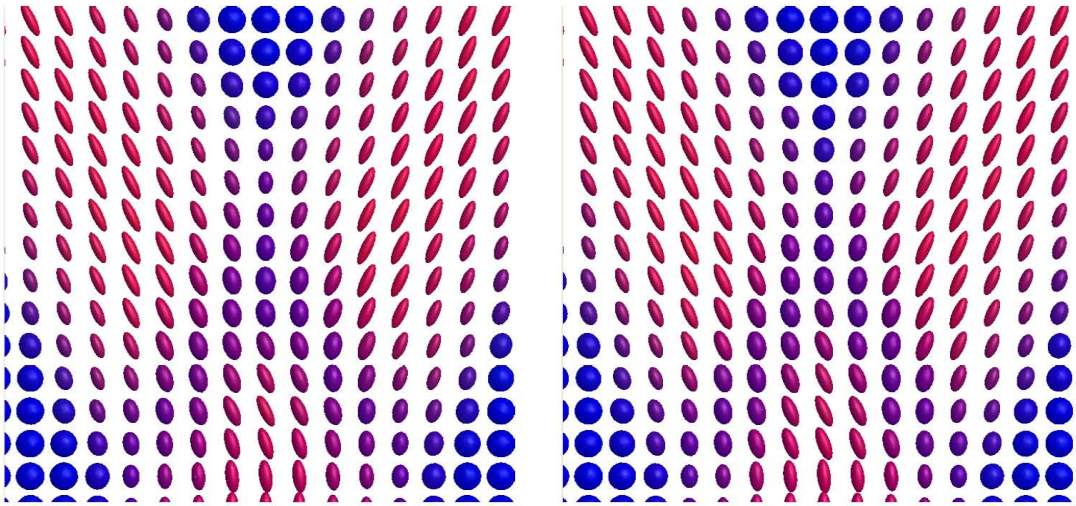

Figure 5.8: Details on the responses of different tensor regularization methods. Top Row: Gaussian Smoothing (Left). Wiener Filter (Right). Middle Row: Root-Squares Homomorphic Filtering. $H\{\cdot\}$ is Gaussian filter (Left) and Wiener filter (Right). Bottom Row: Log-Exponential Homomorphic Filtering. $H\{\cdot\}$ is Gaussian filter (Left) and Wiener filter (Right).

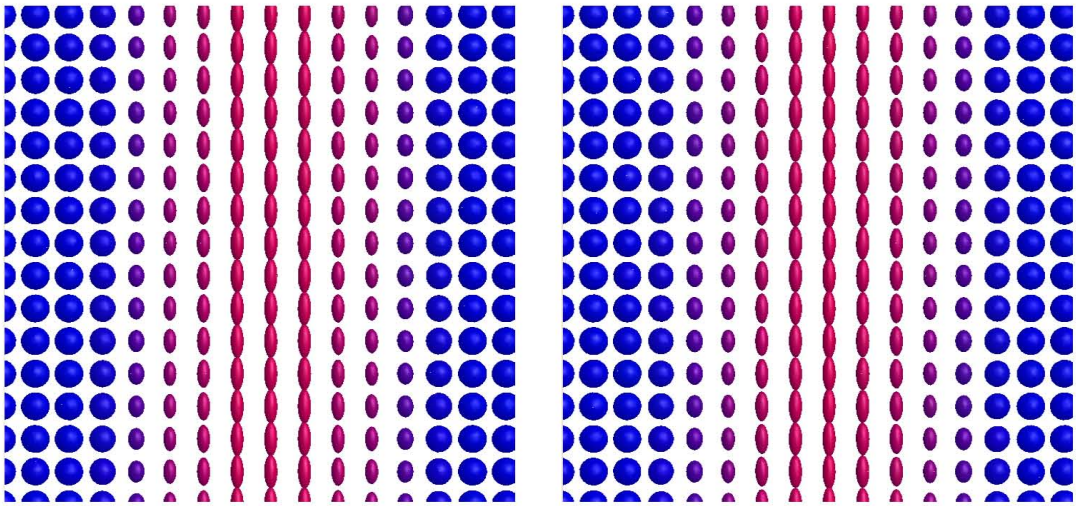

Figure 5.9: Details on the responses of different tensor regularization methods. Top Row: Gaussian Smoothing (Left). Wiener Filter (Right). Middle Row: Root-Squares Homomorphic Filtering. $H\{\cdot\}$ is Gaussian filter (Left) and Wiener filter (Right). Bottom Row: Log-Exponential Homomorphic Filtering. $H\{\cdot\}$ is Gaussian filter (Left) and Wiener filter (Right).

	Mean Error	Std Deviation	Max	Min
Anisotropic Riemannian Filtering	0.4216	0.1816	1.7076	0.1327
Nonlinear Diffusion	0.4240	0.1590	1.6562	0.1617

Table 5.4: Statistics of the error measured following Eq. 5.25 for experiment 2 using the different regularization schemes proposed in this chapter.

5.6.2 Real DT-MRI Data

Figure 5.10 (top left) shows the estimated diffusion tensors. On the top right, we display the regularized image using the Riemannian filtering approach, while bottom images are regularized using nonlinear diffusion, both with 10 iterations, but different time steps: 0.001 on the left and 0.01 on the right.

If we analyze the different structures found on this axial slice, we can see that tensors orientation within the *splenium of the corpus callosum* (CC(S) in the image) and in the *genu of the corpus callosum* (CC(G) in the image) is more coherent with our Riemannian filtering scheme. Anisotropy in these areas is also better preserved than with the nonlinear diffusion case, which yields blurred areas most likely because of the properties of the Euclidean gradient. In addition, the *ventricles* areas (VE in the image), since they are mainly homogeneous structures, are better regularized with our approach, as inhomogeneities do not disappear with nonlinear diffusion. Finally, the *corona radiata* (CR in the image) is well preserved in our approach while it is completely smoothed away from the image with longer diffusion time.

On Fig. 5.11, we show a complete human brain volume where fiber orientation is color coded as follows: Red: Right-Left / Green: Anterior-Posterior / Blue: Inferior-Superior. Original data is shown at the top of the image, while the filtered version is shown at the bottom. An axial slice from that volume is presented on Fig. 5.12, where we compare original data (on the left) with the filtered version (on the right) using our approach. It is clear that tensors belonging to particular fiber bundles are more coherent while the interfaces between the various tracts have been preserved.

5.7 Conclusions

We have presented a novel differential geometrical approach for the anisotropic regularization of tensor fields, seen as fields of multivariate normal distributions. We focused on the properties of the space of multivariate normal distributions to introduce an affine invariant Riemannian metric and notions such as the mean and spatial gradient which provide a well-founded framework to develop a non iterative anisotropic filtering algorithm for tensor data.

The anisotropic behavior is introduced through the gradient magnitude, simply computed by using the geodesic distance between distributions. This gradient magnitude, contrary to the Euclidean one, benefits from the affine invariance of the underlying distance. It is not sensitive to the scale of the tensors which allows to better discriminate tissues interfaces and regularize misoriented tensors because of the noise as shown in our numerical experiments.

Our filtering scheme is also compared to nonlinear diffusion of matrix-valued data to point out its added value over the PDE-based approaches and to show that our approach can easily solve some of their limitations, yielding better results on synthetic and real DT-MRI data.

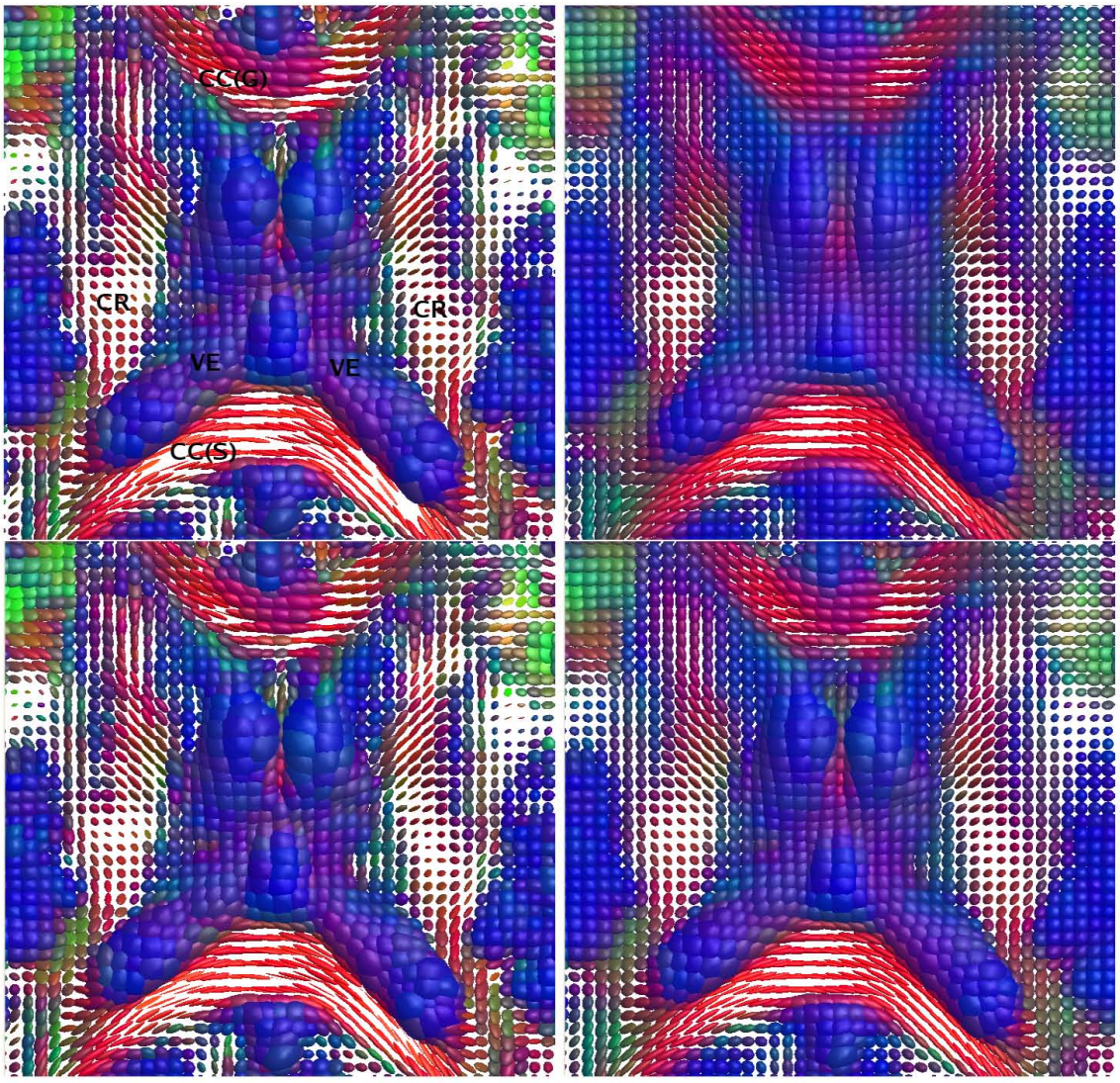

Figure 5.10: Results on real DT-MRI data. Top Left: Original DT-MRI data. CC(S): Splenium of the Corpus Callosum. CC(G): Genu of the Corpus Callosum. VE: Ventricles. CR: Corona Radiata. Top Right: anisotropic Riemannian filtering. Bottom Left: nonlinear diffusion (time step 0.001, 10 iter.). Bottom Right: nonlinear diffusion (time step 0.01, 10 iter.)

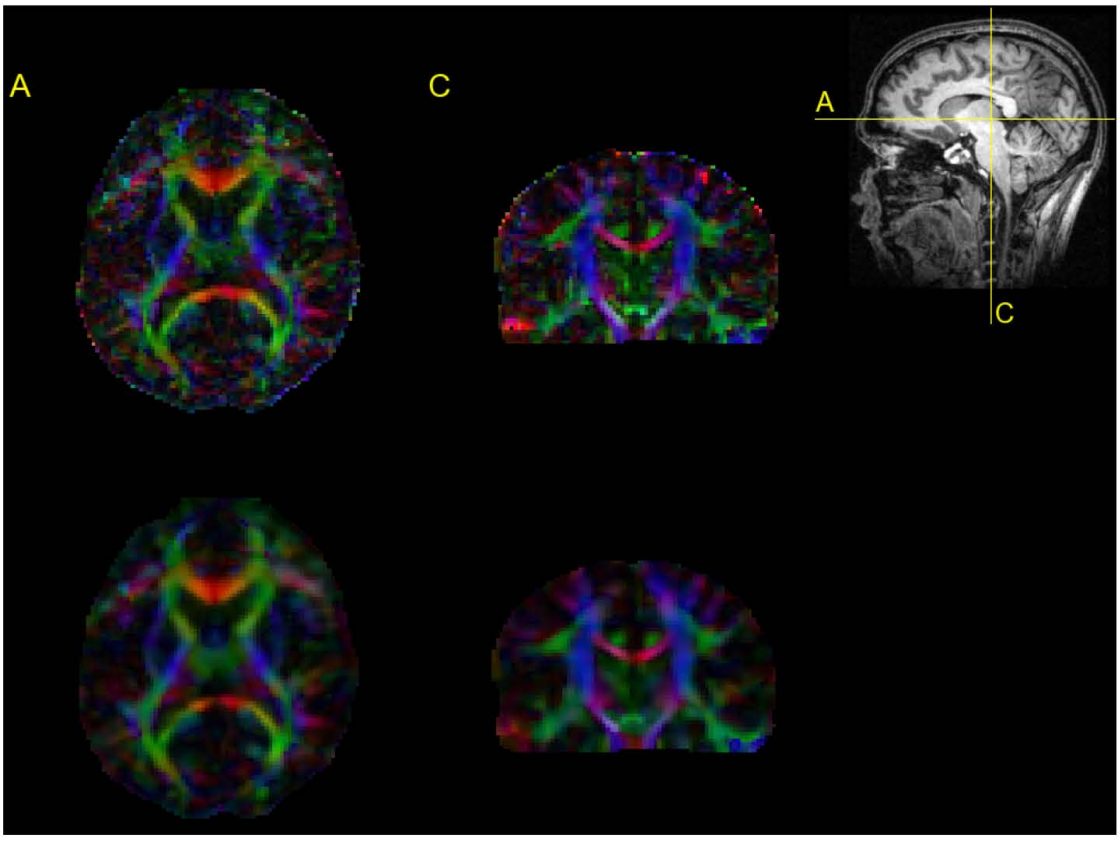

Figure 5.11: Real data volume of a human brain.

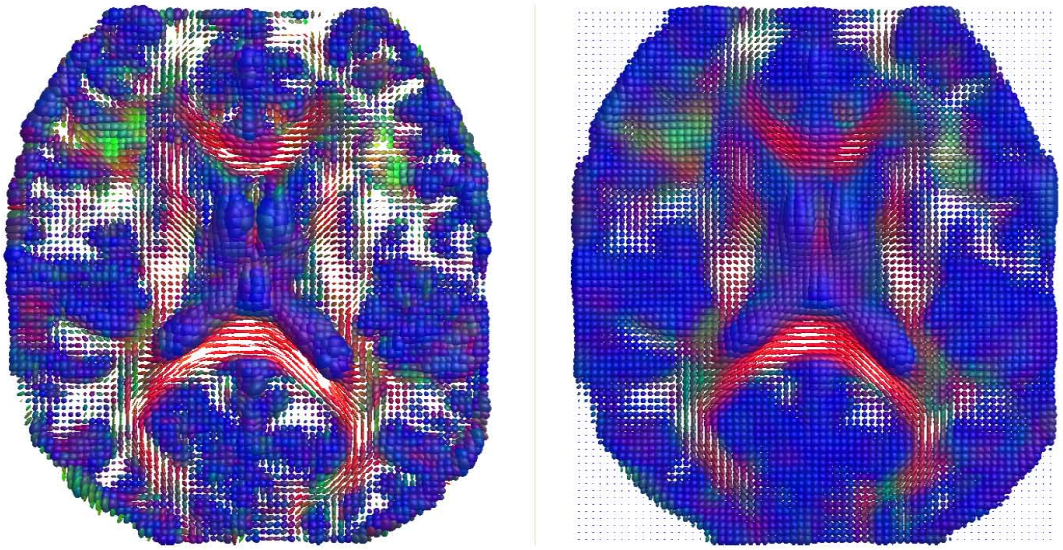

Figure 5.12: Axial view of DT-MRI data. Left: Raw tensor field. Right: Regularized version of the tensor field.

Chapter 6

Conclusions

6.1 Conclusions and Discussions

The aim of this dissertation is the development of *New Schemes for Tensor Signal Processing* to deal with conventional signal processing problems, but with the special requirements that tensor datasets demand, since intrinsic algebraic relationships among the elements of the tensor and between adjacent tensors have to be preserved.

Furthermore, tensors have also become an important signal processing tool, specially in the domain of image processing approaches, mainly motivated by the use of the local structure tensor for the measurement of spatial signal variation. The tensor representation presents the advantage that provides information about the dominant direction of signal variation as well as the uncertainty of being actually dominant. This fact resolves certain ambiguity which arises in conventional structure descriptors based on a vector representation, such as the gradient.

In chapter 3, we have studied the local structure tensor as an image processing tool to develop algorithms for scalar and tensor-valued signals. Motivated by the fact that several methods have been proposed in the literature to estimate that tensor, mainly, those based on the outer product of the gradient and those based on the computation of the signal local energy, we have studied the robustness of these methods against noise. From our results, we have reached the conclusion that the postprocessing smoothing step usually applied to introduce an scale factor into the estimated tensor field usually yields to structure delocalization, which can be reduced by means of a nonlinear smoothing technique. Also from our results, we verified that energy-based methods are more robust against noise that those based on the outer product of the gradient.

Then, we presented an anisotropic filtering scheme which uses nonlinear structure tensors to define the neighborhood to be used in the estimation and to drive an anisotropic gaussian function. On the one hand, the definition of the neighborhood by means of the local structure tensor lead us to a general framewok to build anisotropic versions of classical linear estimators, such as Wiener or constrained LMMSE. On the other hand, we introduced the use of nonlinear structure tensors in a well known filtering approach, as it is anisotropic gaussian filtering.

The local structure tensor can also be used to derive models of the signal covariance function taking into account its own structure. Statistical second order signal characterization is important in the field of signal processing since it yields to the derivation of filters that are grounded on a bayesian framework, interpreting signals as fields of random variables, using statistics to perform estimations. In this context, the use of the local structure tensor contributes to obtain covariance models that better fit the real signal behavior, yielding to improved signal estimators.

The previous ideas were also used to interpolate tensor fields, which is essential for many important tasks managing digital imagery and, in particular for data of low resolution such as clinical DT-MRI data. We presented a new method to perform interpolation, preserving boundaries. Our approach interpolates samples using the natural neighbors of the interpolation point, in a regular grid, with weights proportional to the inverse squared distance between the samples and the interpolation point, using the inverse of a generalization of the local structure tensor as a metric to compute the distances.

Both signal processing systems, those used for image filtering and the latter used to perform interpolation, can be straightforwardly generalized for tensor-valued signals with the inherent advantage that they preserve tensors semidefinite positive since they are weighted by positive values.

In chapter 4, we have addressed the specific problem of regularization of tensor fields from a new perspective. We presented a generalization of the homomorphic processing framework for the regularization of tensor fields. The mathematical background relies on the algebraical interpretation of the vector space of symmetric matrices and the set of symmetric positive definite matrices. Although these two algebraical structures seem different, there exists a relationship between them that we exploit to generalize the homomorphic theory for tensors.

In this sense, the properties of the generalized theory differ from the usual homomorphic decomposition, even though the mathematical formulation is completely analogous, using the matrix logarithm and the matrix exponential as input and output subsystems, respectively, in the processing cascade since it is the natural mapping which transforms symmetric positive definite matrices into elements of the vector space of symmetric matrices and viceversa. We show that this is not the only possibility. For instance, we relaxed some requirements to propose the use of the matrix square root and matrix squares, respectively, as input and output subsystems of the processing cascade. This approach takes the advantage that it also deals with symmetric positive semidefinite tensors.

To validate our algorithms we compared the outputs of the homomorphic processing cascades to the output of the filter used in the middle of the processing cascade. In our experiments with synthetic and true data, we obtained better results in all cases with the homomorphic framework than with the filter itself.

Finally, in chapter 5, we have presented a novel differential geometrical approach for the anisotropic regularization of tensor fields, seen as fields of multivariate normal distributions. We focused on the properties of the space of multivariate normal distributions to introduce an affine invariant Riemannian metric and notions such as the mean and spatial gradient which provide a well-founded framework to develop a non

iterative anisotropic filtering algorithm for tensor data.

The anisotropic behavior is introduced through the gradient magnitude, simply computed by using the geodesic distance between distributions. This gradient magnitude, contrary to the Euclidean one, benefits from the affine invariance of the underlying distance. It is not sensitive to the scale of the tensors which allows to better discriminate tissues interfaces and regularize misoriented tensors because of the noise as shown in our numerical experiments.

Our filtering scheme is also compared to nonlinear diffusion of matrix-valued data to point out its added value over the PDE-based approaches and to show that our approach can easily solve some of their limitations, yielding better results on synthetic and real DT-MRI data. A major advantage of our approach is the fact that it is almost parameter-free, since it only depends on the neighborhood used to calculate the weighted intrinsic mean. From our experience, we always get the better results with a $3 \times 3 \times 3$ averaging neighborhood, so it can be considered a default value. In addition, its implementation yields a quite computationally efficient algorithm since, to regularize a $50 \times 50 \times 50$ volume of 3×3 tensors, we obtain an average processing time of 8 minutes. Moreover, it is easy to automatically detected the convergence of the gradient descent by checking the evolution speed and stopping whenever its Frobenius norm, for instance, has reached a certain threshold. Hence not only do we ensure the convergence of the weighted mean but we also discard the need for a parameter such as the number of iterations for the gradient descent algorithm.

6.2 Related Publications

In this section we show a short description of the papers that have been published in the context of this thesis.

- **Homomorphic Filtering of DT-MRI Fields** [Castaño03b]:

  In this paper, we propose the embryonic foundations of the homomorphic processing cascade that guarantees PSD tensor output motivated by the fact that DT-MRI tensor fields must remain symmetric positive definite even when these datasets are filtered, something that is not allways true when working with real data.

- **Filtrado Homomórfico de Datos Tensoriales** [Castaño03a]:

  DT-MRI tensor fields must be symmetric positive definite. However, due to a number of reasons this is not true in real data. Furthermore, it would be desirable to maintain that condition when tensor data is filtered. This paper complements the work done in [Castaño03b] by means of a homomorphic cascade that guarantees this property.

- **Anisotropic Interpolation of DT-MRI** [Castaño04b]:

  In this paper, we present a new technique to interpolate the diffusion tensor field, preserving boundaries and the constraint of positive-semidefiniteness. Our approach is based on the use of the inverse of the local structure tensor as a metric to compute the distance between the samples and the interpolation point. Interpolation is an

essential step in managing digital image data for many different applications. Results on resampling (zooming) synthetic and clinical DT-MRI data are used to illustrate the technique. This new scheme provides a new framework for anisotropic image processing, including applications on filtering, registration or segmentation.

- **Esquema Variacional para el Filtrado de Imágenes Médicas Tensoriales** [Castaño04a]:

  In this paper, we propose a filtering scheme to regularize DT-MRI tensor fields. Our approach is based on variational methods combined with the computation of a local structure measure of this non-scalar data. Some examples with synthetic and DT-MRI data illustrate the performance of the method.

- **Estudio Comparativo de Estimadores no Lineales del Tensor de Estructura Local** [Castaño05]:

  In this paper, we present a method to improve energy estimators of the structure tensor based on nonlinear diffusion. Furthermore, we perform a comparative analysis on the quality of different estimators presented in the literature, measuring the accuracy in the corner detection task, since it is one of the more important applications of the structure tensor.

- **A Generalized Local Structure Measure to Regularize Tensor Fields** [SS05]:

  In this work we describe some approaches to tensor statistical signal processing based on local structure. The local structure tensor, obtained from initial data, is used as a key element in regularization. A stochastic point of view as well as a phase-invariant implementation are included in this chapter. Furthermore, we present a general filtering scheme for multidimensional tensor images, and applications on multidimensional interpolation an registration of tensor data.

- **Anisotropic Filtering with Nonlinear Structure Tensors** [Castaño06b]:

  In this paper, we present an anisotropic filtering scheme which uses a nonlinear version of the local structure tensor to dynamically adapt the shape of the neighborhood used to perform the estimation. In this way, only the samples along the orthogonal direction to that of maximum signal variation are chosen to estimate the value at the current position, which helps to better preserve boundaries and structure information. This idea sets the basis of an anisotropic filtering framework which can be applied for different kinds of linear filters, such as Wiener or LMMSE, among others. In this paper, we describe the underlying idea using anisotropic gaussian filtering which allows us, at the same time, to study the influence of nonlinear structure tensors in filtering schemes, as we compare the performance to that obtained with classical definitions of the structure tensor.

- **A Homomorphic Filtering Framework for DT-MRI** [Castaño06c]:

  In this paper we set the mathematical foundations of a filtering framework for tensor signals using the theory of vector spaces. From this point of view, signals are regarded as elements of vector spaces and operators as mappings from the input space to the output space. Hence, it is possible to generalize the principle of superposition to

any operator defined on the signal spaces. Systems that obey that generalization of the principle of superposition are referred to as homomorphic and they can be decomposed in a cascade of three homomorphic subsystems: the first one operates on the input signal space, the second one is a linear system in the usual sense and the third one operates on the output signal space. Thus, suitable input and output subsystems can be chosen to deal with input signals, which defines a whole family of homomorphic filters. To apply this idea for DT-MRI signals, which consist of positive semi-definite matrices, we identify input and output signal spaces as the set of those real symmetric positive semi-definite matrices. Our homomorphic filtering framework not only guarantees a positive-semidefinite output tensor field whatever linear filter is used to regularize the noisy input, but also reduces the swelling effect produced by a faster regularization of diffusivities rather than orientations, as demonstrate the encouraging results that have been carried out.

- **A Fast and Rigorous Anisotropic Smoothing Method for DT-MRI** [Castaño06]:

  In this paper, we exploit the theoretically well-founded differential geometrical properties of the space of multivariate normal distributions, where an affine-invariant Riemannian metric can be defined, to develop some statistics on the manifold of symmetric positive definite matrices. We focus on the contributions of these statistical tools to the anisotropic smoothing problem of tensor fields.

- **A Riemannian Approach to Anisotropic Filtering of Tensor Fields** [Castaño06a]:

  Up to now, algorithms and tools developed to deal with tensors were founded on the assumption of a matrix vector space with the constraint of remaining symmetric positive definite matrices. On the contrary, our approach is grounded on the theoretically well-founded differential geometrical properties of the space of multivariate normal distributions, where it is possible to define an affine-invariant Riemannian metric and express statistics on the manifold of symmetric positive definite matrices. In this paper, we focus on the contribution of these tools to the anisotropic filtering and regularization of tensor fields. To validate our approach we present promising results on both, synthetic and real DT-MRI data.

6.3 Future Work

Following the work presented in this dissertation, further research can still be done in order to develop new concepts and/or algorithms for tensor signal processing. Among others, we can distinguish the following research topics:

- An interesting task is to perform a complete characterization of anisotropic versions of traditional signal estimators (Wiener, LMMSE, etc.) under the anisotropic processing framework presented in this thesis.

- The use of the local structure tensor as a metric tensor to compute distances between any two samples used in our interpolation algorithm can still be exploited in other

conventional problems, such as image segmentation or registration. These two problems, although out of the scope of this thesis, are quite important in the image processing world. Hence, the use of the local structure tensor is expected to improve the current results.

- Concerning the homomorphic and Riemannian frameworks, further research have to be done in order to find the relationship among them. When the equations associated to each framework are compared to the other, it is quite surprising that both frameworks provide similar expressions, specially when the exponential and logarithm maps are used in the input and output subsystems, respectively, of the homomorphic chain.

Bibliography

[Albers00] G. Albers, M. Lansberg, A. Norbash, D. Tong, M. O'Brien, A. Woolfenden, M. Marks, M. Meseley. Yield of Diffusion-Weighted MRI for Detection of Potentially Relevant Findings in Stroke Patients. *Neurology*, vol. 54, pags. 1562–1567, 2000.

[Alvarez92] L. Alvarez, P. Lions, J. Morel. Image Selective Smoothing and Edge Detection by Nonlinear Diffusion (II). *SIAM Journal of Numerical Analysis*, vol. 29, pags. 845–866, 1992.

[Alvarez94] L. Alvarez, L. Mazorra. Signal and Image Restoration using Shock Filters and Anisotropic Diffusion. *SIAM Journal of Numerical Analysis*, vol. 31, num. 2, pags. 590–605, 1994.

[Alzola01] J. R. Alzola, R. Kikinis, C. Westin. Detection of point landmarks in multidimensional tensor data. *Signal Processing*, vol. 81, pags. 2243–2247, 2001.

[Amari90] S. Amari. Differential geometrical methods in statistics. *Lecture Notes in Statistics, Springer-Verlag*, vol. 1, , 1990.

[Anderson01] A. Anderson. Theoretical analysis of the effects of noise on diffusion tensor imaging. *Magnetic Resonance in Medicine*, vol. 46, num. 6, pags. 1174–1188, 2001.

[Andreu01] F. Andreu, C. Ballester, B. Caselles, J. Mazón. Minimizing total variation flow. *Differential and Integral Equations*, vol. 14, num. 3, pags. 321–360, Mar 2001.

[Anwander02] A. Anwander, C. Wolters, M. Dumpelmann, T. Knosche. Sensitivity of source localization towards conductivity anisotropy in high resolution finite element head models. *Proc. of the International Conference on Biomagnetism (BIOMAG)*, 2002.

[Ardekani03] B. Ardekani, J. Nierenberg, M. Hotman, D. Javitt, K. Lim. MRI Study of White Matter Diffusion Anisotropy in Schizophrenia. *NeuroReport*, vol. 14, num. 16, pags. 2025–2029, 2003.

[Atkinson81] C. Atkinson, A. Mitchell. Rao's Distance Measure. *Sankhya: The Indian Journal of Stats.*, vol. 43, num. A, pags. 345–365, 1981.

[Baird98] A. Baird, S. Warach. Magnetic Resonance of acute stroke. *J. Cerebral Blood Flow Metabolism*, vol. 18, pags. 582–609, 1998.

[Basser94a] P. Basser, J. Mattiello, D. L. Bihan. Estimation of the effective self-diffusion tensor from the nmr spin echo. *Journal of Magnetic Resonance*, vol. B, num. 103, pags. 247–254, 1994.

[Basser94b] P. Basser, J. Mattiello, D. L. Bihan. MR Diffusion Tensor Spectroscopy and Imaging. *Biophysical Journal*, vol. 66, pags. 259–267, 1994.

[Basser96] P. Basser, C. Pierpaoli. Microstructural and physiological features of tissues elucidated by quantitative-diffusion tensor MRI. *J. Magn. Reson.*, vol. 111, pags. 209–219, 1996.

[Basser00] P. Basser, S. Pajevic, C. Pierpaoli, J. Duda, A. Aldroubi. In vivo fiber tractography using DT-MRI data. *Magnetic Resonance in Medicine*, vol. 44, pags. 625–632, 2000.

[Bigün87] J. Bigün, G.-H. Granlund. Optimal orientation detection of linear symmetry. *IEEE First International Conference on Computer Vision - June - London, Great Britain*, pags. 433–438, 1987.

[Bihan86] D. L. Bihan, E. Breton, D. Lallemand, P. Grenier, E. Cabanis, M. Laval-Jeantet. MR Imaging of Intravoxel Incoherent Motions: Application to Diffusion and Perfusion in Neurologic Disorders. *Radiology*, vol. , pags. 401–407, 1986.

[Bihan89] D. L. Bihan, J. Delannoy, R. Levin. Temperature mapping with MR imaging of molecular diffusion: Application to hyperthermia. *Radiology*, vol. 171, num. 3, pags. 853–857, 1989.

[Bihan01] D. L. Bihan, J.-F. Mangin, C. Poupon, C. Clark, S. Pappata, N. Molko, H. Chabriat. Diffusion Tensor Imaging: Concepts and Applications. *Magn. Reson. Imaging J.*, vol. 13, pags. 534–546, 2001.

[Björck83] A. Björck, S. Hammarling. A Schur method for the square root of a matrix. *Linear Algebra Appl.*, vol. 52, num. 53, pags. 127–140, 1983.

[Blair95] W. Blair, J. Conte, T. Rice. An instructive example of homomorphic signal processing. *IEEE Transactions on Education*, vol. 38, num. 3, pags. 211–216, 1995.

[BMtHR94] Bart M. ter Haar Romeny. *Geometry-driven diffusion in computer vision.* Computational imaging and vision. Kluwer Academic Publishers, 1994.

[Brox02] T. Brox, J. Weickert. Nonlinear matrix diffusion for optic flow estimation. *Proc. DAGM Symposium*, pags. 446–453, 2002.

[Brox06] T. Brox, J. Weickert, B. Burgeth, P. Mrázek. Nonlinear structure tensors. *Image and Vision Computing*, vol. 24, num. 1, pags. 41–55, January 2006.

[Burbea82] J. Burbea, C. Rao. Entropy Differential Metric, Distance and Divergence Measures in Probability Spaces: A Unified Approach. *Journal of Multivariate Analysis*, vol. 12, pags. 575–596, 1982.

[Burbea86] J. Burbea. Informative geometry of probability spaces. *Expositiones Mathematica*, vol. 43, num. A, pags. 345–365, 1986.

[Calvo91] M. Calvo, J. Oller. An explicit solution of information geodesic equations for the multivariate normal model. *Statistics and Decisions*, vol. 9, pags. 119–138, 1991.

[Campbell03] J. Campbell, K. Siddiqi, B. Vemuri, G. Pike. A geometric flow for white matter fibre tract reconstruction. *IEEE International Symposium on Biomedical Imaging Conferece Proceedings*, pags. 505–508, 2003.

[Castaño03a] C.-A. Castaño, J. Ruiz-Alzola. Filtrado Homomórfico de Datos Tensoriales. *Actas del XVIII Symposium de la Unión Científica de Radio-URSI*, La Coruña, sep 2003.

[Castaño03b] C.-A. Castaño, C.-F. Westin, J. Ruiz-Alzola. Homomorphic Filtering of DT-MRI fields. *Medical Image Computing and Computer Assisted Intervention, Lecture Notes in Computer Science*, vol. 2879, , Noviembre 2003.

[Castaño04a] C.-A. Castaño, L. Álvarez, M.-A. Rodríuez-Florido, J. Ruiz-Alzola. Esquema Variacional para el Filtrado de Imágenes Médicas Tensoriales. *Actas del XIX Symposium de la Unión Científica de Radio-URSI*, Barcelona, sep 2004.

[Castaño04b] C.-A. Castaño, M.-A. Rodríguez-Florido, L. Álvarez, C.-F. Westin, J. Ruiz-Alzola. Anisotropic Interpolation of DT-MRI. *Medical Image Computing and Computer Assisted Intervention, Lecture Notes in Computer Science*, vol. 3216, , 2004.

[Castaño05] C.-A. Castaño, J. Ruiz-Alzola. Estudio Comparativo de Estimadores No Lineales del Tensor de Estructura Local. *Actas del XX Symposium de la Unión Científica de Radio-URSI*, Gandía, Spain, sep 2005.

[Castaño06a] C.-A. Castaño, C. Lenglet, R. Deriche, J. Ruiz-Alzola. A Riemannian Approach to Anisotropic Filtering of DT-MRI. *Signal Processing. Special Issue on Tensor Signal Processing*, vol. In press, , 2006.

[Castaño06b] C. Castaño, J. Ruiz-Alzola. Anisotropic Filtering with Nonlinear Structure Tensors. *Proc. SPIE conference on Electronic Imaging*, page In press, San Jose, CA (USA), 2006.

[Castaño06c] C. Castaño, C.-F. Westin, J. Ruiz-Alzola. A Homomorphic Filtering Framework for DT-MRI. *Proc. SPIE conference on Medical Imaging*, page In press, San Diego, CA (USA), 2006.

[Castaño06] C. Castaño, C. Lenglet, R. Deriche, J. Ruiz-Alzola. A Fast and Rigorous Anisotropic Smoothing Method for DT-MRI. *Proc. IEEE Intl. Symposium on Biomedical Imaging: From Nano to Macro*, Arlington, VA, April 2006.

[Chan99] T. Chan, J. Shen. Variational restoration of non-flat image features : Models and algorithms. *Research Report. Computational and applied mathematics department of mathematics Los Angeles.*, vol. , , jun 1999.

[Charbonnier94] P. Charbonnier, G. Aubert, M. Blanc-Fraud, M. Barlaud. Two deterministic half-quadratic regularization algorithms for computed imaging. *Proceedings of the International Conference on Image Processing*, volumen II, pags. 168–172, 1994.

[Chefd'hotel02] C. Chefd'hotel, D. Tschumperlé, R. Deriche, O. Faugeras. Constrained Flows on Matrix-Valued functions : application to diffusion tensor regularization. *Proceedings of ECCV'02*, Jun. 2002.

[Cheng01] S. Cheng, N. Higham, C. Kenney, A. Laub. Approximating the logarithm of a matrix to specified accuracy. *SIAM J. Matrix Anal. Appl.*, vol. 22, num. 4, pags. 1112–1125, 2001.

[Cicarelli03] O. Cicarelli, A. Toosy, G. Parker, C. M. Wheeler-Kingshott, G. Barker, D. Miller, A. Thompson. Diffusion Tractography Based Grou p Mapping of Major White Matter Pathways in the Human Brain. *NeuroImage*, vol. 19, pags. 1545–1555, 2003.

[Coulon01] O. Coulon, D. Alexander, S. Arridge. A geometrical approach to 3D diffusion tensor magnetic resonance image regularisation. Technical report, Department of Computer Science. University College London, 2001.

[Cressie93] N. A. Cressie. *Statistics for Spatial Data.* Wiley Series in Probability and Mathematical Statistics. J. Wiley and Sons, 1993.

[Curtis87] M. Curtis. *Matrix Groups.* Springer-Verlag New York Berlin Heidelberg Tokyo, 2nd edition edition, 1987.

[Dibos00] F. Dibos, G. Koepfler. Global total variation minimization. *SIAM Journal on Numerical Analysis*, vol. 33, num. 2, pags. 646–664, 2000.

[Douek91] P. Douek, R. Turner, J. Pekar, N. Patronas, D. LeBihan. MR color mapping of myelin fiber orientation. *J. Computer Assisted Tomography*, vol. 15, pags. 923–929, 1991.

[Dudgeon83] D. Dudgeon, R. Merserau. *Multidimensional Digital Signal Processing.* Signal Processing Series. Prentice-Hall, Upper Saddle River, 1983.

[Eriksen86] P. Eriksen. Geodesics Connected with the Fisher Metric on the Multivariate Manifold. Technical Report 86-13, Institute of Electronic Systems, Aalborg University, 1986.

[Farnebäck02] G. Farnebäck. *Polynomial Expansion for Orientation and Motion Estimation.* Tesis Doctoral, Linköping University. Dissertation No 790., Sweden, 2002.

[Fletcher04] P. Fletcher, S. Joshi. Principal Geodesic Analysis on Symmetric Spaces: Statistics of Diffusion Tensors. *Proc. Computer Vision Approaches to Medical Image Analysis*, pags. 87–98, Prague, may 2004.

[Förstner86] W. Förstner. A Feature Based Corresponding Algorithm for Image Matching. *Int. Arch of Photogrammetry and Remote Sensing*, vol. 3, num. 3, pags. 150–166, 1986.

[Förstner87] W. Förstner, E. Gülch. A fast operator for detection and precise location of distinct points, corners and centres of circular features. *Proc. ISPRS Intercommission Conference on Fast Processing of Photogrammetric Data*, pags. 281–305, Interlaken, Switzerland, June 1987.

[Förstner99] W. Förstner, B. Moonen. A metric for covariance matrices. Technical report, Stuttgart University, Dept. of Geodesy and Geoinformatics, 1999.

[Frank02] L. Frank. Characterization of Anisotropy in High Angular Resolution Diffusion Weighted MRI. *Magnetic Resonance in Medicine*, vol. 47, pags. 1083–1099, 2002.

[Freeman91] W. T. Freeman, E. H. Adelson. The design and use of steerable filters. *IEEE Trans. Pattern Analysis and Machine Intelligence*, vol. 13, num. 9, pags. 891–906, 1991.

[Freeman92] W. Freeman. *Steerable filters and the local analysis of image structure.* Tesis Doctoral, MIT Dept. Media Arts and Sciences., September 1992.

[Gabor46] D. Gabor. Theory of Communication. *J. Inst. Elec. Eng.*, vol. 93, num. 26, pags. 429–457, 1946.

[Gallier05] J. Gallier. *Group Actions, Manifolds, Lie Groups and Lie Algebras.* Springer, to be published edition, 2005.

[Geusebroek03] J. M. Geusebroek, A. W. M. Smeulders, J. van de Weijer. Fast Anisotropic Gauss Filtering. *IEEE Trans. Image Processing*, vol. 12, num. 8, pags. 938–943, 2003.

[Golub96] G. Golub, C. V. Loan. *Matrix Computations.* Johns Hopkins University Press, 3rd edition edition, 1996.

[Granlund95] G.-H. Granlund, H. Knutsson. *Signal Processing for Computer Vision.* Kluwer Academic Publishers, 1995.

[Haimes99] R. Haimes, D. Kenwright. The Velocity Gradient Tensor and Fluid Feature Extraction. *Proc. AIAA 14th Computational Fluid Dynamics Conference*, 1999.

[Harris88] C. Harris, M. Stevens. A combined corner and edge detector. *4th Alvey Vision Conf.*, pags. 147–151, Manchester, August 1988.

[Haueisen02] J. Haueisen, D. Tuch, C. Ramon, P. Schimpf, V. Wedeen, J. George, J. Belliveau. The influence of brain tissue anisotropy on human EEG and MEG. *Neuroimage*, vol. 15, pags. 159–166, 2002.

[Higham86] N. Higham. Newton's method for the matrix square root. *Math. Comp.*, vol. 46, num. 174, pags. 537–549, April 1986.

[Higham87] N. Higham. Computing real square roots of a real matrix. *Linear Algebra Appl.*, vol. 88, num. 89, pags. 405–430, 1987.

[Higham97] N. Higham. Stable iterations for the matrix square root. *Numerical Algorithms*, vol. 15, num. 2, pags. 227–242, 1997.

[Higham01] N. Higham. Evaluating Padé approximants of the matrix logarithm. *SIAM J. Matrix Anal. Appl.*, vol. 22, num. 4, pags. 1126–1135, 2001.

[Higham05a] N. Higham. Functions of Matrices. Technical Report 2005.21, University of Manchester, 2005.

[Higham05b] N. Higham. The scaling and squaring method for the matrix exponential revisited. *SIAM J. Matrix Anal. Appl.*, vol. 26, num. 4, pags. 1179–1193, 2005.

[Horsfield02] M. Horsfield, D. Jones. Applications of Diffusion-Weighted and Diffusion Tensor MRI to white matter diseases - a review. *NMR Biomed.*, vol. 15, num. 7-8, pags. 570–7, 2002.

[Hunt87] J. Hunt. Vorticity and vortex dynamics in complex turbulent flows. vol. 11, num. 1, pags. 21–35, 1987.

[Isham89] C.-J. Isham. *Lectures on Groups and Vector Spaces for Physicists.* World Scientphic Publishing, 1989.

[Karcher77] H. Karcher. Riemannian centre of mass and mollifier smoothing. *Comm. Pure Appl. Math*, vol. 30, pags. 509–541, 1977.

[Kass87] M. Kass, A. Witkin. Analyzing oriented patterns. *Computer Vision Graphics and Image Processing*, vol. 37, pags. 362–385, 1987.

[Kay93] S. Kay. *Fundamentals of Statistical Signal Processing: Estimation Theory*, volumen 1 de *Signal Processing Series.* Prentice-Hall, Upper Saddle River, 1993.

[Kenney89] C. Kenney, A. Laub. Condition estimates for matrix functions. *SIAM J. Matrix Anal. Appl.*, vol. 10, num. 2, pags. 191–209, 1989.

[Kimmel00] R. Kimmel, R. Malladi, N. Sochen. Images as embedded maps and minimal surfaces: movies, color, texture and volumetric medical images. *International Journal of Computer Vision*, vol. 39, num. 2, pags. 111–129, 2000.

[Kindlmann04] G. Kindlmann. Superquadric tensor glyphs. *Proc. IEEE TVCG/EG Symposium on Visualization*, pags. 147–154, 2004.

[Knutsson89] H. Knutsson. Representing local structure using tensors. *6th Scandinavian Conference on Image Analysis. Oulu, Finland*, pags. 244–251, 1989.

[Knutsson03a] H. Knutsson, M. Andersson. Loglets: Generalized quadrature and phase for local spatio-temporal structure estimation. J. Bigün, T. Gustavsson, editors, *Proc. of SCIA03. LNCS.*, volumen 2749, pags. 741–748. Springer, 2003.

[Knutsson03b] H. Knutsson, M. Andersson. What's so Good About Quadrature Filters? *2003 IEEE International Conference on Image Processing*, 2003.

[Koenderink84] J. Koenderink. The structure of images. *Biological Cybernetics*, vol. 50, pags. 363–370, 1984.

[Köthe03] U. Köthe. Integrated Edge and Junction Detection with the Boundary Tensor. *9th Intl. Conf. on Computer Vision*, volumen 1, pags. 424–431, Nice, 2003. IEEE Computer Society.

[Laidlaw98] D. H. Laidlaw, E. T. Ahrens, D. Kremers, M. J. Avalos, C. Readhead, R. E. Jacobs. Visualizing Diffusion Tensor Images of the Mouse Spinal Cord. *Proceedings of IEEE Visualization 1998*, pags. 127–134. IEEE Computer Society Press, October 1998.

[Lazar03] M. Lazar, D. Weinstein, J. Tsuruda, K. Hasan, K. Arfanakis, M. Meyerand, B. Badie, H. Rowley, V. Haughton, A. Field, A. Alexander. White Matter Tractography Using Diffusion Tensor Deflection. *HBM*, vol. 18, pags. 306–321, 2003.

[Lenglet05a] C. Lenglet, R. Deriche, O. Faugeras, S. Lehéricy, K. Ugurbil. A Riemannian approach to Diffusion tensor estimation and streamline-based fiber tracking. *Proceedings of 11th Annual Meeting of the Organization for Human Brain Mapping*, Toronto, 2005.

[Lenglet05b] C. Lenglet, M. Rousson, R. Deriche, O. Faugeras. Statistics on the Manifold of Multivariate Normal Distributions: Theory and Application to Diffsuion Tensor MRI. *Journal of Mathematical Imaging and Vision, Special Issue MIA'04*, vol. In press, , 2005.

[Lim90] J. Lim. *Two-Dimensional Signal and Image Processing.* Englewood Cliffs, NJ: Prentice Hall, 1990.

[Lin03] C. Lin, V. Weeden, J. Chen, C. Yao, W. Tseng. Validation of Diffusion Spectrum Magnetic Resonance Imaging with Manganese-enhanced Rat Optic Tracts and ex Vivo Phantoms. *Neuroimage*, vol. 19, pags. 482–495, 2003.

[Lovric05] M. Lovric, M. Min-Oo, E.-A. Ruh. Multivariate normal distributions parametrized as a Riemannian symmetric space. *J. Multivariate Analysis*, vol. 74, num. 1, pags. 36–48, 2005.

[Lucas81] B. D. Lucas, T. Kanade. An Iterative Image Registration Technique with an Application to Stereo Vision. *Proc. of the 7th IJCAI*, pags. 674–679, Vancouver, Canada, 1981.

[Lukin05] A. Lukin, D. Kalinkina, D. Kubasov. Adaptive Multiresolution filter Banks for Image and Audio Processing. *Graphicon-2005*, Russia, 2005.

[Mester01] R. Mester, M. Mühlich. Improving motion and orientation estimation using an equilibrated total least squares approach. *Proc. IEEE International Conference on Image Processing (ICIP 2001)*, pags. 640–643, Thessaloniki, Greece, October 2001.

[MF04] M. Martin-Fernandez, C.-F. Westin, C. Alberola-Lopez. 3D Bayesian Regularization of Diffusion Tensor MRI Using Multivariate Gaussian Markov Random Fields. *Medical Image Computing and Computer Assisted Intervention, Lecture Notes in Computer Science*, vol. 3216, pags. 351–359, 2004.

[Micchelli05] C.-A. Micchelli, L. Noakes. Rao Distances. *J. Multivariate Analysis*, vol. 92, pags. 97–115, 2005.

[Moakher05] M. Moakher. A Differential Geometric Approach to the Geometric Mean of Symmetric Positive-Definite Matrices. *SIAM J. Matrix Anal. Appl.*, vol. 26, num. 3, pags. 735–747, Apr. 2005.

[Moler78] C. Moler, C. V. Loan. Nineteen dubious ways to compute the exponential of a matrix. *SIAM Rev.*, vol. 20, num. 4, pags. 801–836, 1978.

[Moon99] T.-K. Moon, W.-C. Sterling. *Mathematical Methods and Algorithms for Signal Processing.* Prentice-Hall, 1999.

[Mori99] S. Mori, B. Crain, V. Chacko, P. van Zijl. Three Dimensional Tracking of Axonal Projections in th Brain by Magnetic Resonance Imaging. *Ann Neurol*, vol. 45, num. 2, pags. 265–269, 1999.

[Morrone87] M. Morrone, R. Owens. Feature detection from local energy. *Pattern Recognition Letters*, vol. 6, pags. 303–313, 1987.

[Moseley99] M. Moseley, Y. Cohen, J. Kucharczyk, J. Mintorovitch, H. Asgari, M. Wendland, J. Tsuruda, D. Norman. Diffusion Weighted MR Imaging of anisotropic water diffusion in cat central nervous system. *Radiology*, vol. 176, pags. 439–445, 1999.

[Muller94] M. Muller, P. Prasad, B. Siewert. Abdominal Diffusion Mapping with use of a whole-body echo-planar system. *Radiology*, vol. 190, pags. 475–478, 1994.

[Niethammer06] M. Niethammer, R. San-Jose Estepar, S. Bouix, M. Shenton, C.-F. Westin. On Diffusion Tensor Estimation. *28th IEEE EMBS*, pags. 2622–2625, New York City, NY, USA, September 2006.

[Nitzberg92] M. Nitzberg, T. Shiota. Nonlinear image filtering with edge and corner enhancement. *IEEE Trans. Pattern Anal. Mach. Intell.*, vol. 8, pags. 318–327, 1992.

[O'Donnell02] L. O'Donnell, S. Haker, C.-F. Westin. New approaches to estimation of white matter connectivity in diffusion tensor MRI: Elliptic PDEs and geodesics in a tensor warped space. *Fifth International Conference on Medical Image Computing and Computer-Assisted Intervention*, 2002.

[Oppenheim65] A. Oppenheim. Superposition in a Class of Nonlinear Systems. Technical Report 432, Laboratory of Electronics, MIT, Cambridge, Mass., 1965.

[Oppenheim67] A. Oppenheim. Generalized Superposition. *Information Control*, vol. 11, num. 5-6, pags. 528–536, November-December 1967.

[Oppenheim68a] A. Oppenheim, R. Schafer. Homomorphic Analysis of Speech. *IEEE Transactions on Audio and Electroacustics*, vol. AU-16, num. 3, pags. 221–226, June 1968.

[Oppenheim68b] A. Oppenheim, R. Schafer, T. Stockham. Nonlinear Filtering of Multiplied and Convolved Signals. *IEEE Transactions on Audio and Electroacustics*, vol. AU-16, num. 3, pags. 437–466, September 1968.

[Oppenheim97] A. Oppenheim, A. Willsky, I. Young. *Signals and Systems*. Prentice-Hall International, 1997.

[Pajevic03] S. Pajevic, P. Basser. Parametric and non-parametric statistical analysis of DT-MRI data. *Journal of Magnetic Resonance*, vol. 106, pags. 1–14, 2003.

[Parker02] G. Parker, C. Wheeler-Kingshott, G. Barker. Estimating Distributed Anatomical Connectivity Using Fast Marching Methods and Diffusion Tensor Imaging. *Transactions on Medical Imaging*, vol. 21, num. 5, pags. 505–512, 2002.

[Parker03] G. Parker, D. Alexander. Probabilistic Monte Carlo Based Mapping of Cerebral Connections Utilising Whole-Brain Crossing Fibre Information. *Proc. of Information Processing in Medical Imaging*, pags. 684–695, 2003.

[Parlett76] B. Parlett. A recurrence among the elements of functions of triangular matrices. *Linear Algebra Appl.*, vol. 14, pags. 117–121, 1976.

[Paterson73] M. Paterson, L. Stockmeyer. On the number of nonscalar multiplications necessary to evaluate polynomials. *SIAM J. Comput.*, vol. 2, num. 1, pags. 60–66, 1973.

[Pennec04] X. Pennec, P. Fillard, N. Ayache. A Riemannian Framework for Tensor Computing. Technical Report 5255, INRIA, Sophia Antipolis, Jul. 2004.

[Pennec05] X. Pennec, P. Fillard, N. Ayache. A Riemannian Framework for Tensor Computing. *International Journal of Computer Vision*, vol. 65, num. 1, , 2005.

[Perona90] P. Perona, J. Malik. Scale-space and Edge Detection Using Anisotropic Diffusion. *IEEE Transactions on Pattern Analysis and Machine Intelligence*, vol. 12, num. 7, pags. 629–639, Jul. 1990.

[Pierpaoli96a] C. Pierpaoli, P. Basser. Toward a Quantitative Assessment of Diffusion Anisotropy. *Magn. Res. Med.*, vol. 36, num. 6, pags. 893–906, 1996.

[Pierpaoli96b] C. Pierpaoli, P. Jezzard, P. Basser, A. Barnett, G. D. Chiro. Diffusion Tensor MR Imaging of Human Brain. *Radiology*, vol. 201, pags. 637–648, 1996.

[Poupon99] C. Poupon. *Detection des faisceaux de fibres de la substance blanche pour l'etude de la connectivite anatomique cerebrale.* Tesis Doctoral, Ecole Nationale Superieure des Telecommunications, 1999.

[Poupon00] C. Poupon, C. Clark, V. Frouin, J. Regis, D. L. Bihan, I. Bloch, J. Mangin. Regularization Diffusion-Based Direction Maps for the Tracking of Brain White Matter Fascicles. *Neuroimage*, vol. 12, pags. 184–195, 2000.

[RA05] J. Ruiz-Alzola, C. Alberola-Lopez, C.-F. Westin. Kriging Filters for Multidimensional Signal Processing. *Signal Processing*, vol. 85, num. 2, pags. 413–439, 2005.

[Raffel98] M. Raffel, C. Willert, J. Kompenhans. *Particle Image Velocimetry. A Practical Guide.* Springer Verlag, 1998.

[Rao45] C. Rao. Information and Accuracy Attainable in the Estimation of Statistical Parameters. *Bull. Calcutta Math. Soc.*, vol. 37, pags. 81–91, 1945.

[Rao91] A.-R. Rao, B.-G. Schunck. Computing oriented texture fields. *CVGIP: Graphical Models and Image Processing*, vol. 53, num. 2, pags. 157–185, 1991.

[Reese95] T. Reese, R. Weisskoff, R. Smith. Imaging myocardial fiber architecture in vivo with magnetic resonance. *Magnetic Resonance Medicine*, vol. 34, pags. 786–791, 1995.

[RF01] M.-A. Rodriguez-Florido, K. Krissian, J. Ruiz-Alzola, C.-F. Westin. Comparison Between Two Restoration Techniques in the Context of 3D Medical Imaging. *LNCS - Springer-Verlag*, vol. 2208, pags. 1031–1039, 2001.

[RF03] M. Rodriguez-Florido. *Procesado Anisótropo de Campos Tensoriales Multidimensionales y sus Aplicaciones al Filtrado y Segmentación de Imágenes Médicas.* Tesis Doctoral, Universidad de Las Palmas de Gran Canaria, Centro de Tecnología Médica, 2003.

[RF04] M.-A. Rodriguez-Florido, C.-F. Westin, J. Ruiz-Alzola. DT-MRI Regularization Using Anisotropic Tensor Field Filtering. *2004 IEEE International Symposium on Biomedical Imaging - April 15-18 - Arlington,VA (USA)*, pags. 336–339, 2004.

[Rieger04] B. Rieger, L. Vlieet. A systematic approach to nD orientation representation. *Image and Vision Computing*, vol. 22, num. 6, pags. 453–459, 2004.

[Rohr94] K. Rohr. Localization properties of direct corner detectors. *Journal of Mathematical Imaging and Vision*, vol. 4, pags. 139–150, 1994.

[Rousson04] M. Rousson. *Cues Integrations and Front Evolutions in Image Segmentation.* Tesis Doctoral, Nice-Sophia Antipolis University, INRIA-Project Odyssée, 2004.

[San Jose05] R. San Jose. *Local Structure Tensor for Multidimensional Signal Processing. Applications to Medical Image Analysis.* Tesis Doctoral, Universidad de Valladolid, E.T.S. Ingenieros de Telecomunicación, February 2005.

[Sapiro01] G. Sapiro. *Geometric Partial Differential Equations and Image Analysis.* Cambridge University Press, 2001.

[Skare00] S. Skare, T. Li, B. Nordell, M. Ingvar. Noise considerations in the determination of diffusion tensor anisotropy. *Magnetic Resonance in Medicine*, vol. 18, num. 6, pags. 659–669, 2000.

[Skovgaard81] L. Skovgaard. A Riemannian Geometry of the Multivariate Normal Model. Technical Report 81/3, Statistical Research Unit, Danish Medical Research Council, Danish Social Science Research Council, 1981.

[Sotak02] C. Sotak. The role of diffusion tensor imaging (dti) in the evaluation of ischemic brain injury. *NMR Biomed.*, vol. 15, pags. 561–569, 2002.

[SS03] E. Suárez-Santana. *Un marco general para la normalización geométrica de datos tensoriales y su aplicación al registrado de imágenes médicas.* Tesis Doctoral, Universidad de Las Palmas de Gran Canaria, Centro de Tecnología Médica, 2003.

[SS05] E. Suarez-Santana, M. Rodriguez-Florido, C. Castaño-Moraga, C.-F. Westin, J. Ruiz-Alzola. A Generalized Local Structure Measure to Regularize Tensor Fields. J. Weickert, H. Hagen, editors, *Visualization and Image Processing of Tensor Fields*, Mathematics and Visualization. Springer-Verlag, 2005.

[Stejskal65] E. Stejskal, J. Tanner. Spin diffusion measurements: spin echoes in the presence of a time-dependent field gradient. *Journal of Chemical Physics*, vol. 42, pags. 288–292, 1965.

[Talos03] I. Talos, L. O'Donnell, C.-F. Westin, S. Warfield, W. Wells-III, S. Yoo, L. Panych, A. Golby, H. Mamata, S. Maier, P. Ratiu, C. Guttmann, P. Black, F. Jolesz, R. Kikinis. Diffusion tensor and functional mri fusion with anatomical mri for image-guided neurosurgery. *Sixth International Conference on Medical Image Computing and Computer-Assisted Intervention (MICCAI'03)*, pags. 407–415, Montreal, Canada, November 2003.

[Torquato90] S. Torquato, A. Sen. Conductivity Tensor of Anisotropic Composite Media from the Microstructure. *Journal of Applied Physics*, vol. 67, num. 3, pags. 1145–1155, 1990.

[Torquato02] S. Torquato. *Random Heterogeneous Material, Microstructure and Macroscopic Properties, Mechanics and Materials.* Springer, 2002.

[Tschumperlé01] D. Tschumperlé, R. Deriche. Diffusion Tensor Regularization with Constraints Preservation. *IEEE Computer Society Conference on Computer Vision and Pattern Recognition*, Kauai Marriott, Hawaii, dec 2001.

[Tschumperlé03a] D. Tschumperlé, R. Deriche. DT-MRI Images : Estimation, Regularization and Application. J. R. R. Moreno-Diaz Jr, A. Quesada-Arencibia, editor, *EUROCAST'2003*, 9th International Workshop on Computer Aided Systems Theory, Las Palmas de Gran Canaria, 2003.

[Tschumperlé03b] D. Tschumperlé, R. Deriche. Variational Frameworks for DT-MRI Estimation, Regularization and Visualization. *Proceedings of the 9th International Conference on Computer Vision*, Nice, France, 2003. IEEE Computer Society, IEEE Computer Society Press.

[Tschumperle03c] D. Tschumperle, R. Deriche. Vector-Valued Image Regularization with PDE's: A common framework for different applications. *In IEEE Conference on Computer Vision and Pattern Recognition*, 2003.

[Tschumperlé03] D. Tschumperlé, R. Deriche. DT-MRI Images: Estimation, Regularization and Application. R. M. Díaz, A. Q. Arencibia, editors, *Proc. of th 9th International Workshop on Computer Aided Systems Theory*, pags. 46–47, Las Palmas de Gran Canaria (Spain), February 2003. Universidad de Las Palmas de Gran Canaria.

[Tuch01] D. Tuch, M. Wiegell, T. Reese, J. Belliveau, V. Weeden. Measuring Cortico-cortical Connectivity Matrices with DSI. *Int. Soc. Magn. Resonance in Medicine*, vol. 9, pags. 502, 2001.

[Tuch02a] D. Tuch. Mapping cortical connectivity with diffusion mri. *In Proc. ISBI*, pags. 392–394, 2002.

[Tuch02b] D. Tuch, T. Reese, M. Wiegell, N. Makris, J. Belliveau, V. Wedeen. High angular resolution diffusion imaging reveals intravoxel white matter fiber heterogeneity. *Magnetic Resonance in Medicine*, vol. 48, pags. 577–582, 2002.

[Vemuri01] B. Vemuri, Y. Chen, M. Rao, T. McGraw, Z. Wang, T. Mareci. Fiber Tract Mapping from Diffusion Tensor MRI. *Proceedings of the IEEE Workshop on Variational and Level Set Methods (VLSM'01)*. IEEE, 2001.

[vG94] P. van Gelderen, M. de Vleeschouwer, D. Despres, J. Pekar, P. van Zijl, C. Moonen. Water diffusion and acute stroke. *MR in Medicine*, vol. 31, pags. 154–163, 1994.

[Vilanova05] A. Vilanova, S. Zhang, G. Kindlmann, D. Laidlaw. An Introduction to Visualization of Diffusion Tensor Imaging and Its Applications. J. Weickert, H. Hagen, editors, *Visualization and Image Processing of Tensor Fields*, Mathematics and Visualization. Springer-Verlag, 2005.

[Wang03] Z. Wang, B. Vemuri, Y. Chen, T. Mareci. Simultaneous smoothing and estimation of the tensor field from diffusion tensor mri. *IEEE Conference on Computer Vision and Pattern Recognition*, pags. 461–466, 2003.

[Ward77] R. Ward. Numerical computation of the matrix exponential with accuracy estimate. *SIAM J. Numer. Anal.*, vol. 14, num. 4, pags. 600–610, 1977.

[Weickert98] J. Weickert. *Anisotropic Diffusion in Image Processing.* Teubner-Verlag, 1998.

[Weickert99] J. Weickert. Coherence Enhancing diffusion filtering. *International Journal of Computer Vision*, vol. 31, num. 2/3, pags. 111–127, 1999.

[Weickert02] J. Weickert, T. Brox. Diffusion and regularization of vector- and matrix-valued images. *Inverse Problems, Image Analysis and Medical Imaging. Contemporary Mathematics*, vol. 313, pags. 251–268, 2002.

[Westin94] C.-F. Westin. *A Tensor Framework for Multimiensional Signal Processing.* Tesis Doctoral, Linkoping University, Sweden, 1994. Dissertation No 348.

[Westin97] C. Westin, S. Peled, H. Gudbjartsson, R. Kikinis, F. Jolesz. Geometrical Diffusion Measures for MRI from Tensor Basis Analysis. *Proc. of the International Society for Magnetic Resonance Medicine (ISMRM)*, Vancouver (Canada), April 1997.

[Westin02a] C.-F. Westin, S. Maier, H. Mamata, A. Nabavi, F.-A. Jolesz, R. Kikinis. Processing and Visualization for Diffusion Tensor MRI. *Medical Image Analysis*, vol. 6, num. 2, pags. 93–108, June 2002.

[Westin02b] C. Westin, S. Maier. A dual tensor basis solution to the stejskal-tanner equations for dt-mri. *Proc. of International Society for Magnetic Resonance in Medicine*, 2002.

[Wolters01] C. Wolters, A. Anwander, M. K. S. Reitzinger, M. Kuhn, M. Svensen. Influence of head tissue conductivity anisotropy on human EEG and MEG using fast high resolution finite element modeling, based on a parallel algebraic multigrid solver. Numero ISSN: 0176-2516 en Forschung und wissenschaftliches Rechnen, pags. 111–157. 2001.

[Zhang04] Zhang. Diffusion Tensor MRI Visualization. Tech. Report., November 2004.

List of Figures

List of Tables

List of Acronyms

Acronym	Definition
A/D	Analog to Digital
ADC	Apparent Diffusion Coefficients
CAT	Computed Axial Tomography
CT	Computed Tomography
DT-MRI	Diffusion Tensor Magnetic Resonance Imaging
DWI	Diffusion Weighted Imaging
EAE	Experimental Allergic Encephalomyelitis
EEG	Electro-EncephaloGraphy
ESI	Electromagnetic Source Imaging
FA	Fractional Anisotropy
FIR	Finite Impulse Response
IIR	Infinite Impulse Response
LI	Lattice Intex
LMMSE	Linear Minimum Mean Square Error
LS	Least Squares
LST	Local Structure Tensor
MD	Mean Diffusivity
MEG	Magneto-ElectroencephaloGraphy
MRI	Magnetic Resonance Imaging
MRT	Magnetic Resonance Tomography
MSE	Mean Squared Error
NMR	Nuclear Magnetic Resonance
PDE	Partial Differential Equation
PSD	Positive Semi-Definite

Acronym	Definition
RA	Rational Anisotropy
RF	Radio Frequency
RGB	Read Green Blue
SNR	Signal-to-Noise Ration
TV	Television
TV	Total Variation
VR	Volume Ratio

Index